For Reference

NOT TO BE TAKEN FROM THIS ROOM

Ex libris
universitatis
albertaensis

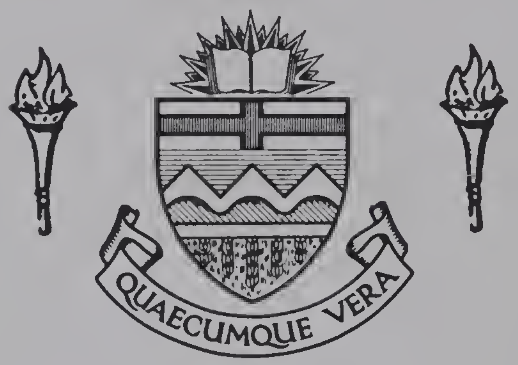

The University of Alberta
Printing Department
Edmonton, Alberta

THE UNIVERSITY OF ALBERTA

RELEASE FORM

NAME OF AUTHOR: Edward Wong

TITLE OF THESIS: Study of ^{37}Ar and the Statistical Compound Nuclear Model

DEGREE FOR WHICH THESIS WAS PRESENTED: Ph. D.

YEAR THIS DEGREE GRANTED: 1975

Permission is hereby granted to THE UNIVERSITY OF ALBERTA LIBRARY to reproduce single copies of this thesis and to lend or sell such copies for private, scholarly or scientific research purposes only.

The author reserves other publication rights, and neither the thesis nor extensive extracts from it may be printed or otherwise reproduced without the author's written permission.

THE UNIVERSITY OF ALBERTA

STUDY OF ^{37}AR AND THE STATISTICAL COMPOUND NUCLEAR MODEL

by

Ⓒ EDWARD WONG

A THESIS

SUBMITTED TO THE FACULTY OF GRADUATE STUDIES AND RESEARCH
IN PARTIAL FULFILLMENT OF THE REQUIREMENTS FOR THE DEGREE
OF DOCTOR OF PHILOSOPHY
IN
PHYSICS

DEPARTMENT OF PHYSICS

EDMONTON, ALBERTA

SPRING, 1975

THE UNIVERSITY OF ALBERTA

FACULTY OF GRADUATE STUDIES AND RESEARCH

The undersigned certify that they have read, and recommend to the Faculty of Graduate Studies and Research, for acceptance, a thesis entitled STUDY OF ^{37}AR AND THE STATISTICAL COMPOUND NUCLEAR MODEL submitted by Edward Wong in partial fulfillment of the requirements for the degree of Doctor of Philosophy in Physics.

ABSTRACT

The levels in ^{37}Ar below 3.30 MeV excitation have been studied using the ^{37}Cl(p,n)^{37}Ar and the ^{37}Cl(p,nγ)^{37}Ar reactions. These levels were identified from neutron time-of-flight spectra and their energies from deexcitation γ-ray spectra. A level at 3185 keV excitation has been positively confirmed. The mean lifetimes of these levels were determined by the Doppler-shift attenuation method with the γ rays measured in coincidence with neutrons and in singles. Gamma-ray angular distributions were obtained at various incident energies and compared with the statistical compound nuclear (SCN) model. Spins,parities and mixing ratios have been deduced in conjunction with transition strengths based on Weisskopf estimates. Neutron differential cross sections were also measured using the time-of-flight method and compared with the statistical (Hauser-Feshbach) calculations.

The spin and parity assignments and mean lifetimes have been extracted for the following levels of ^{37}Ar: 1410 keV ($J^\pi = 1/2^+$, $\tau = 943^{+170}_{-100}$ fs), 1611 keV ($J^\pi = 7/2^-$, $\tau > 3000$ fs), 2217 keV ($J^\pi = 7/2^+$, $\tau = 510^{+75}_{-60}$ fs), 2488 keV ($J^\pi = 3/2^-$, $\tau = 660^{+250}_{-160}$ fs), 2795 keV ($J^\pi = 5/2^+$, $\tau = 22^{+16}_{-12}$ fs), 3171 keV ($J^\pi = 5/2^+$, $\tau = 85^{+40}_{-30}$ fs), 3185 keV ($J^\pi = 9/2^-$, $\tau = 285^{+70}_{-55}$ fs) and 3274 keV ($J^\pi = 5/2^\pm$, $\tau = 50^{+21}_{-16}$ fs). The results of the present investigation are

compared with previous experimental and theoretical works.

A study of the $^{29}Si(p,p'\gamma)^{29}Si$ reaction was undertaken to investigate statistical limitations of the SCN model. Using a thin target angular distributions of γ-rays deexciting from the 1st and 2nd states of ^{29}Si were measured. Proton energies were varied from 3.00 to 3.60 MeV in 10 keV intervals. Angular distributions for progressively thicker targets were constructed from the thin target yields and compared with predictions of the SCN model. An estimate of the number of levels required for successful application of the model was thus obtained.

ACKNOWLEDGEMENT

I would like to thank my supervisor, Dr. W.C. Olsen, for his advice, encouragement and above all his patience throughout all phases of this work.

I am especially grateful to my co-supervisor, Dr. D.M. Sheppard for his assistance and invaluable discussions.

I would like to express my gratitude to Drs. B.C. Robertson and K.V.K. Iyengar who shared and helped in the ^{37}Ar project. I am also indebted to Dr. G.C. Neilson for his guidance in the neutron experiment. Thanks are also extended to Dr. P.J. Twin for introducing me to the (p,n) reaction.

I am very grateful to Dr. D.A. Hutcheon who read the manuscript and was always ready to explain the finer points of nuclear physics.

Many thanks to my colleagues: Orla Aaquist, Georges Carola, Woon Chung, Sayed El-bakr, Paul Gutowski, Jim Pasos, Tilak Sharma and in particular, Peter Green whose assistance is greatly appreciated.

To Dr. W.K. Dawson and Jim Easton, my sincere gratitude for providing an excellent data acquisition system and their advice and assistance in computer programming. Thanks also go to 'Uncle Jock' Elliott, Lars Holm and the other members of the Nuclear Research Centre technical staff for their co-operation and help.

I would like also to thank Mrs. Mary Yiu for her beautiful and expeditious typing of this thesis.

I wish to acknowledge the financial assistance of the Atomic Energy Control Board of Canada and the University of Alberta.

Finally, I would like to thank my wife, Cora, who typed the manuscript and assisted in her way to make this work possible. To my children, Brigette and Teddy, my appreciation for their cheerful disposition that brightened many a moment of despair.

To Cora
1975

TABLE OF CONTENTS

PAGE

CHAPTER 1 INTRODUCTION 1

CHAPTER 2 MEAN LIFETIMES OF ^{37}Ar 7

2.1 Doppler-Shift Attenuation Method 7

2.2 Experimental Details 11

2.3 Analysis 18

2.4 Results and Discussion 23

2.4.1 Level energies 23

2.4.2 Lifetimes 26

CHAPTER 3 GAMMA-RAY ANGULAR DISTRIBUTION OF ^{37}Ar 39

3.1 Condition of Nuclear Alignment 39

3.1.1 Gamma-ray decay of aligned state 41

3.1.2 Application of the statistical compound nuclear model 45

3.2 Experimental Arrangement 48

3.3 Analysis 53

3.3.1 Chi-square analysis 54

3.3.2 Branching ratios 55

3.4 Results and Discussion 55

3.4.1 The 1410 keV level 58

3.4.2 The 1611 keV level 63

3.4.3 The 2217 keV level 67

3.4.4 The 2488 and 2795 keV levels 69

3.4.5 The 3171 keV level 72

PAGE

CHAPTER 3 (cont'd)

3.4.6 The 3185 keV level 72

3.4.7 The 3274 keV level 76

CHAPTER 4 NEUTRON TIME-OF-FLIGHT STUDIES OF THE $^{37}Cl(p,n)^{37}Ar$ REACTION 80

4.1 Compound Nucleus and Statistical Theory 81

4.2 Experimental Method 87

4.2.1 Neutron identification 90

4.2.2 Neutron angular distribution 92

4.3 Analysis 92

4.3.1 Hauser-Feshbach calculation 95

4.4 Results and Discussion 96

CHAPTER 5 SUMMARY OF ^{37}Ar 111

CHAPTER 6 A STUDY OF THE STATISTICAL MODEL WITH THE $^{29}Si(p,p'\gamma)^{29}Si$ REACTION 118

6.1 Motivation 118

6.2 Experiment 121

6.3 Results and Discussion 123

6.3.1 Thin target 123

6.3.2 Thick target 136

6.4 Conclusion 138

REFERENCES 143

PAGE

Appendix A Modification of F(τ) due to Cascade Feeding 149

Appendix B MAGPOP - A Program to Calculate Angular Distribution Coefficients of γ Rays in Terms of Magnetic Population Parameters 153

Appendix C WAVY - A Program to Calculate Yield Average and Least Square Fit to Legendre Polynomial Series 163

Appendix D Positive Parity States of ^{40}K 172

Appendix E A Study of γ Rays of ^{37}Ar 175

Appendix F Listing of 'OXDS' - a program to calculate F(τ) 188

LIST OF TABLES

TABLES		PAGE
2.1	Summary of Levels of ^{37}Ar	24
2.2	Attenuation Factors and Lifetimes of ^{37}Ar	32
2.3	Summary of Lifetimes in ^{37}Ar	33
3.1	Legendre Polynomial Coefficients for Gamma-ray Angular Distributions of ^{37}Ar	59
3.2	Mixing Ratios of the 1611 keV Level	60
3.3	Summary of Mixing Ratios in ^{37}Ar for $\chi^2 < 0.1\%$ Confidence	61
3.4	Recommended Upper Limits for Gamma-ray Transition Strengths	62
4.1	Optical Model Parameters	97
4.2	Legendre Polynomial Coefficients of the Neutron Angular Distributions	106
5.1	Electromagnetic Transition Strengths in ^{37}Ar	112
6.1	Optical Model Parameters for the ^{29}Si(p,p'γ)^{29}Si Reaction	126
6.2	Angular Distribution Coefficients and Mixing Ratios of ^{29}Si	141

LIST OF FIGURES

FIGURE PAGE

2.1 Experimental arrangement of target and detectors. 13

2.2 Block diagram of electronics. 15

2.3 F(τ) vs τ curves for the 2795 keV level. θ_n is the angle of the outgoing neutron and v_o is the initial recoil velocity. The two curves represent the coincidence ($\theta_n = 170°$) and the singles (θ_n = ave) cases. 22

2.4 A typical γ-ray spectrum observed in coincidence with neutrons from the ^{37}Cl(p,nγ)^{37}Ar reaction at $E_p = 5.70$ MeV. The γ rays were detected at $\theta_\gamma = 0°$ with the annular neutron detector at 180° to the beam direction. 27

2.5 Plots of energy vs cos θ for γ-ray transitions in ^{37}Ar observed at $E_p =$ 5.70 MeV. γ rays detected in coincidence with neutrons (COIN) and in singles (SINGLES) are shown for comparison. The dashed lines represent full energy shifts while the solid lines correspond to the least square fits of the experimental shifts.

a) The 1410 keV state 28

b) The 1611 and 2217 keV states 29

c) The 2488 and 2795 keV states 30

d) The 3171, 3185 and 3274 keV states 31

2.6 Direct γ-ray spectra from the ^{37}Cl(p,nγ)^{37}Ar reaction exhibiting Doppler-shifts of the γ rays originating from the 1611, 3185 and 3274 keV states. 37

3.1 A schematic diagram of the A(p,nγ)B* reaction. 40

3.2 Target arrangement for γ-ray angular distribution measurements. 50

FIGURE PAGE

3.3 The angular distribution of the 1410 keV transition to the ground state. 52

3.4 Energy levels and decay scheme of ^{37}Ar. 56

3.5 A γ-ray spectrum for the ^{37}Cl(p,nγ)^{37}Ar reaction observed with the Ge(Li) detector at 90° and E_p = 5.15 MeV. Energies of all the peaks are identified and the primes and double primes denote 1st and 2nd escape peaks respectively. 57

3.6 The angular distribution and χ^2 plot for the 1611 keV transition to the ground state. 64

3.7 Excitation function of the 1611 keV γ rays observed at θ = 90° for proton beam energies from 3.30 to 5.40 MeV. Arrows indicate energies at which the angular distributions were measured. 65

3.8 The angular distribution and χ^2 plot for the 2217 keV transition to the ground state. 68

3.9 The angular distribution and χ^2 plot for the 2488 keV transition to the ground state. 70

3.10 The angular distribution and χ^2 plot for the 2795 keV transition to the ground state. 71

3.11 The full energy peaks of the 3163 and 3171 keV γ rays of the ^{35}Cl and ^{37}Ar respectively. The dots are experimental points. The solid curves represent the Gaussian fits of the 3163 keV γ rays with linear backgrounds which were removed to give intensities of the 3171 keV γ rays. 73

3.12 The angular distribution and χ^2 plot for the 3171 keV transition to the ground state. The difference in the angular distribution errors is due to the uncertainties of fitting. 74

FIGURE PAGE

3.13 The angular distribution and χ^2 plot for the 1574 keV transition to the 1611 keV state. 75

3.14 The angular distribution and χ^2 plot for the 3274 keV transition to the ground state. 77

3.15 The angular distribution and χ^2 plot for the 1663 keV transition to the 1611 keV state. 78

4.1 A block diagram of the neutron time-of-flight electronics. 89

4.2 Neutron time-of-flight spectrum of the $^{37}Cl(p,n)^{37}Ar$ reaction observed with a flight path of 6.3 m at E_p = 5.90 MeV. A total charge of 50,000 μC was collected on the target. The neutron groups are indicated by their energies as determined from this experiment. 91

4.3 A detector efficiency vs neutron energy curve. 94

4.4 Differential cross sections of neutrons leading to states in the ^{37}Ar nucleus.

a) The ground state 98

b) The 1410 keV state 99

c) The 1611 keV state 100

d) The 2217 keV state 101

e) The 2488 keV state 102

f) The 2795 keV state 103

g) The 3274 keV state 104

5.1 The measured and calculated energy levels of ^{37}Ar. 115

6.1 The energy level scheme of ^{29}Si. 120

6.2 Observed Legendre polynomial coefficients vs energy for the 1273 and 2028 keV γ rays. 125

FIGURE PAGE

6.3 Legendre polynomial coefficients calculated with the modified SCN model. 129

6.4 Angular distribution coefficients obtained from averaging process.

a) Energy interval of 50 keV 131

b) Energy interval of 100 keV 132

c) Energy interval of 200 keV 133

d) Energy interval of 400 keV 134

6.5 Angular distribution coefficients obtained using the thick target. 135

6.6 Angular distribution of the 1273 and 2028 keV γ rays measured with the thick target. 137

6.7 χ^2 vs mixing ratio for the 1273 keV γ rays. 139

6.8 χ^2 vs mixing ratio for the 2028 keV γ rays. 140

CHAPTER 1

INTRODUCTION

Nuclei near doubly-closed shells are of considerable interest due to the relatively simple shell model configuration expected and because experimental data can be readily compared in detail with theoretical predictions. The ^{37}Ar nucleus which lacks a neutron and two protons from the 'magic' ^{40}Ca nucleus is of particular interest because its low-lying excited states extend into the next shell; hence states of both parities are observed. Its odd mass can also permit studies involving models of coupling a single particle to an even-even core.

In addition to its interest from a nuclear structure point of view, the ^{37}Ar nucleus also has astrophysical implications. It has been reported that the detection of solar neutrinos by the ^{37}Cl(ν_e,e$^-$)^{37}Ar reaction involves some excited states in ^{37}Ar (Ba 64, Da 68 and Ba 68). Thus knowledge of the low-lying levels could lead to better understanding of the solar energy generation process.

At the time when this experiment was initiated most of the experimental information on the ^{37}Ar nucleus had been obtained by charged particle spectroscopy (En 67 and Na 68). As a result, excitation energies contained

large uncertainties (±15 keV) and electromagnetic properties were incomplete; only the lifetime of the 1611 keV level had been reported (Go 67).

The present investigation was undertaken to provide a more complete experimental description of the low-lying states of ^{37}Ar. One of the intentions was to determine more precisely the energies of the excited states in order to separate perhaps previously unresolved states. The study of γ-ray deexcitation of these states could then lead to information of their decay modes, branching ratios and spins and parities (J^{π}). Also measurement of Doppler-shifted γ rays could yield mean lifetimes for the excited states as well as infer limits on their J^{π} values. Several different experimental observations, however, were necessary to obtain the desired information and these will be discussed separately.

The ^{37}Cl(p,n)^{37}Ar reaction ($Q = -1.596$ MeV) was chosen for this investigation for several reasons. The (p,n) reaction would populate all energetically allowed states and its negative Q-value would also permit one to excite only up to the levels of interest unlike the (d,p) reaction for example. Furthermore, experimental information on this reaction had been lacking; neutron emission threshold energies of the lowest four excited states in ^{37}Ar and the angular distribution of the ground state

neutron group had been the only observations reported (Fe 59 and Iy 66). Finally at low incident proton energies (<6 MeV) the (p,n) reaction would proceed mainly through the compound nuclear mechanism and experimental conditions could be suitably arranged to justify the statistical analysis. Such results are necessary for a comparison with those obtained using the direct interactions or model independent approaches to provide a better understanding of the SCN model.

The lifetimes of all the levels up to 3274 keV in ^{37}Ar have been studied using the Doppler shift attenuation method (DSAM). Enriched ^{37}Cl targets were bombarded by 5.70 MeV protons from the van de Graaff accelerator at the Nuclear Research Centre of the University of Alberta. The Doppler-shifted γ rays from the excited states were observed using a Ge(Li) detector at 0°, 90° and 120° with respect to the beam direction. The spectra were collected in singles and in coincidence with neutrons detected at 180 degrees by an annular detector. From the energy shifts of the detected γ rays, mean lifetimes could be determined according to the method of Warburton (Wa 67). The description of the experiment and results are contained in Chapter 2.

Chapter 3 reports the γ-ray yields and angular distributions measured with different target thickness and incident energies. The results were compared with

the statistical compound nuclear (SCN) model to predict the spins and parities of the level and to find multipole mixing ratios of their deexcitation γ rays; lifetime results were utilized to restrict some of these assignments. A comparison of the SCN model and model-independent analysis was also made for the 1611 keV level. Branching ratios were extracted from the zero-order term of the Legendre polynomial expansion of the angular distributions.

Since the reaction was assumed to proceed mainly through the compound nuclear (CN) process, it was of interest to measure the neutron angular distributions in search of symmetry around 90° in the center-of-mass system which is characteristic of the CN interaction (En 66). Neutron angular distributions also provided knowledge of the average ^{37}Ar recoil velocity which was helpful in our DSAM singles analysis. Of course, neutron spectra would also show which excited states are populated, thereby aiding the proper identification of the γ rays. This resulted in the confirmation (from the neutron spectrum) of the existence of a new level at 3185 keV which did not decay to the ground state. The time-of-flight technique was used to record the neutron spectra and is presented in Chapter 4.

The summary of the ^{37}Ar nucleus and comparison with Shell model calculations are contained in Chapter 5.

In the analysis, the SCN model and model-independent calculations have been compared. The agreement is good; however, it was felt that a more detailed investigation of the applicability of the SCN model was desirable. An extensive angular distribution study using the $^{29}Si(p,p'\gamma)^{29}Si$ reaction was therefore undertaken. The selection of this reaction and the result of the investigation are described in Chapter 6. Basically, the experiment consists of measuring γ-ray angular distributions with a thin target over a range of bombarding energies, in small energy increments. Hence variations of the angular distribution as a function of yield and target thickness may be studied to afford an insight into the statistical process.

During the course of this project several investigations on the ^{37}Ar nucleus have been published including part of this dissertation (Wo 72 and Appendix E). Inspite of the numerous lifetime determinations of the low-lying states, agreement has not been satisfactory. The level energies, decay modes and J^{π} assignments have, however, agreed more consistently. Detail comparison of these and present results will be made in the discussion of the respective subjects.

Several calculations within this study require modification of standard formula and computer codes to expedite calculations. A short description of these

together with published papers are presented in the Appendices.

Appendix A describes modification of the Doppler-shift attenuation factor to include both the direct (particle) and cascade (γ ray) feeding of the state. A program, 'MAGPOP', written for the model independent study of the 1611 keV level in the ^{37}Ar nucleus (Section 3.4.2), is presented in Appendix B. In Chapter 6, the procedure to simulate yields of thicker targets by summing and averaging yields from a thin target is described by the code, 'WAVY', in Appendix C.

A paper on the positive parity states in ^{40}K which introduced the author to (p,nγ) studies and the SCN model is contained in Appendix D. Finally, part of this dissertation which has been published is included in Appendix E and the listing of the code 'OXDS' (Ro 69) is given in Appendix F.

CHAPTER 2

MEAN LIFETIMES OF ^{37}Ar

2.1 Doppler Shift Attenuation Method

Electromagnetic transition strength is usually expressed in terms of mean lifetime, τ, for the emission of a γ ray of a particular multipolarity between a pair of nuclear energy levels or in terms of corresponding radiative width, Γ, according to the uncertainty principle, $\Gamma\tau = \hbar$. The measured strength of the transition can then give important clues as to the properties of the nuclear energy levels involved.

The Doppler shift attenuation method (DSAM) (Wa 67a) has been adopted in the present investigation to determine lifetimes of the ^{37}Ar levels. This method relies on the rapid slowing down of swiftly moving atoms in a solid. In short, γ rays emitted by an excited nucleus in motion will exhibit the familiar Doppler shift in energy. The average (centroid) energy of the γ rays emitted by recoiling nuclei of varying velocities is given by (Wa 63 and Ol 66)

$$E_{\gamma}(\theta) = E_{\gamma 0}[1 + F(\tau) \frac{v_o}{c} \cos \theta] \qquad (2.1)$$

where $E_{\gamma 0}$ specifies the γ-ray energy emitted by nuclei at rest and θ is the angle between the gamma emission and the bombarding direction. v_o is the average component of

the initial recoil velocity along this axis and c is the velocity of light. $F(\tau)$ is the Doppler-shift attenuation factor whose deviation from unity ($0 \leq F(\tau) \leq 1$) describes the effect on $E_\gamma(\theta)$ due to the slowing down process of the recoiling nuclei.

This attenuation factor may be obtained experimentally by observing the average γ-ray energies at two detection angles, θ_1 and θ_2. From the energy difference between these measurements one gets,

$$F(\tau) = \frac{E_\gamma(\theta_1) - E_\gamma(\theta_2)}{E_{\gamma 0}\,\frac{v_o}{c}\,(\cos\theta_1 - \cos\theta_2)} \quad . \qquad (2.2)$$

The denominator may be recognized as the maximum energy difference ($F(\tau) = 1$) and it can be calculated from reaction kinematics. Thus one rewrites Equation 2.2

$$F(\tau) = \frac{[E_\gamma(\theta_1) - E_\gamma(\theta_2)]_{\text{observed}}}{[E_\gamma(\theta_1) - E_\gamma(\theta_2)]_{\text{maximum}}} \quad . \qquad (2.3)$$

In the present experiment, $^{37}Cl(p,n)^{37}Ar$, the initial recoil velocity of the ^{37}Ar nuclei was restricted to the forward direction (in the same direction as the incident protons) by requiring the γ rays to be in coincidence with the neutrons detected in the backward direction. This requirement ensured maximum initial recoil velocity and hence maximum Doppler shift according to Equation 2.1. However, for the higher excited states

(which had low yields), γ-ray shifts were measured in singles only. The mean initial recoil velocity in this case was derived from the independently measured neutron angular distributions (Chapter 4) as well as from the method of Warburton (Wa 67). For the lower energy levels, the lifetimes have been obtained by both coincidence and singles methods.

The theoretical derivation of the attenuation factor, $F(\tau)$ has been described extensively (Wa 63, Bl 66, Ro 69 and Gu 70) and hence only a brief outline will be given here. The $F(\tau)$ that was given by Warburton et al (Wa 63) was modified by Blaugrund (Bl 66) to include the $\overline{\cos\,\phi(t)}$ term and can be written as

$$F(\tau) = \frac{1}{v_o\ \tau} \int_0^\infty v(t)\ \overline{\cos\,\phi(t)}\ e^{-t/\tau}\ dt \qquad (2.4)$$

where τ is the lifetime, v_o and $v(t)$ are the initial and instantaneous velocities respectively, $\phi(t)$ is the angle between v_o and $v(t)$ and $e^{-t/\tau}$ is the probability of decay. The term, $\overline{\cos\,\phi(t)}$, was introduced to account for the large angle scattering of the recoiling nucleus and can be calculated from multiple scattering consideration (Le 50).

$$\overline{\cos\,\phi} = \exp(-\int_0^x K_\phi\ dx) \qquad (2.5)$$

in which x is the distance travelled in the stopping medium and

$$K_{\phi} = N \int_{\phi} (1 - \cos \phi)\ d\sigma(\phi) \qquad (2.6)$$

where N represents the number of scatterers per cm^3 and $d\sigma(\phi)$ the differential scattering cross section of the recoil.

It has been shown (Po 61) that the velocity function v(t) in Equation 2.4 varies linearly with stopping power, $\frac{dE}{dx}$, of the stopping material for the recoiling nuclei and can be expressed in terms of it. The stopping power, however, may be divided into electronic and nuclear stopping components. The electronic process involves energy loss of the recoiling ion due to collision with electrons in the stopping material and the nuclear process involves collision with atoms in the stopping medium. According to Lindhard et al (Li 61 and Li 63)

$$\left(\frac{dE}{dx}\right)_{\text{electronic}} = k \left(\frac{E}{M}\right)^{1/2} \qquad \text{keV.cm}^2\text{/mg} \qquad (2.7)$$

where E is the energy of the moving ion, M is its mass and

$$k = \frac{73.0\ Z_1^{1/6}\ Z_1\ Z_2}{M_2 (Z_1^{2/3} + Z_2^{2/3})^{3/2}} \qquad \text{for} \quad v \leq \frac{e^2}{\hbar} Z_1^{2/3} = \frac{1}{137} C Z_1^{2/3} \qquad (2.8)$$

where Z and M are the charge and mass and the subscripts, 1 and 2, denote the moving ion and the stopping material respectively.

In similar notation, the nuclear stopping is given by

$$\left(\frac{dE}{dx}\right)_{\text{nuclear}} = N\ B_n\ \ln \left[\frac{2\,E\,M_2\,\hbar^2}{(M_1+M_2)\ Z_1\ Z_2\ e^4\,(Z_1^{2/3}+Z_2^{2/3})^{1/2}}\right] \qquad (2.9)$$

where

$$B_n = \frac{2\,\pi\,Z_1^2\ Z_2^2\ M_1\ e^4}{M_2\ E} \quad .$$

The total stopping power is simply the sum of Equations 2.7 and 2.9. Calculations of the theoretical F(τ) from the total stopping power were performed using a computer code 'OXDS' (Ro 69 and Appendix F). The program has provision to vary the electronic and nuclear contributions to the stopping power. Thus mean lifetimes may be obtained from comparison of the observed attenuation factor and the theoretical F(τ) vs τ curves.

2.2 Experimental Details

Lifetimes of the low-lying levels in ^{37}Ar below 3.274 Mev excitation have been determined by the Doppler-shift attenuation method. These levels were populated via the ^{37}Cl(p,nγ)^{37}Ar reaction using a 5.70 MeV proton beam. The target consisted of 0.5 mg/cm^2 of PbCl$_2$ (enriched to 87% in ^{37}Cl) evaporated onto a 0.5 mm thick Au backing. Gamma rays were detected both in coincidence with neutrons and in singles using a 45 cm^3 Ge(Li) γ-ray

detector placed 10 cm from the target at 0°, 90° and 120° with respect to the incident beam direction. The detector provided a resolution of 4 keV at 1.33 MeV under experimental conditions. Neutrons were detected in a 5.1 cm thick annular (17.8 cm O.D., 25 cm I.D.) NE 218 liquid scintillation counter which subtended angles between 157° and 177° to the beam direction. It was placed 15.8 cm from the target (Figure 2.1). The γ flux in the neutron detector was suppressed by a 1.95 cm thick lead shield.

In order to detect only the γ rays emitted by the excited states of ^{37}Ar, stringent neutron coincidence restrictions were imposed on the Ge(Li) signals. These requirements consisted of distinguishing neutrons and γ rays arriving at the neutron detector by their time-of-flight separation and also by their rise time differences in the detector. A detailed description of the n-γ discrimination and all electronic circuitry will follow after a brief outline of the general experimental arrangement.

Gamma-gamma coincidence between the Ge(Li) detector and a 7.5 cm × 7.5 cm NaI (Tl) γ-ray detector was also arranged. This allowed γ rays from known sources placed nearby to be recorded simultaneously during the experiment to serve as internal calibration lines as well as a continuous monitor of the system stability.

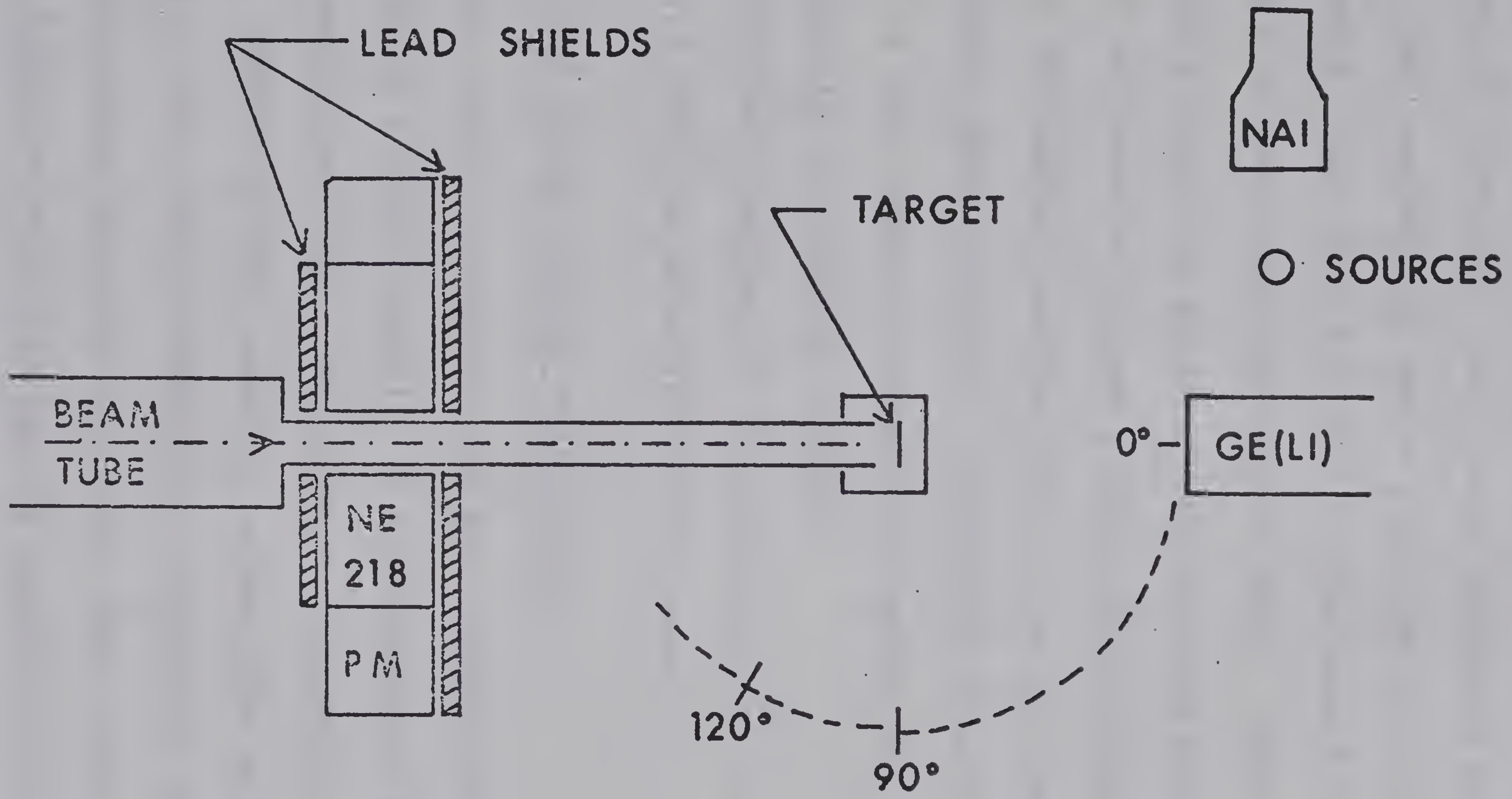

Figure 2.1 Experimental arrangement of target and detectors

The n-γ and γ-γ coincidence signals were accumulated in parallel and added so that a single analog-to-digital converter (ADC) was used. The advantage of using one ADC for all the γ rays detected by the Ge(Li) whether they satisfied the n-γ or the γ-γ coincidence requirement, was that all the γ rays would then be subjected to the same conversion gain. Thus the known γ-ray peaks from the sources may be used directly as internal calibration lines without gain correction arising from the use of another ADC. The n-γ and γ-γ coincidences were, however, separated into different regions of the computer memory by using the γ-γ coincidence signals as routing pulses.

A block diagram of the electronics is shown in Figure 2.2 and its description follows.

Neutron and γ-ray timing coincidence

The Ge(Li) detector has two output signals; an energy and a timing signal. A combination of timing filter amplifier (TFA) and constant fraction pulse height trigger (CFPHT 1) were used to obtain the starting time signal for the time-to-amplitude converter (TAC 1). The stop pulses were obtained from the fast output of the neutron detector with the use of another (CFPHT 2). Two gate and delay generators (G&D 1 and 2) were employed to sychronize the start and stop signals so that they fall

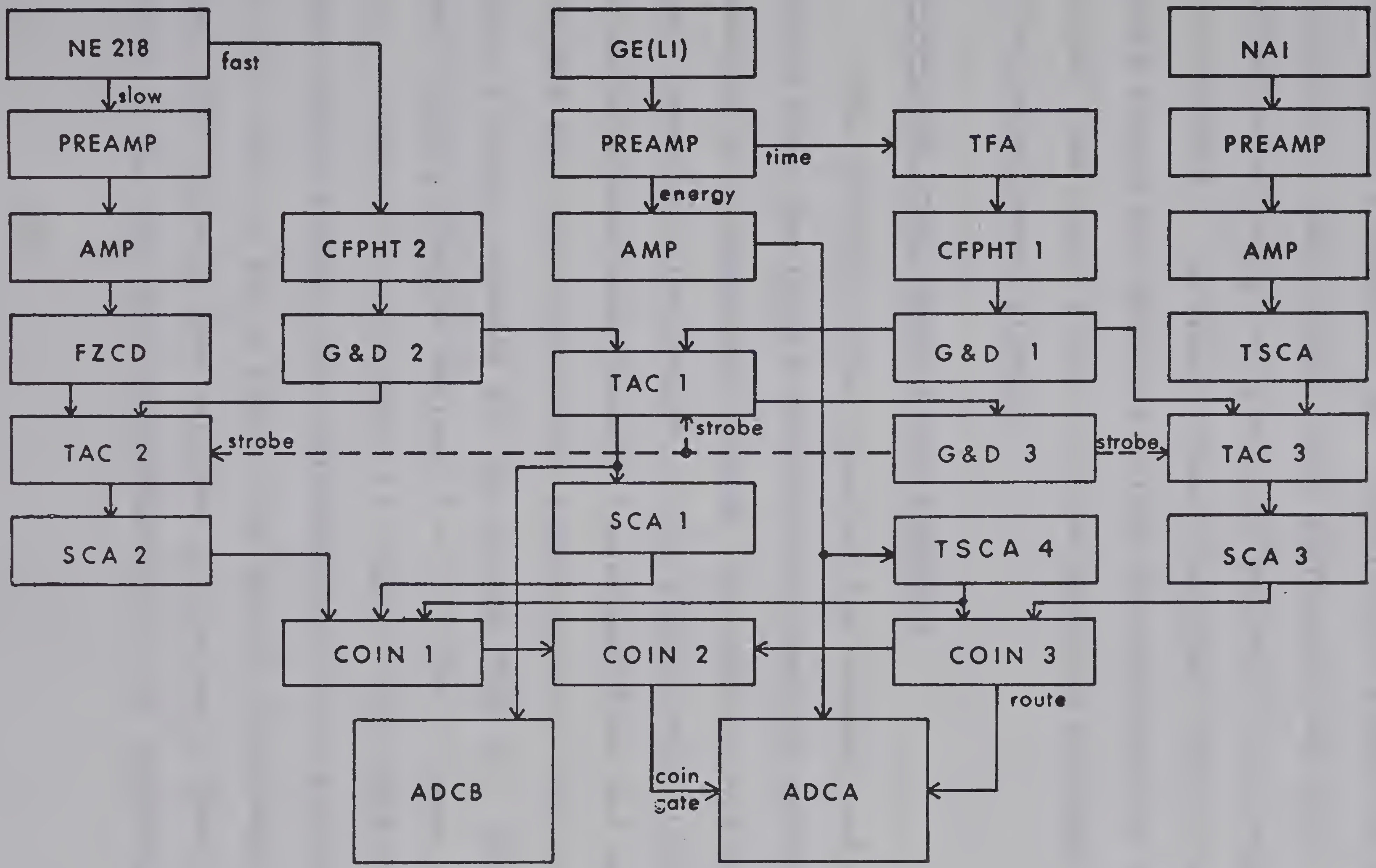

Figure 2.2 Block diagram of electrons

[illegible]

within the time range (50 ns) of the (TAC 1). The different velocities between the neutrons and the γ rays caused their arrival at the liquid scintillator to be separated by their flight time difference and this yielded essentially two groups of pulses at the output of the (TAC 1). A single channel analyzer (SCA 1) window placed around the group of pulses corresponding to the neutron time peak of the n-γ time spectrum provided one of the coincidence signals.

Neutron and γ-ray shape discrimination

The different rise times of the neutron and γ-ray signals from the liquid scintillator provided another method of discriminating between the neutrons and the γ rays. From the slow output of the liquid scintillator, the signals were sent through a pre-amplifier and amplifier and fast zero cross-over discriminator (FZCD) to obtain starting signals for the second (TAC 2). The same stopping signals derived for the (TAC 1) were used to stop (TAC 2). The output of (TAC 2) consisted of two pulse height groups; one corresponding to the neutrons and the other to the γ rays. The second coincidence signal for (COIN 1) was obtained by placing a (SCA 2) window around the peak corresponding to the neutrons.

Gamma-gamma coincidence

To record simultaneously known γ-ray lines from the sources and to use them as internal calibration lines, a γ-γ coincidence arrangement was employed using a NaI(Tl) crystal as a second γ-ray detector. The two γ-ray sources ^{88}Y and ^{60}Co, placed between the two γ-ray detectors provided calibration lines at 898, 1836, 1173, and 1332 keV. The NaI(Tl) detector was mounted with the Ge(Li) detector, 8 cm directly above it. A third (TAC 3) was used to generate a coincidence time peak between the signals of these two detectors and it was triggered by the same starting pulses that triggered (TAC 1). The timing signals extracted from the NaI crystal through a pre-amplifier, amplifier and timing single channel analyzer (TSCA) system provided the stopping pulses. Once again the coincidence signals were derived by placing a (SCA 3) window around the time peak.

Coincidence requirements

It was essential that all coincidence signals arrived at the universal coincidence (COIN 1 and 3) at the same time. This was accomplished by using the true start signals from (TAC 1) and (G&D 3) to strobe all the (TAC'S). The linear signals from the Ge(Li) detector were self-gated (TSCA 4) in order to eliminate low energy part of the spectrum and they provided additional coincidence signals for (COIN 1 and 3). Thus a triple

coincidence between the linear, n-γ time and n-γ shape signals was required for each n-γ event accepted by the (COIN 1). The linear and γ-γ time signals constituted the coincidence requirement for the γ-γ events accepted by the (COIN 3). The outputs of both (COIN 1 and 3) were sent to another (COIN 2) whose output was used to gate the analog-to-digital converter (ADCA). This caused the (ADCA) to accept the n-γ and γ-γ events. The output of (COIN 3) was also used for routing the γ-γ events into a separate region of the computer memory.

The ungated n-γ time spectra were obtained from the output of the (TAC 1) and accumulated during all runs in a second analog-to-digital converter (ADCB). Both (ADC'S) were interfaced to a Honeywell 516 on-line computer.

2.3 Analysis

The centroids of all γ-ray peaks of interest were carefully calculated and checked. Each spectrum was then calibrated using the centroid positions of the known γ rays from the ^{60}Co (1173 and 1332 keV) and ^{88}Y (898 and 1836 keV) sources. Since our known γ rays were available, the coefficients, a_ν, of calibration were determined by polynomial fits to the equation,

$$E_\gamma = \sum_{\nu=0}^{2} a_\nu x^\nu \qquad (2.10)$$

where E_γ is the energy of the γ ray and x is the channel number. There were no significant deviations from the linear relationship, $E_\gamma = a_o + a_1 x$ for all spectra. Nevertheless, to ensure that the calibrations were indeed linear even at the high energy region (>1836 keV), the channel-separations of first, second and full energy peaks of all identified high energy γ rays were checked and found to be consistent. Hence the calibrations were extended to the regions outside the calibration lines.

Having determined the average Doppler shifted energies of all the γ rays concerned, the experimental attenuations were calculated according to Equation 2.1

$$E_\gamma = E_{\gamma 0} \ (1 + F(\tau) \ \frac{v_o}{c} \cos \theta) \quad . \tag{2.1}$$

This equation has the same form as the first order Legendre polynomial expansion

$$\sum_{k=0}^{1} A_k \ P_k \ (\cos \theta) = A_o \ (1 + \frac{A_1}{A_o} \cos \theta) \tag{2.11}$$

where A_k are the coefficients and P_k (cos θ) are the Legendre polynomials. Hence the average γ-ray energies, E_γ, were least square fitted to the first order polynomial series and the experimental attenuations were determined from the ratios of the coefficients, A_1/A_o, once the v_o was specified.

The mean initial recoil velocity, v_o, was determined from kinematics, after the energy loss of the

incident beam through the target was taken into account (i.e., incident beam energy was taken at center of target). For the n-γ coincidence runs, the finite angle of the neutron detector was also taken into account by using the mean angle subtended by the neutron detector. For the singles experiment, the mean initial recoil velocities, $\bar{v}_o$, were determined from the formula (Wa 63):

$$\bar{v}_o = v_{cm} \frac{\int_{-1}^{+1} (1 + \epsilon^{-1} \cos \theta_{cm}) \sigma(\theta_{cm}) \, d \cos \theta_{cm}}{\int_{-1}^{1} \sigma(\theta_{cm}) \, d \cos \theta_{cm}} \qquad (2.12)$$

in which

v_{cm} ≡ velocity of the center-of-mass in the laboratory system

ϵ ≡ ratio of velocity of the center-of-mass in the laboratory system to the velocity of the recoiling nuclei in the center-of-mass system

θ_{cm} ≡ the angle of the outgoing particles (i.e. neutrons) in the center-of-mass system

$\sigma(\theta_{cm})$ ≡ differential cross section of the neutrons in the center-of-mass system.

The neutron differential cross sections were independently measured for levels up to 3274 keV excitation using time-of-flight technique (Chapter 4).

At a bombarding energy of 5.70 MeV, the $^{37}Cl(p,n)^{37}Ar$ reaction is assumed to proceed predominantly through the compound nucleus mechanism. The neutron differential cross section in the center-of-mass system will therefore exhibit symmetry about 90° (Section 4.1). This symmetry property applied to Equation 2.12 leads to the result that $\bar{v}_o = v_{cm}$. In other words, a symmetric angular distribution has the same influence on the average initial recoil velocity as an isotropic angular distribution. The average initial recoil velocities determined by the two methods (i.e. by weighting with the neutron differential cross section or by a straight average) agreed to within one per cent.

The expected $F(\tau)$ vs τ curves were calculated using the computer code, OXDS, (Ro 69) which used the formulae of Lindhard (Li 61 and Li 63) to calculate electronic and nuclear stopping. Large angle scattering was also taken into account. A typical plot of the $F(\tau)$ vs τ curves is shown in Figure 2.3.

Since the target was not infinitely thick, some of the recoiling ions would escape and stop in the Au backing. In such cases the attenuation factor, $F(\tau)$, was adjusted for the effect of the recoil stopping in the Au backing. The target was considered to be divided into N layers such that the attenuation factor for the ith layer may be written as

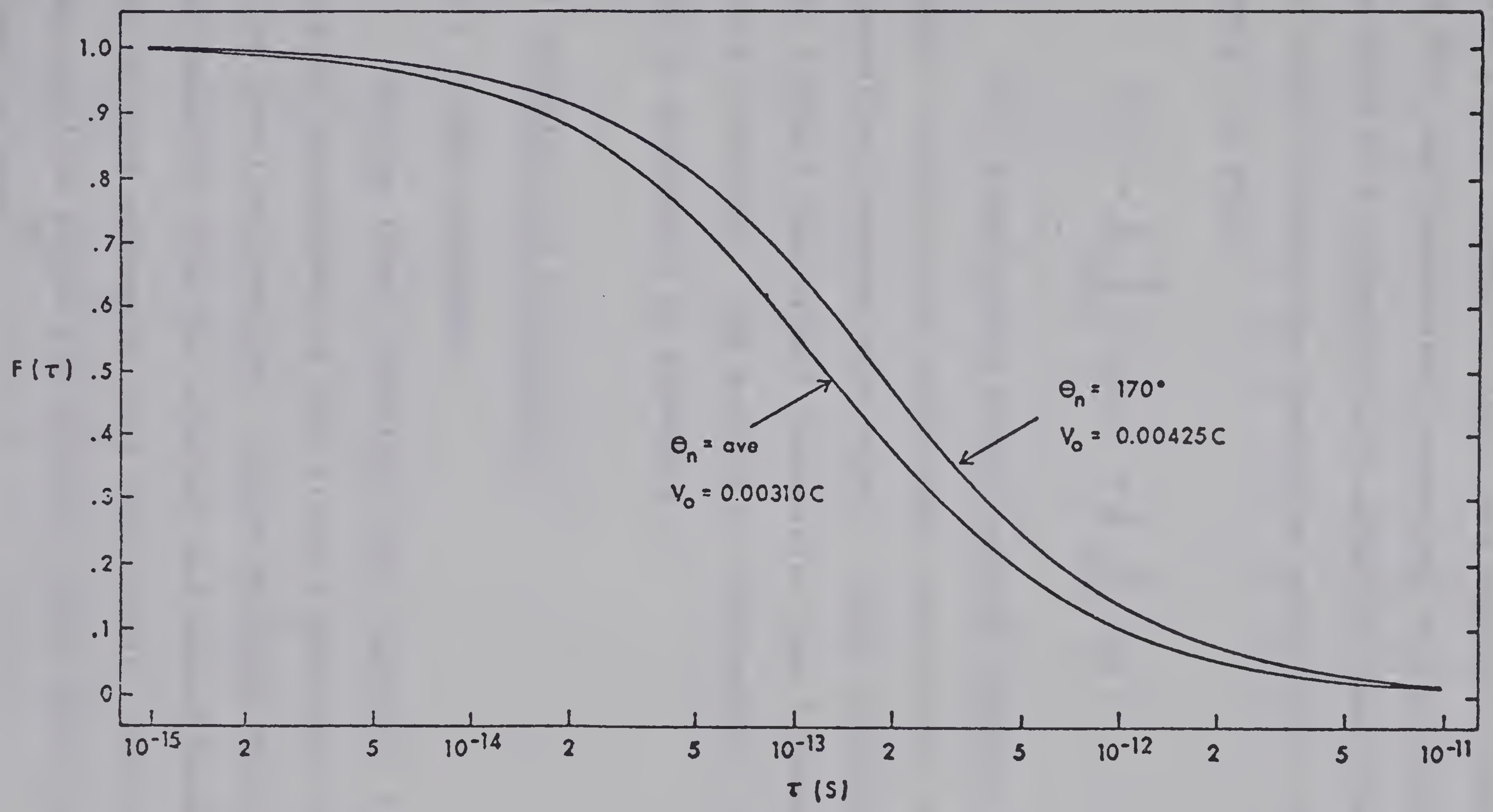

Figure 2.3 F(τ) vs τ curves for the 2795 keV level. θ_n is the angle of the outgoing neutron and v_o is the initial recoil velocity. The two curves represent the coincidence ($\theta_n = 170°$) and the singles (θ_n = ave) cases.

$$F_i(\tau) = F_{1i}(\tau) + F_{2i}(\tau) \qquad (2.13)$$

where 1 and 2 denote target and backing respectively and they are calculated according to Equation 2.4 with the limits of integration bounded by the thickness of the layer. Hence the composite attenuation factor is simply the sum:

$$F(\tau) = \frac{1}{N}\sum_{i=1}^{N} F_{1i}(\tau) + \frac{1}{N}\sum_{i=1}^{N} F_{2i}(\tau) \ . \qquad (2.14)$$

For some levels where cascade feeding from higher energy levels occurs additional corrections to the attenuation factors were made. These corrections took into account the direct population and lifetimes of the levels involved. The method of determining the correction is presented in Appendix A.

2.4 Results and Discussion

2.4.1 Level energies

Energy level positions were inferred from γ-ray energies determined by the fitting procedure described in the previous section. These energies were determined independently from the singles and coincidence data and were in good agreement with each other. The results are summarized in Table 2.1 together with other available determinations.

Table 2.1

Summary of Levels of ^{37}Ar

Champlin et al (Ch 71)	Ivascu et al (Iv 71)	Ragan et al (Ra 71)	Taras (Ta 71)	Caraca et al (Ca 71)	Luketina et al (Lu 72)	Present Result
1408.8±1.5	1408.9±1.3	1410±1	1409.7±0.4	1409.0±0.6	1409.8±0.1	1409.8±0.5
1611.2±0.8	1611.3±1.2	1611±1	1611.5±0.4	1610.7±1.0	1611.3±0.1	1611.3±0.5
2218.2±1.5	2219.8±1.5	2217±1		2216.4±1.5	2217.1±0.4	2216.6±0.9
2490.6±1.3	2491.2±1.5	2489±1		2489.0±1.0	2490.0±0.4	2488.0±0.8
2796.3±1.8	2799 ± 2	2796±2		2795.1±1.3	2795.5±0.6	2794.6±1.4
3171.3±1.7	3168 ± 2			3171 ± 3	3169.7±0.8	3171.0±2.0
3186.4±1.7	3189 ± 2			3184 ± 3	3184.9±1.0	3185.1±1.5
3273.4±1.6	3270 ± 3			3272 ± 3	3271.7±1.0	3273.6±1.5

The presence of the 1574 keV γ ray in both the singles and coincidence data indicates that it originated from a state in the ^{37}Ar. Its energy, however, did not fit into the decay scheme known at that time. From the yield curve study, its threshold corresponded closely to the level at 3.17 MeV but a 14 keV discrepancy would then exist if it were indeed the 3.17 → 1.611 MeV transition. It was, therefore, postulated that the 3.17 MeV level was a doublet of 3171 and 3185 keV where the former would decay by the ground state transition and the latter would decay 100% to the 1611 keV level. To obtain direct confirmation of the presence of the proposed 3185 keV level, a neutron time-of-flight spectrum was accumulated at an incident proton energy of 5.90 MeV. The experimental set-up which is described in Chapter 4 was arranged to provide optimum conditions for the separation of the doublet. A neutron group corresponding to the proposed level is indeed present in the time-of-flight spectrum (Figure 4.2) giving direct confirmation of the 3185 keV level.

The 3185 keV level has since been inferred by other γ-ray experiments (Table 2.1) but to date no other direct confirmation by particle identification has been reported.

The present energy level determinations are in agreement (within experimental uncertainties) with other

results with the exception of those of Ivascu et al (Iv 71). This discrepancy may be attributed to the low yield of the coincidence experiment using the (^{3}He,p) reaction.

2.4.2 Lifetimes

The liftimes of levels up to an excitation of 2795 keV were investigated using the coincidence technique and up to an excitation of 3274 keV using the singles technique. A typical γ-ray spectrum in coincidence with neutrons is shown in Figure 2.4. Gamma-ray energy shifts corresponding to θ between 0° and 120° for all the levels whose lifetimes were measured are presented in Figure 2.5. The corrected attenuation factors and inferred lifetimes for both the coincidence and singles experiments are presented in Table 2.2. A summary of all published lifetimes are compared to the present results in Table 2.3.

The 1410 keV level The 1410 keV level was partially populated (∿20%) by cascade decays from the 3517 keV level (Iv 71). The attenuation factors and lifetimes listed in Table 2.2 have been corrected for this effect and they also include a 10% correction due to recoils decaying in the target backing. The final lifetime, $\tau = 943^{+170}_{-100}$ fs, is in good agreement with the result of

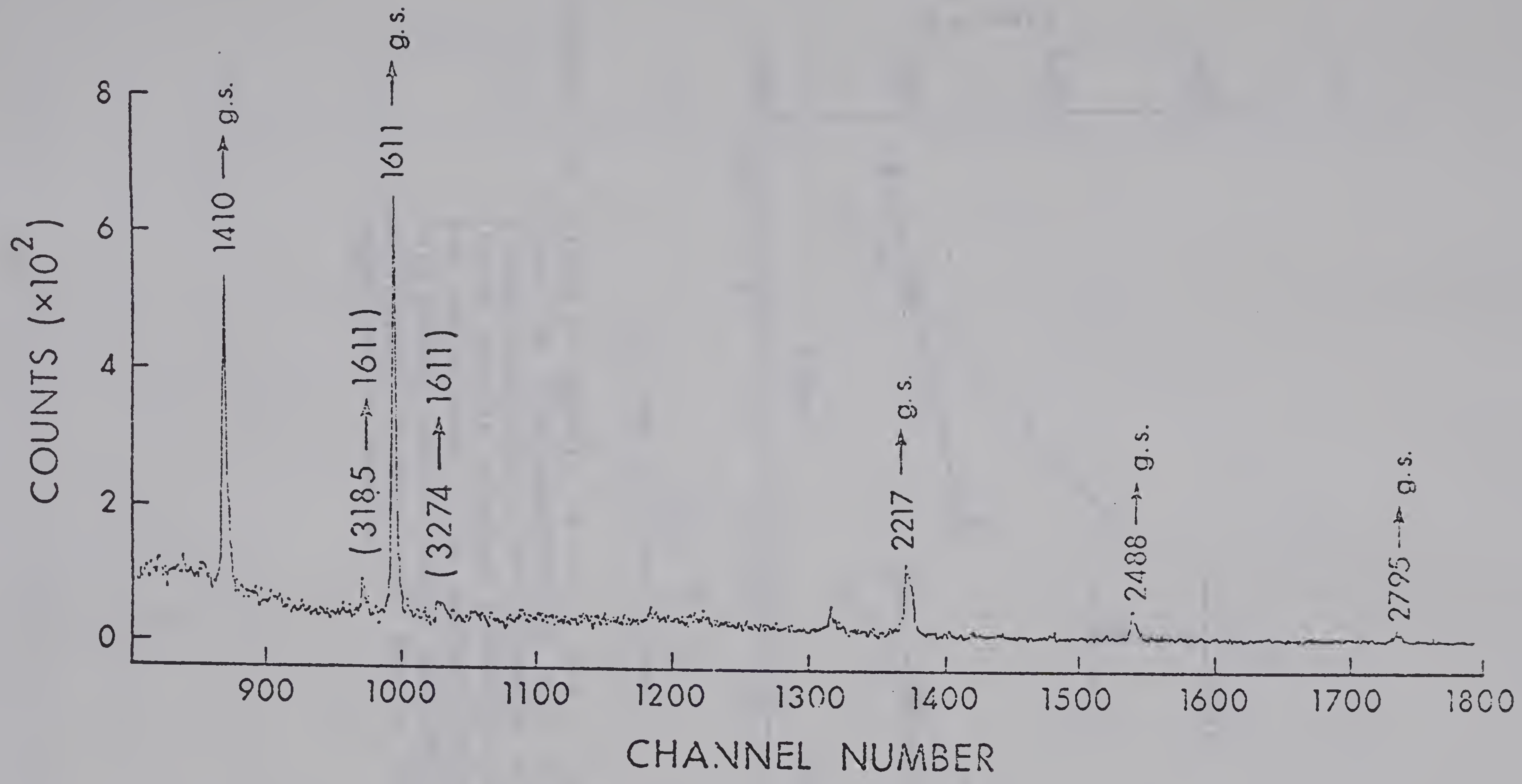

Figure 2.4 A typical γ-ray spectrum observed in coincidence with neutrons from the ^{37}Cl(p,nγ)^{37}Ar reaction at E_p = 5.70 MeV. The γ rays were detected at θ_γ = 0° with the annular neutron detector at 180° to the beam direction.

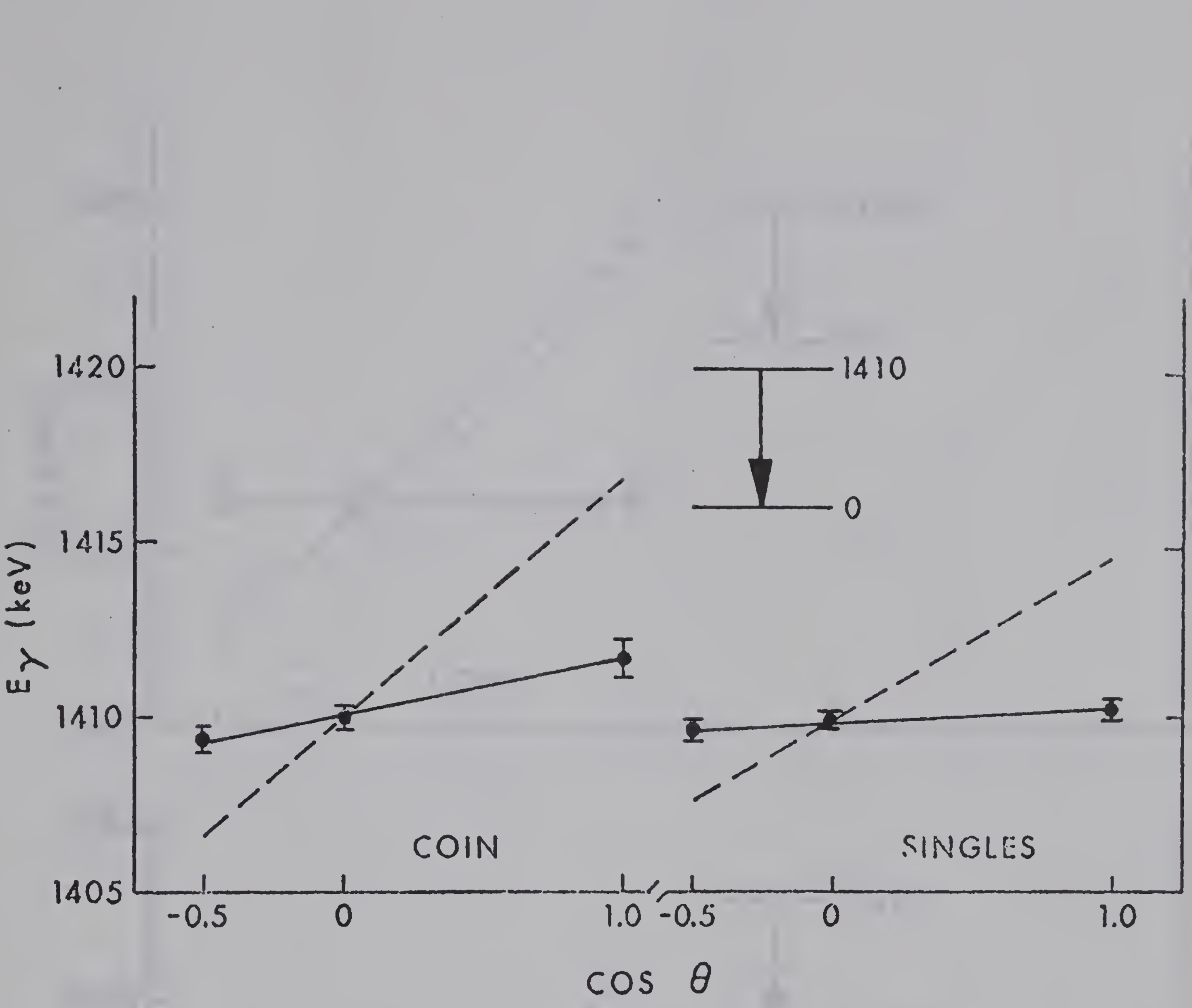

a) the 1410 keV state

Figure 2.5 Plots of energy vs cos θ for γ-ray transitions in ^{37}Ar observed at $E_p = 5.70$ MeV. γ rays detected in coincidence with neutrons (COIN) and in singles (SINGLES) are shown for comparison. The dashed lines represent full energy shifts while the solid lines correspond to the least square fits of the experimental shifts.

[illegible]

[illegible]

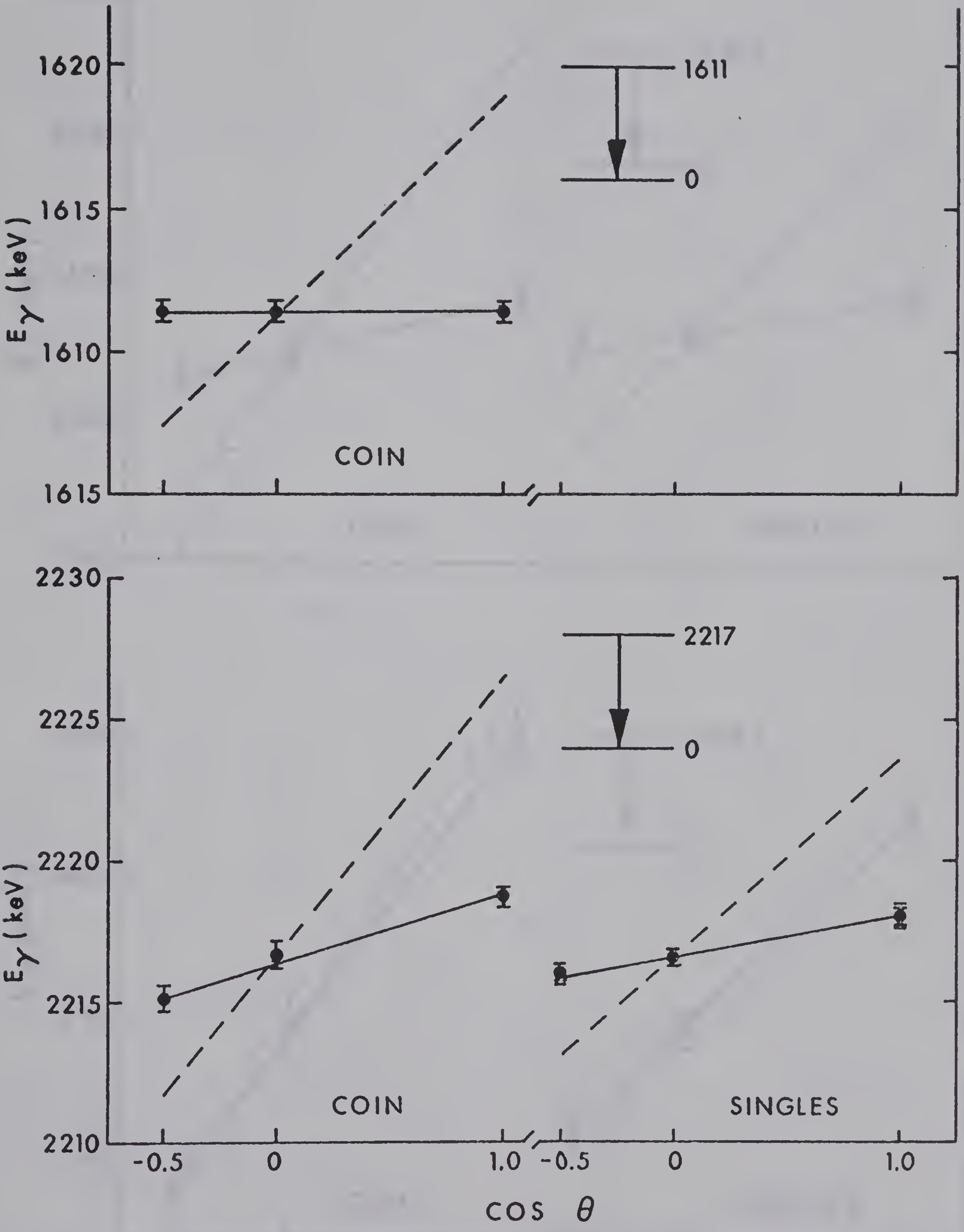

Figure 2.5 b) The 1611 and 2217 keV states

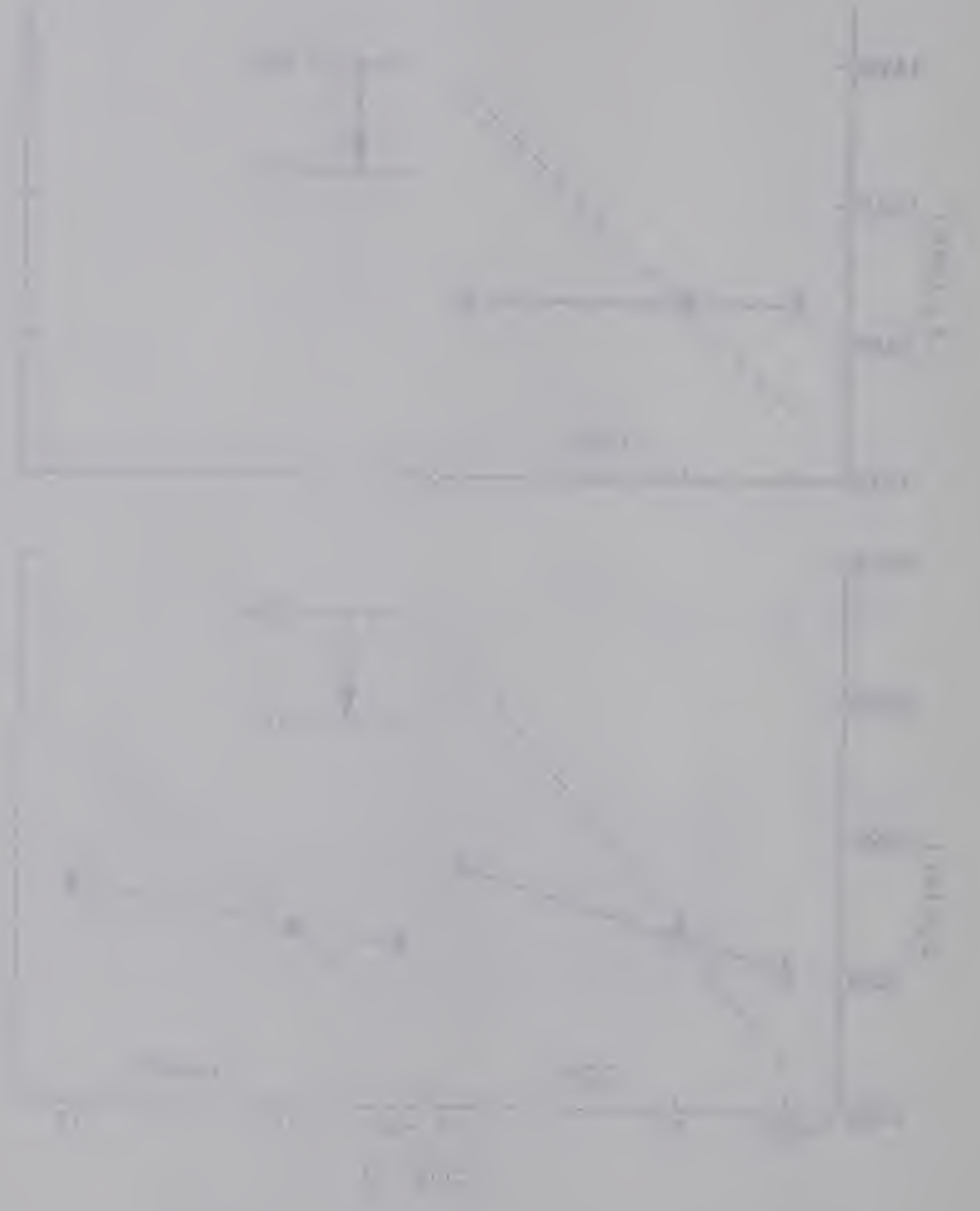

[illegible]

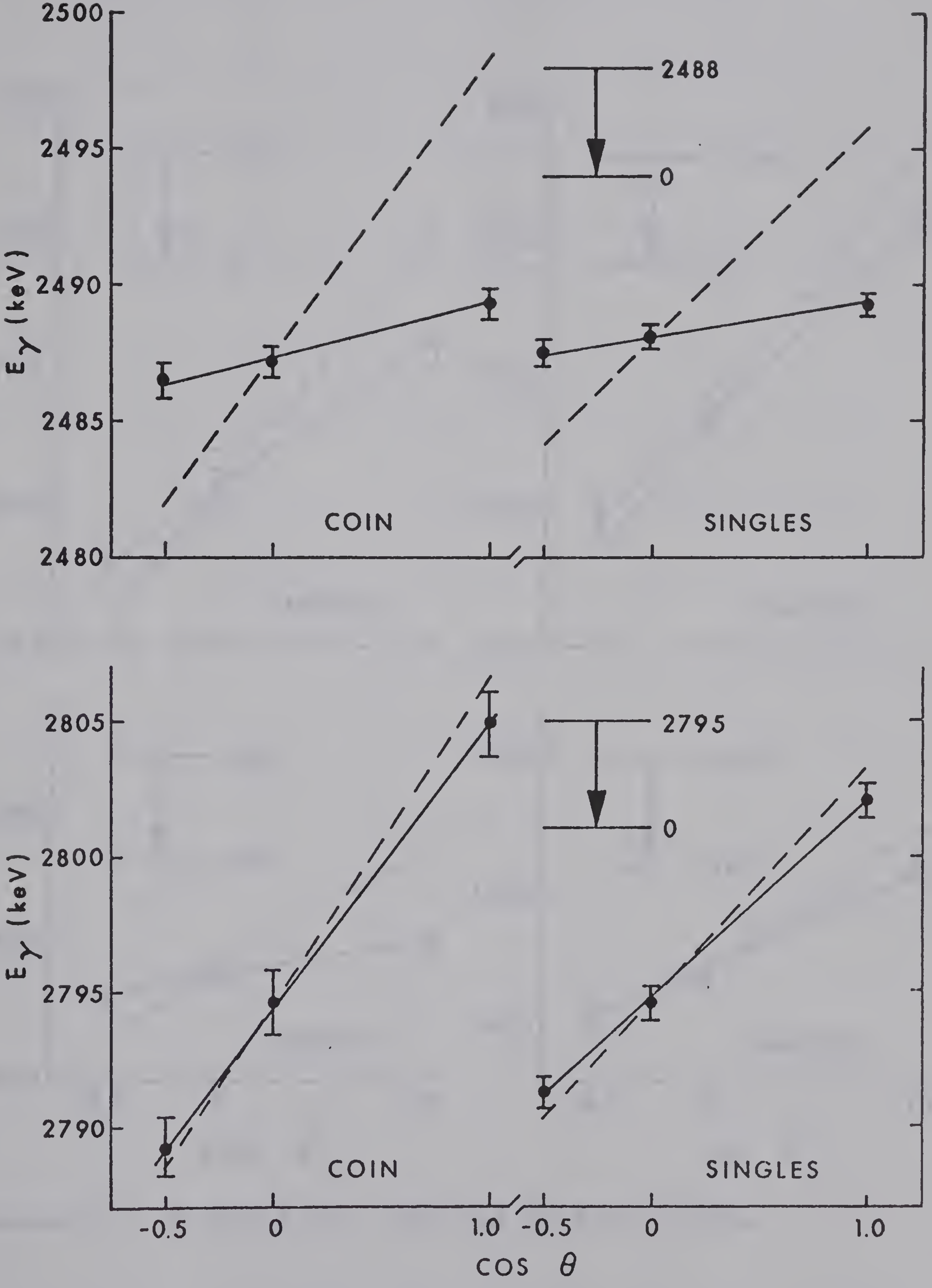

Figure 2.5 c) The 2488 and 2795 keV states

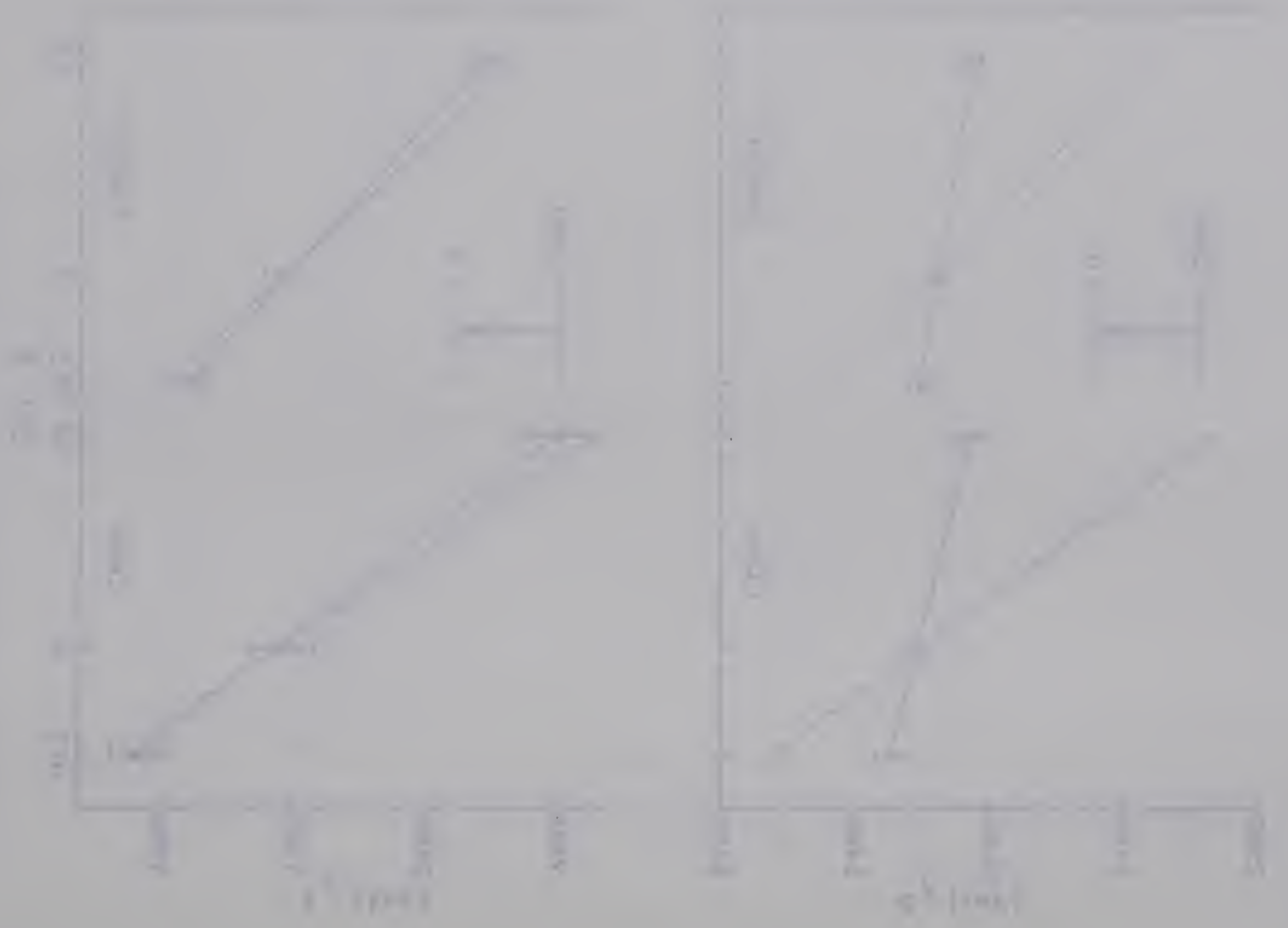

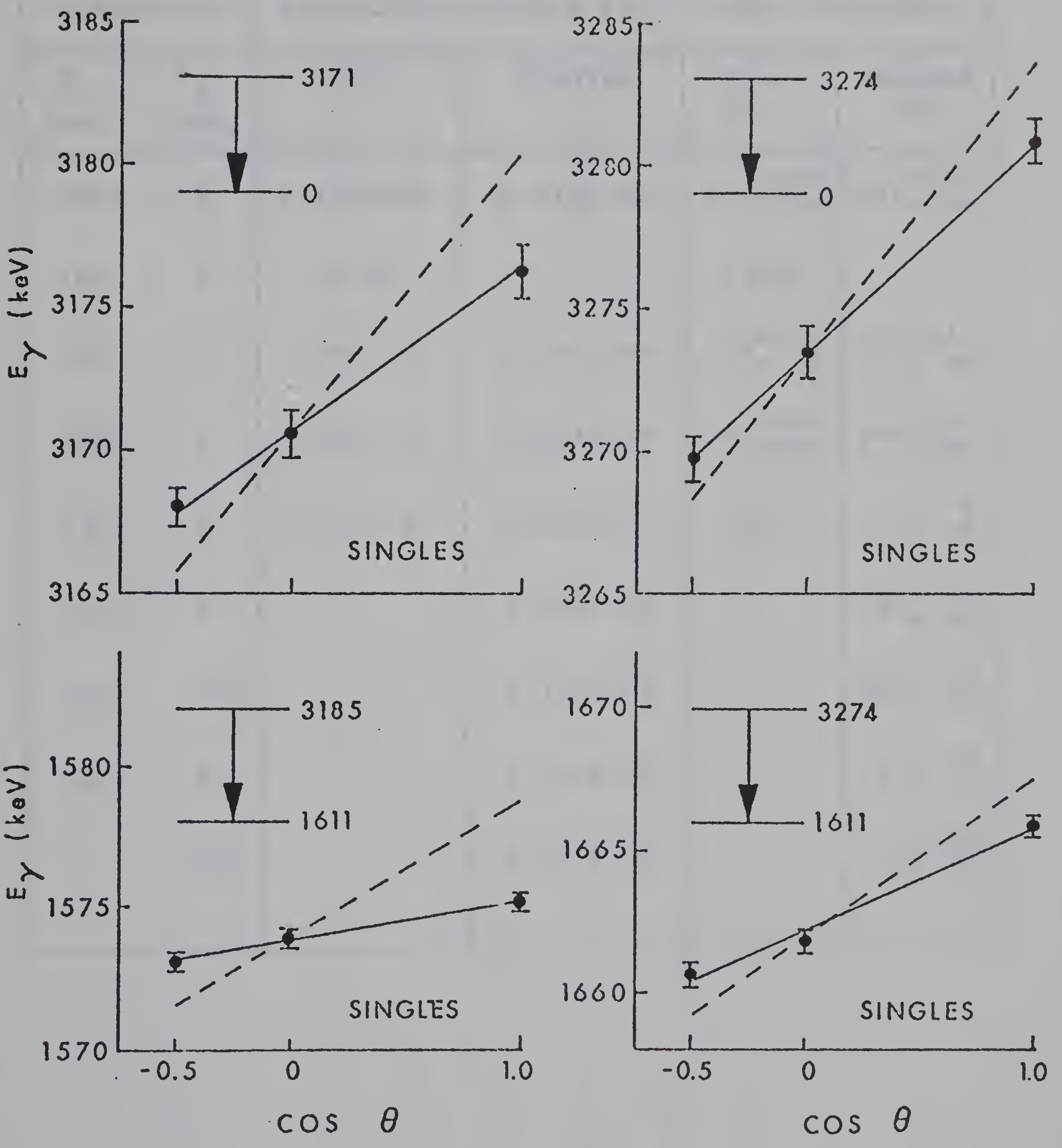

Figure 2.5 d) The 3171, 3185 and 3274 keV states

Table 2.2

Attenuation Factors and Lifetimes of ^{37}Ar

Transition		Attenuation Factor F(τ)		Mean Lifetimes	
E_i (keV)	E_f (keV)	Coin	Singles	Coin (fs)	Singles (fs)
1410	0	0.17±0.02	0.11±0.02	945^{+200}_{-120}	940^{+300}_{-160}
1611	0	<0.05		>3000	
2217	0	0.26±0.03	0.20±0.04	520^{+100}_{-80}	500^{+110}_{-80}
2488	0	0.19±0.05	0.16±0.04	700^{+460}_{-260}	640^{+300}_{-200}
2795	0	0.91±0.07	0.88±0.12	22^{+21}_{-17}	21^{+26}_{-18}
3171	0		0.61±0.11		85^{+40}_{-30}
3185	1611		0.31±0.05		285^{+70}_{-55}
3274	0		0.75±0.12		47^{+29}_{-25}
	1611		0.72±0.10		52^{+29}_{-21}

Table 2.3

Summary of Lifetimes in ^{37}Ar

Ex (keV)	MEAN LIFETIMES τ (fs)						
	Ivascu et al (Iv 71)	Ragan et al (Ra 71)	Caraca et al (Ca 71)	Luketina et al (Lu 72)	Kruzek et al (Kr 73)	Present Experiment	Endt and Van der Leun (En 73)
1410	650±350	1080^{+170}_{-130}	370^{+190}_{-110}	1220±150	620±185	943^{+170}_{-100}	980±110
1611	>10,000			>10,000		>3000	$(6.3\pm0.2)\times10^6$
2217	600±180	380±50		910±180	540±145	510^{+75}_{-60}	520±70
2488	400±130	775^{+105}_{-89}	88±24	1040±190	755±170	660^{+250}_{-160}	700±90
2795	<25	14±11	<8	<40	23±8	22^{+16}_{-12}	30±7
3171	30±15			100±20	81±15	85^{+40}_{-30}	70±20
3185	950±450			300±60	310±80	285^{+70}_{-55}	300±40
3274	45±30			60±20	38±15	50^{+21}_{-16}	50±10

$\tau = 1080^{+170}_{-130}$ fs obtained by Ragan et al (Ra 71). However, agreement with other lifetime determinations using similar (p,n) reaction varies from fair (Lu 72 and Kr 73) to very poor (Ca 71).

The 2217 keV level The lifetimes of the 2217 level obtained by the singles and coincidence methods show good agreement and the average value, $\tau = 510^{+75}_{-60}$ fs, is also in good agreement with the results of $\tau = 600 \pm 180$ fs and $\tau = 540 \pm 145$ fs determined by Ivascu et al (Iv 71) and Kruzek et al (Kr 73) respectively. Fair agreement is achieved in comparison with the value, $\tau = 380 \pm 50$ fs, obtained by Ragan et al (Ra 71). In the latter work, the analysis of the 2217 → g.s. transition was complicated by the presence of a 2232 keV γ ray due to the first excited state in ^{32}S which may account for the discrepancy between the values. The lifetime, $\tau = 910 \pm 180$ fs, reported by Luketina et al (Lu 72) is, however, considerably longer than that of all other determinations.

The 2488 keV level The attenuation factor for the 2488 → g.s. transition was modified to account for recoils decaying in the target backing and it amounted to a correction of about 10% in the lifetime. The resulting lifetime, $\tau = 660^{+250}_{-160}$ fs is in agreement with the lifetimes of 775^{+105}_{-89} fs and 755 ± 170 fs determined by Ragan et al (Ra 71) and Kruzek et al (Kr 73) respectively.

Fair agreement is obtained in comparison with $\tau = 400\pm130$ fs of Ivascu et al (Iv 71). The other lifetimes reported by Caraca et al (Ca 71) and Luketina et al (Lu 72) of $\tau = 88\pm24$ fs and $\tau = 1040\pm190$ fs respectively, are in very poor agreement with the present determination.

The 2795 keV level The 2795 keV level has the shortest observed lifetime in ^{37}Ar. Our value of $\tau = 22^{+16}_{-12}$ fs, extracted from the average of the singles and coincidence measurements of 21 and 23 fs respectively, has been corrected for cascade feeding from the 3274 keV level. The branching ratio presented by Ivascu et al (Iv 71) was used. In general, all reported lifetimes are in good agreement.

The 3171 keV level The 100% ground state transition of the 3171 keV level was weakly excited in the coincidence spectra and hence its lifetime was determined from the singles spectra only. Separation of the 3163 keV γ rays from the ^{35}Cl(p,p'γ)^{35}Cl reaction was necessary and resulted in a slight increase in the errors of the lifetime, $\tau = 85^{+40}_{-30}$ fs, which is in good agreement with $\tau = 100\pm20$ fs and $\tau = 81\pm15$ fs of Luketina et al (Lu 72) and Kruzek et al (Kr 73) respectively; both of these determinations have used the (p,n) reaction. The only other reported lifetime for this level is that by Ivascu et al (Iv 71) of $\tau = 30\pm15$ fs which is in considerable

discrepancy with the present measurement.

The 3185 keV level A spectrum of the 3185 → 1611 keV transition accumulated at the three angles is shown in Figure 2.6 together with the neighboring 1611 → g.s. and 3274 → 1611 keV transitions. The resulting lifetime of $\tau = 285^{+70}_{-50}$ fs is in excellent agreement with $\tau = 300 \pm 60$ fs and 310±80 fs reported by Luketina et al (Lu 72) and Kruzek et al (Kr 73) respectively. The lifetime, $\tau =$ 950±450 fs, inferred by Ivascu et al (Iv 71) is more than three times longer than the present value and this disagreement may again be attributed to the low experimental yield that was mentioned in Section 2.4.1.

The 3274 keV level The 3274 → g.s. and 3274 → 1611 keV transition yielded lifetimes of $\tau = 47^{+29}_{-25}$ fs and 52^{+29}_{-21} fs respectively for the 3274 keV level. Our adopted lifetime, $\tau = 50^{+21}_{-16}$ fs, is in excellent agreement with all other reported values.

An overall comparison of the several measurements of the lifetimes of ^{37}Ar by DSAM shows large variation for the levels below and including the 2488 keV level. An explanation of this variation in the mean lifetimes may be due to the fact that for different experiments, the recoiling nuclei slowed down in different materials. It has been reported (Br 73) that the lifetimes determined by DSAM vary with atomic number of the slowing down

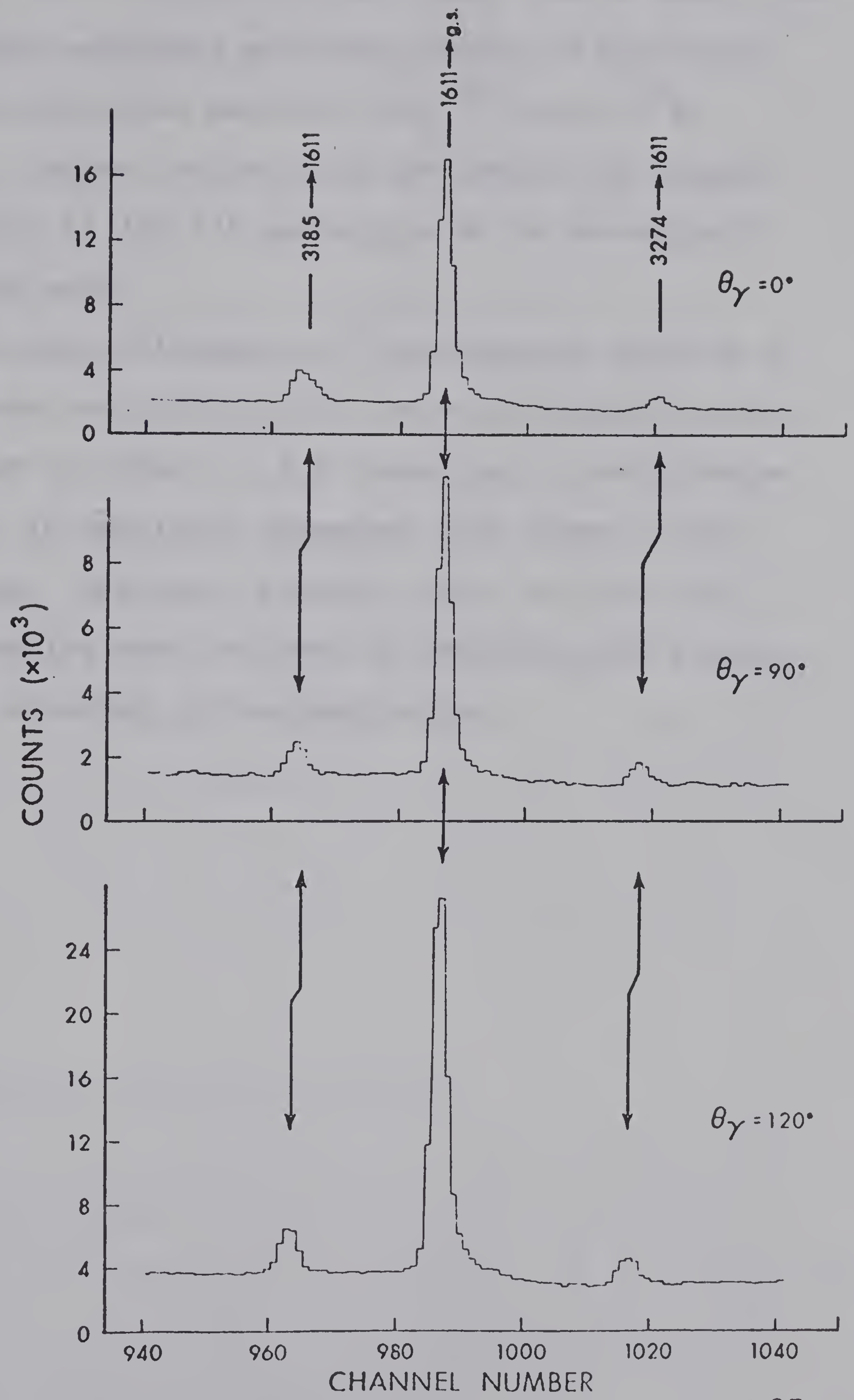

Figure 2.6 Direct γ-ray spectra from the $^{37}Cl(p,n\gamma)^{37}Ar$ reaction exhibiting Doppler-shifts of the γ rays originating from the 1611, 3185 and 3274 keV states.

material. The lifetimes of the higher levels show, however, better agreement with each other, in particular those determinations made with the $^{37}Cl(p,n\gamma)^{37}Ar$ reaction. Except for the 1410 keV level, the report of Kruzek et al (Kr 73) appears to be in accord with the present work.

The mean lifetimes of ^{37}Ar compiled recently by Endt and van der Leun (En 73) has been included in the last column of Table 2.3 for comparison. Our lifetime values are in excellent agreement with those of the compilation. One must, however, point out that the present results were included in obtaining the average lifetimes reported in the compilation.

CHAPTER 3

GAMMA-RAY ANGULAR DISTRIBUTION OF ^{37}Ar

The study of γ-ray angular distributions from aligned nuclear states is a useful tool for extracting information of spins and decay modes of these states. To define nuclear alignment one considers a reaction of the type A(a,b)B*. If neither the beam of particles, a, nor the target A is polarized then the γ-radiation from the residual state, B*, will exhibit axial symmetry about the beam direction. Furthermore, if the excited state, $|J_2M_2>$, of B* has definite parity then reflection about a plane normal to the beam direction would also be symmetric. Under these conditions the state $|J_2M_2>$ is said to be aligned i.e. $P(M_2) = P(-M_2)$ where $P(M_2)$ is the population of the magnetic substate M_2.

3.1 Condition of Nuclear Alignment

There are several possible ways to obtain alignment in the nucleus of decaying state, one of which is the A(p,nγ)B* reaction near threshold. At low bombarding energy the (p,n) reaction proceeds mainly through the compound nucleus (see Figure 3.1).

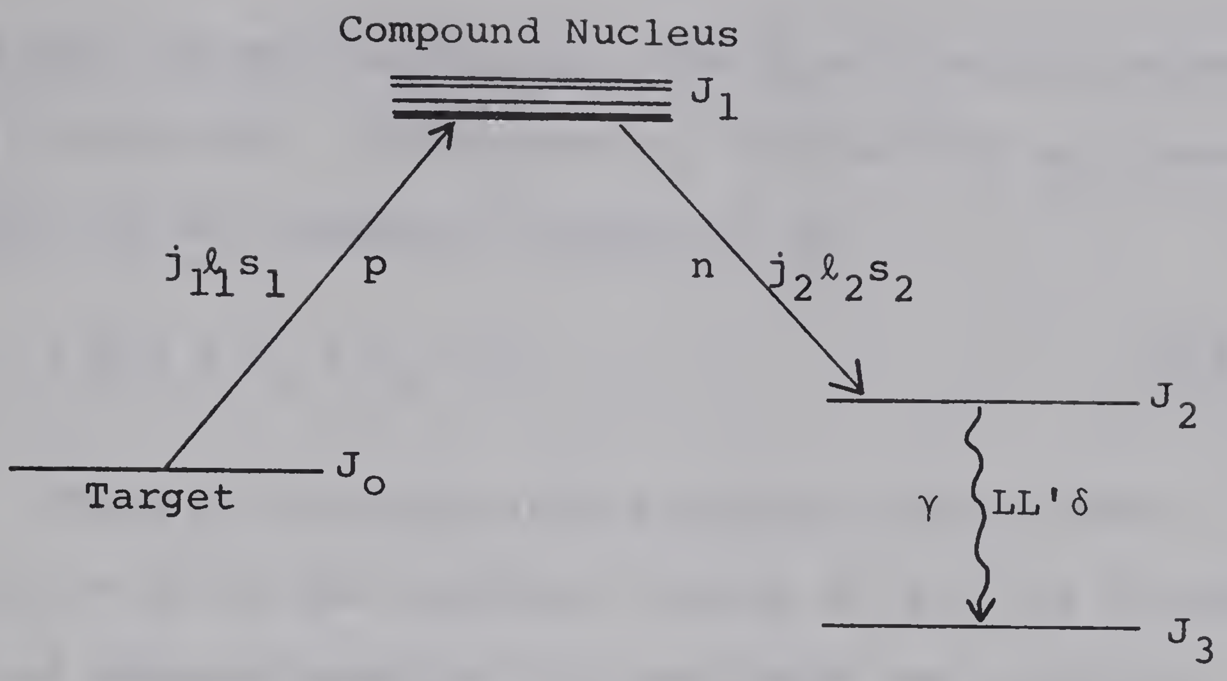

Figure 3.1

The compound nuclear model describes the reaction as proceeding in two stages; the formation of the compound nuclear states, $|J_1M_1>$, by the projectile and the target nucleus and the eventual decay of $|J_1M_1>$ into two reaction products (in this case the neutron and the residual nucleus B*). If the incident proton direction is chosen as the axis of quantization then the maximum spin projection along this axis for any compound nuclear state is

$$|M_1| \leq J_o + s_1 \tag{3.1}$$

where J_o is the target spin and s_1 is the spin of proton; the projection of the orbital angular momentum of the proton will not contribute because the orbital angular momentum is perpendicular to the quantization axis.

Now if the reaction proceeds near threshold the outgoing neutron will have low orbital angular momentum

and hence one may assume that the $l_2 = 0$ partial waves will predominate. Consequently, the maximum spin projection of the residual nucleus B* is

$$|M_2| \leq J_o + s_1 + s_2 \quad . \tag{3.2}$$

Thus for an unpolarized system, states with $J_2 > (J_o + 1)$ in the residual nucleus B* will be strongly aligned because Equation 3.2 precludes the magnetic substates greater than $(J_o + 1)$ from being populated. A nuclear state is said to be strongly aligned if its highest magnetic substate $(|M_2| = J_2)$ is not populated. This results from the fact that the asymmetry of the angular distribution is most sensitive to the lack of population of the highest magnetic substate.

3.1.1 Gamma-ray decay of aligned state

The theoretical derivation of the angular distribution of γ-ray decay from an aligned state has been treated in detail by Litherland and Ferguson (Li 61), Poletti and Warburton (Po 65) and Rose and Brink (Ro 67). The outline presented below follows the notation and sign conventions of Rose and Brink.

Consider the γ-ray transition of the state $|J_2M_2>$ to the state $|J_3M_3>$. The probability amplitude, $A^q_{M_2M_3}(\vec{k})$, for emission of a photon along $\vec{k}$ with circular polarization q is given by

$$A_{M_2M_3}^{q}(\vec{k}) = -\left(\frac{k}{2\pi\hbar}\right)^{\frac{1}{2}} \sum_{LM\pi} q^{\pi} \langle J_2M_2|T_{LM}^{<\pi>}|J_3M_3\rangle \mathcal{D}_{Mq}^{L}(R) \tag{3.3}$$

where $T_{LM}^{<\pi>}$ is the electromagnetic operator with $\pi = 0$ or 1 for electric and magnetic interaction respectively. $\mathcal{D}_{Mq}^{L}(R)$ is the rotation matrix and $R = (\alpha\beta\gamma)$ describes the rotation that takes the quantization or beam axis to the direction of $\vec{k}$.

When the orientation of the spin, J_3, is not observed the transition probability for emission must be summed over M_3, namely

$$\sum_{M_3} |A_{M_2M_3}^{q}(\vec{k})|^2 \tag{3.4}$$

If the radiating system is cylindrically symmetric, the total radiative probability for photons along $\vec{k}$ is obtained by weighting the contribution from each substate M_2 by its population parameter, $P(M_2)$

$$\sum_{M_2} P(M_2) \sum_{M_3} |A_{M_2M_3}^{q}(\vec{k})|^2 \quad . \tag{3.5}$$

Using the normalization condition

$$\sum_{M_2} P(M_2) = 1 \tag{3.6}$$

the Wigner-Eckart theorem

$$\langle J_2M_2|T_{LM}^{<\pi>}|J_3M_3\rangle = (-1)^{2L}(J_3LM_3M|J_2M_2)\langle J_2||T_{L}^{<\pi>}||J_3\rangle \tag{3.7}$$

and the properties of rotation matrices and vector coupling, the expression for the total radiative probability or angular distribution formula becomes

$$W(J_2 \rightarrow J_3;kq) = (\frac{k}{2\pi\hbar}) \sum_{KLL'\pi\pi'} B_K(J_2)(P_K(\cos\theta)(-)^{q+J_2-J_3+L'-L-K}$$

$$\times\ (2J_2 + 1)^{\frac{1}{2}}(LL'q-q|KO)W(J_2J_2LL';KJ_3)$$

$$\times\ q^{\pi+\pi'}<J_2||T_L^{<\pi>}||J_3><J_2||T_{L'}^{<\pi'>}||J_3> \qquad (3.8)$$

with

$$B_K(J_2) = \sum_{M_2} P(M_2)(-)^{J_2-M_2}(2J_2 + 1)^{\frac{1}{2}}(J_2J_2M_2-M_2|KO) \qquad (3.9)$$

$$B_o(J_2) = 1$$

in which $(J_1M_1J_2M_2|JM)$ is a Clebsch-Gordan coefficient, $W(J_1J_1LL';KJ_2)$ is a Racah coefficient and $<J_1||T_L^{<\pi>}||J_2>$ is a reduced matrix element.

If polarization is not measured then one sums over the circular polarization quantum number, q,

$$W(J_2 \rightarrow J_3;k) = W(J_2 \rightarrow J_3;k1) + W(J_2 \rightarrow J_3;k-1)\ . \qquad (3.10)$$

Equation 3.8 can be written in a more compact form if one introduces the mixing ratio

$$\delta_L^{<\pi>} = \frac{<J_2||T_L^{<\pi>}||J_3>/(2L + 1)^{\frac{1}{2}}}{<J_2||T_{\bar{L}}^{<\bar{\pi}>}||J_3>/(2\bar{L} + 1)^{\frac{1}{2}}} \qquad (3.11)$$

where $\bar{L}$, $\bar{\pi}$ is the lowest multipolarity and the coefficient

$$R_K(LL'J_2J_3) = (-)^{1+J_2-J_3+L'-L-K}\{(2J_2+1)(2L+1)(2L'+1)\}^{\frac{1}{2}}$$

$$\times\ (LL'1-1|K0)W(J_2J_2LL';KJ_3)\quad . \qquad (3.12)$$

Hence the formula of angular distribution for γ rays in terms of the mixing ratio when circular polarization is not observed is

$$W(J_2\rightarrow J_3;k) \equiv W(\theta) = \sum_{LL'\pi\pi'K}\{B_K(J_2)R_K(LL'J_2J_3)P_K(\cos\ \theta)$$

$$\times\ [1-(-1)^{L+L'+\pi+\pi'-K}]\,\delta_L^{<\pi>}\delta_{L'}^{<\pi'>}\}/2\sum_{L\pi}|\delta_L^{<\pi>}|^2 . \qquad (3.13)$$

The multipolarities (L, L') must, however, satisfy the triangular relationship,

$$|J_2 - J_3| \leq L,L' \leq (J_2 + J_3)\quad . \qquad (3.14)$$

In all but a few rare cases, only the two lowest multipolarities are important as contributions (γ-ray transition probability decreases rapidly with increasing multipole order). Hence one needs to consider only the lowest two multipolarities, L and L', whereby $L = |J_2 - J_3|$ and $L' = L + 1$. It follows that for transitions between definite parity states, the quantity $[1 - (-)^{L+L'+\pi+\pi'-K}]$ in Equation 3.13 will vanish when K is odd. Moreover, one arrives at the same result that the odd K terms

disappear if the decaying state $|J_2M_2>$ is aligned. This manifests itself from the definition of the $B_K(J_2)$ coefficients (Equation 3.9) that they vanish for odd K values. Therefore the γ-ray angular distribution from an aligned state when only the lowest two multipolarities are considered is simply:

$$W(\theta) = \sum_{K\ \mathrm{even}} B_K(J_2)P_K(\cos\theta)$$

$$\times \left[\frac{R_K(LLJ_2J_3) + 2\delta R_K(LL'J_2J_3) + \delta^2 R_K(L'L'J_2J_3)}{1+\delta^2}\right] \qquad (3.15)$$

3.1.2 Application of the statistical compound nuclear model

In evaluating the right hand side of the Equation 3.15 one must first calculate the $B_K(J_2)$ defined earlier

$$B_K(J_2) = \sum_{M_2} P(M_2)(-)^{J_2-M_2}(2J_2+1)^{\frac{1}{2}}(J_2J_2M_2-M_2|KO). \qquad (3.9)$$

The $B_K(J_2)$ coefficients describe the nuclear alignment and depend on the population parameter, $P(M_2)$, of the magnetic substates of the decaying state $|J_2M_2>$. When the magnetic substates are equally populated i.e. $P(M_2) = P(M_2')$ for $M_2 \neq M_2'$, the $B_K(J_2)$ coefficients will vanish indicating that the γ-ray angular distribution from such an oriented state will be isotropic. Consequently, $B_K(J_2)$ may be regarded as orientation

coefficients describing the orientation of the magnetic substate and hence the ensuing γ-ray angular distribution. The manner in which the magnetic substates are populated, however, requires the knowledge of the nuclear forces involved in the reaction mechanism. Since nuclear forces are not exactly known one must rely on some nuclear model.

The statistical compound nuclear (SCN) model assumes that the numerous compound nuclear states overlap to a great extent and the interferences between different spin states cancel out. In essence, the formation and decay of the compound nucleus through its various channels may be described by energy averaged transmission coefficients. Consequently, the population parameters can be determined from these transmission coefficients in terms of the penetrability term

$$\tau = T_{\ell j}(E)\left(\frac{T_{\ell' j'}(E')}{\sum\limits_{\ell'' j''} T_{\ell'' j''}(E'')}\right) \tag{3.16}$$

where $T_{\ell j}(E)$ is an energy dependent transmission coefficient with orbital and total angular momenta ℓ and j respectively. The unprimed and primed quantities represent the incoming and outgoing channels respectively and the summation extends over all outgoing channels. In this notation, the term $T_{\ell j}(E)$ in Equation 3.16

describes the formation while the quantity in the bracket that of the decay of the compound nucleus. The transmission coefficients can be obtained by a Hauser-Feshbach calculation.

In terms of the penetrability, τ, the γ-ray angular distribution formula has been derived by Sheldon and Van Patter (Sh 66). For the case of γ-ray decay from an aligned state and considering only the lowest two multipoles the formula reduces to,

$$\begin{aligned} W(\theta) = {} & \frac{1}{(2s_1+1)(2J_o+1)} \sum_{j_1 j_2 K_{\text{even}}} (-)^{J_o+J_3-j_2-s_2} \\ & (2\ell_1+1)(2j_1+1)(2J_1+1)^{\frac{1}{2}}(2J_2+1)^{\frac{1}{2}} \\ & (\ell_1 0 \ell_1 0 | k0) W(L_1 L_1 j_1 j_1, K s_1) W(J_1 J_1 j_1 j_1; K J_o) \\ & W(J_1 J_1 J_2 J_2; K j_2)\, \tau P_K(\cos\theta) \\ & \left(\frac{R_K(LLJ_2J_3) + 2\delta R_K(LL'J_2J_3) + \delta^2 R_K(L'L'J_2J_3)}{1+\delta^2} \right) \end{aligned} \qquad (3.17)$$

with summation over all incoming and decaying channels and even K. The actual calculation of Equation 3.17 is carried out by the computer program, 'AK' (Gr 71).

In order to apply the statistical analysis to the experimental results one must ensure that a large number of compound nuclear states are excited. This is usually achieved by using a very thick target or a broad incident

beam (i.e. beam with poor energy resolution). The thick target method has been chosen for this investigation.

The experimental γ-ray angular distribution can be expanded in a Legendre polynomial series,

$$W(\theta)_{\text{expt.}} = \sum_{K\ \text{even}} A_K Q_K P_K(\cos\theta) \qquad (3.18)$$

in which A_K is the expansion coefficient, $P_K(\cos\theta)$ the Legendre polynomial and Q_K the attenuation factor describing the finite size correction for the γ-ray detector.

Thus by fitting the theoretical and experimental angular distributions (Equations 3.17 and 3.18 respectively) by a least square method (Section 3.3.1) the spin of the decaying state, J_2, may be determined provided the spin of the final state, J_3, is known or vice versa.

3.2 Experimental Arrangement

Angular distributions of the γ rays following the $^{37}Cl(p,n\gamma)^{37}Ar$ reaction were measured at several proton energies between 3.25 and 5.15 MeV. The energies were chosen to be just above the threshold of the levels being investigated in order to achieve the aforementioned alignment of the decaying states. The γ rays were detected by a 33 cm^3 Ge(Li) crystal mounted on a rotating

trolley at a distance of 20 cm from the target. Intensities were measured at 0°, 30°, 45°, 60° and 90° to the beam axis. Each measurement was repeated at least once. A 48 cm^3 Ge(Li) crystal was used in the angular distribution measurement at proton energy of 5.15 MeV. Both detectors provided resolutions of typically 3.5 keV FWHM for the 1.332 MeV ^{60}Co full energy peak.

The signals extracted from the Ge(Li) detector were fed into a pre-amplifier and amplifier system and then sent to a single channel analyzer (SCA). A window was set on the SCA to select the energy region of the spectrum of interest. The output of the SCA was used to gate the analog-to-digital converter which was interfaced to a Honeywell 516 computer.

The $PbCl_2$ target described in the lifetime study (Section 2.2) was used as well as a thick target. The thick target was made by mixing a small amount of enriched ^{37}Cl ($\sim$85%) in the form of KCl into a slurry of polyurethane and benzene and depositing the mixture onto a 0.5 mm thick tantalum backing. The target was placed on a 1.3 mm thick aluminum plate mounted at 30° to the beam direction (Figure 3.2).

Throughout the experiment, the target was cooled by directing a jet of air at the outside surface of the aluminum plate. The beam was well collimated to produce beam spots of less than 2 mm in diameter on the

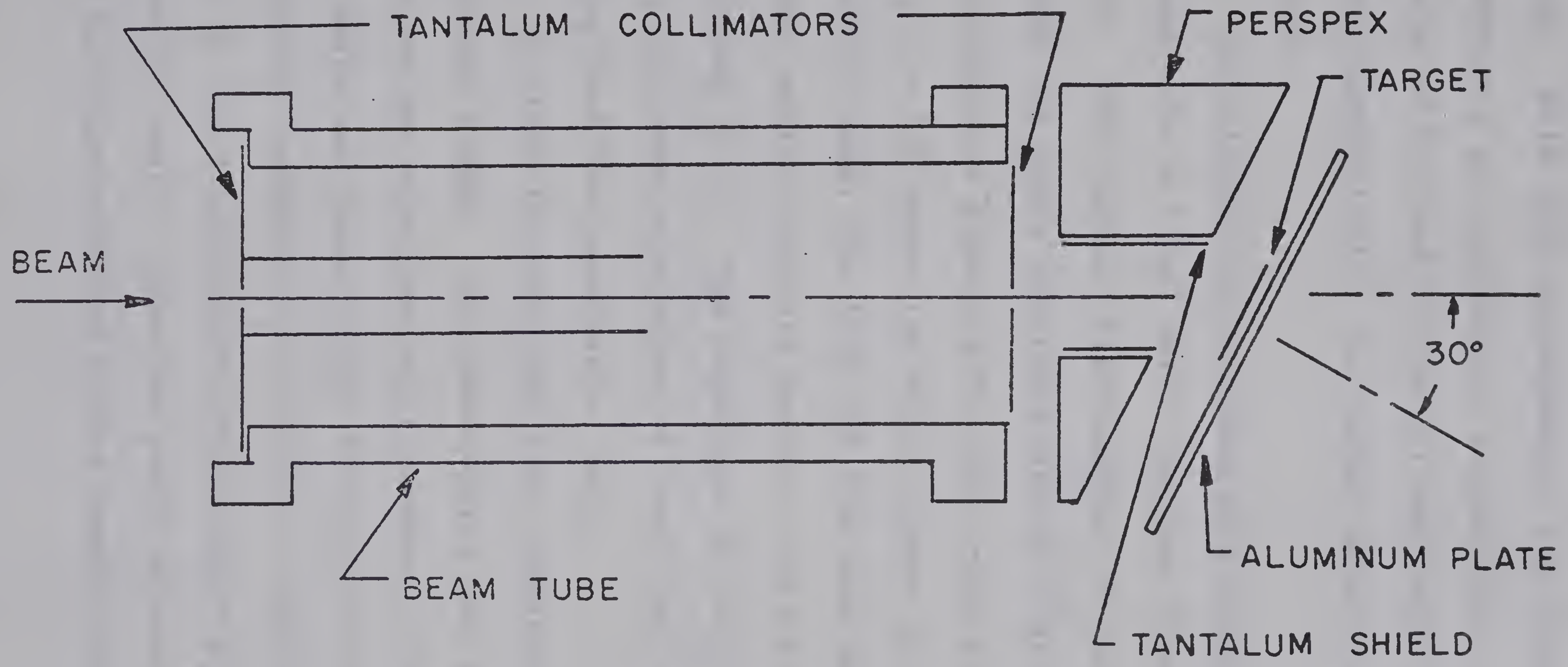

Figure 3.2 Target arrangement for γ-ray angular distribution measurements.

[illegible]

targets. With this arrangement, the counting rate in the detector was maintained around 8000 cps with beam currents of 0.2 and 1.0 μA for the thick and evaporated targets respectively. No target deterioration was observed.

An initial run at bombarding energy of 3.25 MeV was made with a 6 cm^3 Ge(Li) crystal fixed at 90° as monitor. The angular distribution of the 1410 keV γ ray from the first excited state of ^{37}Ar was found to be isotropic as expected for the γ-ray transmission from a J = 1/2 state (Ro 65a) (Figure 3.3). Hence in subsequent runs, the 1410 keV peak was used as an internal monitor and all angular distributions were normalized to it. The existence of an internal monitor also eliminated correction of dead time and anisotropies arising from the correlation table.

A yield function was also obtained with the evaporated target. The beam energy was varied from 3.00-5.40 MeV with the Ge(Li) detector fixed at 55°. This angle was chosen since the second order Legendre polynomial vanishes ($P_2(\theta = 55°) = 0$) and the A_4 coefficient of the distribution, $W(\theta) = A_o + A_2P_2 + A_4P_4$, is usually small. Thus the yield intensities measured would be least affected by the angular distributions.

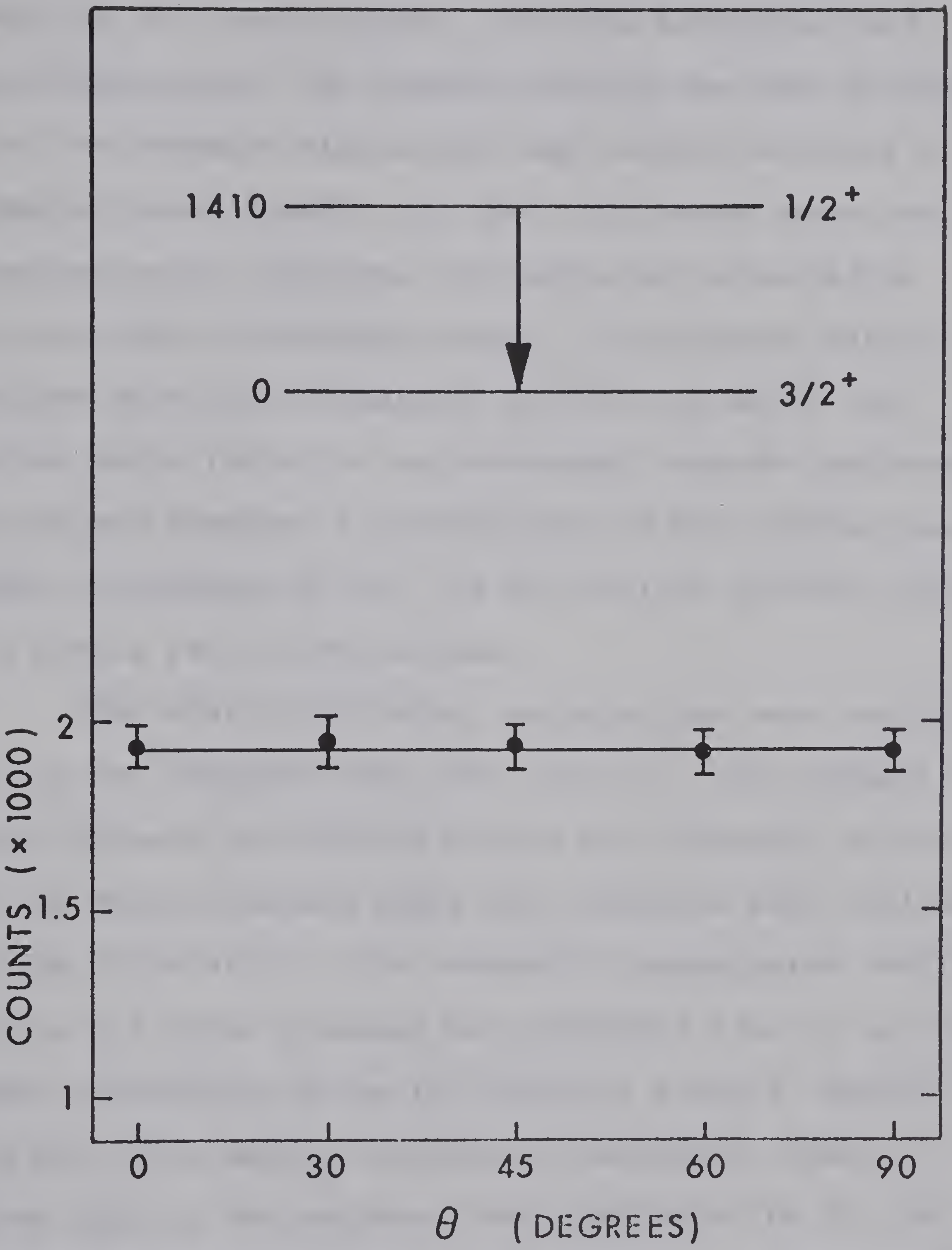

Figure 3.3 The angular distribution of the 1410 keV transition to the ground state.

3.3 Analysis

Gamma-ray intensities were obtained by summing over the full energy peaks after the background had been subtracted. The summing process was done directly from the computer display and was checked later by a computer code 'SUMMIT' (Gr 71a). In cases where unresolved peaks occurred, the sums were extracted by fitting them to Gaussian shapes. The angular distributions were then normalized to the 1410 keV γ ray before being fitted to an even-order Legendre polynomial series and compared to predictions of the statistical model of Sheldon (Sh 66) for the various possible spin and mixing ratio combinations.

The statistical model calculations were carried out by the computer code 'AK' (Gr 71). All kinematically allowed neutron and proton exit channels as well as the four strongest alpha exit channels were included in the calculation. The necessary transmission coefficients for these channels were obtained from an optical model calculation using the computer program 'HAUSER' (Da 69). The optical parameters used were those of Rosen (Ro 65) for protons, Perey and Buck (Pe 62) for neutrons and Davison (Da 69) for alphas. A second set of transmission coefficients was generated using the code 'ABACUS' (Au 64) with the same optical parameters.

Although the absolute values of the two sets of transmission coefficients differed by as much as a factor of two, the ratios, $T_{\ell=1}/T_{\ell=o}$, differed by less than 30% and the resulting statistical calculations yielded A_2/A_o coefficients that differ by 10%. Since the experimental A_2/A_o coefficients (Table 3.1) have uncertainties of this magnitude, the SCN analysis using either set of transmission coefficients would give essentially the same result. This is expected. Pilt (Pi 69) has shown that the usefulness of the statistical calculation results from its insensitivity to the transmission coefficients.

3.3.1 Chi-square analysis

A χ^2 subroutine contained in the 'AK' program provided a test of goodness of fit between the experimental and predicted distributions for various spin and multipole combinations. The quantity, χ^2, is defined as

$$\chi^2 = \frac{1}{n-1} \sum_{i=1}^{n} \frac{[W(\theta_i) - Y(\theta_i)]^2}{[\sigma(\theta_i)]^2} \qquad (3.19)$$

where $W(\theta_i)$ and $Y(\theta_i)$ are respectively the experimental and predicted γ-ray yields at angle θ_i. $\sigma(\theta_i)$ is the statistical uncertainty in $W(\theta_i)$ and n is the number of degrees of freedom.

Normally, a 0.1% confidence limit is set on the χ^2 implying that all spin assignments that fall outside the limit may be rejected with only one chance in a thousand of rejecting the correct spin assignment. Thus for some angular distributions unique spin assignments may be made.

3.3.2 Branching ratios

The γ-ray branching ratios were determined from the angular distributions using the zero-order term of the Legendre polynomial expansion and previously measured efficiencies of the Ge(Li) detectors (Ch 70). They are presented in Figure 3.4 together with the spin and parity assignments extracted from this experiment.

3.4 Results and Discussion

Angular distributions of γ-ray decays for all levels up to 3274 keV excitation in ^{37}Ar were accumulated at incident energies of 3.25, 3.40, 4.05 and 4.30 MeV with the KCl target and at 3.35, 4.55 and 5.15 MeV with the $PbCl_2$ target which yielded a much cleaner spectrum. A typical γ-ray spectrum observed at 5.15 MeV proton energy is shown in Figure 3.5. In fact, contributions of γ rays resulting from proton induced reactions on potassium made it very difficult to extract the yields of the higher energy γ rays from ^{37}Ar.

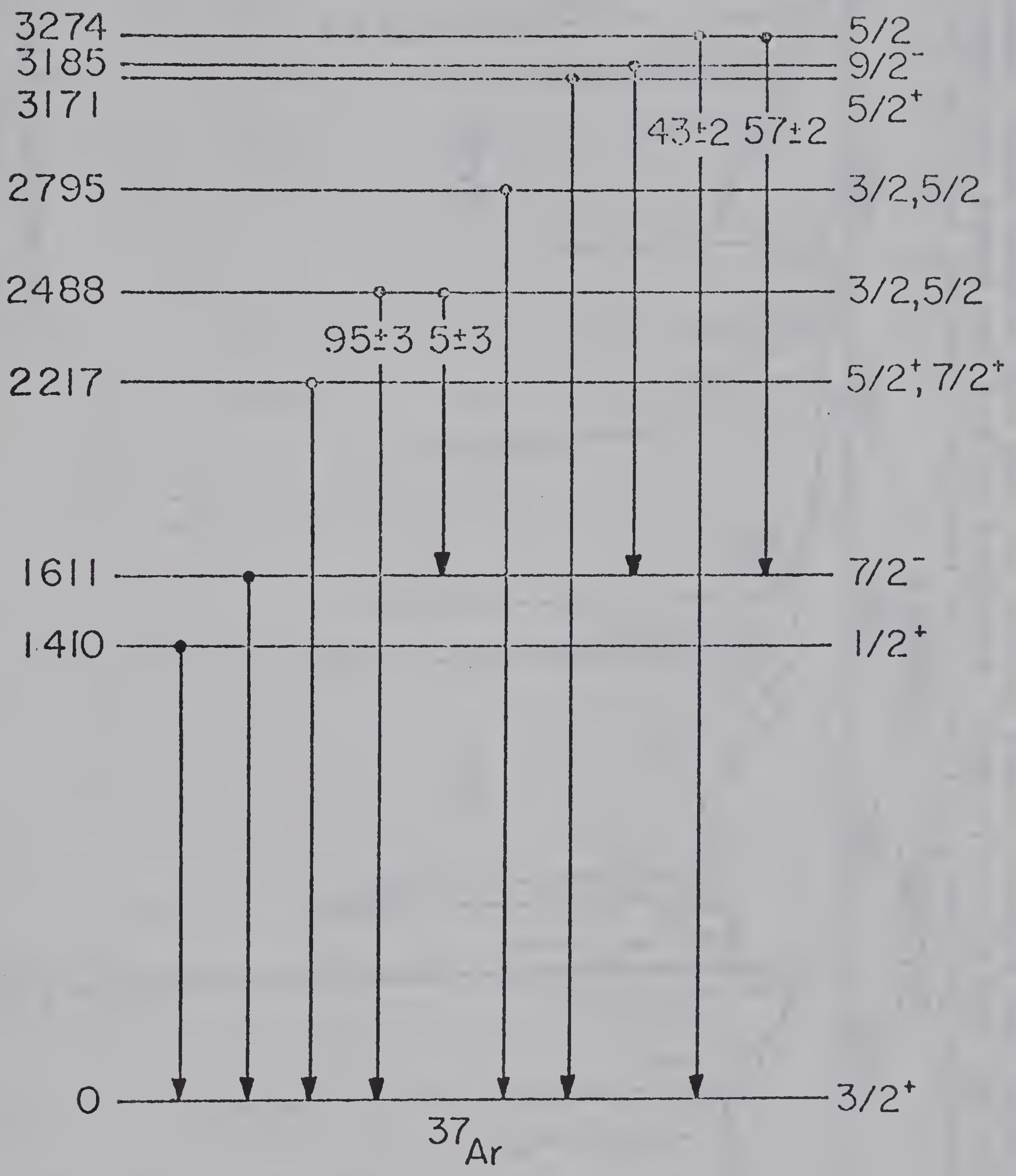

Figure 3.4 Energy levels and decay scheme of ^{37}Ar.

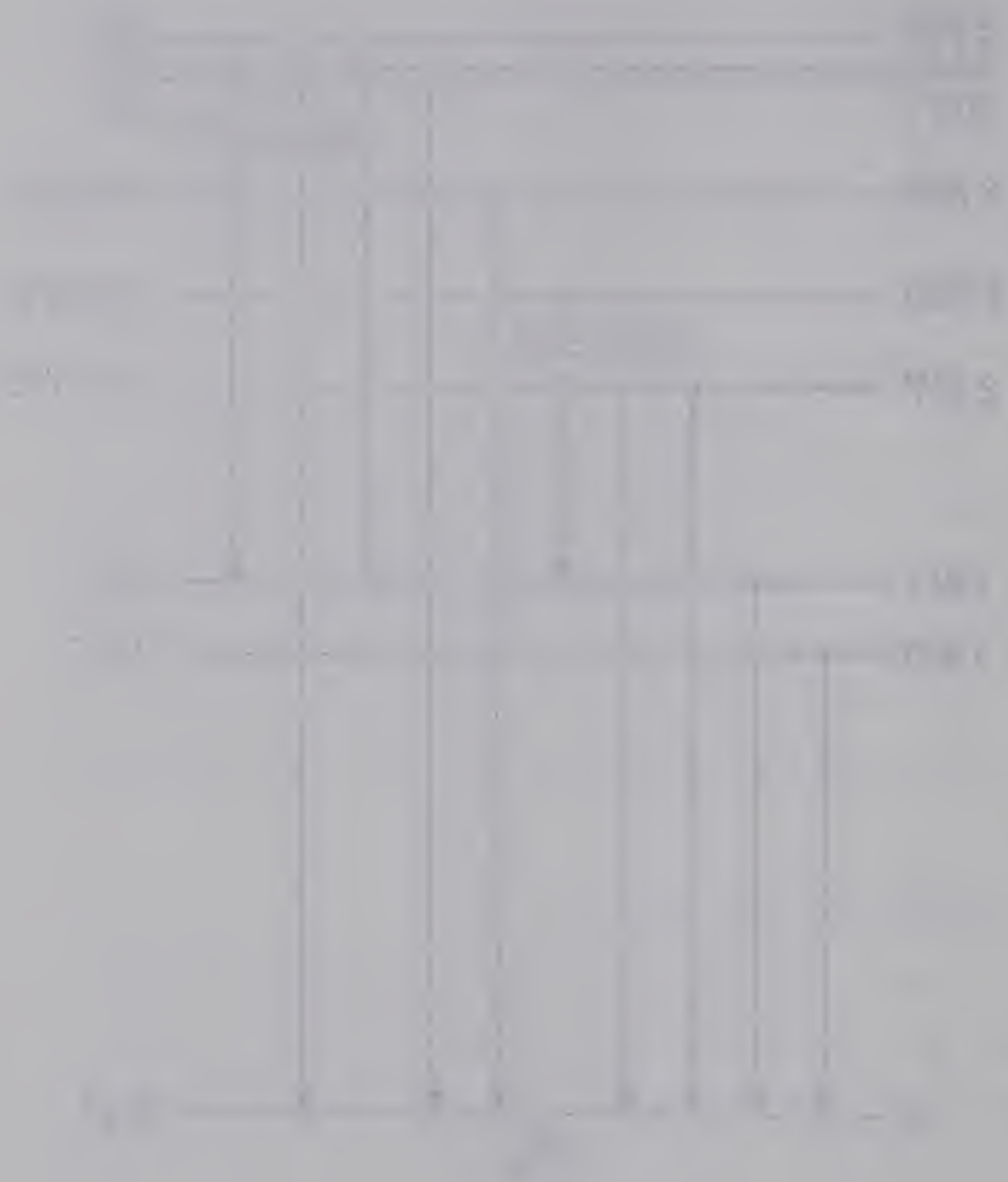

[illegible]

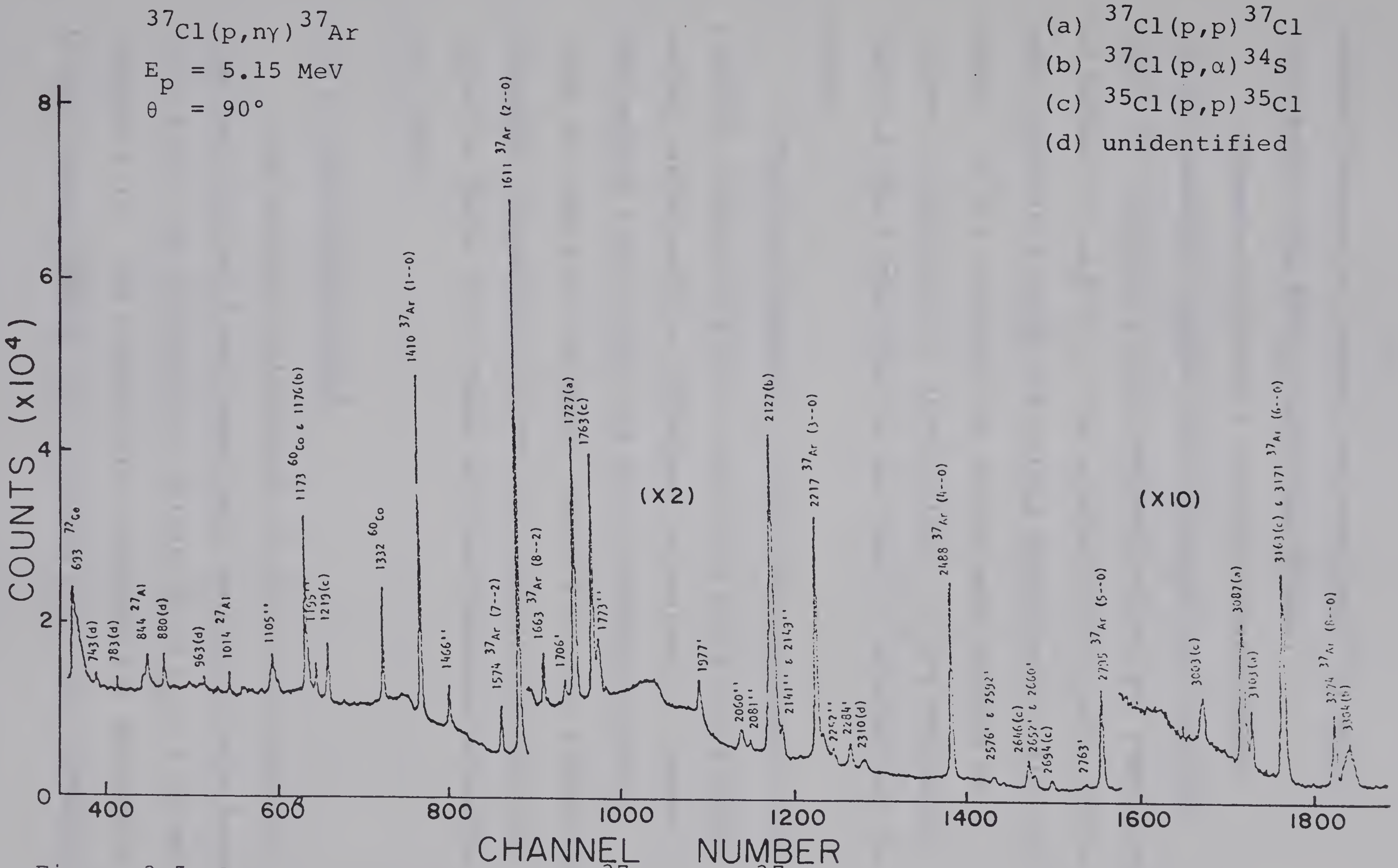

Figure 3.5 A γ-ray spectrum for the $^{37}Cl(p,n\gamma)^{37}Ar$ reaction observed with the Ge(Li) detector at 90° and E_p = 5.15 MeV. Energies of all the peaks are identified and the primes and double primes denote 1st and 2nd escape peaks respectively.

Several targets of natural and enriched ^{37}Cl were tried before the $PbCl_2$ target was chosen.

Legendre polynomial expansion coefficients for all measured angular distributions are listed in Table 3.1 and mixing ratio determinations are summarized in Tables 3.2 and 3.3. The errors in the mixing ratios were calculated using the method described by Cline and Lesser (Cl 70) in which the errors were assumed to follow a statistical F distribution. A 10% confidence limit of the F distribution was used in determining the errors.

The electromagnetic transition strengths of all possible transitions were calculated using the average mixing ratios and the lifetimes determined in Chapter 2. Some mixing ratio, spin and parity combinations were ruled out based on the upper limits for γ-ray transition strengths recommended by Endt and van der Leun (En 74) listed in Table 3.4. These will be discussed below for each level.

3.4.1 The 1410 keV level

The angular distribution of the γ-ray transition from the 1410 keV level whose spin and parity were known ($J^{\pi} = 1/2^{+}$) was isotropic to within 3% at $E_p = 3.25$ MeV (Figure 3.3). The yields were corrected for absorption in the target backing and retaining plate and normalized

Table 3.1

Legendre Polynomial Coefficients for Gamma-ray Angular Distributions of ^{37}Ar

Transition (keV)	Bombarding energy (MeV)	A_2/A_o	A_4/A_o
1410 → g.s.	3.25	-0.01±0.03	0.00±0.03
1611 → g.s.	3.35	0.24±0.02	-0.10±0.02
	3.40	0.18±0.03	-0.07±0.03
	4.05	0.18±0.01	-0.03±0.01
	4.30	0.16±0.01	-0.03±0.01
	4.55	0.17±0.01	-0.08±0.02
2217 → g.s.	4.05	0.29±0.02	-0.01±0.02
	4.30	0.23±0.01	-0.01±0.01
	4.55	0.22±0.01	-0.04±0.01
2488 → g.s.	4.55	0.05±0.01	0.00±0.01
	5.15	0.05±0.01	0.02±0.01
2795 → g.s.	4.55	-0.01±0.03	0.07±0.03
	5.15	0.01±0.01	0.02±0.01
3171 → g.s.	5.15	-0.36±0.08	-0.04±0.08
3185 → 1611	5.15	0.47±0.01	0.02±0.02
3274 → g.s.	5.15	-0.08±0.01	-0.01±0.01

Table 3.2

Mixing Ratios of the 1611 keV Level

E_p (MeV)	S C N Analysis arctan δ (°)	Model Independent Analysis arctan δ (°)
3.35	8 ± 4	8 ± 3
3.40	12 ± 4	13 ± 5
4.05	7 ± 4	10 ± 3
4.30	8 ± 3	8 ± 3
4.55	8 ± 4	10 ± 3

Table 3.3

Summary of Mixing Ratios in ^{37}Ar for $\chi^2 < 0.1\%$ Confidence

E_i (keV)	E_f (keV)	J_i	J_f	E_p (MeV)	Arctan δ (degrees)	Average δ
2217	0	5/2	3/2	4.05	-54 ± 20	$-2.1^{+0.5}_{-0.8}$ or -0.93 ± 0.24
				4.30	-66 ± 10 or -40 ± 10	
				4.55	-60 ± 12 or -48 ± 14	
				5.15	-70 ± 10 or -38 ± 12	
		7/2	3/2	4.05	-6 ± 4 or >88	-0.03 ± 0.04 or 8.1^{+11}_{-3}
				4.30	2 ± 6 or 82 ± 6	
				4.55	0 ± 3 or 84 ± 4	
				5.15	-2 ± 10 or >73	
2488	0	3/2	3/2	4.55	-56 ± 14 or -14 ± 14	$-1.6^{+0.4}_{-0.6}$ or 0.19 ± 0.19
				5.15	-60 ± 8 or -8 ± 8	
		5/2	3/2	4.55	<-84 or -18 ± 6	<-8.1 or 0.32 ± 0.08
				5.15	<-83 or -18 ± 4	
2795	0	3/2	3/2	4.55	$-90\leq\delta\leq90$	$-\infty\leq\delta\leq+\infty$
				5.15	$-90\leq\delta\leq90$	
		5/2	3/2	4.55	-12 ± 11 or >86	0.21 ± 0.13 or >4.7
				5.15	-12 ± 8 or >78	
3171	0	5/2	3/2	5.15	38 ± 20	$0.78^{+0.82}_{-0.46}$
3185	1611	9/2	7/2	5.15	-30 ± 4	-0.58 ± 0.09
		11/2	7/2	5.15	-82 ± 4 or -8 ± 4	$-7.1^{+2.4}_{-7.2}$ or -0.14 ± 0.07
3274	0	3/2	3/2	5.15	$-90\leq\delta\leq90$	$-\infty\leq\delta\leq+\infty$
		5/2	3/2	5.15	-2 ± 8 or 76 ± 8	-0.03 ± 0.14 or $4.0^{+5.5}_{-1.5}$
	1611	5/2	7/2	5.15	<-66 or -16 ± 16	<-2.3 or -0.29 ± 0.31
		7/2	7/2	5.15	40 ± 14	$0.84^{+0.54}_{-0.35}$

Table 3.4

Recommended Upper Limits for Gamma-ray Transition Strengths ¹⁾

Transition	Upper Limits (W.u.)
E1	0.03
E2	100
E3	100
M1	10
M2	3
M3	15 ²⁾

1) Reference En 74

2) Reference Ne 74

to the 1410 keV peak from the monitor detector.

3.4.2 The 1611 keV level

The γ-ray angular distributions of the 1611 keV level to the ground state transition were measured at E_p = 3.35, 3.40, 4.05, 4.30 and 4.55 MeV. The SCN model analysis resulted in a unique spin assignment of 7/2 (see Figure 3.6 of the angular distribution at E_p = 3.35 MeV and its χ^2 fit to the SCN model prediction) which is in agreement with previous assignment of $J^\pi = 7/2^-$ (Ra 71 and Ta 71).

The γ-ray yield curve recorded from 3.00 to 5.40 MeV, however, shows fluctuations (Figure 3.7) indicating that some non-statistical contributions were present. Since the application of the SCN model in the analysis depends on the statistical averaging of all partial waves, these fluctuations reflect enhanced contributions from some dominant partial waves. This may affect the population of the magnetic substates of the decaying level and can result in incorrect mixing ratio and spin assignments. Consequently, in addition to the SCN analysis, all the 1611 keV angular distributions were subjected to a model independent study.

Model independent calculation

In the SCN calculation the population parameters, $P(M_2)$, were determined from the penetration factor, τ.

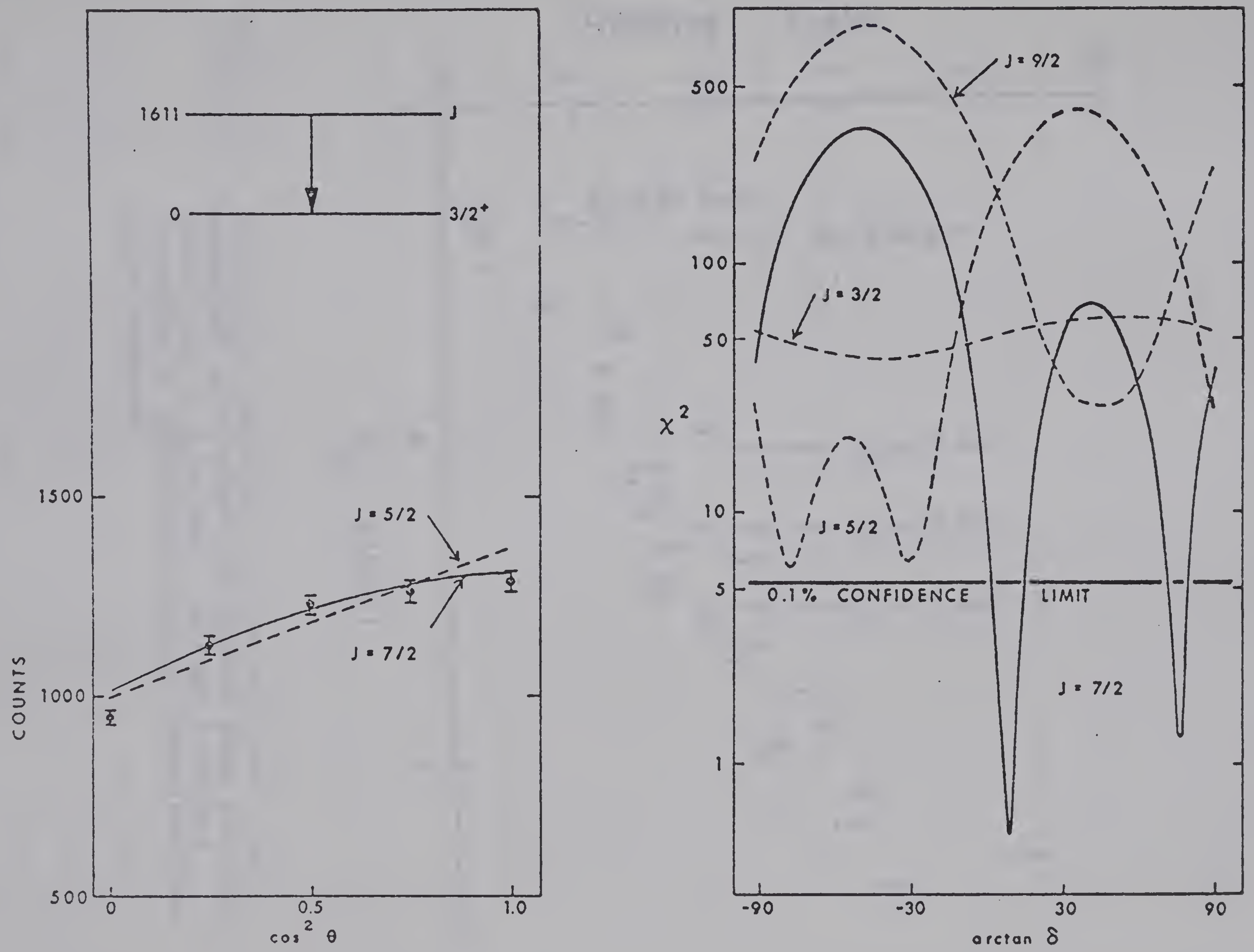

Figure 3.6 The angular distribution and χ^2 plot for the 1611 keV transition to the ground state.

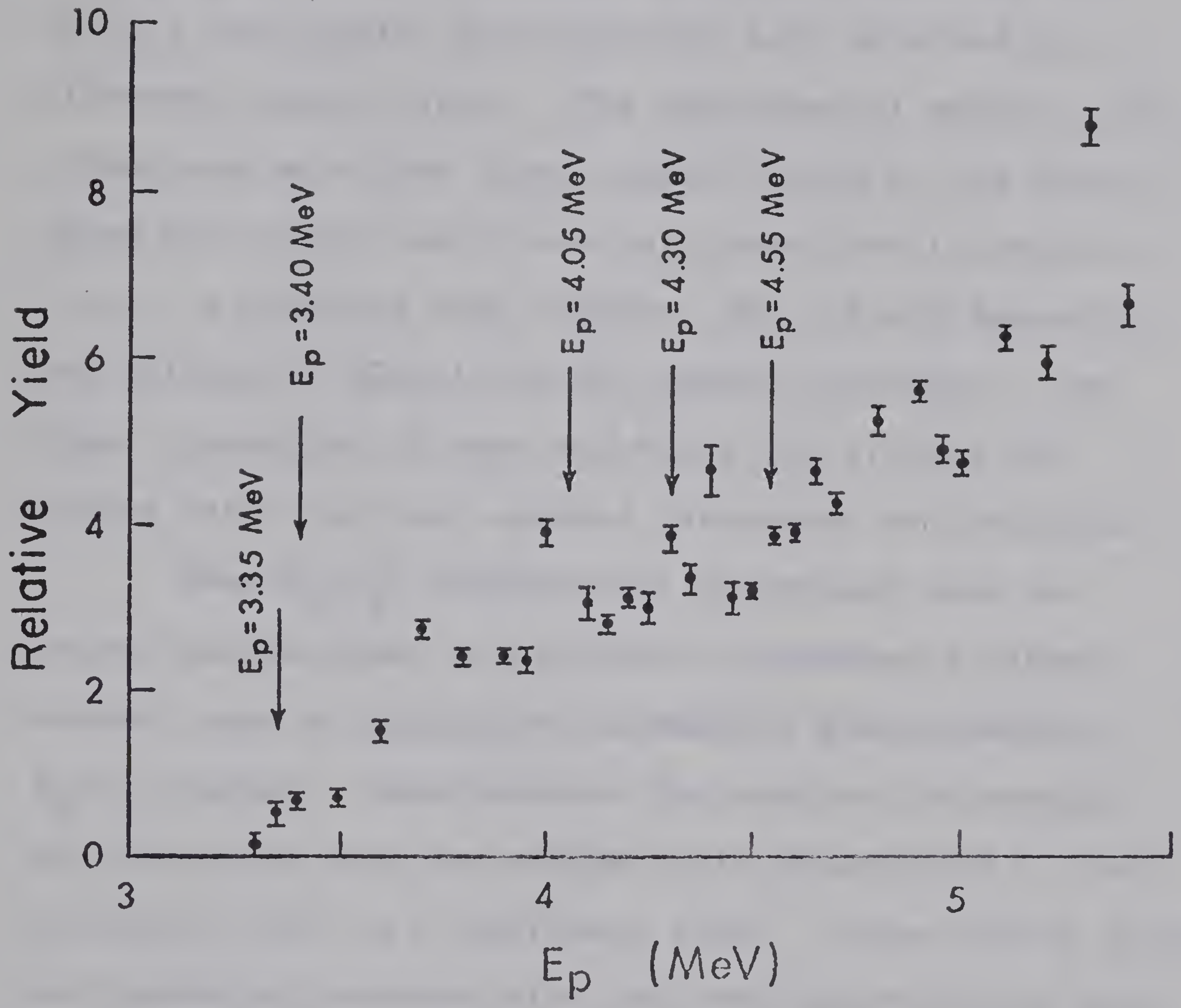

Figure 3.7 Excitation function of the 1611 keV γ rays observed at θ = 90° for proton beam energies from 3.30 to 5.40 MeV. Arrows indicate energies at which the angular distributions were measured.

The model independent calculation, however, allows the population parameters to vary freely in search for best fit with experimental data. For each set of $P(M_2)$, the $B_K(J_2)$ coefficients were calculated and with the $B_K(J_2)$, the angular distributions were obtained for different mixing ratios. The experimental angular distributions were then least square fitted to the calculated ones using the χ^2 analysis described in Section 3.3.1. A computer code 'MAGPOP' (Wo 72a and Appendix B) was written to facilitate the search procedure. The phase convention of Rose and Brink (Ro 67) for the mixing ratio has been adopted throughout the analysis.

Some $B_K(J_2)$ coefficients determined were not unique combinations of population parameters; rather several sets of population parameters yield similar $B_K(J_2)$ values. Nevertheless, for each set of angular distributions only two mixing ratio values have χ^2 that fall below the 0.1% confidence limit. These mixing ratios are presented together with the ones determined by the SCN model calculations in Table 3.2. The mixing ratios are in good agreement for all beam energies.

If one adopts the lifetime of 6.3±0.2 ns for the 1611 keV level (En 73), the spin and parity assignment of $7/2^+$ can be ruled out as it leads to a M3 transition strength >45 W.u. The larger mixing ratio, $\delta = 4.0^{+1.9}_{-1.1}$, for the $7/2^-$ assignment is also ruled out as it would

require an E3 transition strength > 107 W.u.. The accepted value of the mixing ratio, $\delta = 0.16 \pm 0.04$, is in good agreement with the results of Champlin et al (Ch 71) of $\delta = 0.15 \pm 0.04$, Taras et al (Ta 71) of $\delta = 0.22 \pm 0.11$ and Ragan et al (Ra 71) of $\delta = 0.09 \pm 0.03$.

The consistency of the mixing ratio determinations by the SCN and model independent methods and their agreement with previous results indicate that the yield fluctuations do not cause any appreciable error in the SCN model assignments. Therefore the SCN model has been used for the analysis of the other levels.

3.4.3 The 2217 keV level

The 2217 keV level decays to the ground state only and its angular distributions yield a spin assignment of $J = 5/2$ or $7/2$ (Figure 3.8) which is in agreement with the results of Naude et al (Na 68) and Ragan et al (Ra 71).

Negative parities may be ruled out for both spins (5/2 and 7/2) because their transition strengths exceed the upper limits quoted in Table 3.4. In the case where $J = 5/2$, negative parity would lead to a M2 transition strength > 51 W.u. and where $J = 7/2$, the smaller mixing ratio, $\delta = -0.03 \pm 0.04$, would yield a M2 transition strength > 117 W.u., while the larger mixing ratio, $\delta > 8.1^{+11}_{-3}$ would yield an E3 strength $> 1.1 \times 10^{5}$ W.u..

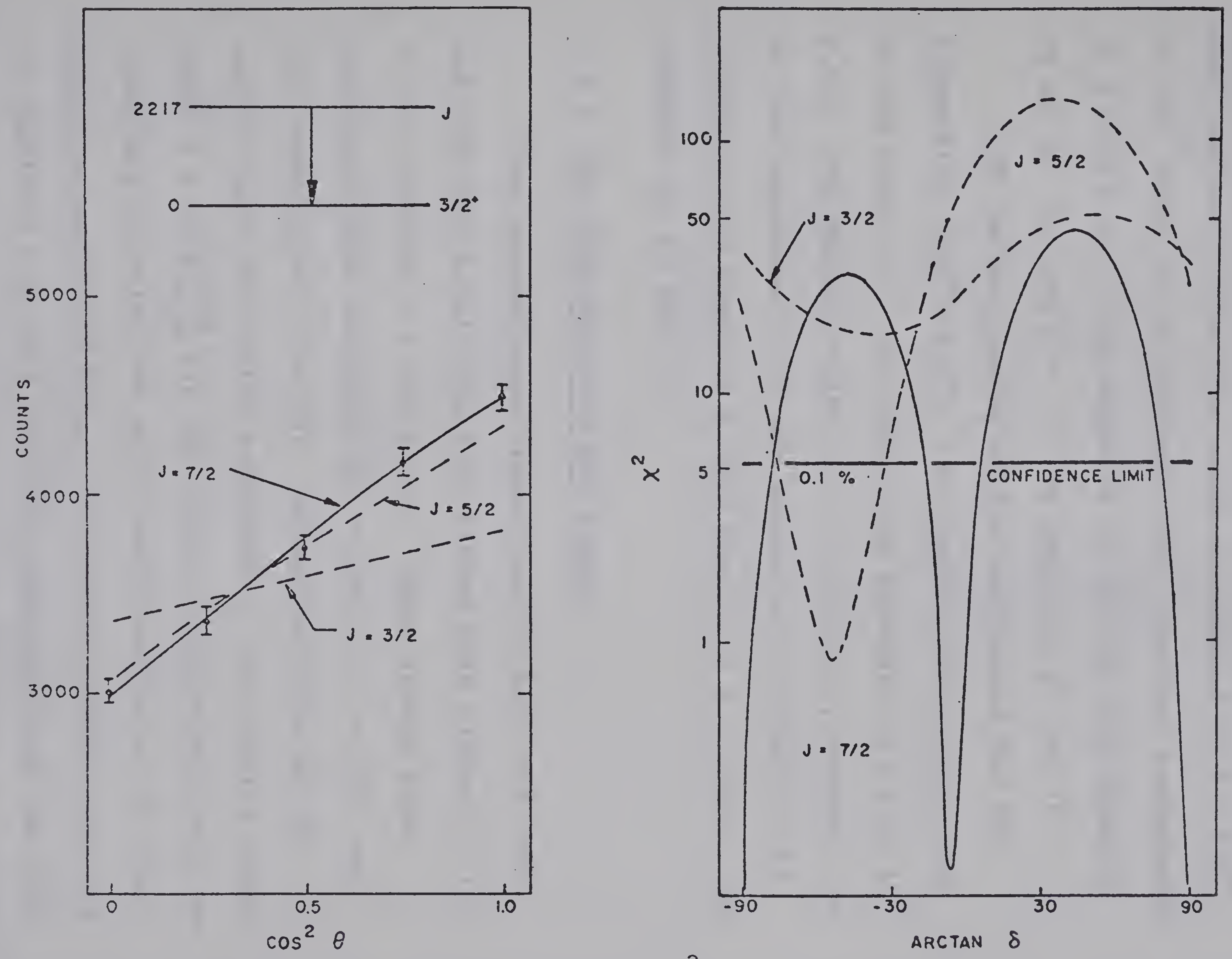

Figure 3.8 The angular distribution and χ^2 plot for the 2217 keV transition to the ground state.

[illegible]

To be consistent with measured lifetime, the spin and parity for this level is limited to $J = 5/2^+$ or $7/2^+$ which is in agreement with previous assignments of J = 5/2 or 7/2 by Naude et al (Na 68) and Champlin et al (Ch 71) and $J = 7/2^+$ by Ragan et al (Ra 71).

Of the two mixing ratios determined for the transition $(7/2^+ \rightarrow 3/2^+)$, the larger one is eliminated on the basis of a M3 transition strength of $> 4.2 \times 10^6$ W.u.. The smaller value ($\delta = -0.03 \pm 0.04$), however, is in good agreement with the values of $\delta = -0.03 \pm 0.04$ determined by Ragan et al and that of $\delta = 0.05 \pm 0.03$ by Champlin et al (Ch 71).

3.4.4 The 2488 and 2795 keV levels

The ground state transitions of both the 2488 and 2795 keV levels could be fitted with either J = 3/2 or 5/2 (Figures 3.9 and 3.10). These levels have previously been assigned the values of $J^\pi = 3/2^-$ and $5/2^+$ respectively (En 73). Accepting these as the correct spin and parity assignments, the smaller mixing ratio $\delta = -1.6^{+0.4}_{-0.6}$ for the transition from the 2488 keV level may be ruled out as it would lead to a M2 transition strength > 24 W.u.. The average mixing ratio of $\delta = -0.21 \pm 0.13$ or > 4.7 for the transition from the 2795 keV level is in agreement with the values of $\delta = 0.00 \pm 0.15$ or 8.0 ± 1.5 obtained by Champlin et al (Ch 71).

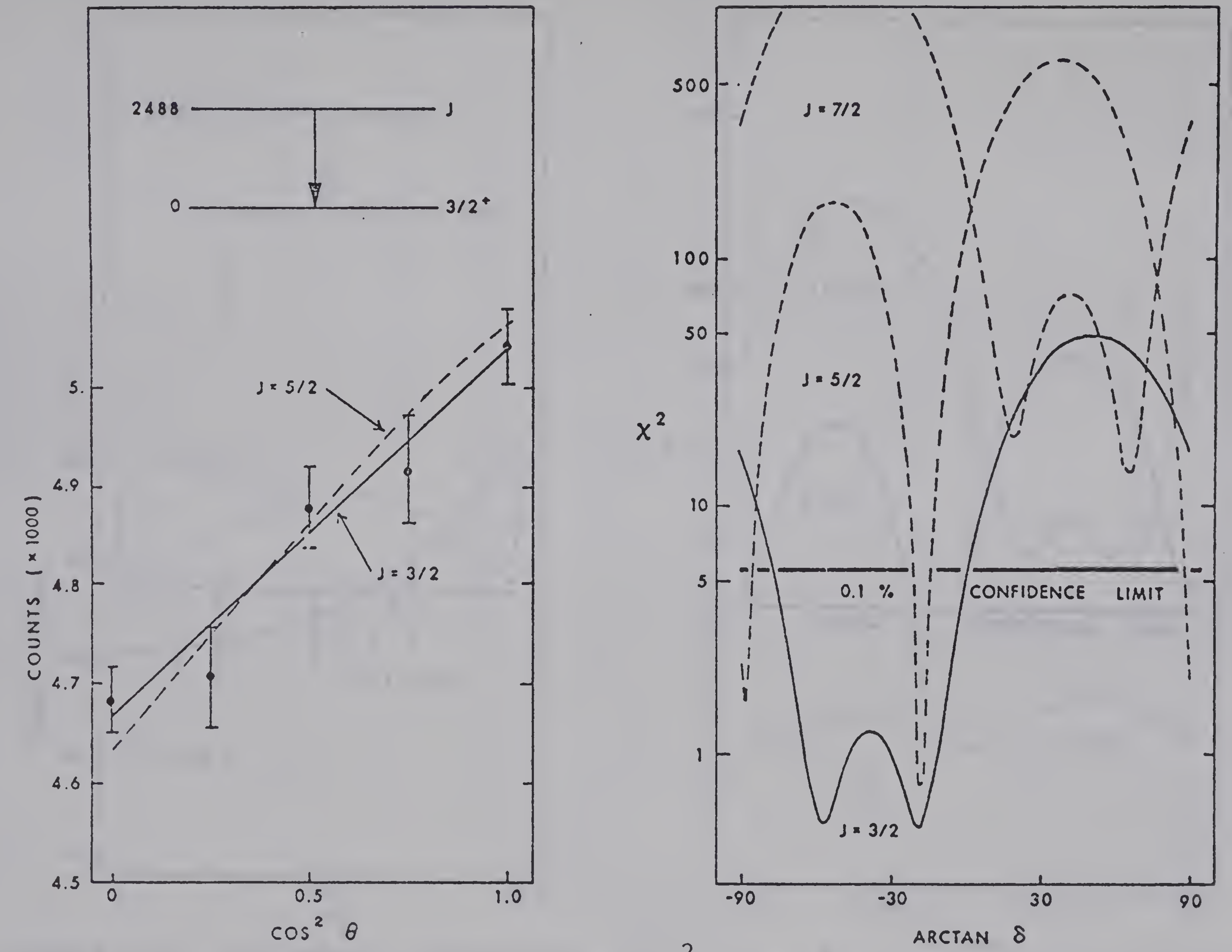

Figure 3.9 The angular distribution and χ^2 plot for the 2488 keV transition to the ground state.

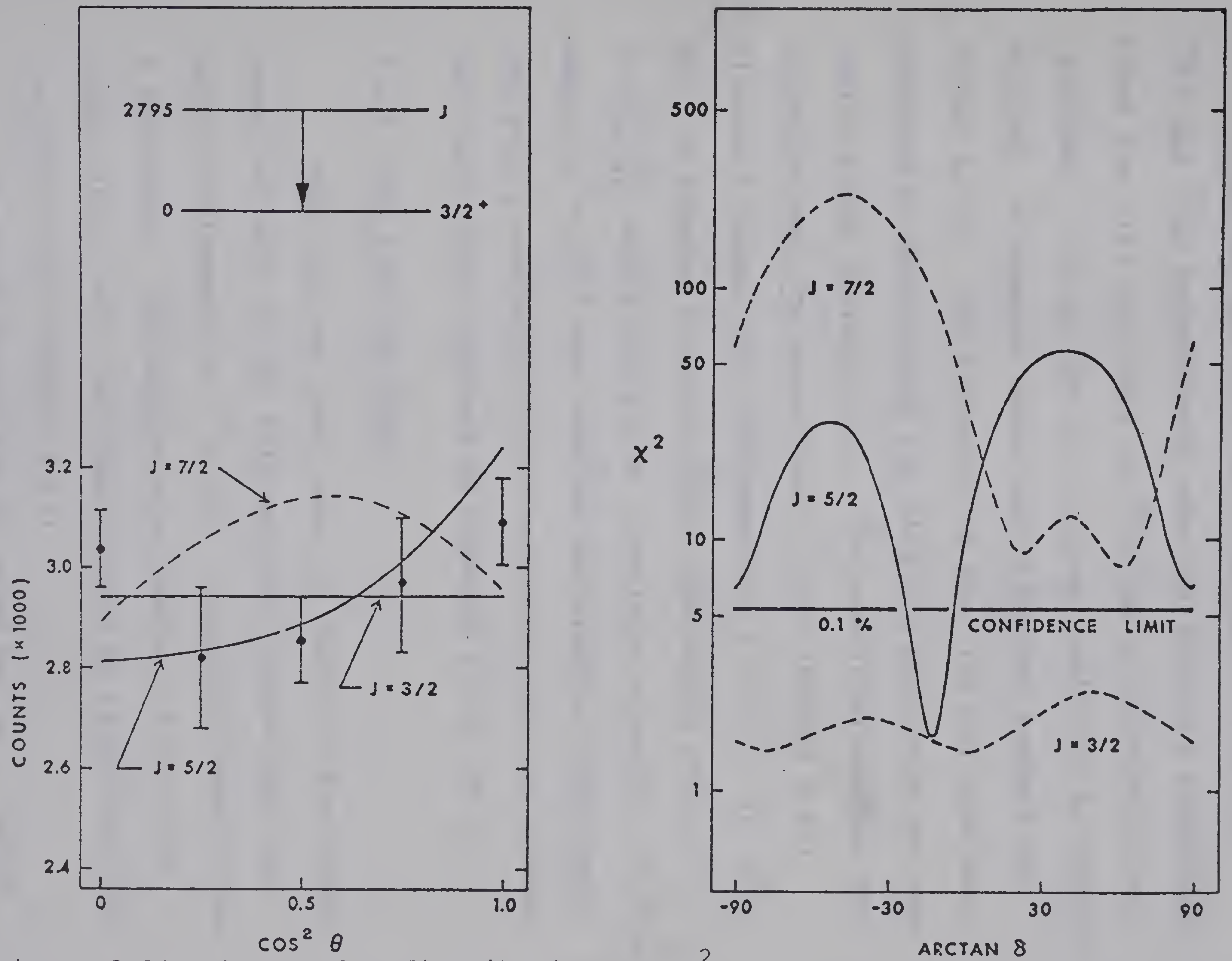

Figure 3.10 The angular distribution and χ^2 plot for the 2795 keV transition to the ground state.

[illegible]

3.4.5 The 3171 keV level

The 3163 and 3171 keV γ-ray peaks from the ^{35}Cl and ^{37}Ar respectively were not resolved completely. Since the 3163 keV level of ^{35}Cl has a relatively long lifetime, $\tau \sim 50$ ps (En 73) its peak would not be Doppler-shifted. A Gaussian shape was therefore assumed and fitted to it. The intensity of the 3171 keV peak was obtained by subtracting the 3163 keV peak from the composite peaks (Figure 3.11). The resulting angular distribution and its associated χ^2 plot (Figure 3.12) yielded a unique spin assignment of $J = 5/2$. If $J^\pi = 5/2^-$ is assumed for this level, the mixing ratio, $\delta = 0.78^{+0.82}_{-0.46}$, would yield a M2 transition strength > 24 W.u. making $J^\pi = 5/2^+$ the accepted assignment. These spin and parity and mixing ratio determinations are consistent with those reported by Champlin et al (Ch 71).

3.4.6 The 3185 keV level

The 3185 keV level does not decay to the ground state but only to the 1611 keV level whose spin and parity assignment is $J^\pi = 7/2^-$, suggesting that it has a high spin. The angular distribution of the 1574 ($3185 \rightarrow 1611$) keV γ ray indeed could be fitted only for $J = 9/2$ or $11/2$ (Figure 3.13).

Positive parity may be ruled out as it would require M2 transition strength > 374 and > 940 W.u. for

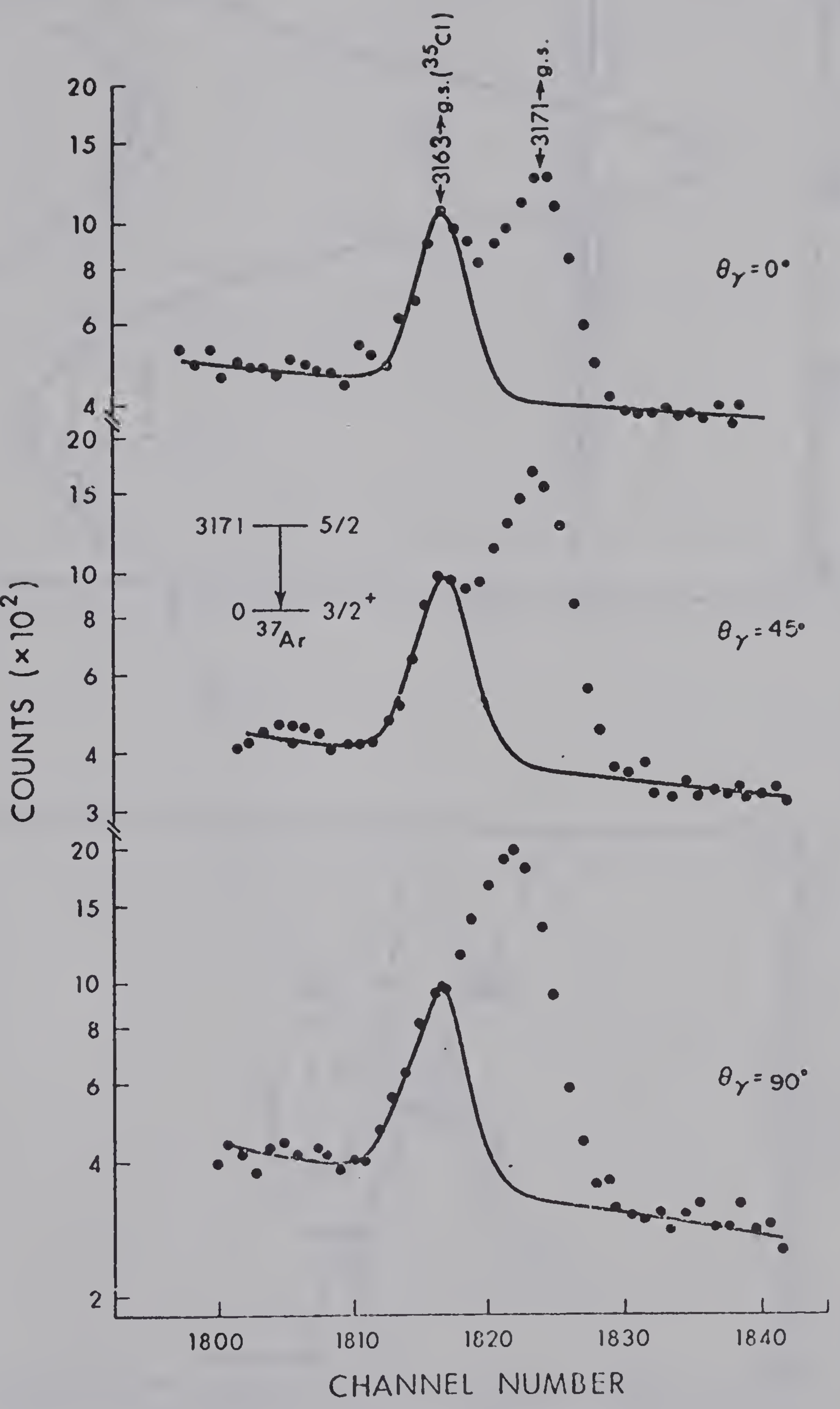

Figure 3.11 The full energy peaks of the 3163 and 3171 keV γ rays of the ^{35}Cl and ^{37}Ar respectively. The dots are experimental points. The solid curves represent the Gaussian fits of the 3163 keV γ rays with linear backgrounds which were removed to give intensities of the 3171 keV γ rays.

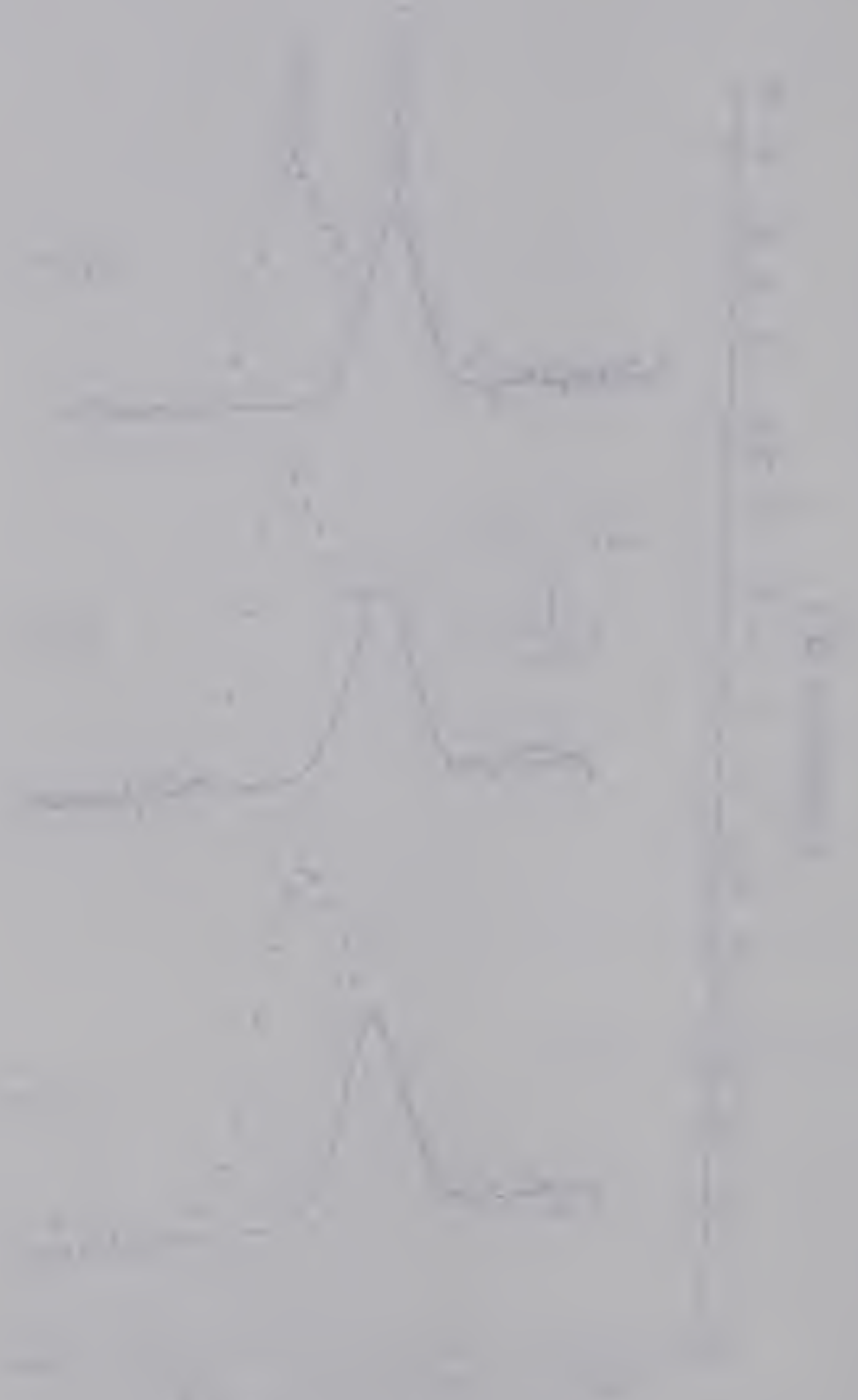

[illegible]

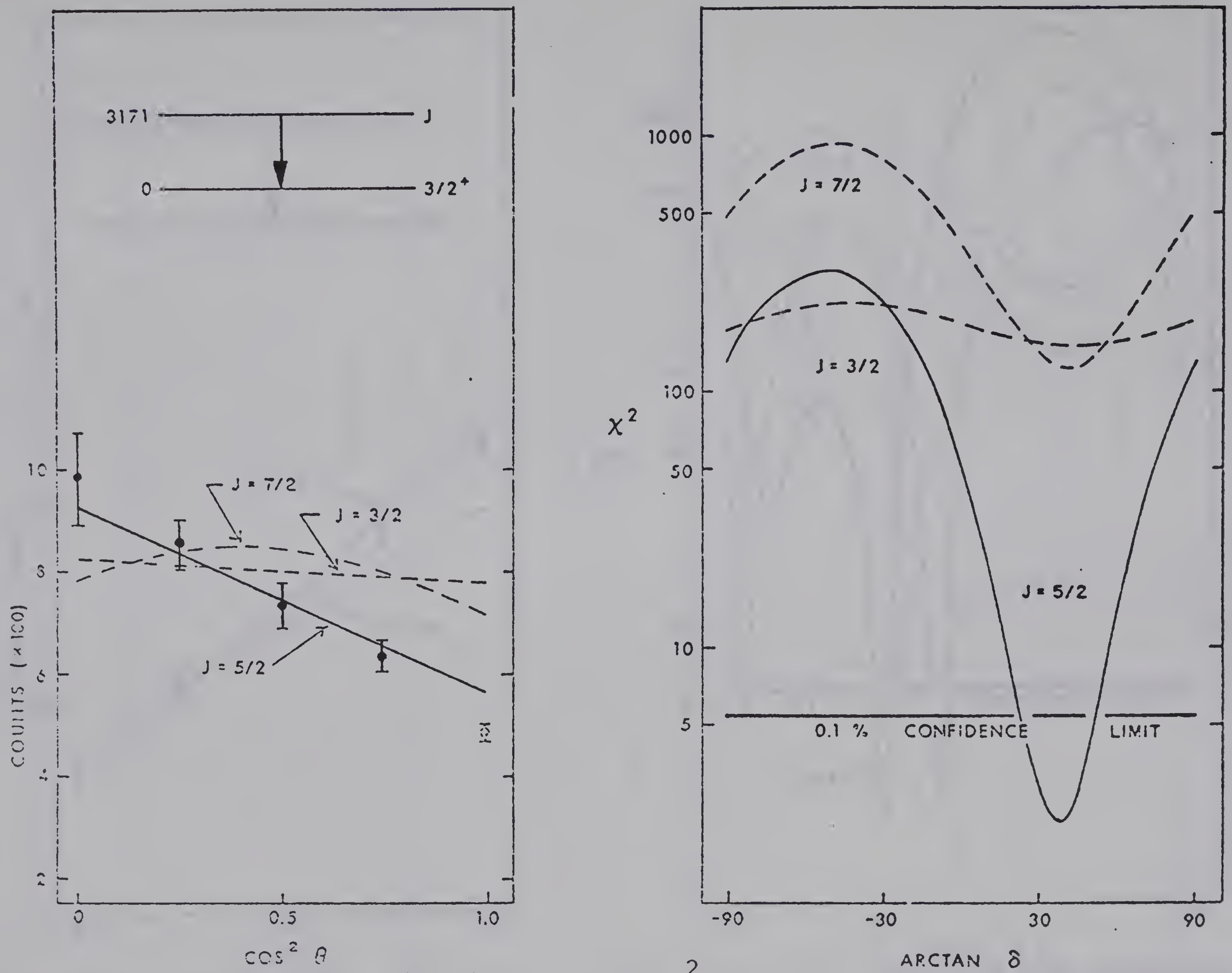

Figure 3.12 The angular distribution and χ^2 plot for the 3171 keV transition to the ground state. The difference in the angular distribution errors is due to the uncertainties of fitting.

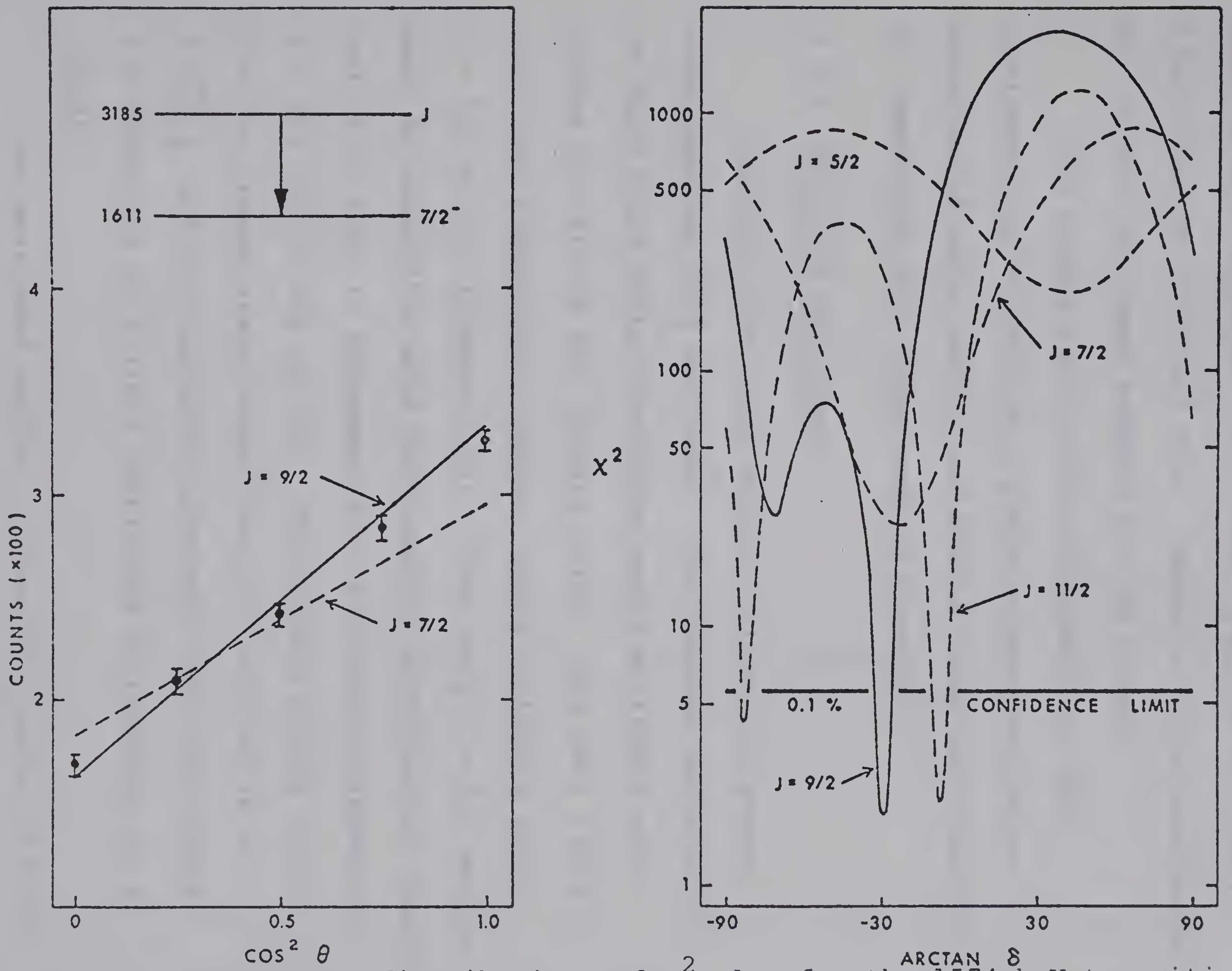

Figure 3.13 The angular distribution and χ^2 plot for the 1574 keV transition to the 1611 keV state.

[illegible]

J = 9/2 and 11/2 respectively. The J = $11/2^-$ assignment is also ruled out as it would require M3 transition strength >5.9×10^6 W.u.. Hence a unique assignment of J = $9/2^-$ has been adopted for this level.

The mixing ratio that corresponds to this assignment is -0.58±0.09. Since no previous determination of spin, parity and mixing ratio were reported, no comparison with other work is possible.

3.4.7 The 3274 keV level

The 3274 keV level decays to both the ground state and the 1611 keV level. The angular distribution of the ground state transition could be fitted with either J = 3/2 or 5/2 (Figure 3.14). The 1663 (3274 → 1611) keV transition, however, could be fitted with J = 5/2 or 7/2 (Figure 3.15). Thus only J = 5/2 assignment is compatible with both angular distribution results and it is also in agreement with previous assignment of J = 5/2 (Iv 71 and Lu 72). The allowed mixing ratio for the ground state transition, $\delta = -0.03 \pm 0.14$ or $4.0^{+5.5}_{-1.5}$, are in reasonable agreement with the values, $\delta = 0.20 \pm 0.25$ or 2.7 ± 0.5 determined by Champlin et al (Ch 71).

As mentioned earlier, during the course of this experiment several investigations have been reported to consolidate the electromagnetic properties of the low-

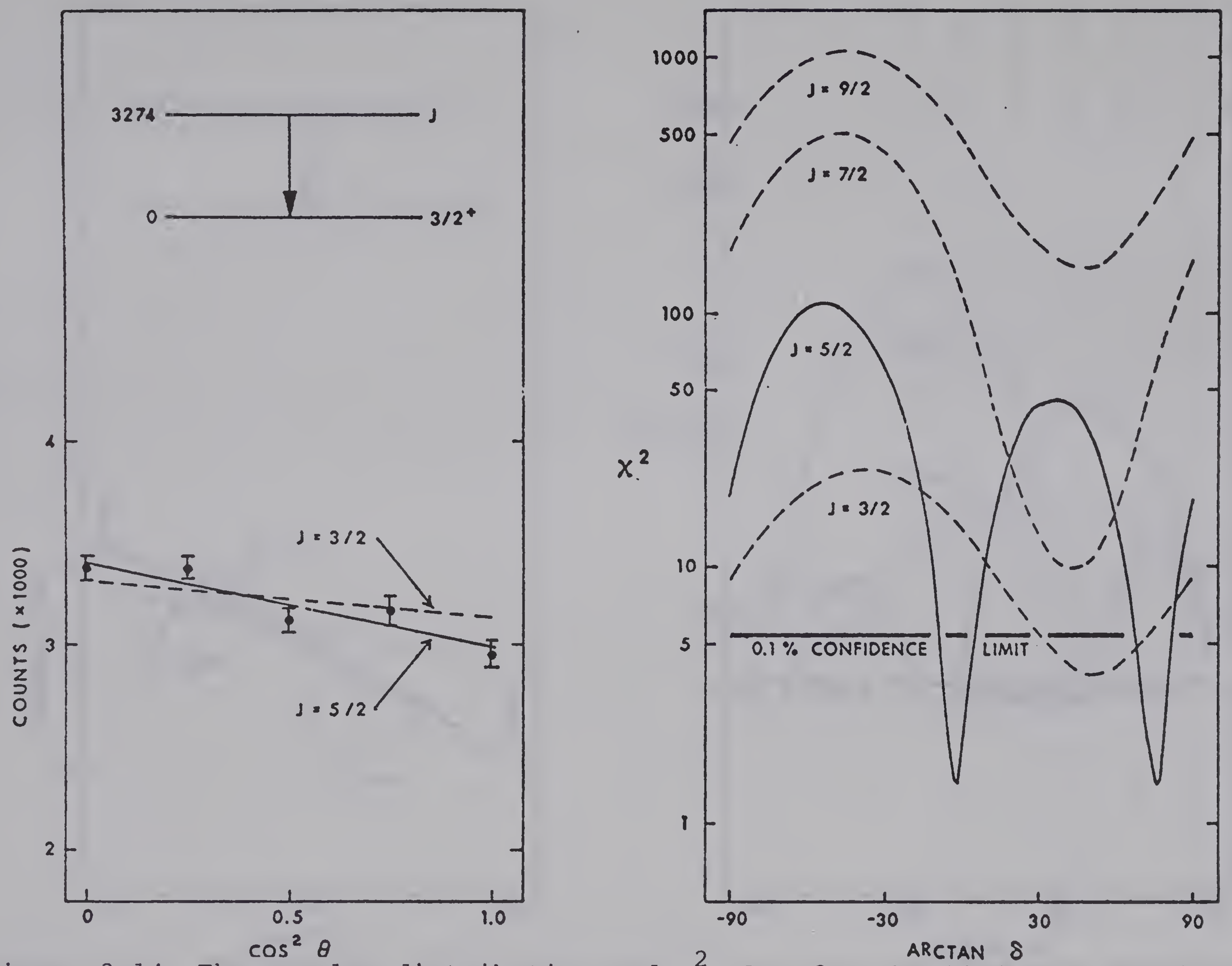

Figure 3.14 The angular distribution and χ^2 plot for the 3274 keV transition to the ground state.

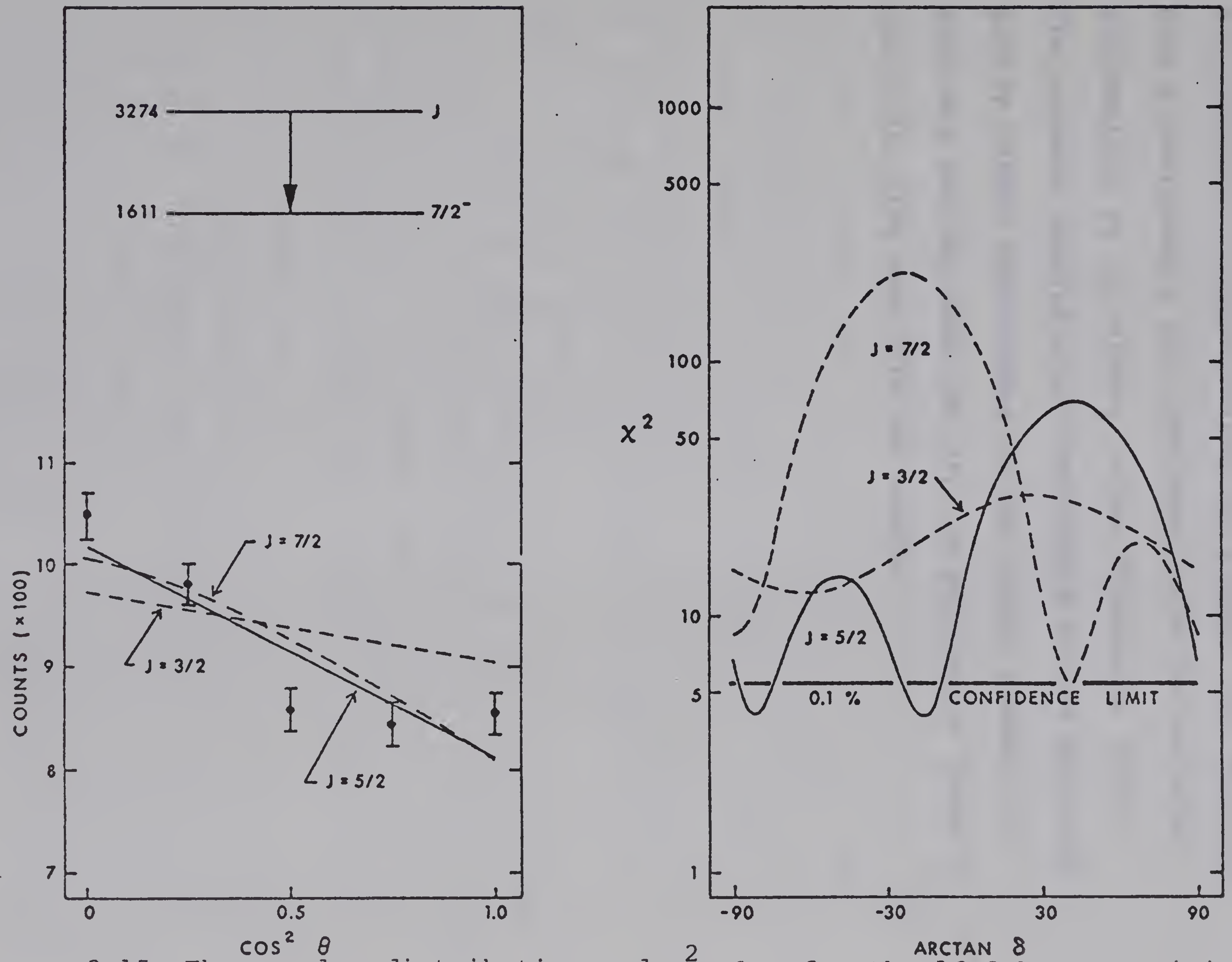

Figure 3.15 The angular distribution and χ^2 plot for the 1663 keV transition to the 1611 keV state.

[illegible]

lying levels in ^{37}Ar. As a result most of the spins and parities of these states are known. Our spin and parity assignments are consistent with the existing information as is evident in the discussion above. The present results also contributed to the spin and parity values established in the recent summary of Endt and van der Leun (En 73); in particular those of the 3171, 3185 and 3274 keV levels.

CHAPTER 4

NEUTRON TIME-OF-FLIGHT STUDIES OF THE $^{37}Cl(p,n)^{37}Ar$ REACTION

In the previous chapter, the statistical compound nuclear (SCN) model was applied in the γ-ray distribution analysis. The model independent analysis of the 1611 keV level has shown that the SCN model predictions were consistent. Nevertheless, its application was based upon the assumptions that the $^{37}Cl(p,n)^{37}Ar$ reaction proceeds via the compound nuclear mechanism and that a large number of levels are excited in the compound nucleus. A study of the neutrons following the reaction could justify these assumptions.

Neutron angular distributions will exhibit symmetry about 90° in the center-of-mass system if the reaction proceeds through the compound nucleus (En 66). Hence a search for this symmetry will indicate the validity of the first assumption.

The differential cross sections may be calculated using the statistical model (Hauser-Feshbach (Ha 52 and La 58)) to provide comparison with measured distributions. This would offer a test for the potentials and parameters used in the calculation as well as a test for the applicability of the statistical theory.

In addition to the justification of the SCN model, the neutron angular distributions would also enable one to determine the average recoil velocity of the residual nucleus ^{37}Ar knowledge of which is essential in the DSAM singles analysis where the outgoing neutrons are not observed (Chapter 1). Moreover, a neutron spectrum would show the levels in ^{37}Ar that are directly excited and thereby aid in the identification of the γ rays.

4.1 Compound Nucleus and Statistical Theory

Nuclear reaction can be classified into compound nuclear reactions or direct interactions according to a certain time scale, the nuclear period. This is defined as the time taken for the average bound nucleon to cross the nucleus and is typically in the order of 10^{-22} s (Pr 62). Direct interaction occurs instantaneously and has a reaction time in a 'nuclear period' region. On the other hand, one pictures the formation of the compound nucleus as a process in which the energy of the incident projectile is randomly distributed among the nucleons in the target. A particle within the compound system may gain sufficient energy through successive collisions to escape, hence the decay of the compound nucleus. Since this process requires many nuclear periods, one assumes that the compound nucleus has no recollection

of its formation when it decays. Consequently, the formation and decay can be considered as two independent processes.

At low energies, the cross section exhibits narrow isolated resonances which correspond to the levels in the compound nucleus. The widths, Γ, of these resonances which vary from around 0.03 to 2.0 eV, equivalent to lifetimes ($\tau = \hbar/\Gamma$) of 2.2×10^{-14} to 3.3×10^{-16} s, are characteristic of the compound nucleus according to the 'nuclear period' time scale. Therefore the average compound nuclear reaction cross section over any resonance structure of spin and parity, J^{π}, can be written as

$$\bar{\sigma}^{J\pi}_{\alpha\alpha'} = \sigma^{J\pi}_{\text{comp}}(\alpha) \left(\frac{G^{J\pi}_{\alpha'}}{\sum\limits_{\alpha''} G^{J\pi}_{\alpha''}} \right) \qquad (4.1)$$

where $\sigma^{J\pi}_{\text{comp}}(\alpha)$ is the cross section for the formation of the compound nucleus through channel α and the factor $[G^{J\pi}_{\alpha'}/\sum_{\alpha''} G^{J\pi}_{\alpha''}]$ is the branching ratio of its decay through channel α'. The summation over α'' extends over all decaying channels.

Since compound nuclear reactions conserve particle flux and are invariant under time reversal, it follows that any reaction and its reverse reaction will satisfy the reciprocity theorem.

$$\frac{k^2_{\alpha}\ \bar{\sigma}^{J\pi}_{\alpha\alpha'}}{g^J_{\alpha}} = \frac{k^2_{\alpha'}\ \bar{\sigma}^{J\pi}_{\alpha'\alpha}}{g^J_{\alpha'}} \qquad (4.2)$$

in which

$$g_\alpha^J \equiv \frac{(2J + 1)}{(2I + 1)(2i + 1)} \tag{4.3}$$

is the statistical spin factor. J is the spin of the compound nucleus. I and i are the spins of the particles in channel α and k_α is the wave number for the relative motion of these particles. The superscript, ', denotes the corresponding quantities for the reverse reaction whose cross section is described by $\bar{\sigma}^{J\pi}_{\alpha'\alpha}$. From Equations 4.1 and 4.2 one obtains the relation,

$$G_\alpha^{J\pi} = \frac{k_\alpha^2 \, \sigma^{J\pi}_{\text{comp}}(\alpha)}{g_\alpha^J} \quad . \tag{4.4}$$

As the mass number and the excitation energy of the compound nucleus increase, the number of resonances excited increases and the average spacing, D, between the resonances decreases. If the experimental condition is such that the spread of the beam energy, ΔE, encompasses many of the resonances ($\Delta E >> D$), the average cross section must take into consideration transitions through all these resonances of different J^π simultaneously, namely,

$$\bar{\sigma}_{\alpha\alpha'} \equiv \sum_{J\pi} \bar{\sigma}^{J\pi}_{\alpha\alpha'} \quad . \tag{4.5}$$

At some energies the average widths of the resonances will exceed the average spacing between them ($\Gamma > D$). The resulting overlap of resonances introduces interference terms in the cross section. In order to deal with these interfering terms, one invokes the statistical theory which assumes that there are many resonances within the energy interval and that their widths and separation energies are randomly distributed. As a result the interference will average out to zero and the interference between the levels of the compound nucleus may be neglected.

Also, it has been shown that the various incoming and outoing partial waves do not interfere among themselves (Bl 52 and Pi 69); a consequence of which is that the average cross section can now be described by energy averaged transmission coefficients which are related to the optical model phase shifts, $\delta_{\alpha\ell}$, according to,

$$T_\ell(\alpha) = 1 - \left| e^{2i\delta_{\alpha\ell}} \right|^2 \quad . \tag{4.6}$$

The optical model views the formation of the compound nucleus as an absorption of the incident particle by the target. Hence the compound nucleus cross section is analogous to the optical-model absorption cross section.

$$\sigma_{abs}(\alpha) \equiv \sum_{J\pi} \sigma^{J\pi}_{comp}(\alpha) \quad . \tag{4.7}$$

In terms of the complex phase shifts, the absorption cross section is

$$\sigma_{abs}(\alpha) = \sum_{J\pi} \pi \frac{g_\alpha^J}{k_\alpha^2} \sum_{s\ell} \left(1 - \left|e^{2i\delta_{\alpha\ell}}\right|^2\right) \tag{4.8}$$

in which the channel spin formalism has been adopted, i.e.

$\vec{I} \equiv$ intrinsic spin of target

$\vec{i} \equiv$ intrinsic spin of projectile

$\vec{\ell} \equiv$ orbital angular momentum of the pair

$\vec{s} = \vec{I} + \vec{i} \equiv$ channel spin

$\vec{J} = \vec{s} + \vec{\ell} \equiv$ total angular momentum.

From Equations 4.4, 4.6, 4.7 and 4.8 it follows that

$$G_\alpha^{J\pi} = \pi \sum_{s\ell} T_\ell(\alpha) \quad . \tag{4.9}$$

The combination of Equations 4.1, 4.8 and 4.9 yields the average compound nuclear reaction cross section in terms of the transmission coefficients (Vo 68)

$$\bar{\sigma}_{\alpha\alpha'} = \frac{\pi}{k_\alpha^2} \sum_{J\pi} g_\alpha^J \sum_{s\ell} T_\ell(\alpha) \frac{\sum_{s'\ell'} T_{\ell'}(\alpha')}{\sum_{s''\ell''} T_{\ell''}(\alpha'')} \quad . \tag{4.10}$$

The unprimed and primed quantities refer to the incoming and outgoing channels respectively. Again the sum in the denominator extends over all channels through which the compound nucleus decays.

In the channel spin notations, the transmission coefficient is independent of J and s. This will no longer be true if spin-orbit coupling is present and one must replace each $\sum_{s\ell} T_\ell(\alpha)$ in Equation 4.10 by $\sum_{j\ell} T_{\ell j}(\alpha)$ where

$$\vec{j} = \vec{i} + \vec{\ell} \qquad (4.11)$$

and $T_{\ell j}(\sigma)$ is related to the optical model phase shift, $\delta_{\ell j\alpha}$ by

$$T_{\ell j}(\alpha) = 1 - \left|e^{2i\delta_{\ell j\alpha}}\right|^2 . \qquad (4.12)$$

One can alternatively define transmission coefficient, $T_{s\ell J}(\alpha)$, to depend on s and J instead of j. The choice of s or j as quantum numbers dictates the angular momentum coupling scheme used. The two transmission coefficients are related by

$$T_{s\ell J}(\alpha) = \sum_j (2j+1)(2s+1)\ W^2(\ell IJi;js)\ T_{\ell j}(\alpha) \qquad (4.13)$$

in which $W(\ell IJi;js)$ is a Racah coefficient. With this choice of transmission coefficient, one simply adds the subscripts, s and J, to each transmission coefficient in Equation 4.10 to include spin orbit coupling.

Based on the approximation that no interference occurs between all incoming and outgoing partial waves, the SCN model can be extended to describe differential

cross sections. The extension, however, concerns only the geometry and not the nuclear physics of the reaction. It involves lengthy calculation of Racah algebra and has been treated by many authors (Bl 52, Sh 66 and Vo 68). The average differential cross section as derived by Vogt (Vo 68) is

$$\frac{d\bar{\sigma}_{\alpha\alpha'}}{d\Omega} = \sum_{L} \frac{1}{4k^2} \sum_{J\pi} \frac{1}{(2I+1)(2i+1)} \sum_{s\ell s'\ell'} \left(\frac{T_{\ell}(\alpha)\; T_{\ell'}(\alpha')}{\sum_{s''\ell''\alpha''} T_{\ell''}(\alpha'')} \right)$$

$$\times\ Z(\ell J \ell J; sL)\, Z(\ell' J \ell' J; s'L)\, (-)^{s-s'}\ P_L(\cos\theta) \tag{4.14}$$

where

$$Z(\ell J \ell' J'; sL) = (i)^{L-\ell+\ell'} \{(2\ell+1)(2\ell'+1)(2J+1)(2J'+1)\}^{\frac{1}{2}}$$

$$\times\ W(\ell J \ell' J'; sL)\,(\ell 0 \ell' 0 | L0)\ . \tag{4.15}$$

The lack of interference has a direct consequence on the shape of the average angular distributions; making them symmetric about 90°. This property of Equation 4.14 is manifested through the coefficient $Z(\ell J \ell' J'; sL)$ which vanishes unless L is even.

4.2 Experimental Method

To study the neutrons from the $^{37}Cl(p,n)^{37}Ar$ reaction, the time-of-flight technique was used. A pulsed

proton beam of 10 ns duration with repetition rate of 1 mHz was obtained from the van de Graaff accelerator and compressed to ∿0.5 ns by a Mobley magnet bunching system (Mc 67).

The electronics associated with the neutron detection and timing is shown in Figure 4.1. A cylindrical capacitive pickoff in front of the target signals the arrival of the protons. These signals are, however, delayed and used to stop the time-to-amplitude converter (TAC 1). Neutrons are detected by a 9 cm diameter by 1.9 cm thick NE213 liquid scillator optically coupled to an RCA 8575 photo-multiplier. The fast output of the detector is sent to a constant fraction pulse height trigger (CFPHT) which provides the (TAC 1) with the starting pulses. The output of the (TAC 1) is a time spectrum and is fed into an analog-to-digital converter (ADC) interfaced to the on-line computer (Honeywell 516).

Gamma rays resulting from the reaction are also detected by the liquid scintillator. In order to reduce the γ-ray background, a n-γ discriminator is set up. This discrimination is based on the different rise times of the neutron and γ-ray pulses and is similar to the arrangement described earlier in Section 2.2. Namely, the fast and slow signals from the detector are used as starting and stopping pulses for a second time-to-amplitude converter (TAC 2). The different rise times

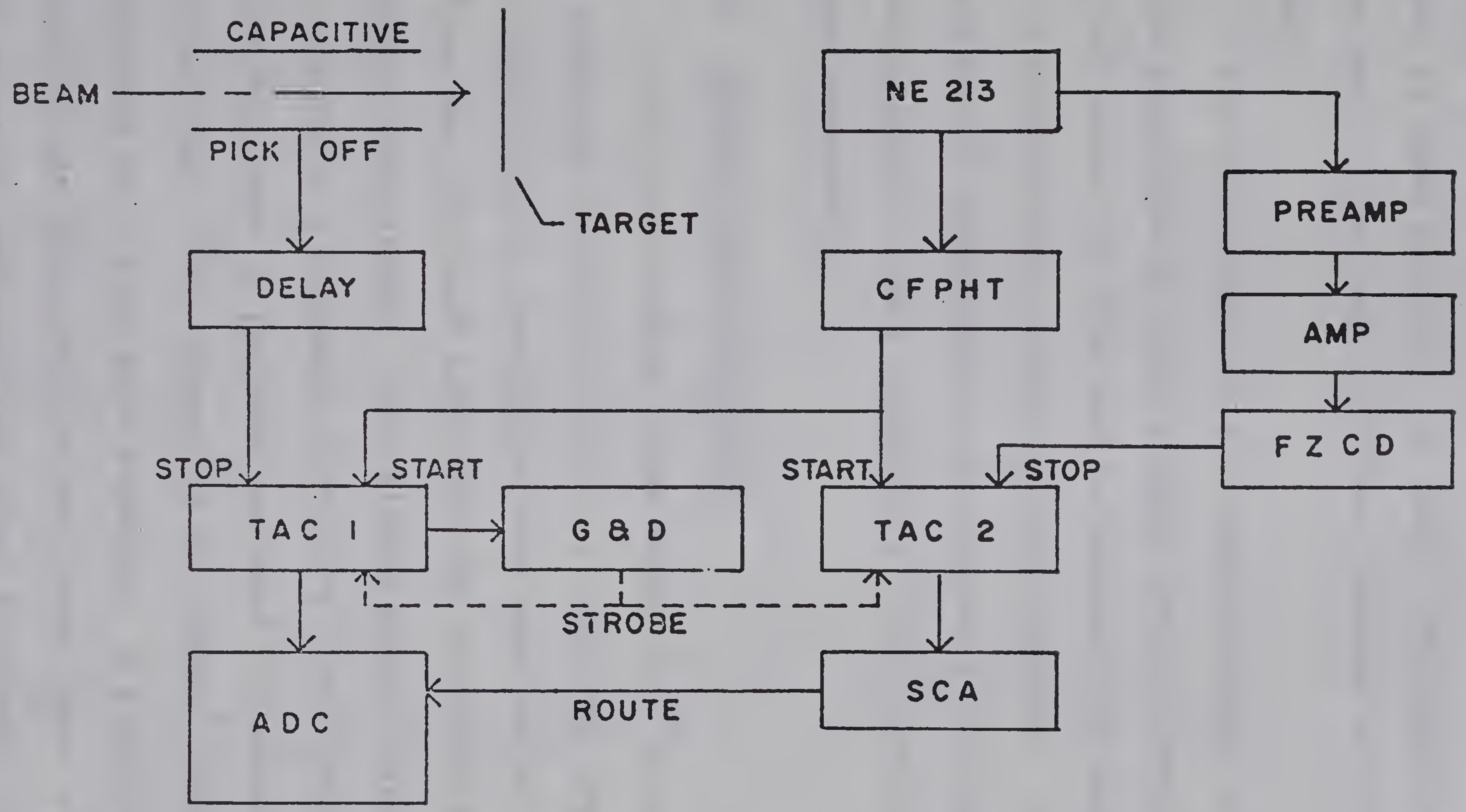

Figure 4.1 A block diagram of the neutron time-of-flight electronics.

of the neutrons and γ rays yield two peaks in the output of (TAC 2). A window is placed on the peak corresponding to γ rays in the single channel analyzer (SCA) whose output is used to route the (ADC) and separate the neutrons and γ rays into different regions of the computer memory.

The objectives of the neutron study as mentioned in the beginning of this chapter are to identify the excited states of ^{37}Ar and to measure the neutron angular distributions leading to these states. Although the experimental arrangements are basically the same for both investigations, other conditions differ and will be discussed separately.

4.2.1 Neutron identification

In γ-ray studies a new level in ^{37}Ar at 3185 keV was proposed (Section 2.4.1). To confirm its existence, good experimental resolution was required to separate it from the 3171 keV level and the conditions were arranged accordingly. The liquid scintillator detector was placed at a distance of 6.32 m from the target at 0°. A 5.90 MeV beam of protons was used to bombard a $PbCl_2$ (78% enriched ^{37}Cl) target of 0.1 mg/cm^2 thickness evaporated on 0.5 mm gold backing. A total charge of 50,000 μC was collected on the target over a period of 10 h to yield the spectrum shown in Figure 4.2.

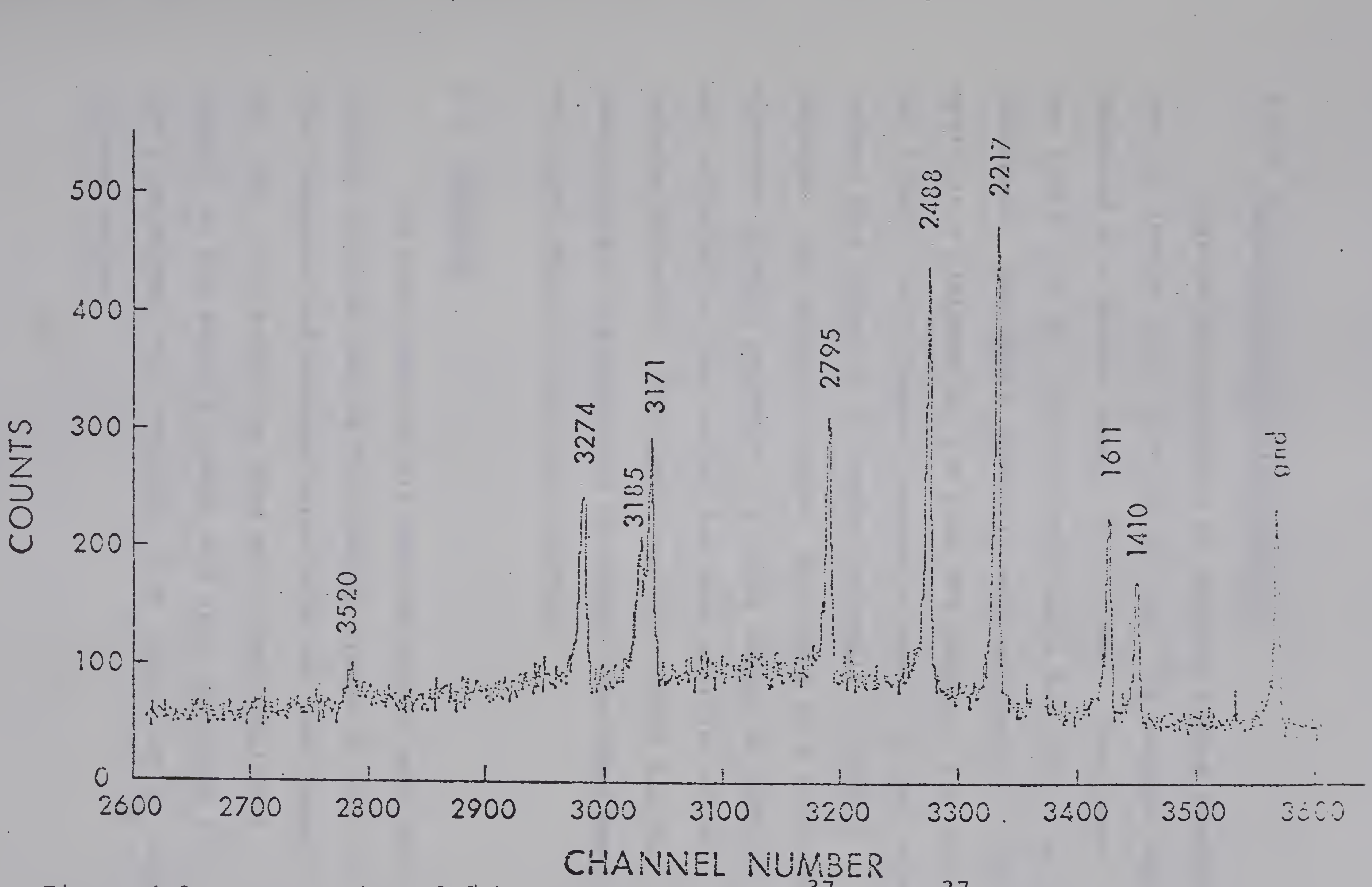

Figure 4.2 Neutron time-of-flight spectrum of the ^{37}Cl(p,n)^{37}Ar reaction observed with a flight path of 6.3 m at $E_p = 5.90$ MeV. A total charge of 50,000 μC was collected on the target. The neutron groups are indicated by their energies as determined from this experiment.

4.2.2 Neutron angular distribution

Angular distributions of neutron groups populating all levels up to 3274 keV in the ^{37}Ar nucleus were measured at a proton energy of 5.75 MeV. The target was similar to the one mentioned above but of 1.0 mg/cm^2 thickness. Two NE213 detectors were mounted on a cart 5° apart at a distance of 4 m from the target. The cart was rotated in 15 degree intervals from 0° to 145° with repeat runs taken at 30 degree intervals. A third detector, the monitor counter, was fixed at 2 m in the opposite forward quadrant. A total charge of 2000 μC was collected on the target for each position of the neutron detector. The target was air cooled and the neutron yield was monitored throughout the experiment. No target deterioration was observed.

4.3 Analysis

The peak areas of all neutron groups were extracted with the aid of the display system of the online computer and checked later with the code 'Summit' (Gr 71a). The resulting sums were normalized with respect to the monitor counts and also corrected for (ADC) deadtimes and conversion from laboratory to center-of-mass angles.

In order to calculate the absolute cross section the efficiencies of the neutron detectors were required. The detector efficiencies versus neutron energies were obtained by a computer code 'Effi' (Gr 67) (Figure 4.3). Since the efficiency curves were particularly sensitive for low energy neutrons the detector thresholds had been determined carefully before and after the runs. Nevertheless, for neutrons below 1.4 MeV in energy the error in efficiency was determined by assuming a 50 keV uncertainty in neutron energy and for the higher energy neutrons, a 5% efficiency error was imposed.

The absolute differential cross section was then calculated according to the formula:

$$\frac{d\sigma}{d\Omega} = \frac{\Delta N}{N\, n\, \Delta x\, \Omega} \tag{4.16}$$

in which ΔN ≡ number of detector neutrons
N ≡ number of incident protons
n ≡ number of target nuclei per unit volume
Δx ≡ thickness of target
Ω ≡ solid angle subtended by detector.

Experimentally, N is determined from the total charge collected on the target and ΔN is determined from the area under the neutron peak after all corrections have been taken into account.

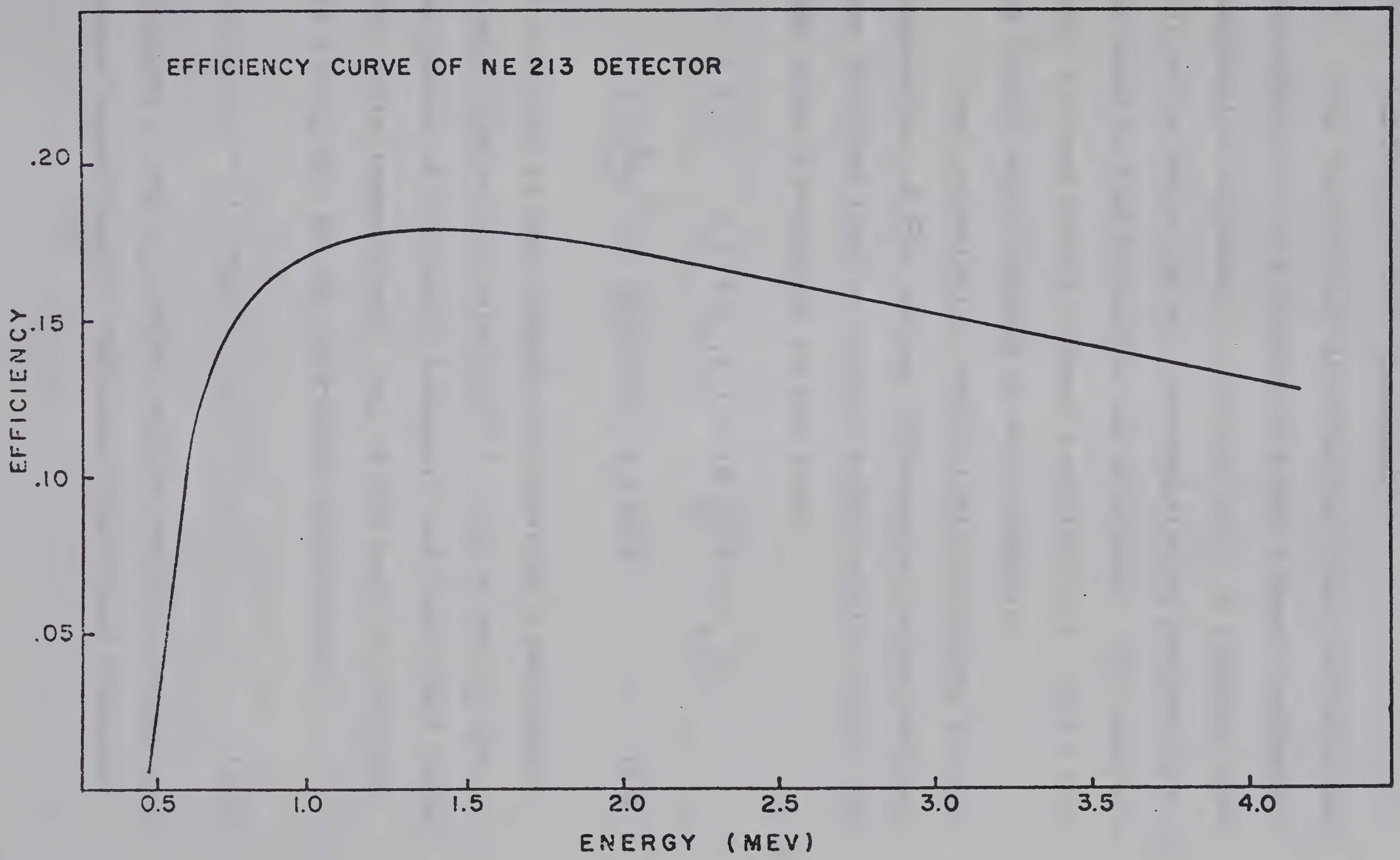

Figure 4.3 A detector efficiency vs neutron energy curve.

4.3.1 Hauser-Feshbach calculation

The theoretical differential cross sections were determined by the statistical model (Hauser-Feshbach) calculation discussed in Section 4.1. A computer code written by Smith (Sm 65) and modified by Davison (Da 69) was used to facilitate the calculations. All energetically allowed proton induced reaction (i.e. (p,p')(p,n) and (p,α)) were included as exit channels.

The transmission coefficients necessary for the computation of the average differential cross section were obtained from an optical model routine within the code using a potential in the form

$$U(r) = V_c(r) - V_o f(r,r_o,a_o) + iW \frac{d}{dr} f(r,r_i,a_i)$$

$$+ \left(\frac{h}{m_\pi c}\right)^2 V_s \frac{d}{rdr}\{f(r,r_o,a_o)\}\vec{\ell}\cdot\vec{\sigma} \qquad (4.17)$$

where $V_c(r)$ is the Coulomb potential of a uniformly charged sphere of radius $r_oA^{1/3}$. V_o, W and V_s are the depths of the real, imaginary and spin-orbit potential wells respectively. m_π is the mass of the pion and $f(r,r_o,a_o)$ is the Wood-Saxon form factor,

$$f(r,r_o,a_o) = \{1+\exp[(r-r_oA^{1/3})/a_o]\}^{-1} \quad . \qquad (4.18)$$

in which r_o and a_o are the radius and diffuseness parameters respectively. The subscripts o and i denote

respectively the quantities contained in the real and imaginary terms involved. One notes that the derivative form of the form factor in Equation 4.17 produces surface absorption.

The optical model parameters that were used in the calculations are tabulated in Table 4.1.

4.4 Results and Discussion

The neutron identification investigation using the thin 0.1 mg/cm^2 target at a proton bombarding energy of 5.90 MeV shows neutron groups leading to the excited states in ^{37}Ar (Figure 4.2). It is evident that a doublet corresponding to the 3171 and 3185 keV levels exists. This is a direct confirmation of the 3185 keV level that was postulated from the γ-ray experiments (Chapters 2 and 3).

Angular distributions of all neutron groups populating states below 3274 keV excitation in ^{37}Ar have been measured at an incident energy of 5.75 MeV. The thicker (1 mg/cm^2) target and shorter flight distance, however, did not allow the 3171 and 3185 keV states to be resolved. Therefore their differential cross sections were not calculated. The differential cross sections of all the other states are presented in Figure 4.4 (a to g).

The theoretical (Hauser-Feshbach) differential cross sections for various spin values are shown by the

Table 4.1

Optical Model Parameters

	Proton (Ro 65)	Neutron (Pe 62)	Alpha (Da 69)
V_0 (MeV)	53.8	41.35	185.0
W (MeV)	7.5	3.95	20.0
V_s (MeV)	5.5	7.2	0.0
r_0 (fm)	1.25	1.32	1.50
r_i (fm)	1.25	1.25	1.70
a_0 (fm)	0.65	0.62	0.80
a_i (fm)	0.70	0.65	0.60

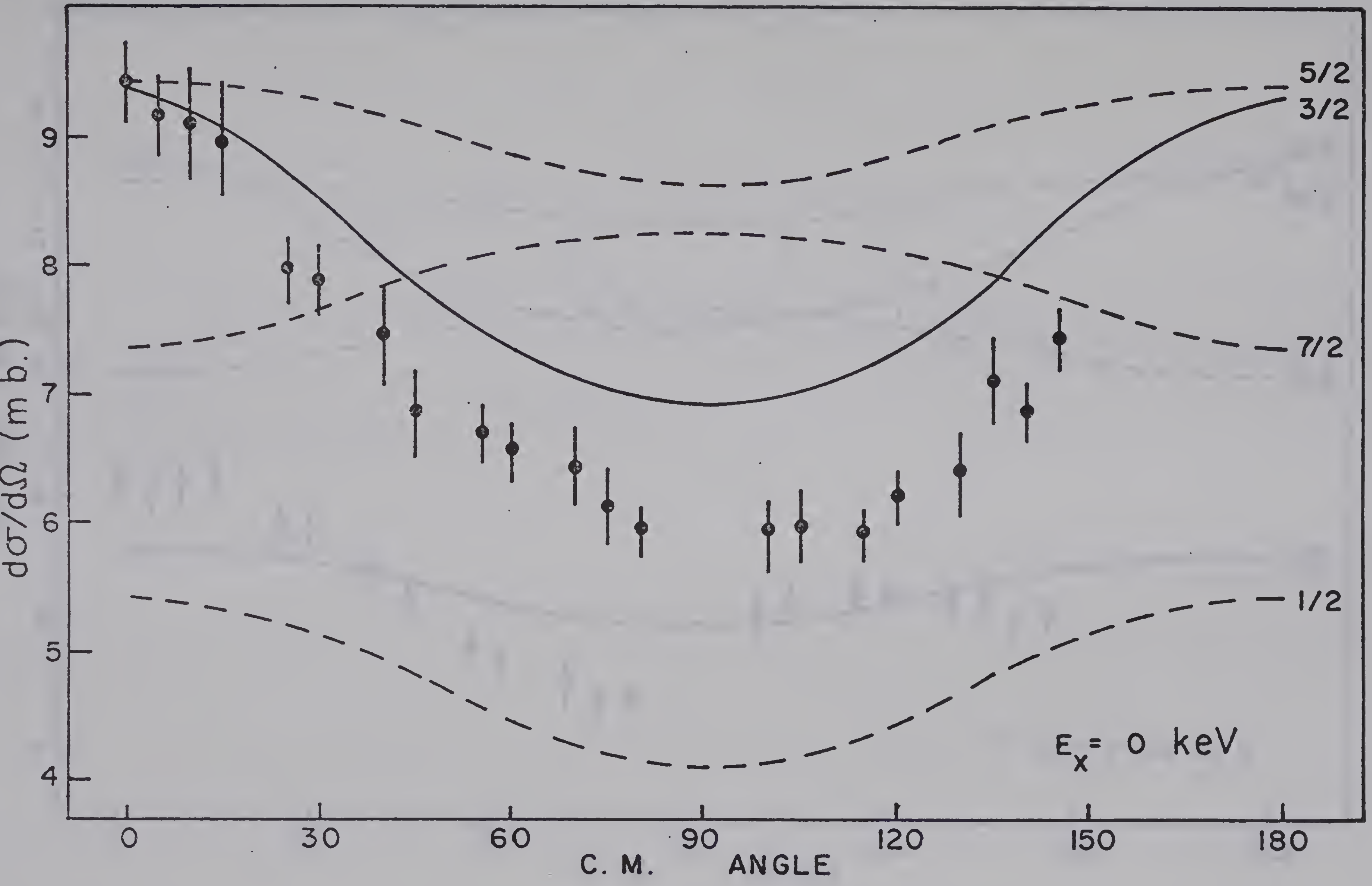

a) The ground state

Figure 4.4 Differential cross sections of neutrons leading to states in the ^{37}Ar nucleus.

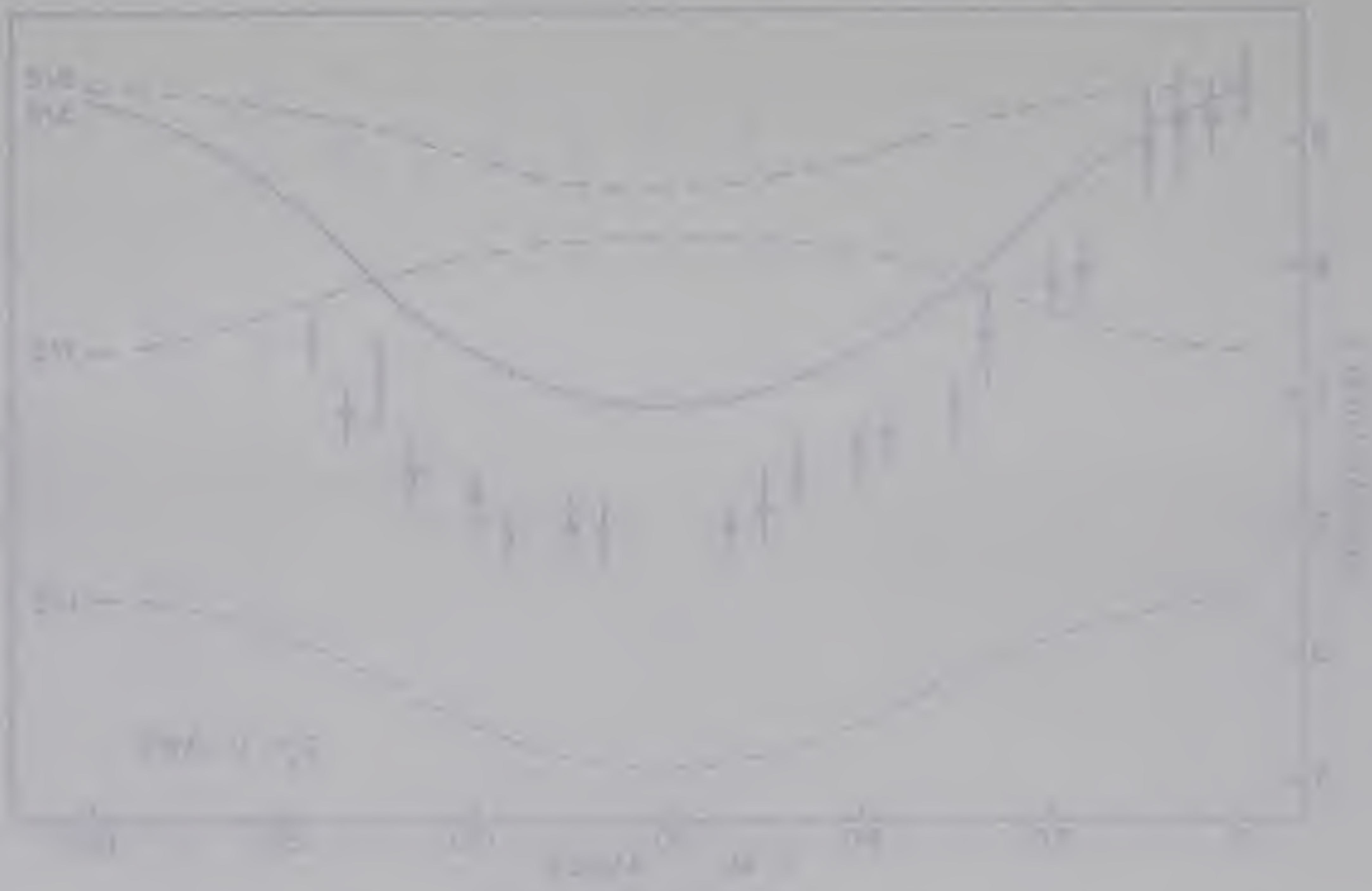

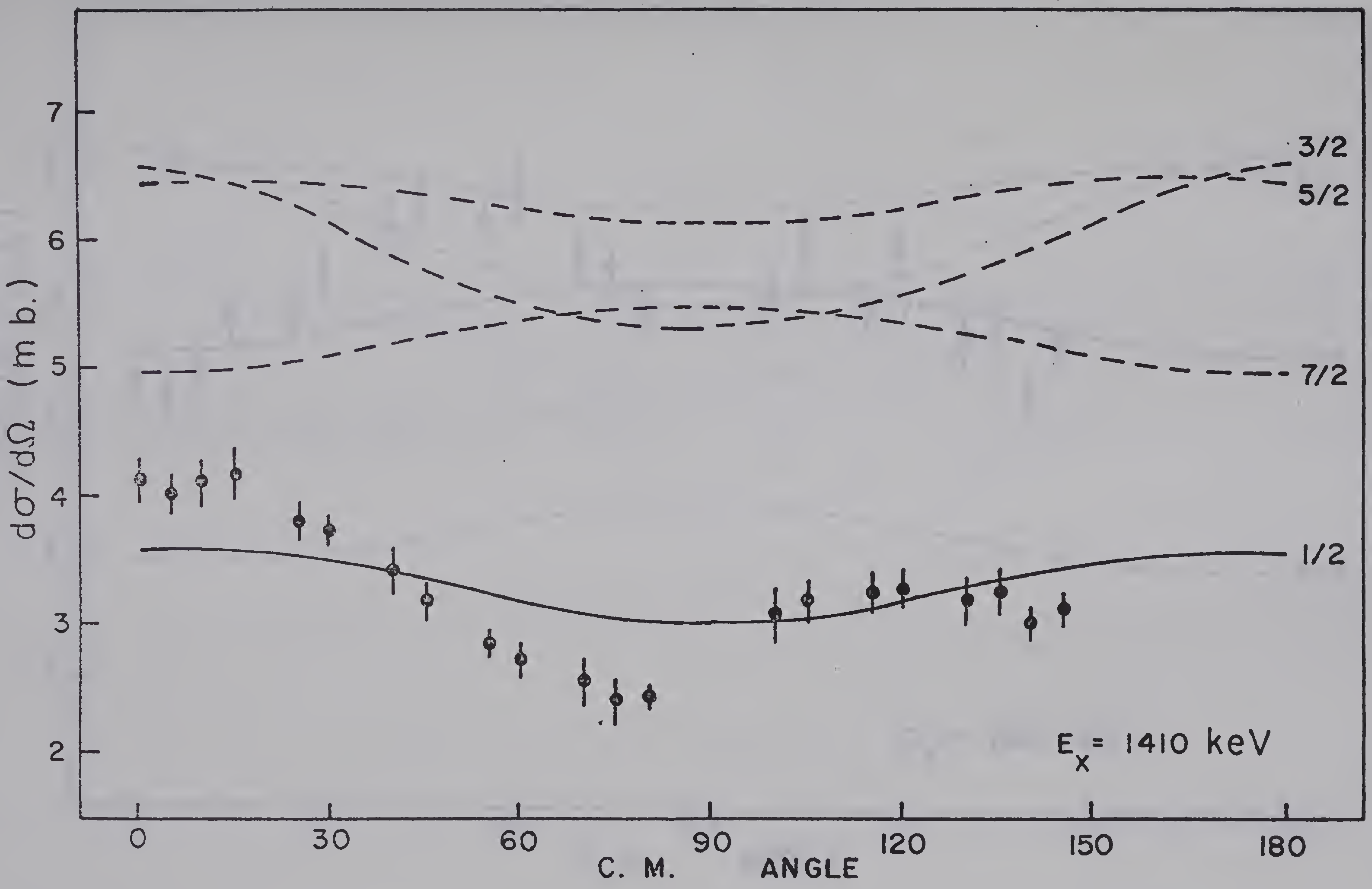

Figure 4.4 b) The 1410 keV state

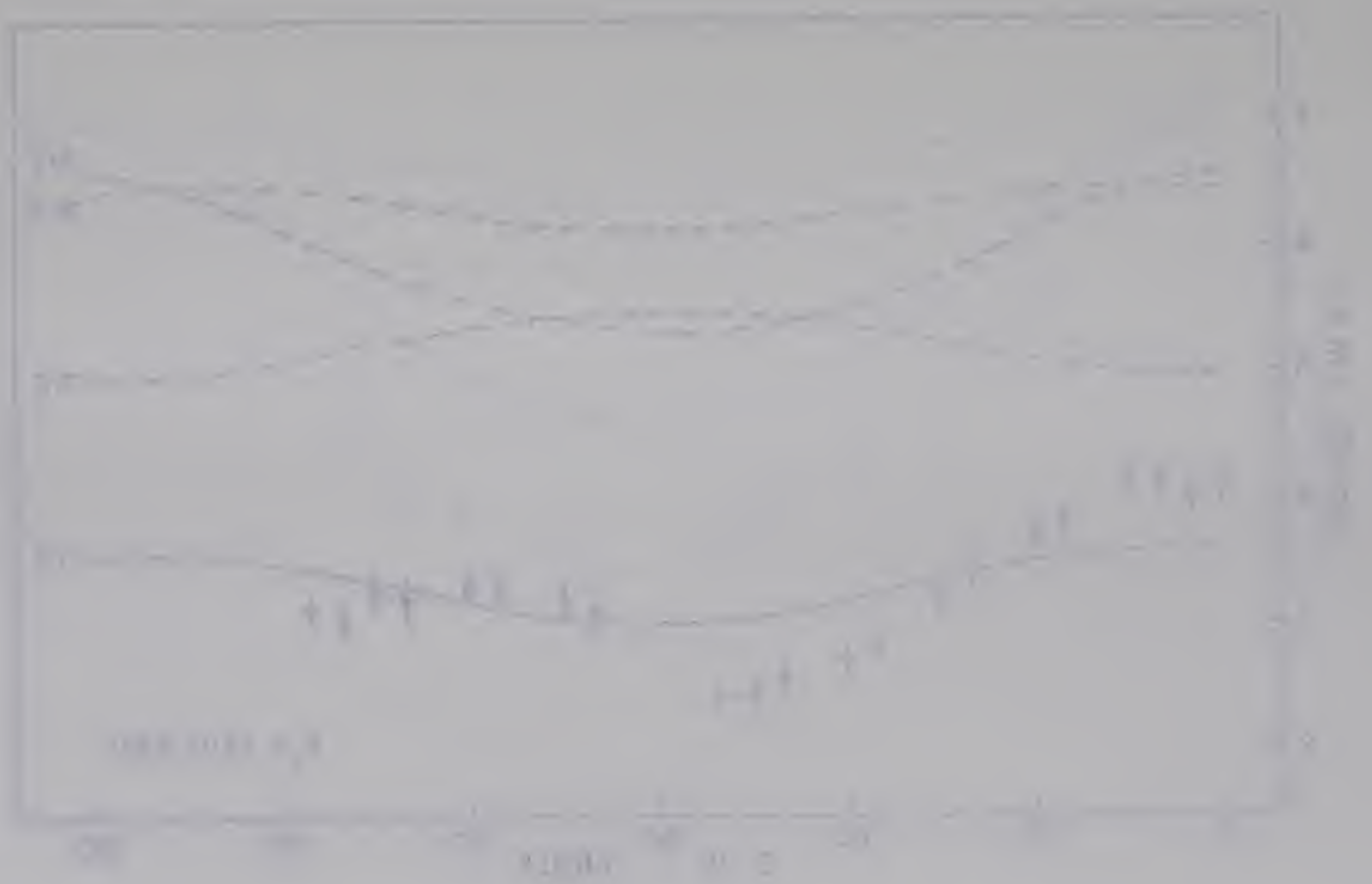

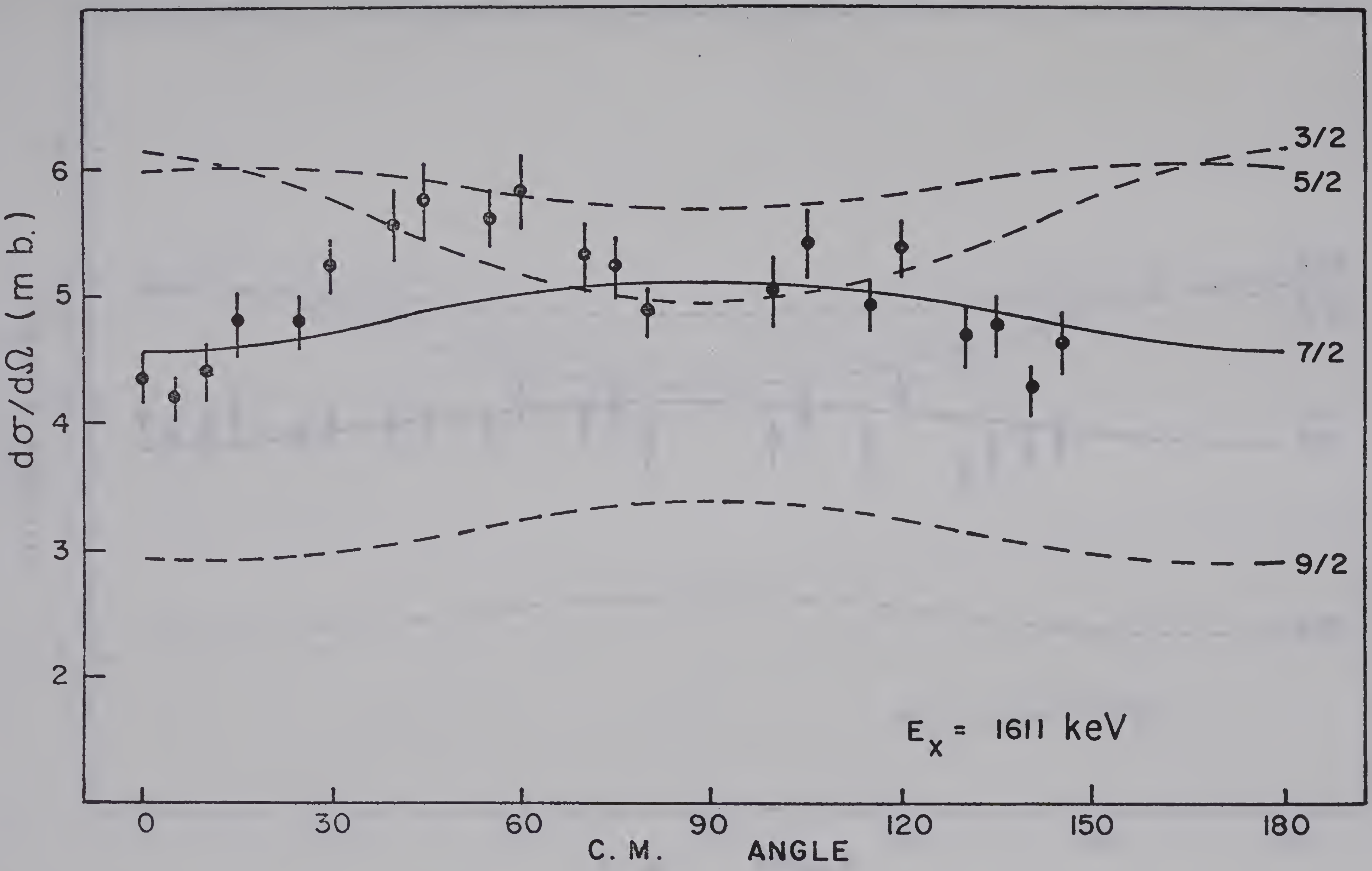

Figure 4.4 c) The 1611 keV state

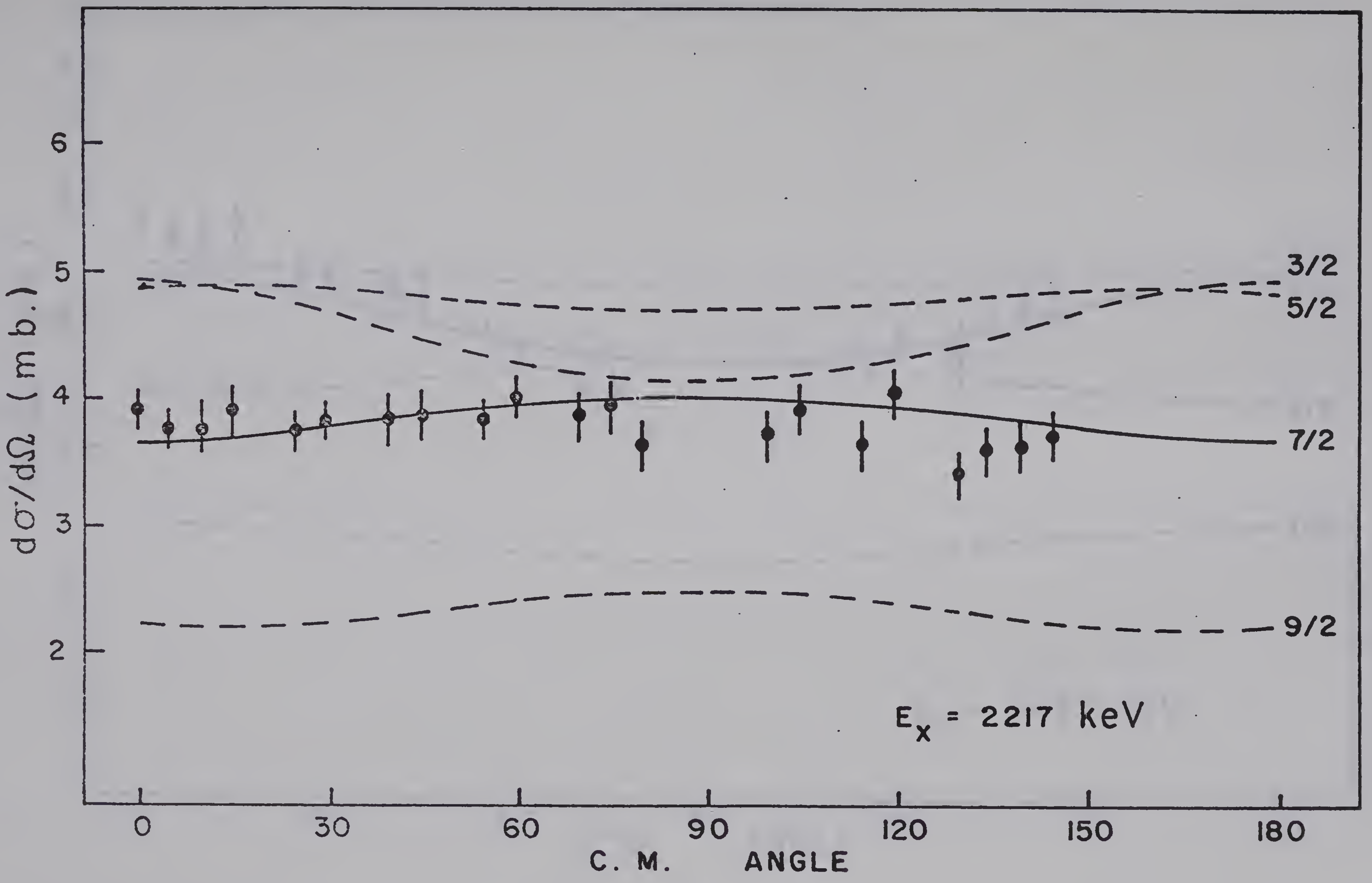

Figure 4.4 d) The 2217 keV state

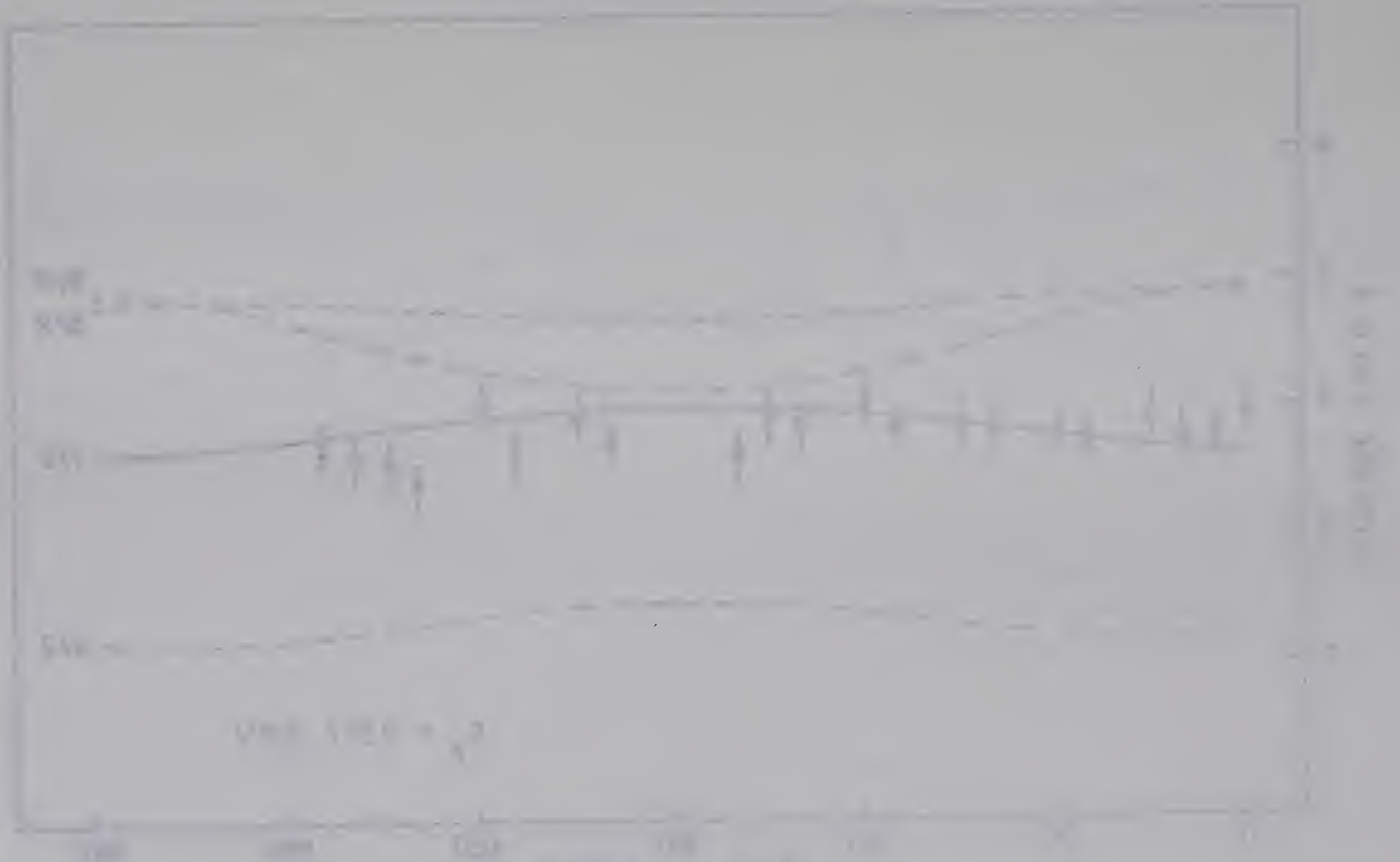

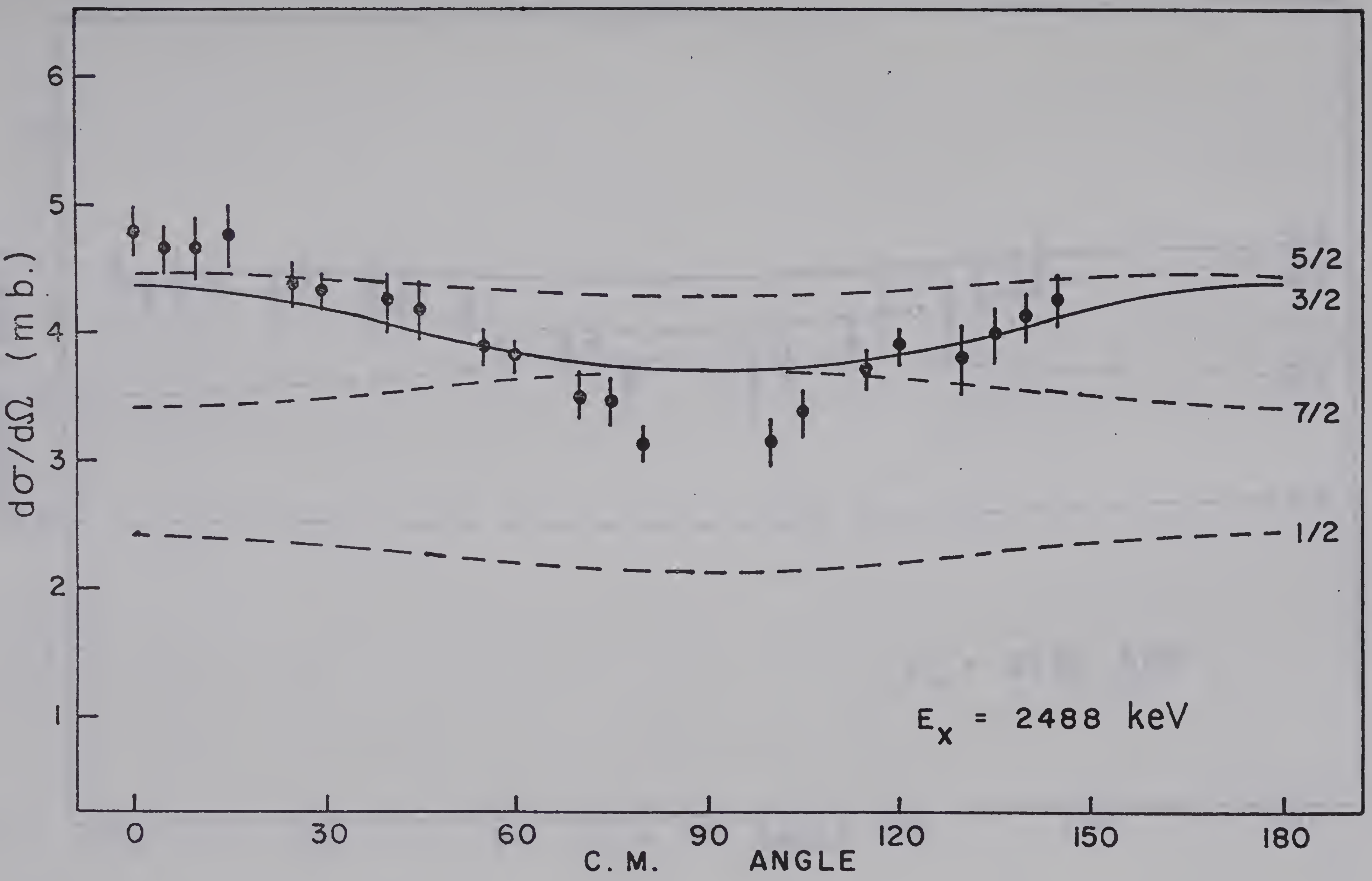

Figure 4.4 e) The 2488 keV state

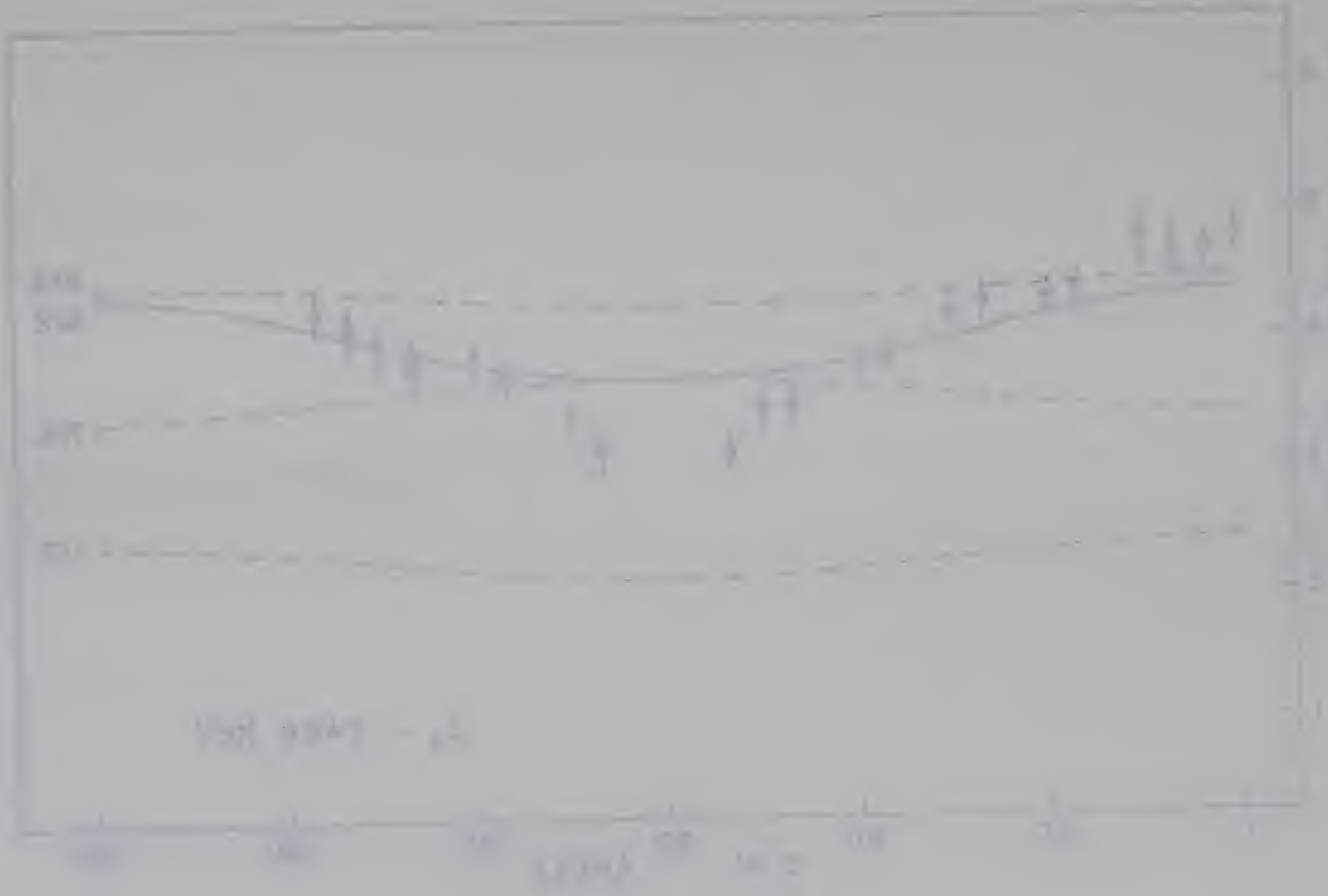

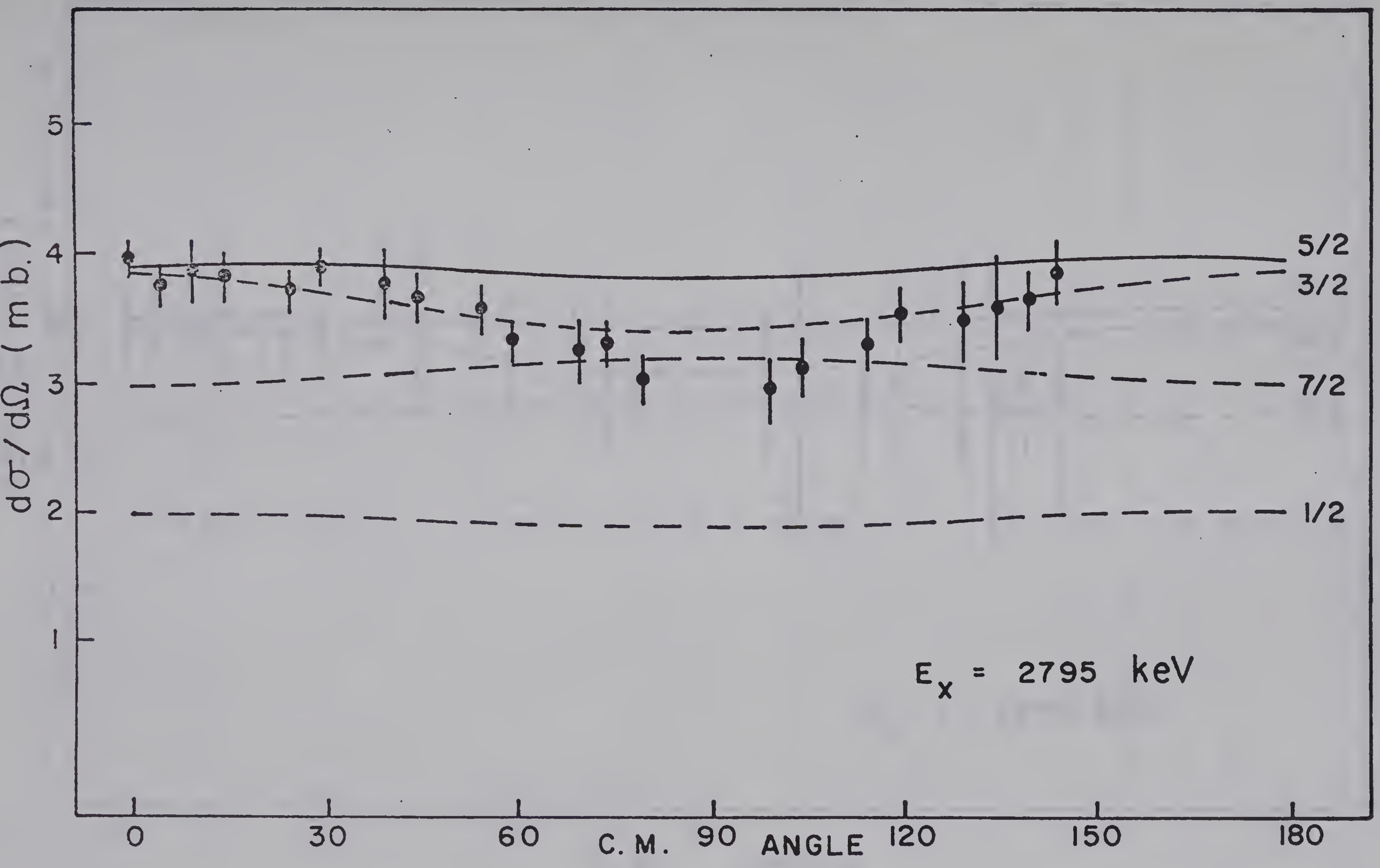

Figure 4.4 f) The 2795 keV state

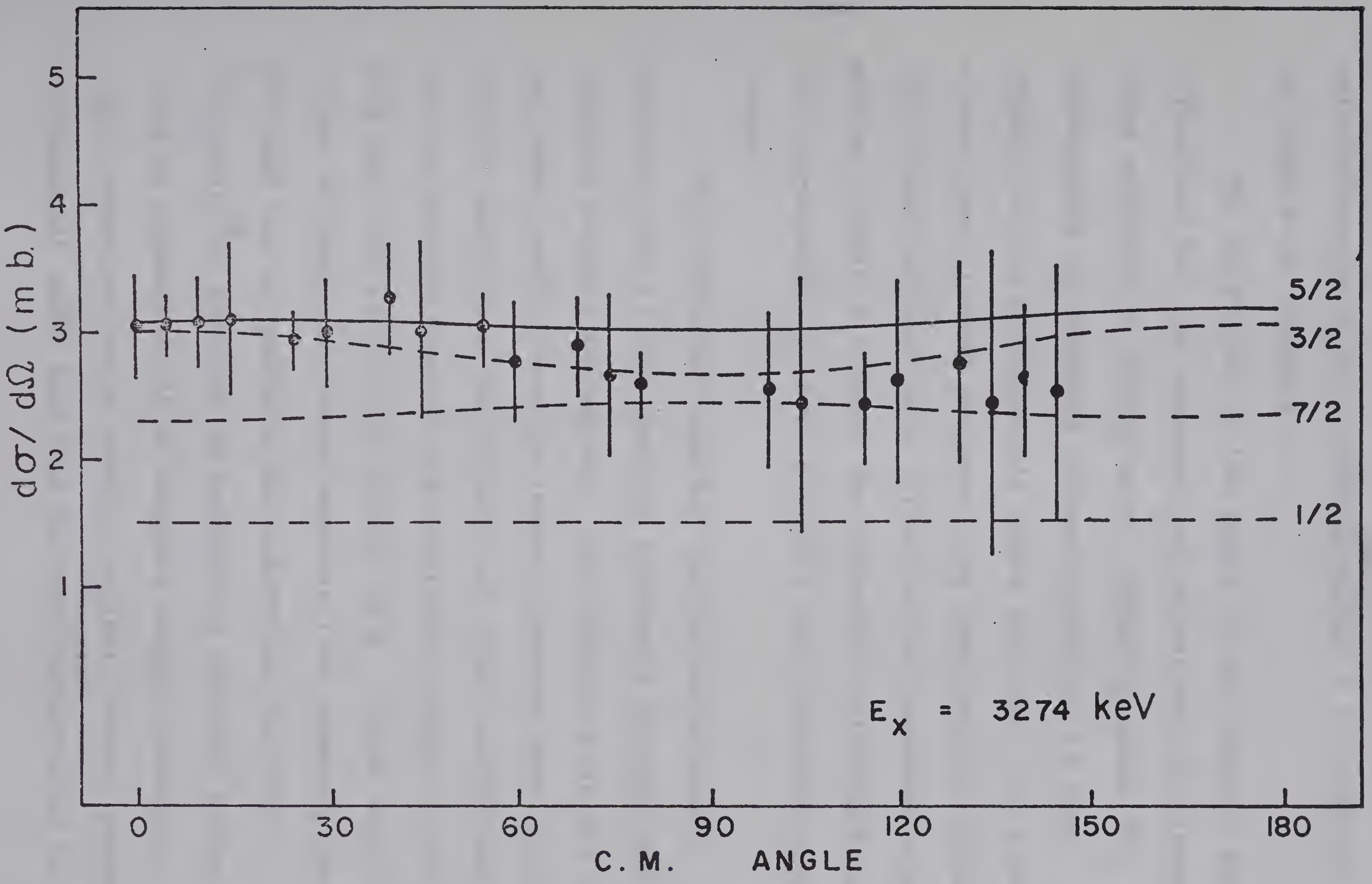

Figure 4.4 g) The 3274 keV state

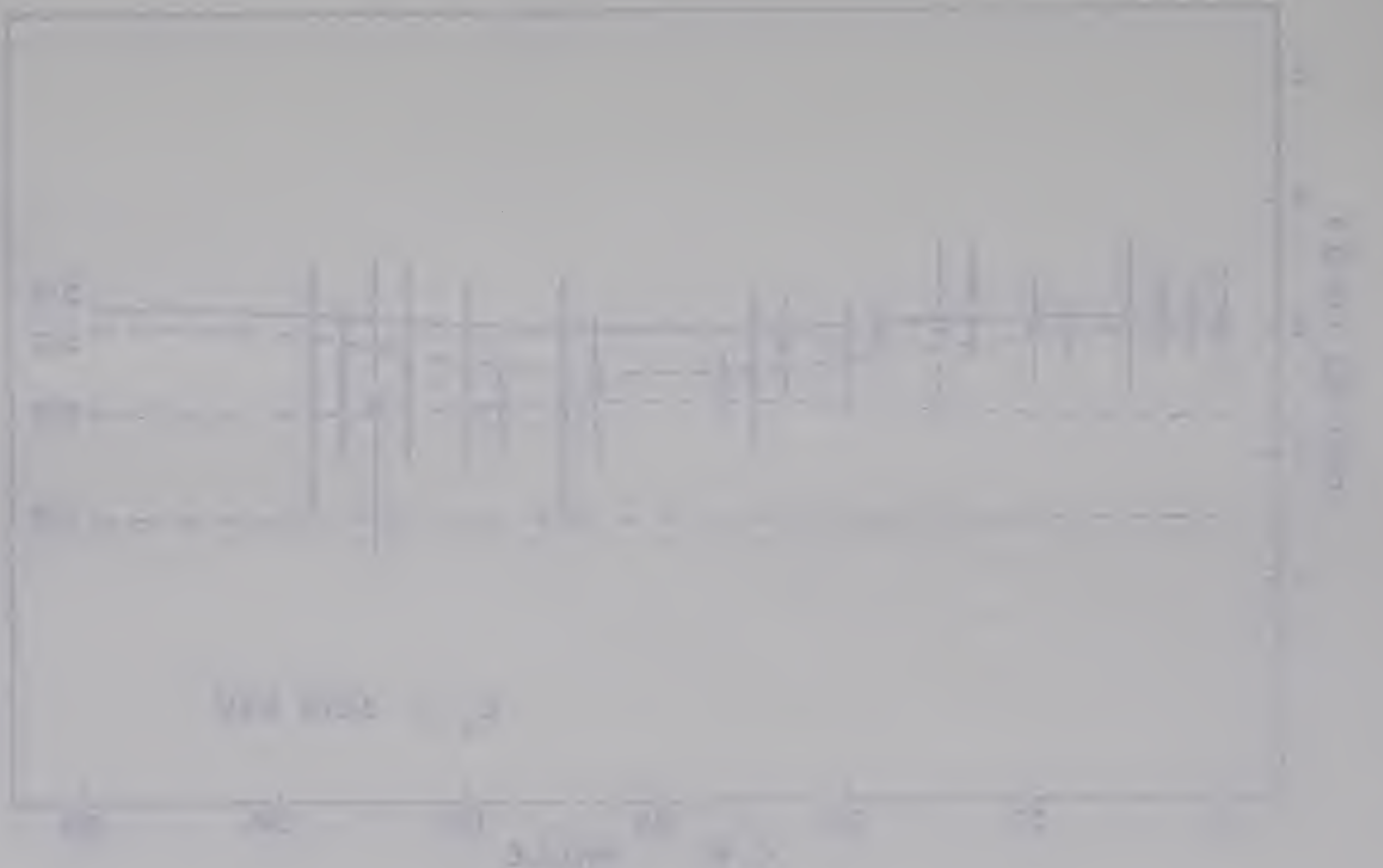

[illegible]

solid and dashed lines; the solid lines represent calculations with the accepted spins, i.e. predicted by γ-ray work (Chapter 3).

The agreement in the shape of the angular distributions for the measured and calculated differential cross sections is fairly good. Symmetry about 90°, a consequence of compound nuclear reaction, is also evident in the differential cross sections. To provide a more quantitative analysis, the experimental differential cross sections were fitted to the Legendre polynomial series. Table 4.2 shows the Legendre coefficients and the chi-squares of their fits for the different neutron groups.

The odd order Legendre coefficients should approach zero if the reaction proceeded through the compound nuclear mechanism. One observes that all the odd order coefficients do indeed approach zero (within errors) except for the 3rd and 1st order coefficients for the neutron angular distributions leading to the 1410 and 1611 keV states respectively. These deviations of the differential cross sections from symmetry about 90° lead one to question the assumption that the $^{37}Cl(p,n)^{37}Ar$ reaction at bombarding energies below 6 MeV is predominantly a compound nuclear reaction. Direct reactions which usually exhibit forward peaked differential cross sections may have contributed to the

Table 4.2

Legendre Polynomial Coefficients of the Neutron Angular Distributions

E_k (keV)	A_1/A_o	A_2/A_o	A_3/A_o	A_4/A_o	χ^2
0	0.03±0.02	0.28±0.03	-0.02±0.03	0.08±0.04	0.34
1410	0.06±0.02	0.14±0.03	0.31±0.04	-0.11±0.04	0.54
1611	0.13±0.02	-0.14±0.03	0.04±0.04	-0.18±0.04	1.12
2217	0.04±0.02	-0.03±0.04	0.00±0.05	-0.02±0.04	0.64
2488	0.02±0.02	0.24±0.03	0.06±0.04	-0.10±0.04	0.50
2795	0.00±0.03	0.12±0.04	0.01±0.06	-0.07±0.05	0.30
3274	0.12±0.12	0.10±0.17	-0.04±0.20	-0.06±0.15	0.09

reaction and caused the asymmetry.

A literature survey of the direct (p,n) reactions shows, however, that direct reaction cross sections are negligible at the present bombarding energies of <6 MeV and are most unlikely to cause the asymmetry in the measured differential cross sections. The arguments against direct reaction contributions are:

a) Direct (p,n) reactions are described as charge-exchange reactions. This occurs most readily in reactions involving isobaric analog states (states with identical spin, J^{π}, and isospin, T) because the initial and final states of the reactions are basically the same. In the $^{37}Cl(p,n)^{37}Ar$ reaction, the ^{37}Cl target has a ground state spin and isospin of J^{π}, T = $3/2^{+}$, 3/2 and hence its isobaric analog state in ^{37}Ar must have the same (J^{π},T). The lowest T = 3/2 state in ^{37}Ar is at 4.989 MeV excitation (Bu 68) and it has been confirmed as the analog to the ground state of ^{37}Cl (Fl 68). Since this is the lowest analog state and it cannot be excited with the present bombarding energies, no direct analog reaction can contribute to our differential cross sections.

b) It is also possible to get charge-exchange by knocking a neutron out with a proton. However, this type of direct reaction does not require the initial and final states to have the same (J^{π},T). In terms of the shell

model description, the proton may enter any orbit after knocking out a neutron from any orbit. In contrast, the direct analog reaction leaves the nucleons of the residual nucleus in the same shell configuration as that of the target nucleus. Hence one would expect the knockout reaction to proceed with a much smaller probability (smaller cross section) than the analog reaction.

Most direct (p,n) reactions have been observed at proton energies above 10 MeV (Ma 69 and Fi 74). With proton energies from 7 to 13.5 MeV, Anderson et al (An 69) found no forward peaking in the ^{27}Al(p,n)^{27}Si reaction cross sections below 10 MeV incident energies. Hence even if knockout should dominate the direct (p,n) reaction, one would expect it to contribute insignificantly to our differential cross sections (proton incident energies <6 MeV).

c) Results of direct (p,n) reactions leading to analog states at $E_p = \sim 18$ MeV yield an average neutron differential cross section of 1 mb/sr at 0° and an average $d\sigma(0°)/d\sigma(120°)$ ratio of four (Ma 69). From theoretical treatment of direct knockout reaction, Atkinson and Madsen (At 68) have shown that its differential cross section formula has the same form as that of the direct analog reaction. Thus assuming the same forward backward ratio in the differential cross section

for the knockout reaction, it would be difficult to account for the asymmetry in the observed differential cross sections (because the knockout cross section is much smaller than that of the analog reaction as mentioned earlier).

d) Finally, if direct reaction is indeed present, one would expect it to be present in all the differential cross sections, especially that of the ground state. This is, however, not the case as the neutron differential cross section leading to the ground state exhibits symmetry about 90° (Figure 4.4a).

The absolute values of the present experimental differential cross sections were, however, lower than those calculated using the Hauser-Feshbach code and a normalization factor of 1.25 was required. This discrepancy could have arisen from the detector efficiency calculations and/or the target thickness. In any case, the general accuracy of the Hauser-Feshbach calculation is not better than 30% because of uncertainties in the value of the transmission coefficients. Taking these errors into consideration, the magnitude of the calculated and measured differential cross sections are in reasonable agreement.

One concludes from these results that the $^{37}Cl(p,n)^{37}Ar$ reaction at incident energies below 6 MeV proceeds mainly through the compound nucleus and that the statistical model is indeed applicable in this case.

CHAPTER 5

SUMMARY OF ^{37}Ar

The results of the various investigations on the ^{37}Ar nucleus are summarized in this chapter and compared with theoretical calculations.

The neutron experiment has identified all the low-lying levels in ^{37}Ar up to 3274 keV (Section 4.2.1) and their energies have been determined from γ rays detected in singles and in coincidence with neutrons (Section 2.4.1). The spin and parity assignments for these levels were derived from the γ-ray angular distributions and transition strengths based on Weisskopf estimates discussed in Section 3.4. Although no unique spins could be extracted from the neutron angular distributions, comparisons of these distributions with the statistical model calculations were consistent with the spins determined from the γ-ray work. The neutron angular distributions do show, however, that in the case of 1410 keV level, the spin, $J = 1/2$ is the most probable assignment. Similarly, the spin, $J = 7/2$ is more probable than $J = 5/2$ for the 2217 keV level.

The electromagnetic transition strengths in ^{37}Ar below 3274 keV excitation have been calculated from the lifetimes (Section 2.4.2) and mixing ratios (Section 3.4) and are tabulated in Table 5.1. Spin and parity

Table 5.1

Electromagnetic Transition Strengths in ^{37}Ar

E_i (keV)	E_f (keV)	J_i	J_f	Mixing Ratio	Multi-pole	Transition Strength (W.u.)	Theory1) (W.u.)	Theory2) (W.u.)
1410	0	$1/2^+$	$3/2^+$		M1 E2	$(1.17\pm0.16)\ 10^{-2}$ 20.4 ± 2.8	2.0×10^{-2} 8.30	1.8×10^{-2} 9.10
1611	0	$7/2^-$	$3/2^+$	0.16 ± 0.04	M2 E3	$(5.3\ \pm0.6)\times10^{-2}$ 16.2 ± 4.0		
2217	0	$7/2^+$	$3/2^+$	0.03 ± 0.04	E2 M3	3.89 ± 0.64 $<4.3\ \times10^5$	4.55	4.95
2488	0	$3/2^-$	$3/2^+$	-0.19 ± 0.19	E1 M2	$(7.9\ \pm3.4)\times10^{-5}$ <23		
2795	0	$5/2^+$	$3/2^+$	-0.21 ± 0.13 >4.7	M1 E2	$(8.1\ \pm5.2)\times10^{-2}$ >14	0.48 2.68	0.42 2.81
3171	0	$5/2^+$	$3/2^+$	$0.78^{+0.82}_{-0.46}$	M1 E2	$(8.3\ \pm5.3)\times10^{-3}$ 2.23 ± 1.6	5.7×10^{-2} 0.91	5.1×10^{-2} 0.59
3185	1161	$9/2^-$	$7/2^-$	-0.58 ± 0.09	M1 E2	$(1.85\pm0.49)\times10^{-2}$ 14.6 ± 4.5		
3274	0	$5/2^+$	$3/2^+$	-0.03 ± 0.14	M1 E2	$(1.85\pm0.78)\times10^{-2}$ $5.3\ \pm2.4$		
		$5/2^-$	$3/2^+$	-0.03 ± 0.14 $4.0^{+5.5}_{-1.5}$	E1 M2	$(5.1\ \pm2.2)\times10^{-4}$ $(1.92\pm0.87)\times10^{2}$		

1) Ref. (Wi 71) using the (11.0 + aspe) potential

2) Ref. (Wi 71) using the (12.5p + ^{17}O) potential

assignments are based on the combined results of the present study except for the 2488 and 2795 keV levels for which the previously established values (En 73) have been adopted.

Several shell model calculations on the mass A = 37 nuclei have been published. The first major study was undertaken by Glaudemans (Gl 64). They used ^{28}Si as the core and confined the remaining nucleons to the $2s_{1/2}$ and $1d_{3/2}$ orbits. More recent calculations by Dieperink and Brussaard (Di 69) and Wildenthal et al (Wi 71) have enlarged the configuration space by allowing the excitation of nucleons from the $1d_{5/2}$ to the $2s_{1/2}$ and $1d_{3/2}$ orbits. Essentially, this established ^{16}O as the inert core and expanded the vector space to include the entire 2s-1d shell. The difference between the latter two calculations lies in the Hamiltonian used.

In the shell model calculation of Wildenthal et al (Wi 71), the transition strengths between positive-parity state in ^{37}Ar were also determined and have been included in Table 5.1 for comparison.

The above shell model calculations yield positive-parity states only. To obtain negative-parity states, Erné (Er 66) performed a calculation using ^{32}S as the core with one nucleon in the $1f_{7/2}$ subshell and the other, extra core, nucleons in the $1d_{3/2}$ subshell.

The results of these calculations together with the properties measured in this investigation are listed in Figure 5.1.

All the Shell model calculations have yielded $J^{\pi} = 3/2^{+}$ for the ground state of ^{37}Ar; corresponding to the last (nineteenth neutron) unpaired neutron being in the $1d_{3/2}$ orbit. The 1410 keV state with $J^{\pi} = 1/2^{+}$ has been identified as a $s_{1/2}$ state with the configuration $(2s_{1/2})^{3}_{1/2}(1d_{5/2})^{6}_{0}$. Since Erné's calculation assumed the $2s_{1/2}$ orbit to be closed, no $s_{1/2}$ state was possible. The calculated energies for this level vary from 1.43 to 1.55 MeV and are in good agreement with the measured value of 1410 keV.

The unique assignment of $J^{\pi} = 7/2^{-}$ for the 1611 keV state (Section 3.4.2) restricts comparison to the 2.07 MeV level in Erné's report (Er 66). According to the model prediction this level has the configuration $(1d_{3/2})^{4}_{0}(1f_{7/2})^{1}_{7/2}$ and contains most of the single particle $f_{7/2}$ strength.

The $J^{\pi} = 7/2^{+}$ state at 2217 keV excitation has been reproduced well by all the calculations. On the contrary, the $J^{\pi} = 3/2^{-}$ assignment for the 2488 keV level cannot be accounted by any of the aforementioned shell model calculations. This is due perhaps to the exclusion of the $2p_{3/2}$ subshell in the calculations. Stripping reactions (Ro 65a and Ch 71) have indicated

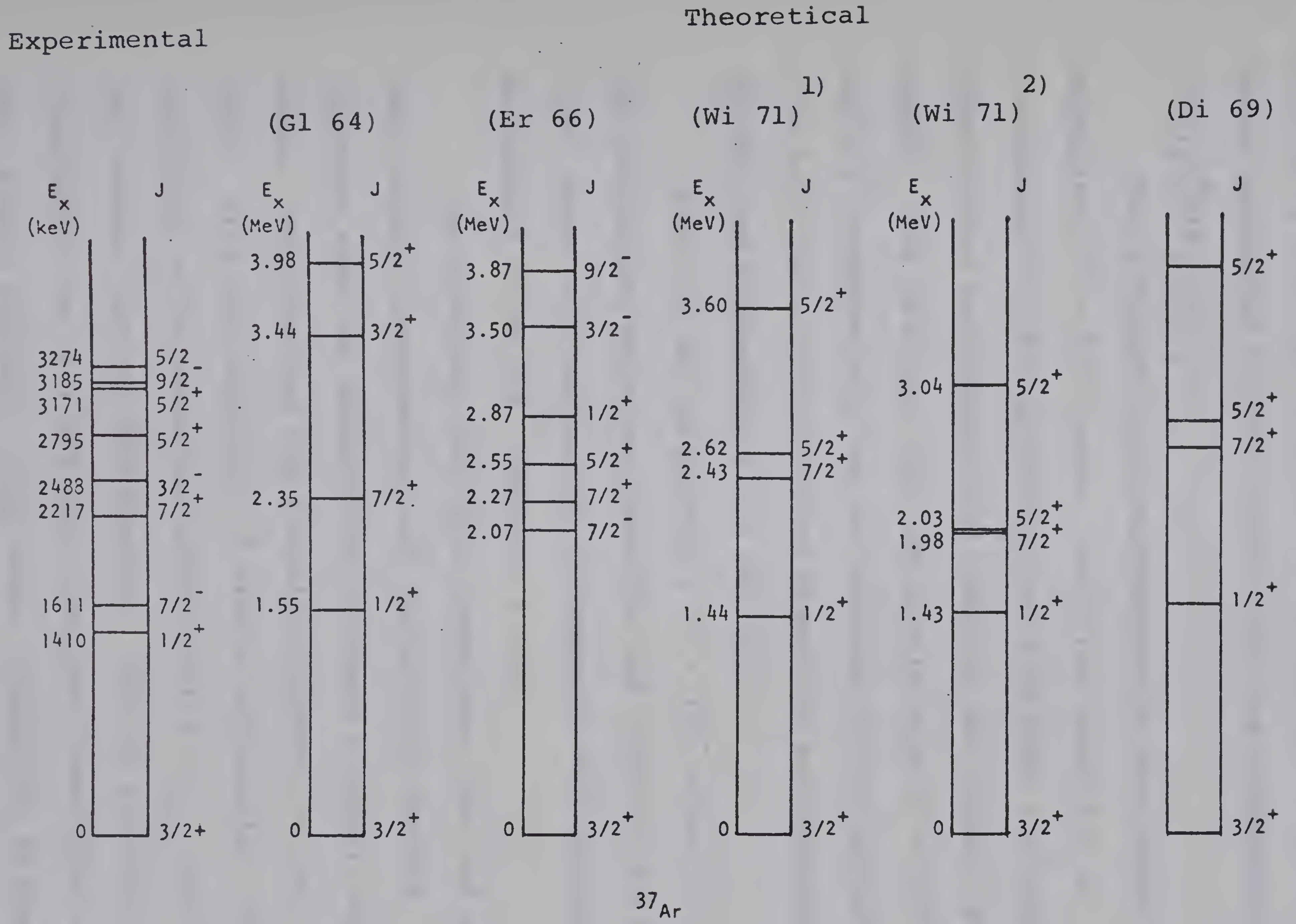

1) Calculated with the (11.0+aspe) potential in Ref. (Wi 71).
2) Calculated with the (12.5p+^{17}O) potential in Ref. (Wi 71).

Figure 5.1 The measured and calculated energy levels of ^{37}Ar.

that this state possesses most of the $2p_{3/2}$ single particle strength. The 3/2 state at 3.50 MeV excitation predicted by Erné (Er 66) has the configuration $(1d_{3/2})^4_2(1f_{7/2})^1_{7/2}$.

The 2795 keV level corresponds to the lowest calculated $J^\pi = 5/2^+$ state. With the exception of Glaudemans' (Gl 64) prediction at 3.98 MeV, all other calculations reproduced this level in the correct energy region. The 3171 and 3274 keV levels with $J^\pi = 5/2^+$ and $5/2^\pm$ respectively may be compared to the second $J^\pi = 5/2^+$ state calculated by Dieperink and Brussaard (Di 69) and Wildenthal et al (Wi 71).

Erne (Er 66) predicted a $J^\pi = 9/2^-$ state at 3.87 MeV excitation which may describe the observed 3185 keV level whose spin and parity assignments were uniquely determined to be $9/2^-$ (Section 3.4.6).

One observes from this comparison that the agreement between experimental and theoretical results improves when the calculation involved a larger vector space. Nevertheless the overall agreement is far from good. With the exception of Erne's calculation, the exclusion of the negative parity orbits $1f_{7/2}$ and $2p_{3/2}$ may account for the discrepancy. This is particularly true since the 1611 keV state has been identified with the 'single particle' $f_{7/2}$ level. Moreover, Wildenthal et al (Wi 71) pointed out that exclusion of negative-

parity states does not affect the calculation of positive-parity states since negative- and positive-parity configurations do not mix. But the results are affected by the exclusion of positive-parity states due to excitation of an even number of particles from the sd to the fp shell.

Finally one must mention that these shell-model calculations were performed when experimental information on ^{37}Ar was lacking. The results of recent investigations and this experiment established most of the properties of the low-lying levels in ^{37}Ar. This will provide a better comparison for future theoretical calculations.

CHAPTER 6

A STUDY OF THE STATISTICAL MODEL WITH THE ^{29}Si(p,p'γ)^{29}Si REACTION

6.1 Motivation

The previous chapters have shown that the statistical compound nuclear (SCN) model was successful in its description of the ^{37}Cl(p,n)^{37}Ar reaction. The assumption that many levels in the compound nucleus were excited was inferred from the use of thick targets. Agreement of the experimental results with model calculations suggests that probably sufficient levels were excited. Nevertheless, it would be interesting to investigate how many levels are required to justify the statistical approach.

One recalls (Section 4.1) that as the mass of the nucleus and also the excitation energy increase, the number of compound nuclear levels increase. In order to study the effect of the number of compound nuclear levels on the statistical theory, one must have an experimental condition whereby one can excite a few or many levels in the compound nucleus by varying the target thickness.

An appropriate mass region to conduct this investigation is in the mid s-d shell ($A \sim 30$) where studies

on structure and resonance have reported (Sh 70 and Ru 72) level densities suitable for the experimental condition mentioned above. In particular, the proton capture and inelastic scattering yields on ^{29}Si nucleus have exhibited considerable fluctuation suggesting low level density (De 70 and Di 71). In addition to its low level density, the ^{29}Si nucleus has several desirable properties which would make it ideal for this investigation.

Firstly, the ^{29}Si nucleus has a ground state spin and parity ($J^{\pi} = 1/2^{+}$) which would enhance nuclear alignment (Section 3.1.1). Secondly, at proton incident energies below 4.8 MeV, only the (p,p') reaction is energetically possible (all other proton induced reactions on ^{29}Si have larger negative Q-values). Lastly, the level energies and electromagnetic properties of the low-lying levels in ^{29}Si are well known to afford comparison.

Particle-gamma angular correlation studies of Becker et al (Be 67) confirmed the spin and γ-decay modes of the low-lying levels in the ^{29}Si nucleus (Figure 6.1). Lifetimes of these states have also been subjected to thorough investigations by many authors using different reactions (Ba 68a, De 70 and Mc 71). Detailed stripping (El 72) and two nucleon transfer (Cu 69, Mc 71 and Na 72) studies which included useful optical model parameters from DWBA analysis have been

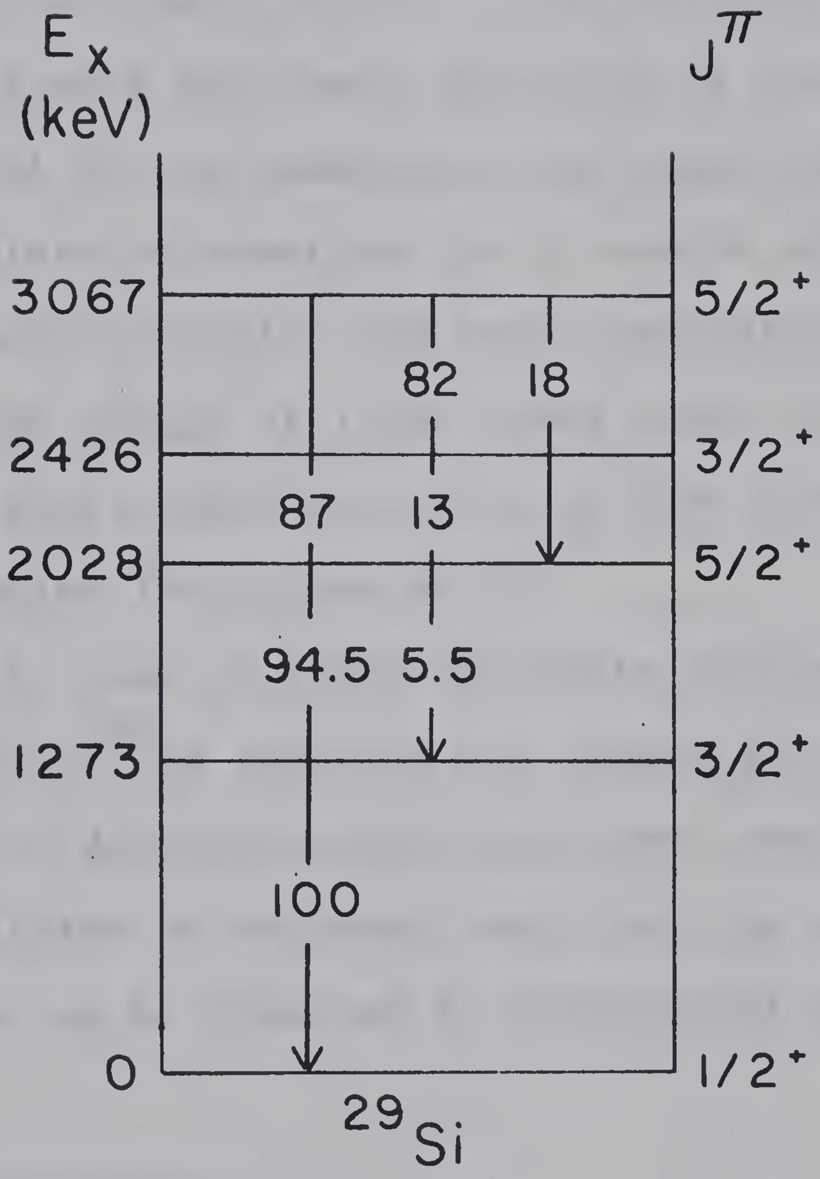

Figure 6.1 The energy level scheme of ^{29}Si.

reported.

The theoretical aspects of the ^{29}Si nucleus have also received considerable attention because it is in the mass region where nuclear deformation changes from prolate to oblate (Br 57). The low-lying positive-parity states have been described in terms of the Nilsson model (Ni 55) as members of two mixed rotational bands with oblate deformation (Br 57 and Hi 69). Single particle interpretation had been unsatisfactory (Ba 68) until the advent of large model space calculations. Recent shell model calculations have given a fair overall description (Vo 72 and Wi 73).

In view of these desirable features, the ^{29}Si(p,p'γ)^{29}Si reaction was chosen for this investigation to determine when sufficient averaging over compound states is achieved such that the experimental results can be compared to statistical theory predictions.

6.2 Experiment

Gamma-ray angular distributions following the ^{29}Si(p,p'γ)^{29}Si reaction were measured with a 52 cc Ge(Li) detector at 0°, 31°, 55° and 90°. Each angle was repeated. A second Ge(Li) detector of 48 cc volume was fixed at 90° in the opposite forward quadrant as a monitor. The detector distance from the target were 12 and 8 cm

respectively. Lead disks of 3 mm thickness were placed in front of both detectors to absorb the low energy γ rays.

The target consisted of 94 $\mu g/cm^2$ of SiO_2 (61% enriched ^{29}Si) evaporated onto a gold backing of 0.13 mm thickness. It was mounted at 30° to the beam direction and air cooled in the arrangement described in Section 3.2.

The energy of the proton beam obtained from the van de Graaff accelerator was varied from 3.00 to 3.60 MeV in 10 keV intervals. To ensure energy stability and accuracy, extreme care was taken in increasing beam energy without changing other conditions. Throughout the experiment, the target current was maintained at $\sim$0.7 μA and monitored by an audio alarm system which would sound if the target current should fall below a preset level. When a run was interrupted the last run was repeated before resuming the experiment. The reproducibility was within the statistical errors and no renormalization was required.

Following the above series of runs, the target was replaced by a thicker one. This target consisted of 90% enriched $^{29}SiO_2$ mixed in a slurry of polyurethane and benzene smeared onto a gold backing. Its estimated thickness was $\sim$5 mg/cm^2. The experiment was repeated in

100 keV intervals with the angular distributions taken at the same angles mentioned earlier and the addition of a point at 71°.

The electronics and computer configuration associated with the detection and data collection were similar to that previously described (Section 3.2).

Intensities of the 1273 and 2028 keV γ-ray transitions to the ground state in ^{29}Si were extracted from the full energy peaks by the same procedure as described in the earlier chapters. They were then normalized with respect to the 1273 keV peaks in the monitor detector and corrected for absorption in the target backing and retaining plate. Dead times in the analog-to-digital converters were also compensated for although they accounted for less than one percent error.

6.3 Results and Discussion

6.3.1 Thin target

Preliminary survey runs with the thin target (94 μg/cm^2) had indicated that the results disagreed with the SCN model predictions. This discrepancy may be attributed to insufficient statistical averaging as a result of too few levels being excited in the compound nucleus. Hence the experimental γ-ray angular distributions measured with the thin target were not subjected

to the normal statistical analysis (Section 3.3). Instead they were least square fitted to the even Legendre polynomial series, $W(\theta) = A_o + A_2Q_2P_2 + A_4Q_4P_4$ (notations similar to Equation 3.18). The coefficients extracted from the fits were expressed as a function of the bombarding energies.

Figure 6.2 show such a plot for the 1273 and 2028 keV γ rays of ^{29}Si. The zeroth order coefficients, A_o, represent the yield function and the higher order coefficients, A_2/A_o and A_4/A_o, the distribution functions. Rather than complicate the graphs only typical error-bars are shown. The distribution coefficients obtained from the SCN calculations are shown by the dotted line for comparison. These theoretical coefficients are calculated with the adopted spins and mixing ratios (En 73). The transmission coefficients required for the statistical calculations were obtained from the code 'Hauser' (Da 69) using the optical model parameters from the report of El-Naiem et al (El 72). They are listed in Table 6.1.

Before analyzing the results further one questions if the resonance-like peaks in the yield curves are authentic, i.e. do they arise from the reaction and not from fluctuation in the experimental conditions? The yield of the 1273 keV γ ray had been measured by Koen (Ko 72) using the same $^{29}Si(p,p'\gamma)^{29}Si$ reaction with a 5 $\mu g/cm^2$ enriched ^{29}Si target. His result shows

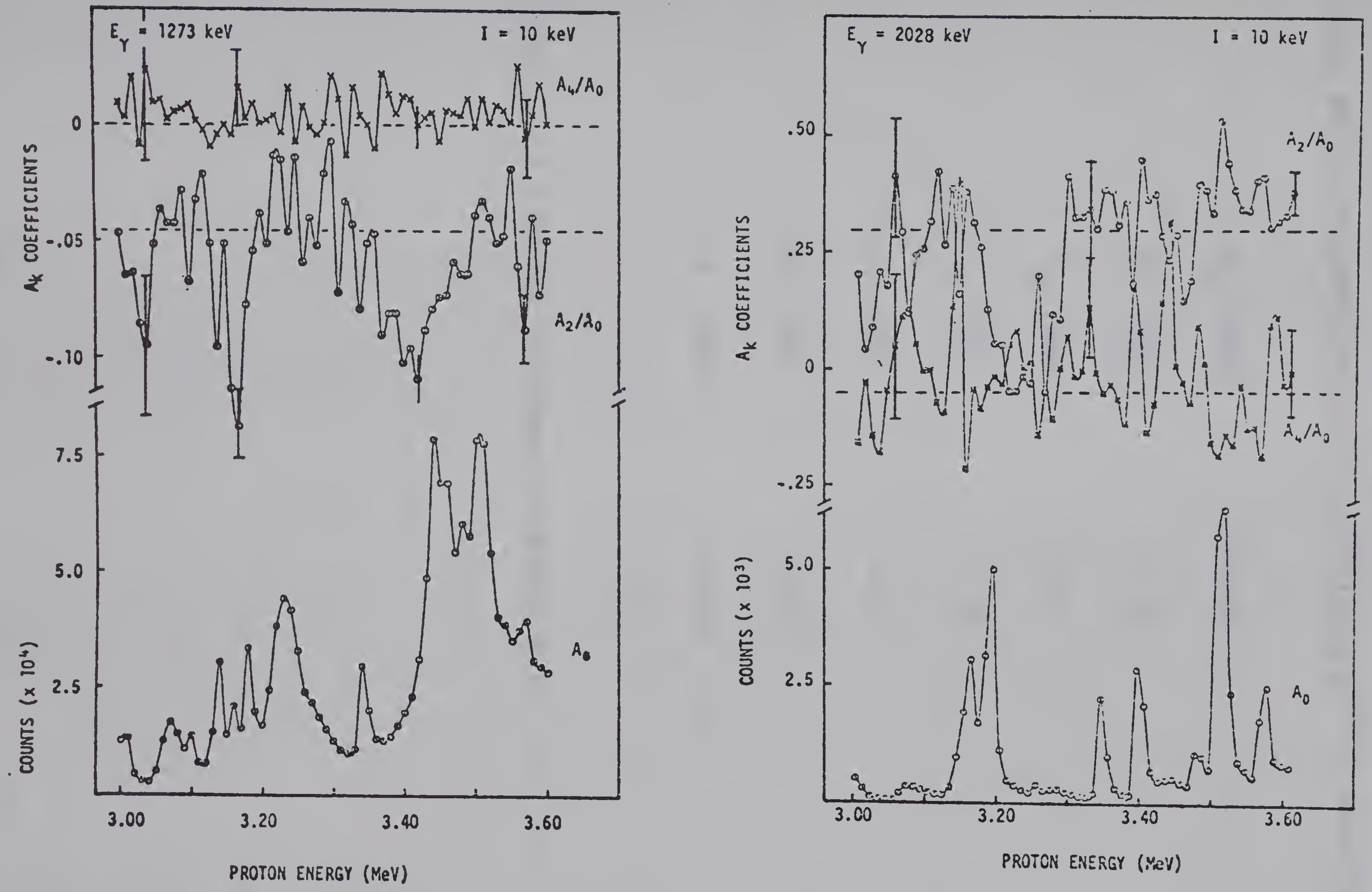

Figure 6.2 Observed Legendre polynomial coefficients vs energy for the 1273 and 2028 keV γ rays.

[illegible]

Table 6.1

Optical Model Parameters for the $^{29}Si(p,p\gamma)^{29}Si$ Reaction[1)]

V_0 (MeV)	50.31
W (MeV)	7.95
V_s (MeV)	6.2
r_0 (fm)	1.25
r_i (fm)	1.25
a_0 (fm)	0.64
a_i (fm)	0.74

1) Notations similar to those in Table 4.1.

resonance-like peaks that occur at the same energies as our peaks. This confirms that the peaks observed in Figure 6.2 are due to resonance structures in the reaction.

The fluctuations of the measured angular distribution coefficients about the SCN line is expected since the thin target was chosen specifically to excite only a few levels in the compound nucleus. Perhaps the properties of these levels do influence the fluctuations in the coefficients and therefore an attempt was made to see if some correlation does exist.

The *statistical* model assumes that compound nuclear levels of all spin and parity combinations are excited provided they satisfy the conservation laws. The calculation then sums (neglecting any possible interference) over partial wave contributions leading to and from all these states. When the compound nuclear level density is low, only a few levels are excited or in the extreme case perhaps only a single level is excited. In these cases a CN model calculation may still provide a reasonable description of the reaction.

To study the effect of low level density on the SCN calculation, one restricts the summation over all incoming and outgoing partial waves in Equation 3.17 to those for a *specific* compound nuclear spin and parity, J_1^{π}. This was accomplished by modifying the summation routine in the code 'AK' (Gr 71) and resulted in a set

of theoretical coefficients for distinct J_1^π values. They are presented graphically in Figure 6.3 for comparison with Figure 6.2.

The range of angular distribution coefficients calculated for a specific J_1^π encompasses all the measured values. This indicates that the CN calculations for specific J_1^π could account for the observed fluctuations in the angular distributions. Comparison of the experimental and theoretical coefficients for specific J_1^π may also yield spin and parity information on possible resonance peaks. The distribution coefficients of both the 1273 and 2028 keV γ rays approach zero at 3.23 MeV suggesting transition through $J_1 = 0$ states in the compound nucleus. Therefore the resonance peak at this energy may correspond to a state of $J_1 = 0$. In practice, however, incomplete averaging of the interference terms could result in disagreement with the simple case of the single CN resonance.

Simulation of Thicker Targets by Yield Averaging

So far the experimental evidence is consistent with the hypothesis that excitation of insufficient levels in the nucleus causes the failure of SCN predictions. It follows then that the inclusion of more compound nucleus levels should overcome the discrepancy. In order to study the effect of averaging over these resonances, one combines the yields from two adjacent measurements of successive energies. By repeating the process at the respective angles one simulates an angular distribution

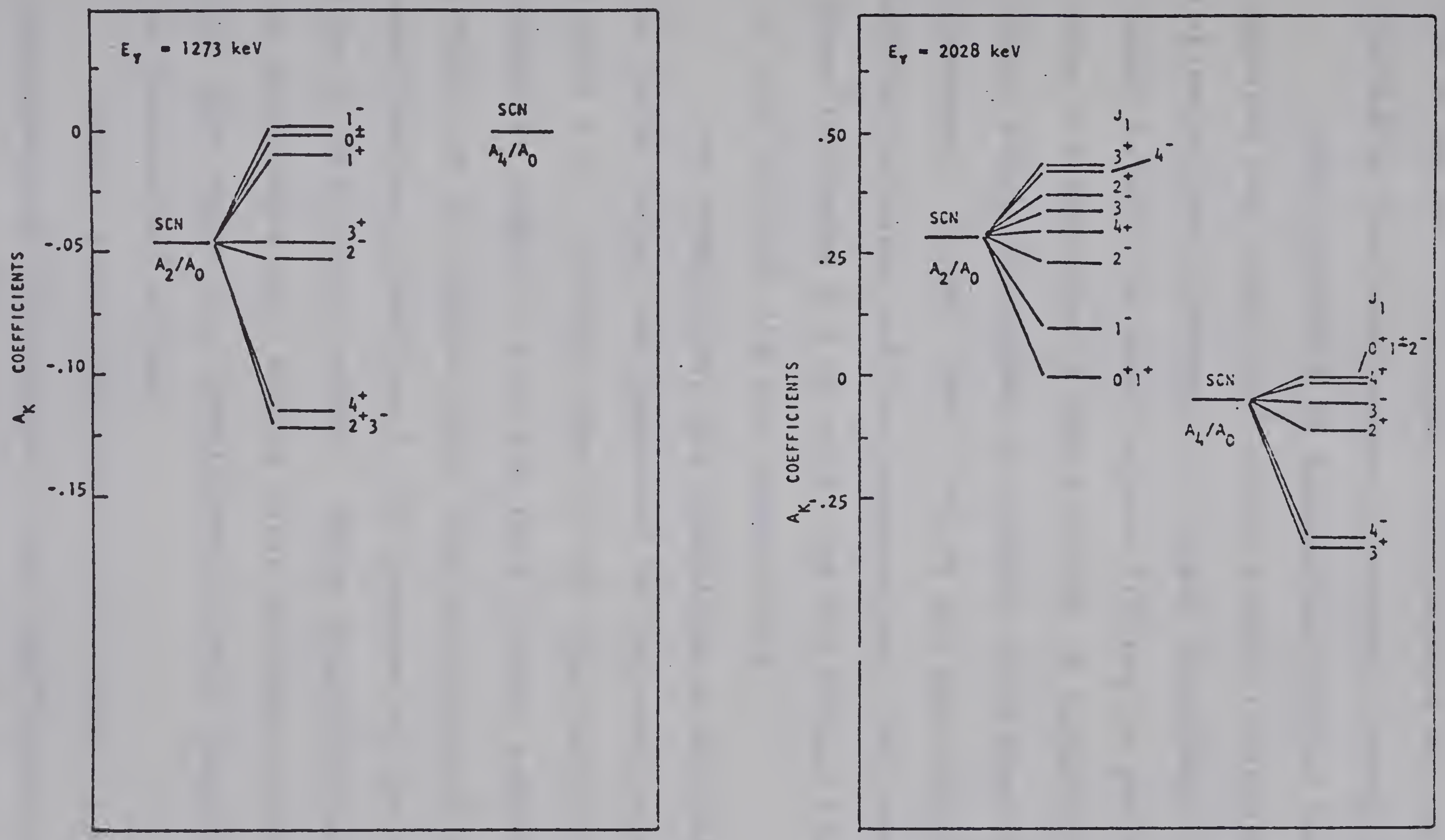

Figure 6.3 Legendre polynomial coefficients calculated with the modified SCN model.

[illegible]

obtained from a target twice the original thickness. Thus a new set of Legendre coefficients may be extracted by the least square procedure already described.

This procedure of simulating thicker targets is repeated for larger and larger energy intervals. Following each increment of target thickness (i.e. energy bite), the least square fitting is performed. Hence one generates a whole series of Legendre coefficients which correspond to gradual increases of target thickness. A code 'WAVY' (Wo 74 and Appendix C) was written to carry out the computation. The results are shown in Figure 6.4 (a to d) for the energy intervals of 50, 100, 200 and 400 keV respectively.

For comparison, the coefficients determined with the thick target are presented in the same manner in Figure 6.5. Although some of the experimental coefficients in Figure 6.5 do not fall (within experimental errors) on the dashed line, they are accepted in the SCN model analysis (Section 6.3.2) because of the uncertainties in the mixing ratios. Since uncertainties are are associated with mixing ratio determinations one must take these into consideration when comparing with the theoretical values.

These graphs show that as the energy interval is increased, the fluctuation in the coefficients are smoothed out. When the energy interval reaches 400 keV

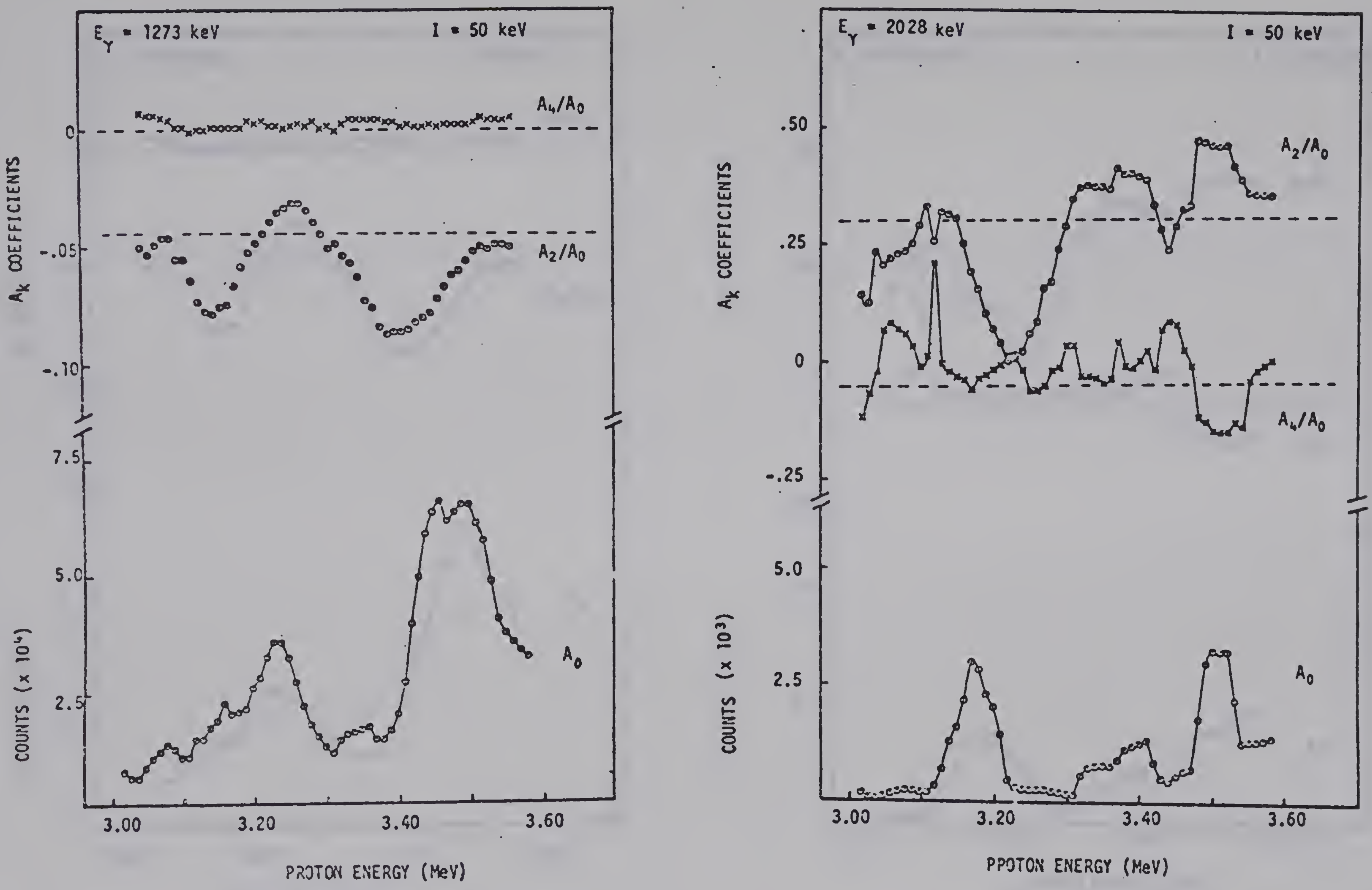

a) Energy interval of 50 keV

Figure 6.4 Angular distribution coefficients obtained from averaging process.

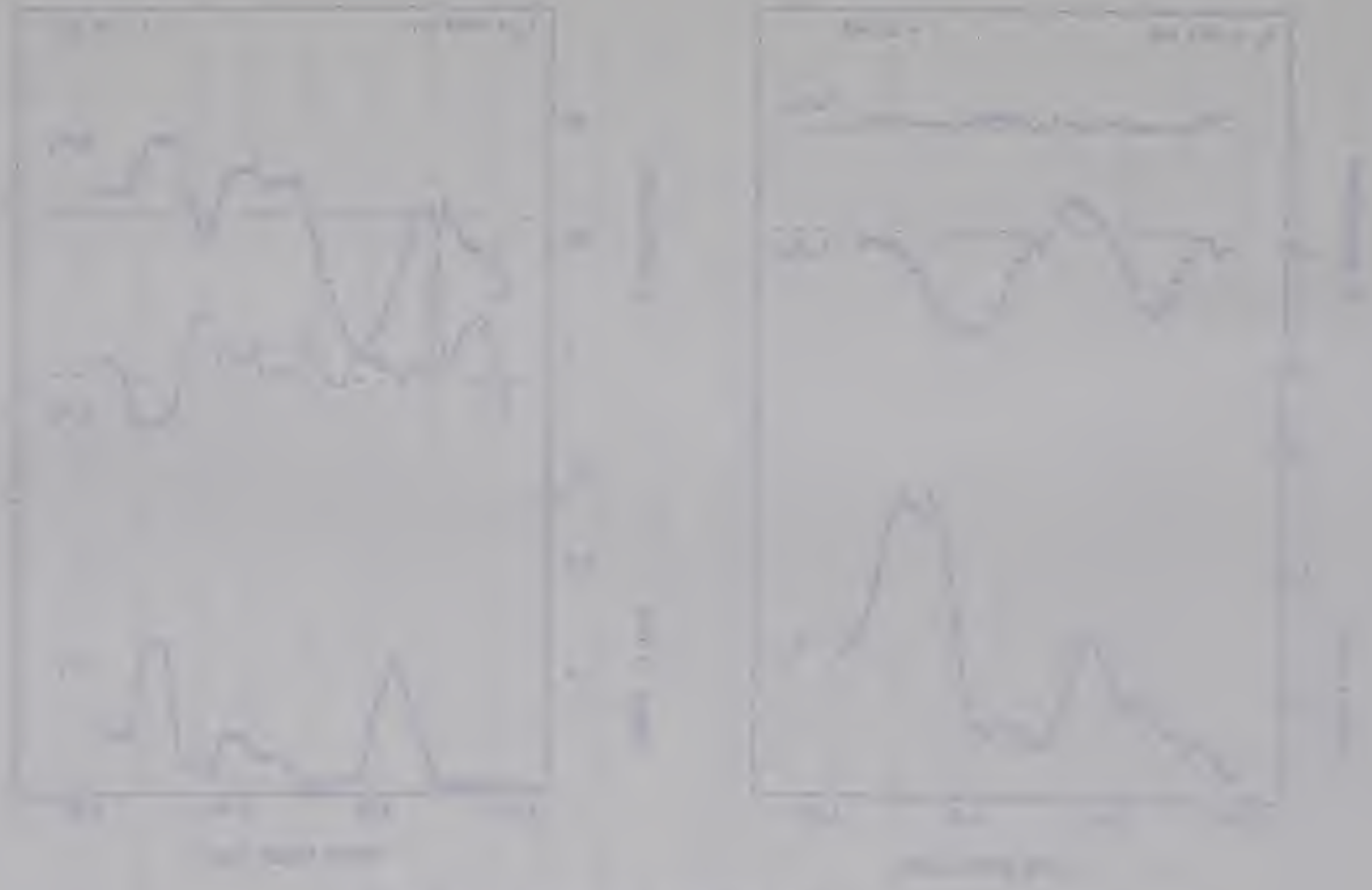

[illegible]

[illegible]

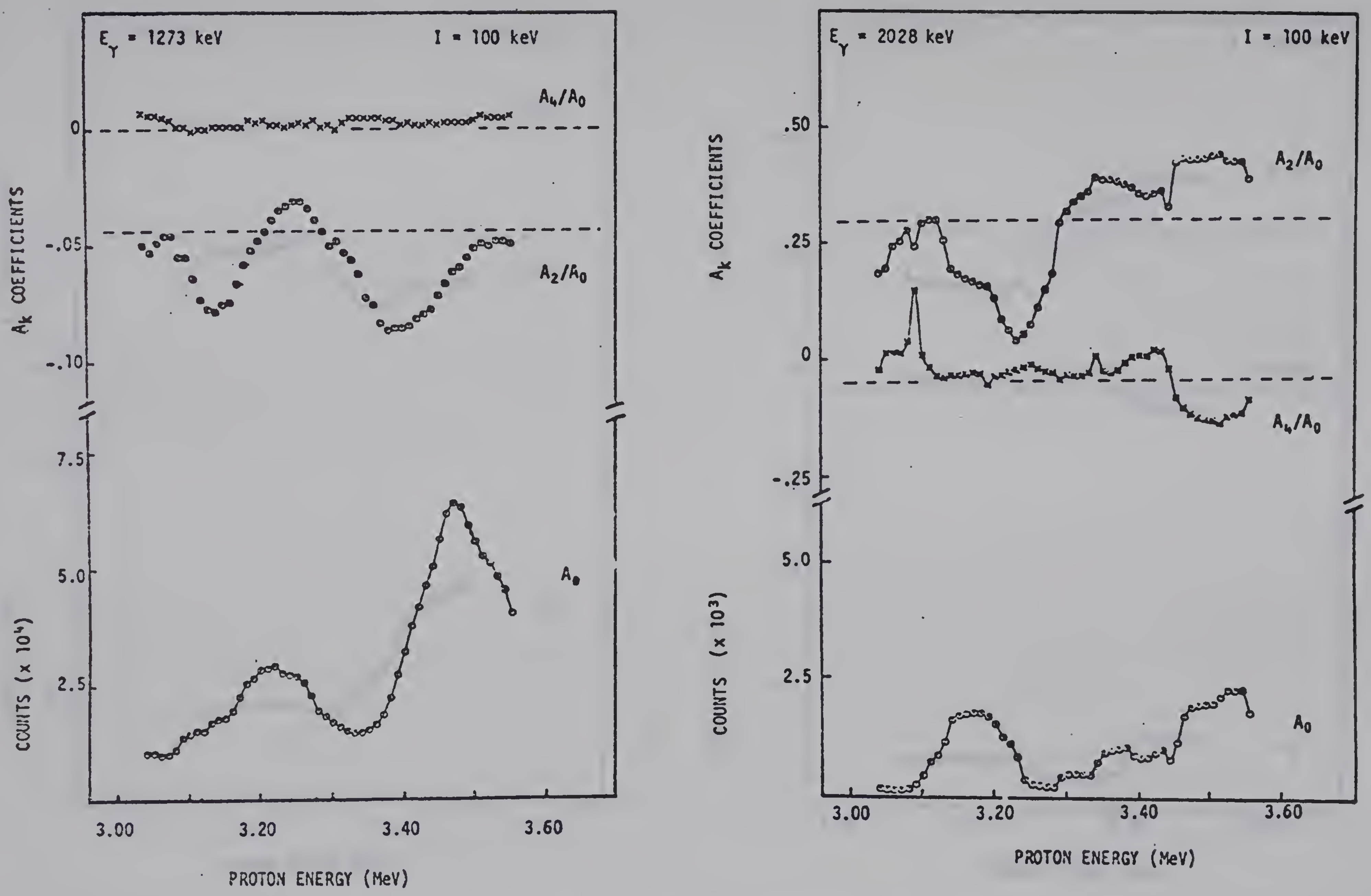

Figure 6.4 b) Energy interval of 100 keV

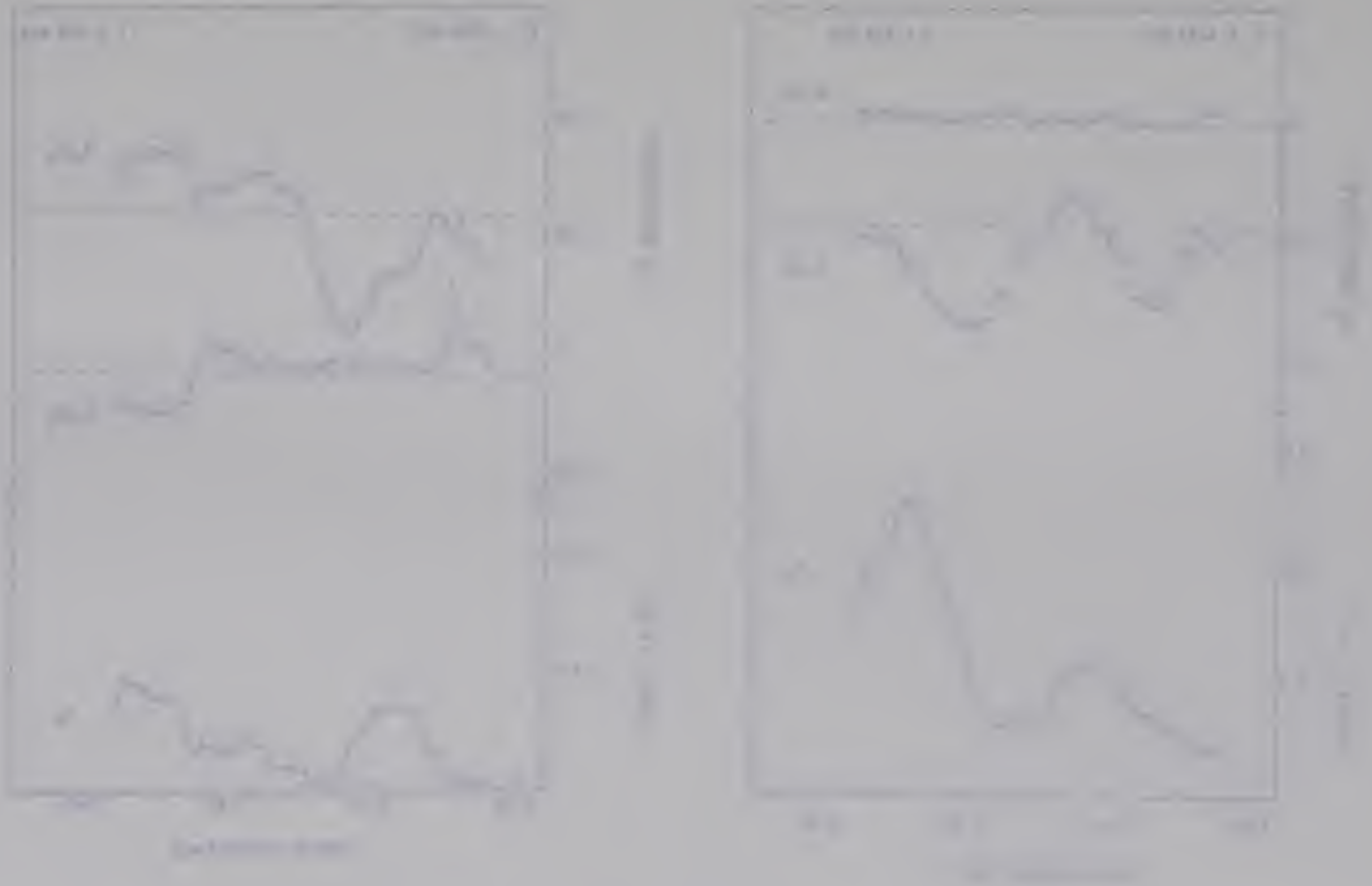

[illegible]

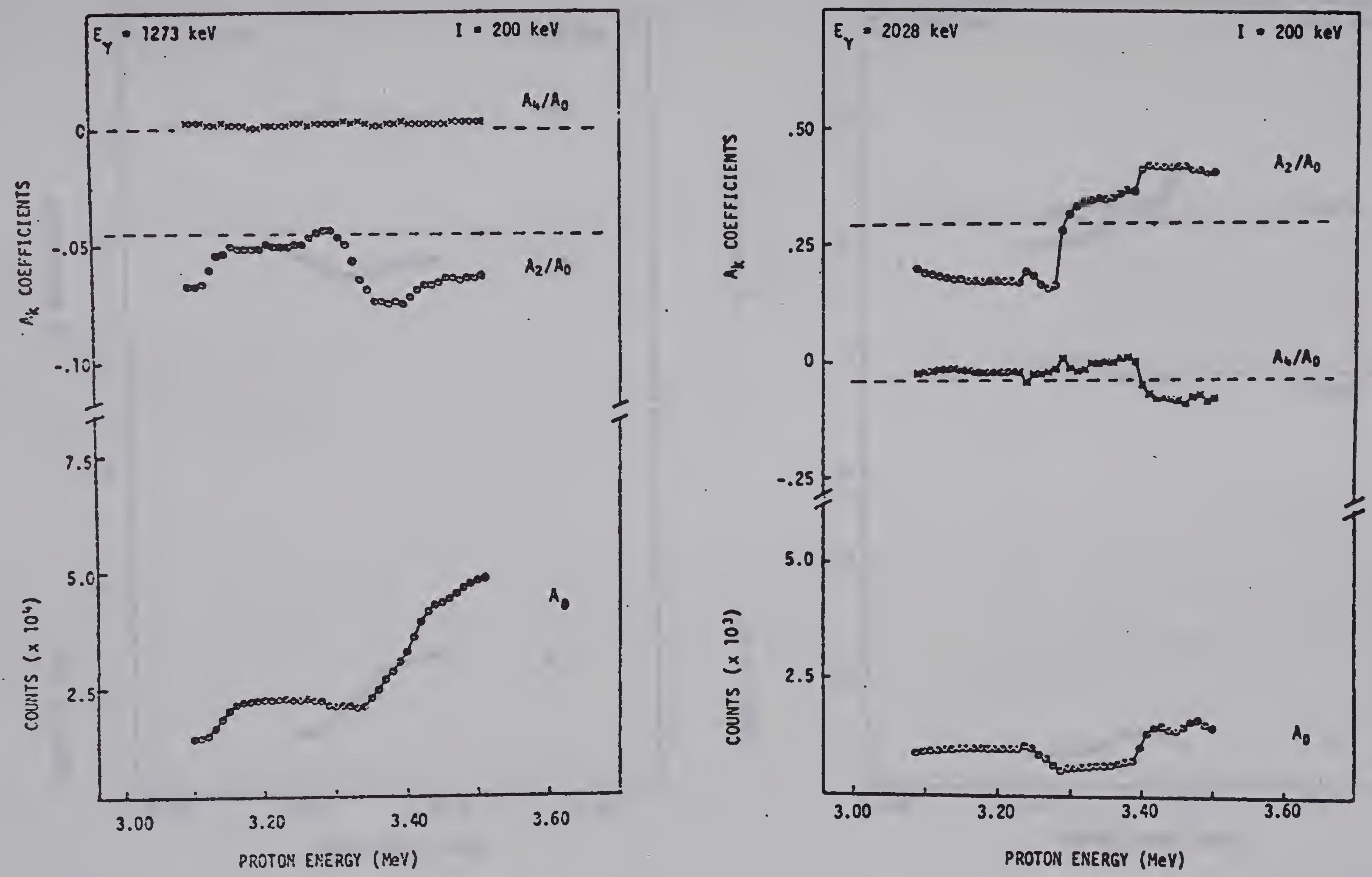

Figure 6.4 c) Energy interval of 200 keV

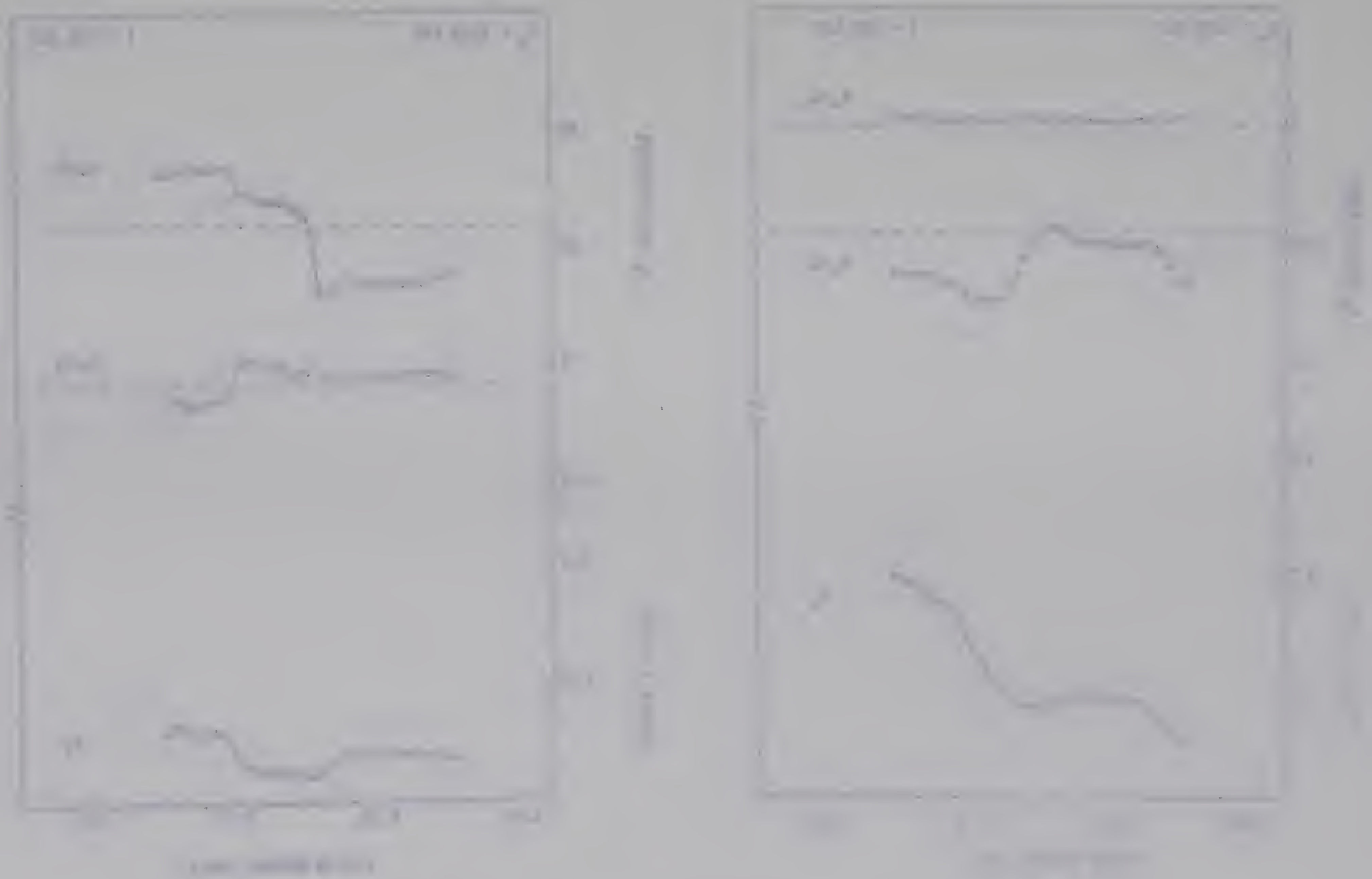

[illegible]

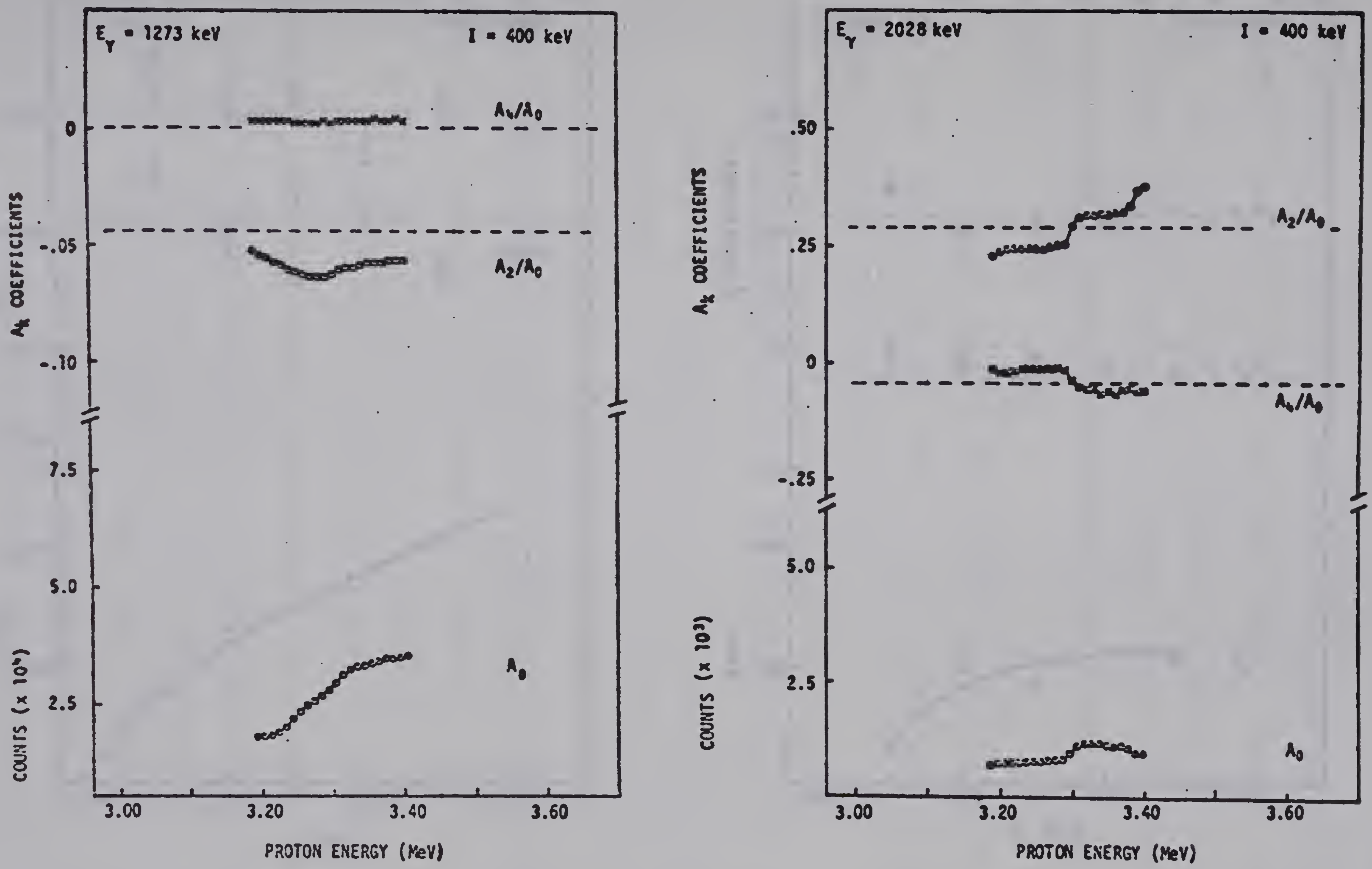

Figure 6.4 d) Energy interval of 400 keV

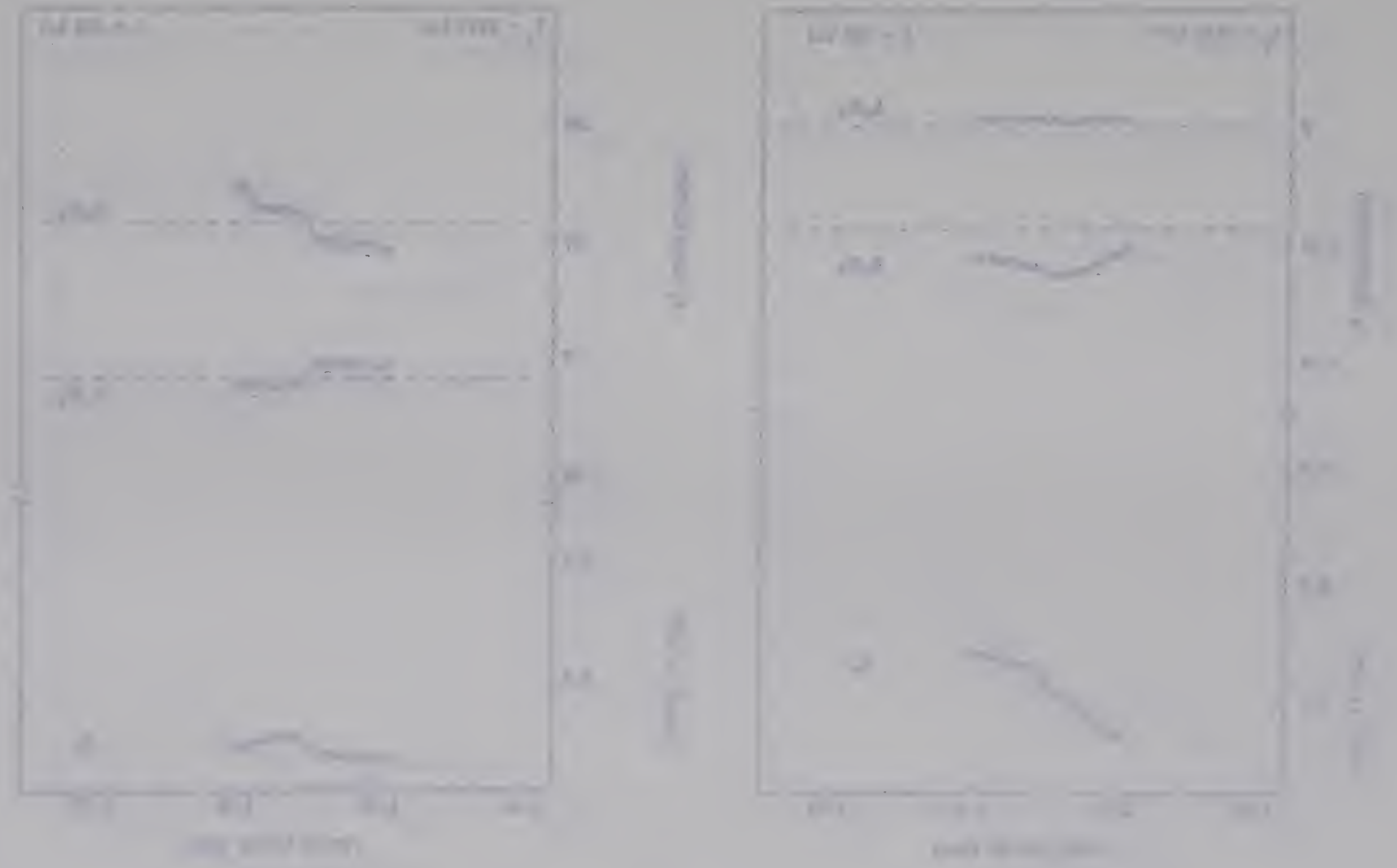

[illegible]

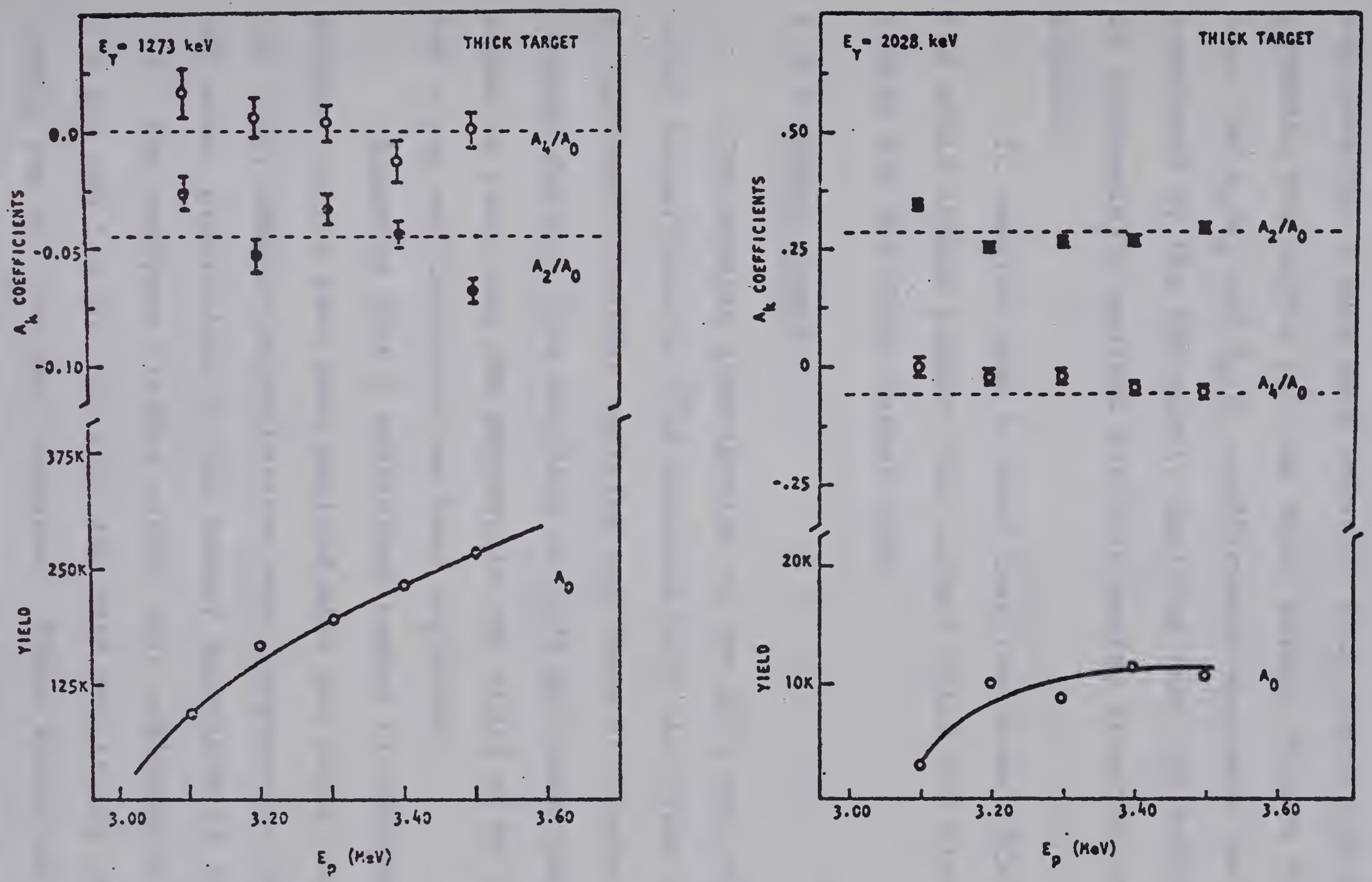

Figure 6.5 Angular distribution coefficients obtained using the thick target.

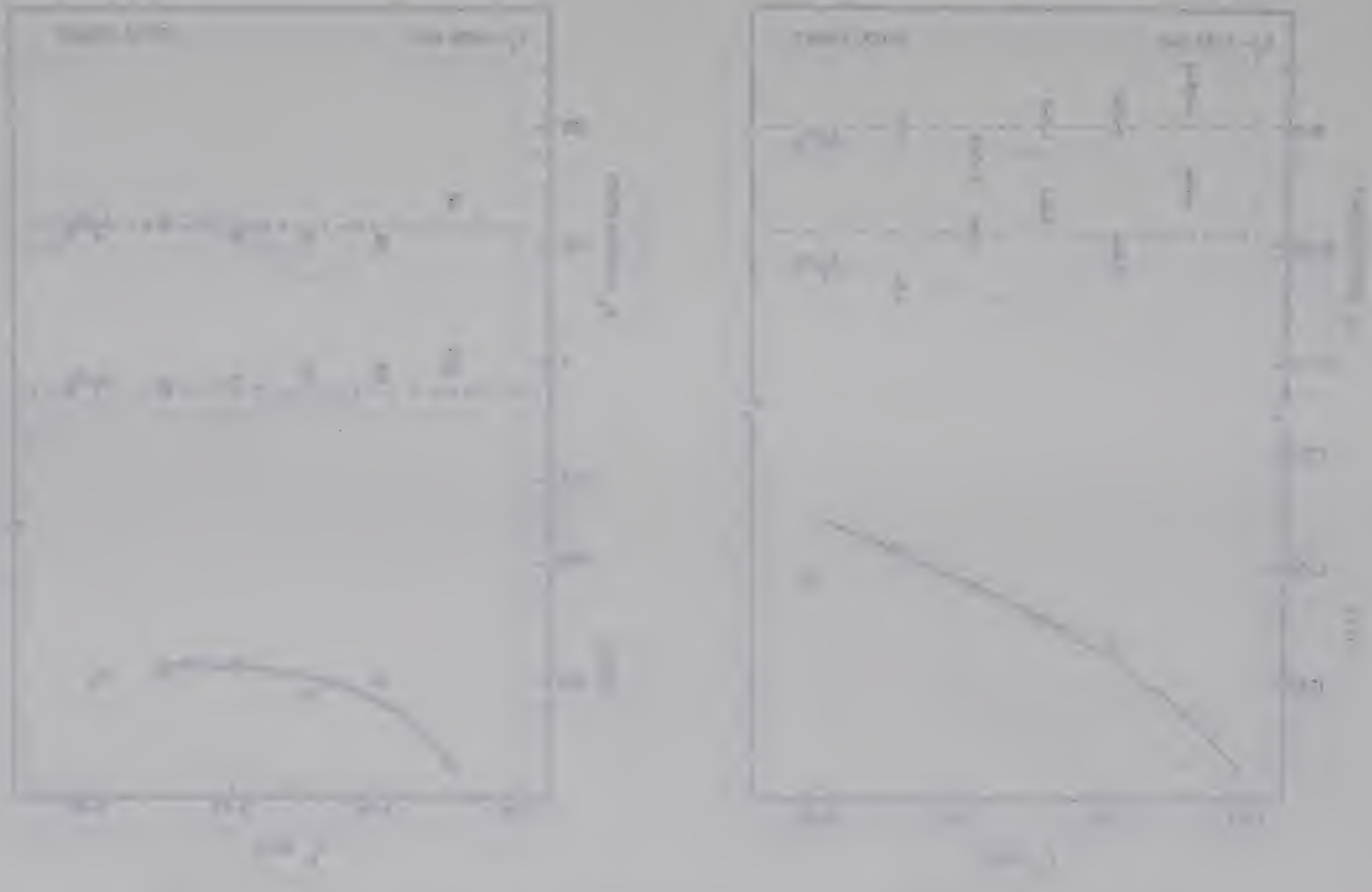

[illegible]

(Figure 6.4d) the coefficients for both the 1273 keV and 2028 keV γ rays vary smoothly with energy and they resemble the curves for the thick target (Figure 6.5). Also the A_2/A_o and A_4/A_o coefficients approach the values predicted by the SCN model; implying that the model may be successfully applied for this energy interval or greater.

It remains then to show that the normal SCN analysis would indeed predict the correct spins and mixing ratios for the thick target case.

6.3.2 Thick target

The angular distribution of the 1273 and 2028 keV γ-ray transitions in ^{29}Si measured with the thick target at different incident energies are shown in Figure 6.6. Cascade feeding from the 2028 to 1273 keV level contributed to less than one percent in the yield of the 1273 keV γ ray and therefore has been neglected.

Assuming that a sufficient number of compound nuclear states have been excited with the thick target, the γ-ray angular distributions were compared to the SCN model predictions in the manner described in Section 3.3. The analyses yielded unique spin assignments of J = 3/2 and 5/2 for the 1273 and 2028 keV levels respectively for all incident energies. These spins are consistent with previous assignments (En 73). Sample chi-

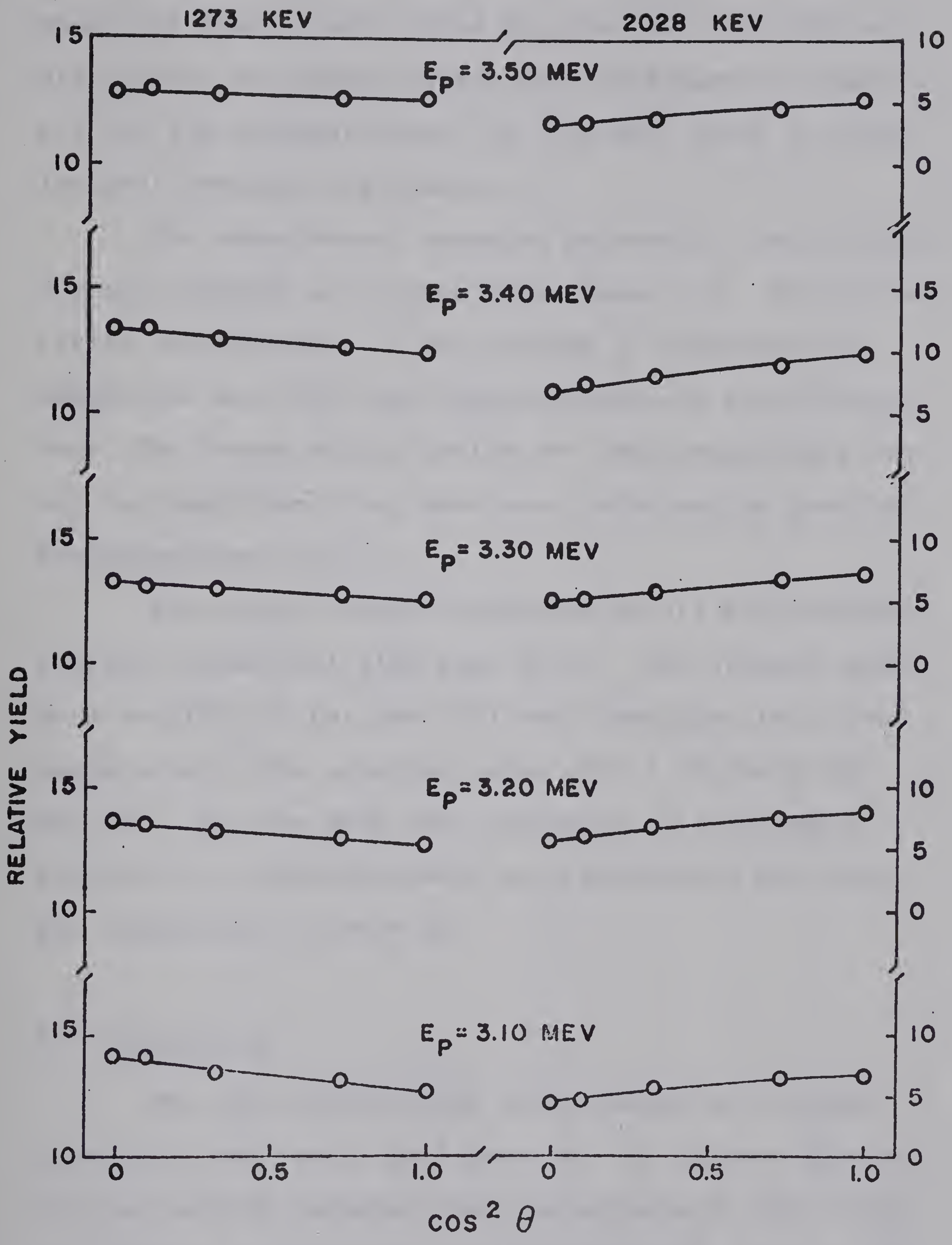

Figure 6.6 Angular distribution of the 1273 and 2028 keV γ rays measured with the thick target.

square vs mixing ratio plots for the 1273 and 2028 keV transitions are shown respectively in Figures 6.7 and 6.8 for the incident energy of 3.40 MeV; plots at other incident energies are similar.

The experimental Legendre polynomial coefficients for all energies are presented in Table 6.2. The mixing ratios corresponding to the minimum χ^2 obtained from comparison with SCN model calculations are also tabulated. The larger mixing ratios for both transitions are not included since they have been ruled out in previous investigations (En 73).

The mixing ratios determined at all the incident energies agree well with each other. The average value of $\delta = -0.18 \pm 0.03$ for the 1273 keV transition is to be compared with the accepted value of $\delta = -0.206 \pm 0.011$ (En 73). For the 2028 keV transition, the average $\delta = 0.07 \pm 0.07$ is consistent with the established fact that the transition is pure E2.

6.4 Conclusion

The thin target study has resulted in a visual picture of the statistical process. By gradual simulation of thicker targets, the fluctuations in the yield and angular distribution coefficients were shown to be damped out. This is analogous to increasing the number of levels for statistical averaging. When sufficient

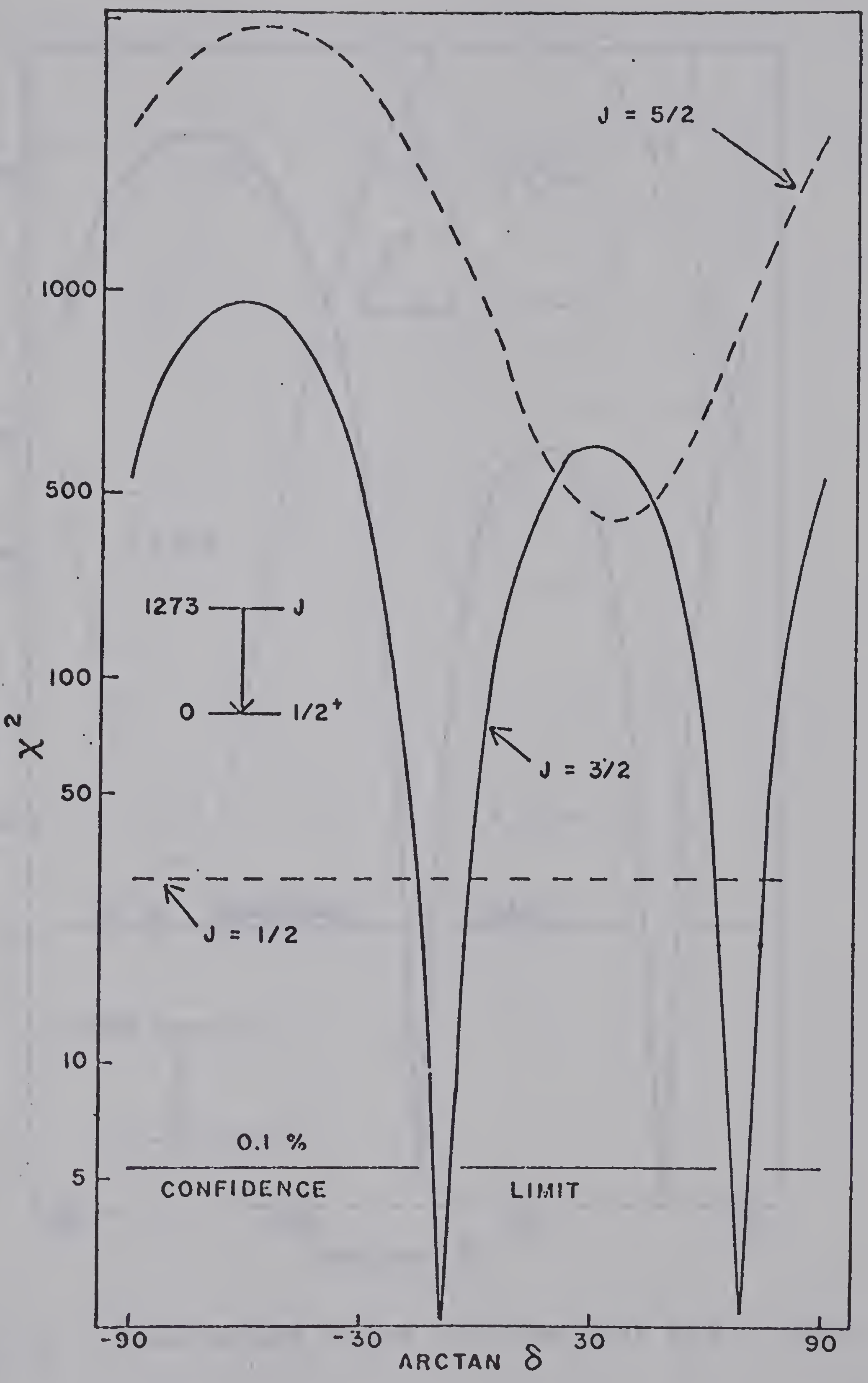

Figure 6.7 χ^2 vs mixing ratio for the 1273 keV γ rays.

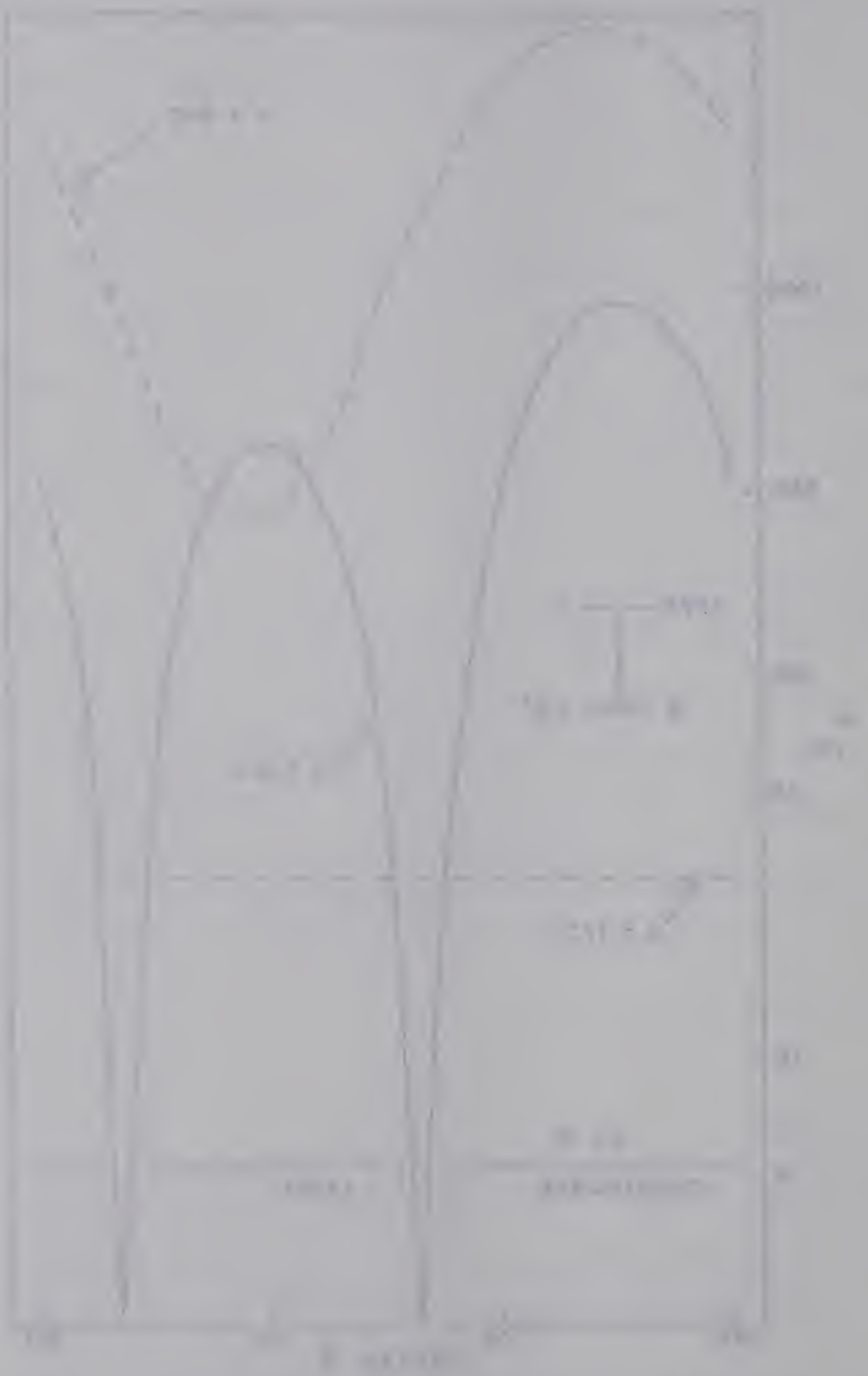

[illegible]

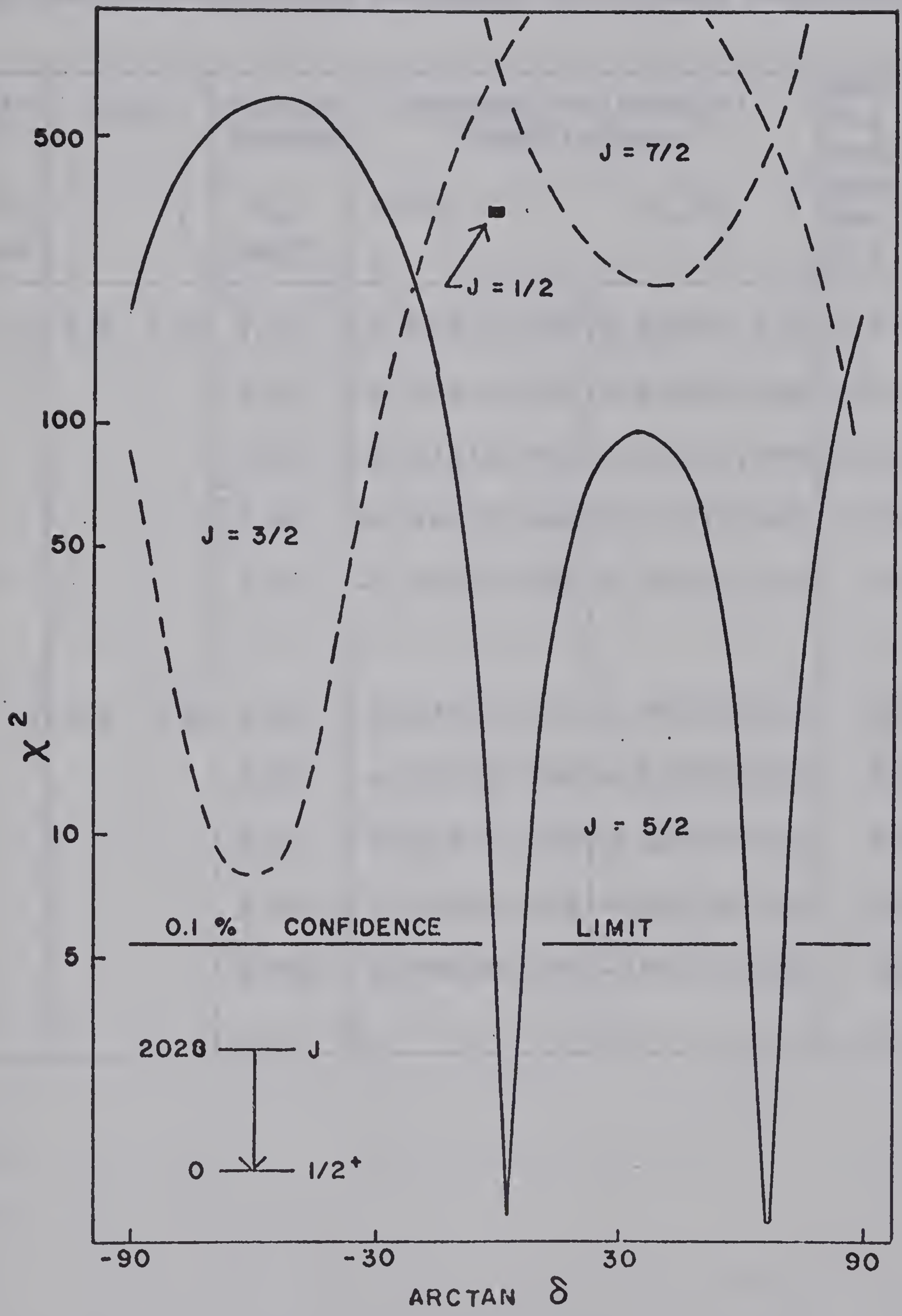

Figure 6.8 χ^2 vs mixing ratio for the 2028 keV γ rays.

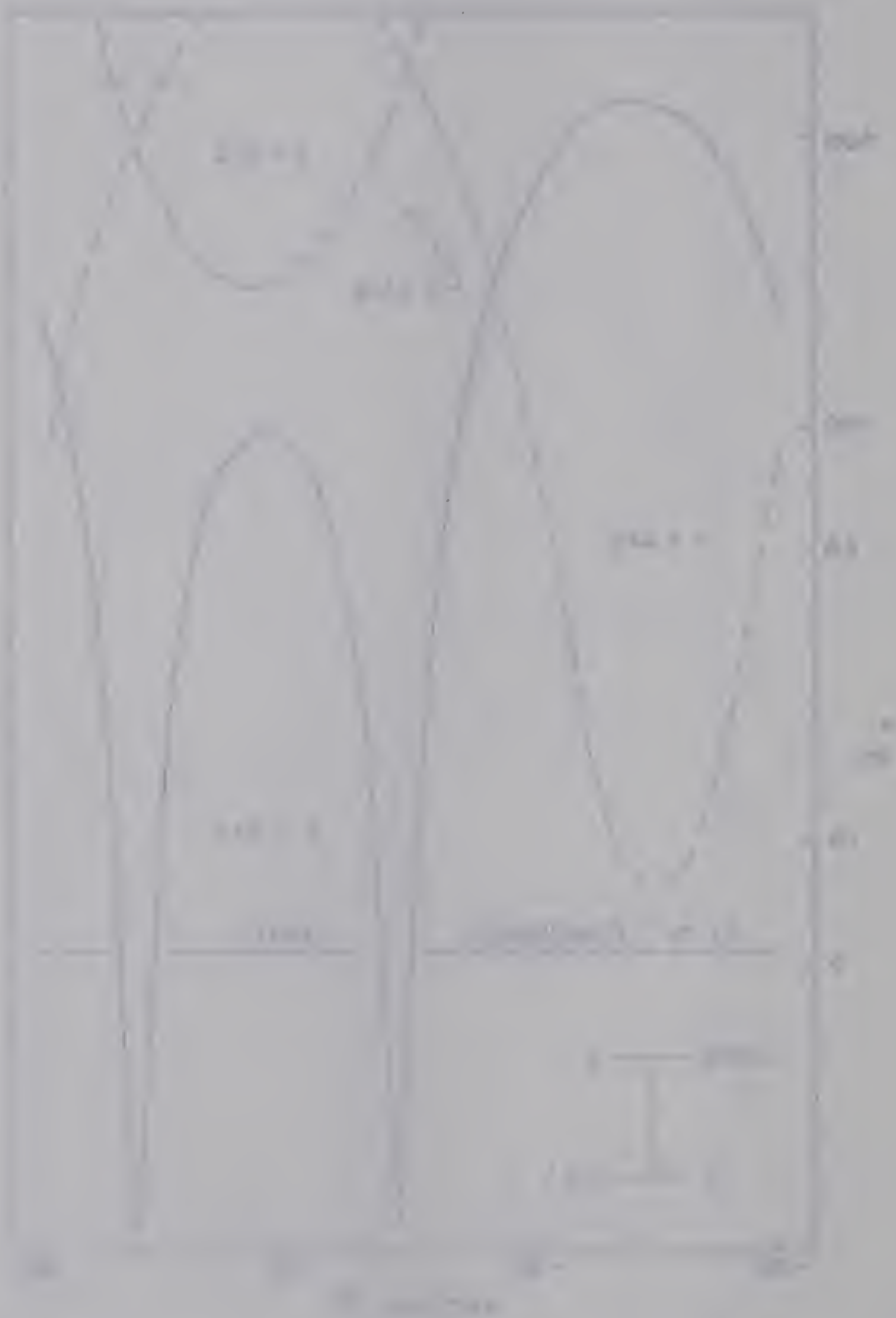

[illegible]

Table 6.2

Angular Distribution Coefficients and Mixing Ratios of ^{29}Si

Transition		Spin		Proton energy	Legendre Polynomial Coefficients		Mixing ratio	Minimum
E_i	E_f (keV)	J_i	J_f	E_p (MeV)	A_2/A_0	A_4/A_0	Arctan δ (°)	χ^2
1273	0	3/2	1/2	3.10	-0.026±0.009	0.016±0.012	-12±4	1.04
				3.20	-0.054±0.007	0.006±0.009	-10±3	0.49
				3.30	-0.033±0.007	0.004±0.008	-12±3	0.29
				3.40	-0.045±0.006	0.014±0.008	-9±4	2.36
				3.50	-0.069±0.006	0.000±0.007	-6±4	1.16
2028	0	5/2	1/2	3.10	0.345±0.016	-0.001±0.021	-4±7	1.31
				3.20	0.252±0.009	-0.022±0.012	8±8	3.96
				3.30	0.264±0.009	-0.026±0.011	6±4	1.47
				3.40	0.265±0.008	-0.050±0.010	4±4	1.13
				3.50	0.296±0.009	-0.057±0.011	4±4	0.81

levels have been included in the statistical treatment, the SCN model becomes applicable. In the $^{29}Si(p,p'\gamma)^{29}Si$ case, sufficient levels required an energy width corresponding to 400 keV in the compound nucleus.

Gilbert et al (Gi 65) reported level density 50 MeV^{-1} for the mass A = 30 region. Using their level density formula and the level information of ^{30}P (En 73), a level density of $\sim$40 MeV^{-1} was obtained for the excitation energy considered. Hence the energy of 400 keV would correspond to $\sim$20 levels (the lower limit for successful statistical averaging).

If one repeats the calculation for the compound nucleus of ^{38}Ar, one obtains a level density of $\sim$1000 MeV^{-1}. Thus to excite $\sim$20 levels in the compound nucleus, one would require a target thickness of only $\sim$20 keV. From proton range calculations (Ja 66), the evaporated target (500 $\mu g/cm^2$ $PbCl_2$) used in the $^{37}Cl(p,n\gamma)^{37}Ar$ experiment has a corresponding thickness of $\sim$25 keV. Hence one is assured that sufficient compound nuclear levels were excited to justify the statistical averaging in the ^{37}Ar experiment.

The agreement between previously established results and the SCN model predictions in both the ^{29}Si and ^{37}Ar studies establishes the wide applicability of the SCN model.

REFERENCES

An 69 J.D. Anderson, S.D. Bloom, C. Wong, W.F. Hornyak and V.A. Madsen, Phys. Rev. 177 (1969) 1416.

At 68 J. Atkinson and V.A. Madsen, Phys. Rev. Lett. 21 (1968) 295.

Ba 64 J.N. Bahcall, Phys. Rev. 135 (1964) B137.

Ba 68 J.N. Bahcall, N.A. Bahcall and G. Shaviv, Phys. Rev. Lett. 20 (1968) 1209.

Ba 68a S.I. Baker and R.E. Segel, Phys. Rev. 170 (1968) 1046.

Be 67 J.A. Becker, L.F. Chase Jr. and R.E. McDonald, Phys. Rev. 157 (1967) 967.

Bl 52 J.M. Blatt and L.C. Biedenharn, Rev. Mod. Phys. 24 (1952) 263.

Bl 66 A.E. Blaugrund, Nucl. Phys. 88 (1966) 501.

Br 57 D.A. Bromley, H.E. Gove, E.B. Paul, A.E. Litherland and E. Almquist, Can. J. Phys. 35 (1957) 1042.

Br 72 J.E. Brock, I.A. Luketina and A.R. Poletti, Phys. Rev. C6 (1972) 1298.

Br 73 C. Broude, Proc. of the Minerva Symp. of Phys. held at the Weizmann Inst. of Science, Rehovet, Israel (1973) 218.

Bu 68 G.W. Butler, J. Cerny, S.W. Cooper and R.L. McGrath, Phys. Rev. 166 (1968) 1096.

Ca 71 J.M.G. Caraca, R.D. Gill, P.B. Johnson and H.J. Rose, Nucl. Phys. A176 (1971) 273.

Ch 71 J.W. Champlin, A.J. Howard and J.W. Olness, Nucl. Phys. A164 (1971) 307.

Cl 70 D. Cline and P.M.S. Lesser, Nucl. Instr. and Meth. 82 (1970) 291.

Cu 69 J.R. Curry, W.R. Coker and P.J. Riley, Phys. Rev. 185 (1969) 185.

Da 68 R. Davis Jr., D.S. Harmer and K.C. Hoffman, Phys. Rev. Lett. 20 (1968) 1205.

Da 69 N.E. Davison, Univ. of Alberta Internal Report UAE-NPL-8 (1969) and private communication.

De 70 P.R. DeKock, J.W. Koen and W.L. Mouton, Nucl. Phys. A140 (1970) 190.

Di 69 A.E.L. Dieperink and P.J. Brussaard, Nucl. Phys. A128 (1969) 34.

Di 71 G.U. Din and J.R. Davis, Aust. J. Phys. 24 (1971) 497.

El 72 A. El-Naiem and R. Reif, Nucl. Phys. A189 (1972) 305.

En 66 H.A. Enge, 'Introduction to Nuclear Physics', Addison-Wesley Publishing Company, Inc., Reading, Mass. (1966).

En 67 P.M. Endt and C. van der Leun, Nucl. Phys. A105 (1967) 1.

En 73 P.M. Endt and C. van der Leun, Nucl. Phys. A214 (1973) 1.

En 74 P.M. Endt and C. van der Leun, Nucl. Data Tables 13 (1974) 67.

Er 66 F.C. Erné, Nucl. Phys. 84 (1966) 91.

Fi 74 H.W. Fielding, S.D. Scherry, D.A. Lind, C.D. Zafiratos and C.D. Goodman, Phys. Rev. C10 (1974) 1560.

Fl 68 D.G. Fleming, J. Cerny and N.K. Glendenning, Phys. Rev. 165 (1968) 1153.

Gi 65 A. Gilbert, F.S. Chen and A.G.W. Cameron, Can. J. Phys. 43 (1965) 1248.

Gl 64 P.W.M. Glaudemans, G. Wiechers and P.J. Brussaard, Nucl. Phys. 56 (1964) 529, 548.

Go 67 D.R. Goosman and R.W. Kavanagh, Phys. Lett. 24B (1967) 507.

Gr 67 T. Grandy, Ph. D. Thesis, University of Alberta (1967).

Gr 71 P.W. Green, University of Alberta Internal Report UAE-NPL-27 (1971).

Gr 71a P.W. Green, University of Alberta Internal Report UAE-NPL-33 (1971).

Gu 70 P.R.H. Gutowski, M. Sc. Thesis, University of Alberta (1970).

Ha 52 W. Hauser and F. Feshbach, Phys. Rev. 87 (1952) 366.

Hi 69 G.R. Hirko, Ph. D. Thesis, Yale University (1969) unpublished.

Iv 71 M. Ivascu, D. Popescu and G. van Middelkoop, Nucl. Phys. A163 (1971) 418.

Ja 66 J.F. Janni, U.S. Air Force Weapons Laboratory Report, New Mexico, AFWL-TR-65-150 (1966).

Ko 72 J.W. Koen, University of Stellenbosch, Stellenbosch, Rep. of S. Africa, private communication.

Kr 73 R.G. Kruzek, G.M. Chenevert, H.G. Leighton and B.D. Kern, Nucl. Phys. A202 (1973) 530.

La 58 A.M. Lane and R.G. Thomas, Rev. Mod. Phys. 30 (1958) 257.

Le 50 H.W. Lewis, Phys. Rev. 78 (1950) 526.

Li 60 A.E. Litherland and G.J. McCallum, Can. J. Phys. 38 (1960) 927.

Li 61 J. Lindhard and M. Scharff, Phys. Rev. 124 (1961) 128.

Li 63 J. Lindhard, M. Scharff and H.E. Schiott, Mat. Fys. Medd. Dan. Vid. Selsk. 33, No. 14 (1963).

Lu 72 I.A. Luketina, J.E. Brock and A.R. Poletti, Phys. Rev. C6 (1972) 196.

Ma 69 V.A. Madsen, 'Nuclear Isospin' Academic Press, New York (1969) 149.

Mc 67 W.J. McDonald, D.A. Gedcke, University of Alberta Internal Report (1967) unpublished.

Mc 71 A.B. McDonald, T.K. Alexander, O. Häuser and G.T. Ewans, Can. J. Phys. 49 (1971) 2886.

Me 71 L. Meyer-Schutzmeister and D.S. Gemmell, Phys.Rev. Lett. 27 (1971) 869.

Na 68 W.J. Naude, A. Bottega and W.R. McMurray, Nucl. Phys. A114 (1968) 551.

Na 72 H. Nann, Mozgovoy, R. Bass and B.H. Wildenthal, Nucl. Phys. A192 (1972) 417.

Ne 74 E.O. de Neijs, M.A. Meyer, J.P.L. Reinecke and D. Reitmann, Nucl. Phys. A230 (1974) 490.

Ni 55 S.G. Nilsson, Mat. Fys. Medd. Dan. Vid. Selsk. 29 (1955) 1.

Ol 66 J.W. Olness and E.K. Warburton, Phys. Rev. 151 (1966) 792.

Pe 62 F.G. Perey and B. Buck, Nucl. Phys. 32 (1962) 353.

Pi 69 A.A. Pilt, M. Sc. Thesis, University of Alberta (1969).

Po 61 D.I. Porat and K. Ramavataram, Proc. Phys. Soc. 78 (1961) 1135.

Pr 62 M.A. Preston, 'Physics of Nucleus', Addison-Wesley Publ. Co. Inc., Reading, Mass. (1962).

Ra 71 C.E. Ragan III, C.R. Gould, N.R. Roberson, G.E. Mitchell and D.R. Tilley, Phys/ Rev. C3 (1971) 1152.
C.E. Ragan III, G.E. Mitchell, D.R. Tilley, C.R. Gould and N.R. Roberson, Phys. Rev. C3 (1971) 2076.

Ra 71a W.L. Randolph, Jr., R.R. Borchers, R. Michaelsen, D.W. Haag and W. Ribbe, Phys. Rev. Lett. 27 (1971) 603.

Ro 65 L. Rosen, Proc. 2nd Int. Symp. on Polarization Phenomena of Nucleons, Karlsruhe (1965).

Ro 65a B. Rosner and E.J. Schneid, Phys. Rev. 139 (1965) B66.

Ro 67 H.J. Rose and D.M. Brink, Rev. Mod. Phys. 39 (1967) 306.

Ro 69 B.C. Robertson, R.A.I. Bell, J. L'Ecuyer, R.D. Gill and H.J. Rose, Nucl. Phys. A126 (1969) 431.

Ru 72 J.P. Russell, W.E. Taylor, F.E. Dunnam and H.A. van Rinsvelt, Nucl. Phys. A187 (1972) 449.

Se 71 S. Sen, C.L. Hollas and P.J. Riley, Phys. Rev. C3 (1971) 2314.

Sh 66 E. Sheldon and D.M. van Patter, Rev. Mod. Phys. 38 (1966) 143.

Sh 70 A.C. Shotter, P.S. Fisher and D.K. Scott, Nucl. Phys. A159 (1970) 577.

Sm 65 W.R. Smith, Oak Ridge National Laboratory Report ORNL-TM-1117 (1965) unpublished.

Ta 71 P. Taras, A. Turcotte, R. Vaillancourt and J. Matas, Can. J. Phys. 49 (1971) 1215.

Ta 72 P. Taras, A. Turcotte and R. Vaillancourt, Can. J. Phys. 50 (1972) 1182.

Va 72 R.J. van Reenen, W.J. Naudé and W.L. Mouton, Nucl. Phys. A183 (1972) 651.

Vo 68 E. Vogt, 'Advances in Nuclear Physics' ed. M. Baranger and E. Vogt, Vol. I, Plenum Press, N.Y. (1968) p.261.

Vo 72 M.J.A. de Voigt, P.W.M. Glaudemans, J. deBoer and B.H. Wildenthal, Nucl. Phys. A186 (1972) 365.

Wa 63 E.K. Warburton, D.E. Alburger and D.H. Wilkinson, Phys. Rev. 129 (1963) 2180.

Wa 67 E.K. Warburton, J.W. Olness and A.R. Poletti, Phys. Rev. 160 (1967) 938.

Wa 67a E.K. Warburton 'Electromagnetic Lifetimes' in Nuclear Research with Low Energy Accelerator eds. J.B. Marion and D.M. van Patter, Academic Press, N.Y. (1967).

Wi 60 D.H. Wilkinson, Nuclear Spectroscopy, ed. F. Ajzenberg-Selove, Academic Press, N.Y. (1960).

Wi 71 B.H. Wildenthal, E.C. Halbert, J.B. McGrory and T.T.S. Kuo, Phys. Rev. C4 (1971) 1266.

Wi 73 B.H. Wildenthal and J.B. McGrory, Phys. Rev. C7 (1973) 714.

Wo 72 E. Wong, B.C. Robertson, K.V.K. Iyengar, D.M. Sheppard and W.C. Olsen, Nucl. Phys. A192 (1972) 279.

Wo 72a	E. Wong and B.O. Aaquist, University of Alberta Internal Report UAE-NPL-47 (1972).
Wo 74	E. Wong, University of Alberta Internal Report UAE-NPL-72 (1974).

APPENDIX A

Modification of $F(\tau)$ due to Cascade Feeding

In lifetime investigations, if the level of interest is fed not only by direct population but also by cascade γ rays from higher energy levels then the observed $F(\tau)$ will have to be appropriately compensated. To simplify the calculations, consider a case where only a single cascade is involved (Figure A1).

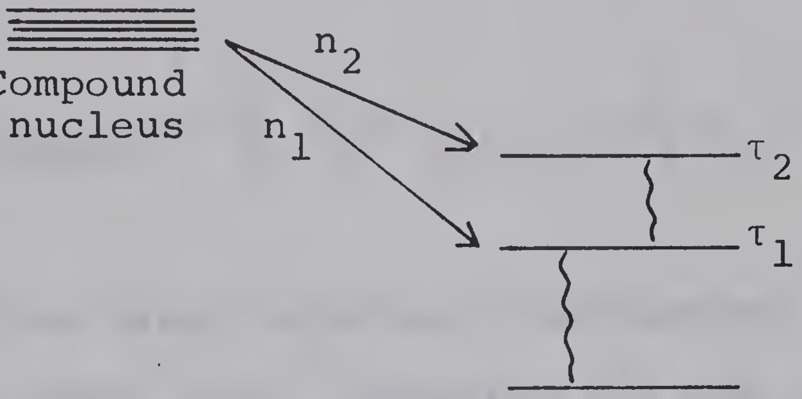

Figure A1

n_1 and n_2 represent the direct population of the states with lifetimes τ_1 and τ_2 respectively and they are normalized. (i.e. $n_1 + n_2 = 1$)

At any time, t, the population of the lower state due to direct contribution can be written as

$$n_1(t)_{\text{direct}} = n_1 e^{-t/\tau_1} \tag{A.1}$$

where e^{-t/τ_1} is the decay probability. Similarly for the upper state:

$$n_2(t)_{\text{direct}} = n_2 e^{-t/\tau_2} . \tag{A.2}$$

The decay rate of the upper state which equals the cascade feeding rate of the lower state is

$$\frac{d}{dt}\,[n_2(t)_{\mathrm{direct}}] = -\frac{1}{\tau_2}\, n_2\, e^{-t/\tau_2}$$

$$= -\frac{1}{\tau_2}\, n_2(t)_{\mathrm{direct}} \quad . \qquad (A.3)$$

From the laws of successive decay it can be shown that the decay rate of the lower state due to cascade feeding is

$$\frac{d}{dt}\,[n_1(t)_{\mathrm{direct}}] = \frac{1}{\tau_2}\, n_2(t)_{\mathrm{direct}} - \frac{1}{\tau_1}\, n_1(t)_{\mathrm{cascade}} \qquad (A.4)$$

in which the terms represent the cascade feeding rate minus its decay rate. Equation A.4 can be integrated to yield:

$$n_1(t)_{\mathrm{cascade}} = \frac{n_2\,\tau_2}{\tau_2-\tau_1}\,[e^{-t/\tau_2} - e^{-t/\tau_1}] \quad . \qquad (A.5)$$

Combining above with Equation A.1, the instantaneous population of the lower state becomes:

$$n_1(t)_{\mathrm{total}} = n_1(t)_{\mathrm{direct}} + n_1(t)_{\mathrm{cascade}}$$

$$= n_1\, e^{-t/\tau_1} + n_2\left(\frac{\tau_1}{\tau_2-\tau_1}\right)[e^{-t/\tau_2} - e^{-t/\tau_1}] \quad . \qquad (A.6)$$

The attenuation factor $F(\tau)$ for directly populated level with lifetime, τ_j, and initial velocity, v_o, has been defined (Section 2.1) as:

$$F_i(\tau_j) = \frac{1}{v_o \tau_j} \int_0^\infty v_i(t)\, \overline{\cos \phi_i(t)}\, e^{-t/\tau_j}\, dt \qquad (A.7)$$

where $v_i(t)$ is the instantaneous velocity and $\phi_i(t)$ is the angle between the initial and instantaneous recoil directions. By abbreviating

$$v_i(t)\, \overline{\cos \phi_i(t)} \equiv V_i(t)$$

we obtain

$$F_i(\tau_j) = \int_0^\infty \frac{V_i(t) e^{-t/\tau_j}}{V_i(0)\, \tau_j}\, dt \quad . \qquad (A.8)$$

Now if one combines Equations A.6 and A.8 with the definition of $F(\tau)$ one gets

$$\overline{F(\tau_1)}_{obs} = \int_0^\infty [n_1 e^{-t/\tau_1} V_1(t) + n_2 \frac{\tau_1}{\tau_2 - \tau_1} (e^{-t/\tau_2} - e^{-t/\tau_1}) V_i(t)]$$

$$= n_1 F_1(\tau_1) + n_2 \left(\frac{\tau_2 F_2(\tau_2) - \tau_1 F_2(\tau_1)}{\tau_2 - \tau_1} \right) \frac{V_2(0)}{V_1(0)} \quad . \qquad (A.9)$$

which reduces to

$$\overline{F(\tau_1)_{obs}} = n_1 F_1(\tau_1) + n_2 \left(\frac{\tau_2 F(\tau_2) - \tau_1 F(\tau_1)}{\tau_2 - \tau_1} \right) \qquad (A.10)$$

when the initial velocities are the same.

To a first approximation the $\overline{\cos \phi_i(t)}$ term may be neglected and the instantaneous velocity can be written as

$$v(t) = v_o\, e^{-t/\alpha} \tag{A.11}$$

where α is the slowing down time. Upon integration, the attenuation factor, $F(\tau)$, becomes

$$F(\tau) = \frac{\alpha}{\alpha + \tau} \tag{A.12}$$

Substituting Equation A.12 into Equation A.10, one arrives at

$$\overline{F(\tau)}_{obs} = n_1 F(\tau_1) + n_2 F(\tau_1) F(\tau_2)\ . \tag{A.13}$$

In this simplified form, the $F(\tau_1)$ factor for the lower state may be extracted if one knows the feeding fractions (n_1 and n_2) and the $F(\tau_2)$ of the upper level.

APPENDIX B

MAGPOP - A Program to Calculate Angular Distribution Coefficients of γ Rays in Terms of Magnetic Population Parameters.

MAGPOP †

E.R. Wong and B.O. Aaquist

Nuclear Research Centre
University of Alberta
Edmonton, Alberta, Canada

Internal Report UAE-NPL-47

August, 1972

---

† Work supported in part by the Atomic Energy Board of Canada

MAGPOP

E.R. Wong and B.O. Aaquist

ABSTRACT

This program is written in FORTRAN II for the XDS 920 computer at the Nuclear Research Centre of the University of Alberta. It calculates the angular distribution coefficients, A_K, of γ-ray decay between levels with spins J_1 and J_2 for all possible combinations of the magnetic population parameter $P(M_1)$ $\{ -J_1 \leq M_1 \leq J_1 \}$ and mixing ratio, δ. A least square fit of the calculated coefficients to the measured γ-ray angular distribution is included.

THEORY

The general γ-ray angular distribution between levels with spin J_1 and J_2 can be expressed as

$$W(\theta) = \sum_{K \text{ even}} A_K P_K(\cos\theta) \tag{1}$$

If J_1 is aligned [ie. $P(M_1) = P(-M_1)$] and we consider only the lowest two multipolarities (usually the case), L and L' = L + 1 then one can write

$$A_K = B_K(J_1) \times \left\{ \frac{R_K(LLJ_1J_2) + 2\delta R_K(LL'J_1J_2) + \delta^2 R_K(L'L'J_1J_2)}{(1+\delta^2)} \right\}^{*} \tag{2}$$

where $$\delta = \frac{(2L+1)^{\frac{1}{2}}}{(2L'+1)^{\frac{1}{2}}} \times \frac{< J_1 || T_{L'} || J_2 >}{< J_1 || T_L || J_2 >}$$

$$R_K(LL'J_1J_2) = (-)^{1 + J_1 - J_2 + L' - L - K} \times \left\{ (2J_1 + 1)\ (2L + 1)\ (2L' + 1) \right\}^{\frac{1}{2}}$$

$$\times\ (LL'1-1|K0)\ W\ (J_1J_1LL';KJ_2)$$

$$B_K(J_1) = \sum_{M_1} \rho_K(J_1M_1)\ P\ (M_1)$$

$$\rho_K(J_1M_1) = (-)^{J_1-M_1}\ (2J_1 + 1)^{\frac{1}{2}}\ (J_1J_1M_1-M|K0)$$

δ is the mixing ratio of the higher to the lower multipole. R_K's and ρ_K's are angular momentum coupling coefficients and have been tabulated (RO67).

The reaction dependent term is the $P(M_1)$. Frequently, compound Nuclear Statistical Model has been used to determine it in terms of the Hauser Feshbach penetrability factor, τ, (SH66). In fact, computer codes like Mandy (SH69) and AK(GR71) have been written to facilitate the calculation.

* Note: phase convention of Rose and Brink

DESCRIPTION OF PROGRAM

In some cases the condition of using the C.N. Statistical Model may not be fully justified and one may wish to perform a model independent analysis. This program has been written to achieve this model independency. For a given γ-ray decay (ie. $J_1 \rightarrow J_2$) it varies the $P(M_1)$'s to calculate the B_K's and A_K's for any given δ or range of δ. It also does a least square fit of the theoretical angular distribution resulting from these calculated A_K's to the experimental measurements.

The program allows the user to specify:

i) range of lowest $P(M_1)$ ie. $P(M_1=\frac{1}{2})$ or $P(M_1=0)$

ii) steps in which the $P(M_1)$ are to be varied

iii) range of δ

iv) steps to vary δ

v) option to output all calculated vales or those that fall below certain χ^2 (to be input by user)

vi) option to input fixed values of $P(M_1)$

PROGRAM INPUT

Program input cards are of the form (see GR71)

```
ICONTR, (DUM(I), I=1,7)         FORMAT (I2, 8X, 7F10.0)
```

where ICONTR dictates the type of input card or those that follow. The program will remember all quantities and perform calculations with them until they are changed. Default values has also been incorporated into the program such that they will be used in case the user did not input them.

ICONTR	DUM(I) I =	VARIABLE	COMMENT
-1			PROGRAM EXITS
0	-	-	The following card is title card (FORMAT 20A4)
1	1	NRHO	Number of RHO coefficients RHO coefficients follow on the next card or cards (FORMAT 8F10.0) in the order $P_2(J_1 - J_1)$, $P_2(J_1 - J_1 + 1)$... $P_2(J_1,J_1)$ for ascending K.
2	1	NRK	Number of R_K coefficients R_K coefficients follow on next and or cards (FORMAT 8F10.0) in the order $R_K(LLJ_1J_2)$, $R_K(LL'J_1J_2)$, $R_K(L'L'J_1J_2)$ for ascending K.
3	1	PMIN	smallest value of lowest magnetic population parameter
	2	PMAX	largest value of lowest magnetic population parameter
	3	PST(1)	value to step lowest population parameter
	4	PST(2)	value to step 2nd lowest population parameter
	5	PST(3)	value to step 3rd lowest population parameter
	6	PST(4)	value to step 4rth lowest population parameter
	7	PST(5)	value to step 5th lowest population parameter
	etc.		

program will read (NRHO|2) of these. Extra cards to input these may be used if necessary.

ICONTR	DUM(I)	VARIABLE NAME	COMMENT
4	1	ANORM	NORMALIZATION FACTOR FOR EXPERIMENTAL ANGULAR DISTRIBUTION (ie. A_0)
	2	SENSIT	The program will print values for which the χ^2 falls below this. Calculation begins after this card.
5	1	NANG	Number of experimental angles (NANG $\leq$ 20) Angles are input on following card or cards (FORMAT 8F10.0)
6		Y(I) (I=1,NANG)	The next card accepts the experimental angular distribution in the order of the angles input earlier (FORMAT 8F10.0)
7	-	E(I)	The next card accepts exp. dist. error (FORMAT 8F10.0)
8	1	DMIN	MINIMUM DELTA values
	2	DMAX	MAXIMUM DELTA values
	3	DSTEP	value to step the delta values
9	1	Q2	Attenuation coefficients
	2	Q4	
10	1	IOPTION	=1 program will print output only if the χ^2 is below the sensitivity ≠1 program will print all output
11	1	NPOP	number of fixed $P(M_1)$ values to follow on the next card (FORMAT 8F10.0)

DEFAULT VALUES

Default values are used unless overriden by input.

DESCRIPTION	VARIABLE
Mixing ratio, δ	DMIN = 0.0 DMAX = 0.0 DSTEP = 30.0
Magnetic Population parameter	PMIN = 0.0 PMAX = 0.5 PST(I) = 0.1 for I = 1,10
Attenuation coefficient	Q2 = 1.0 Q4 = 1.0
Experimental angles	NANG = 5.0 THETH(1) = 0.0 " (2) = 31.0 " (3) = 55.0 " (4) = 71.0 " (5) = 90.0
Output option	IOPTION = 1.0 SENSIT = 4.6

COMMENTS

The program is limited to calculation for initial state of spin, $J_1 \leq 19/2$ and for expansion of angular distribution up to the order $K = 4$. This latter condition restricts unique population combination for each value of B_K for $J_1 \leq 5/2$.

FORTRAN II PROGRAM MAGPOP FLOW CHART

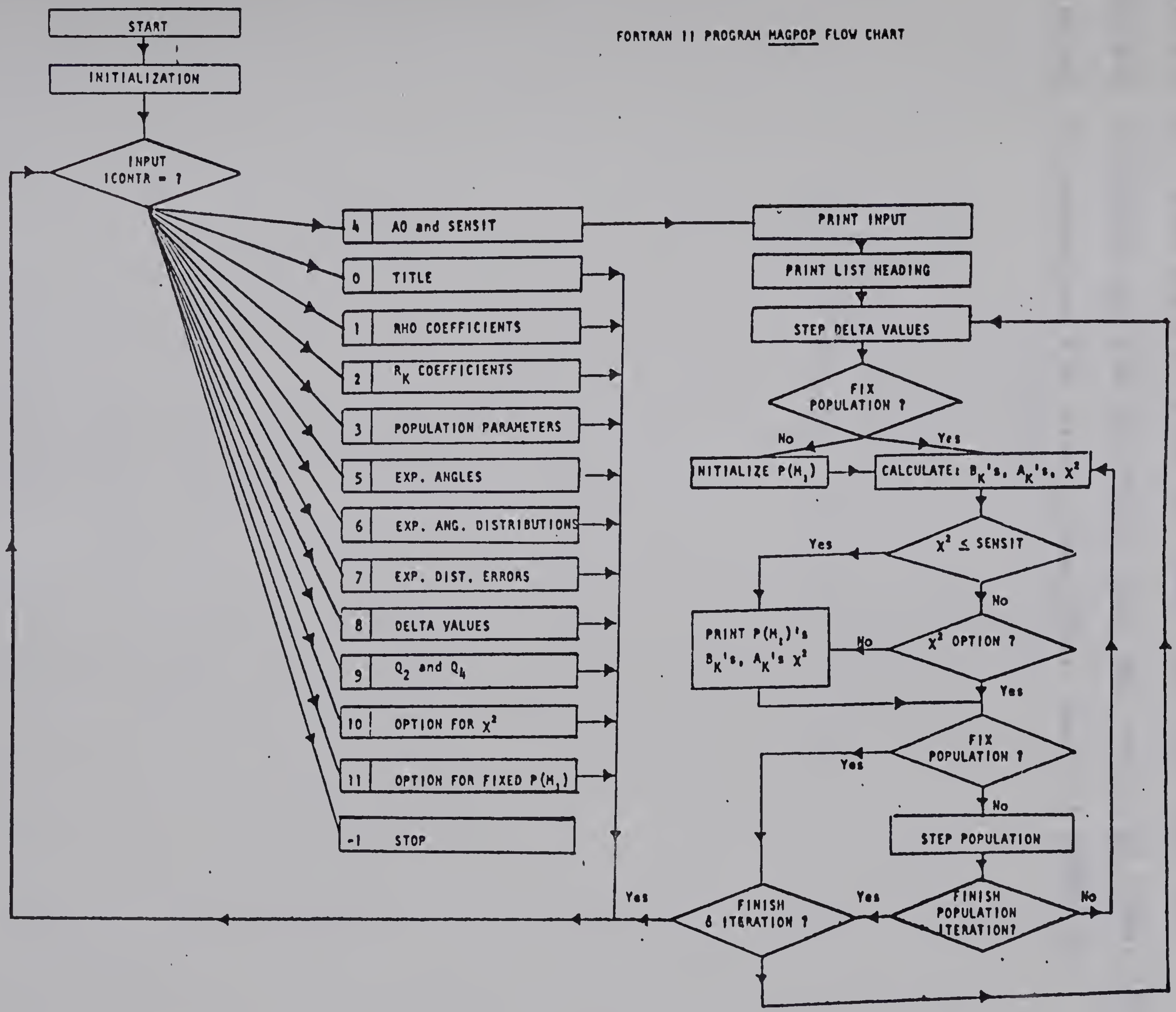

REFERENCES

1) (GR 71) P.W. Green, University of Alberta, Internal Report UAE-NPL-27.

2) (RO 67) H.J. Rose and D.M. Brink, Rev. Mod. Phys., 39 (1967) 306.

3) (SH 66) E. Sheldon and D.M. Van Patter, Rev. Mod. Phys., 38 (1966) 143.

4) (SH 69) E. Sheldon and R.M. Strang, Comp. Phys. Comm., 1 (1969) 35.

APPENDIX C

WAVY - A Program to Calculate Yield Average and Least Square Fit to Legendre Polynomial Series

WAVY

E.R. Wong

Nuclear Research Centre
The University of Alberta
Edmonton, Alberta, Canada

Internal Report

#72

November 1974

---

* Work supported in part by the Atomic Energy Control Board of Canada.

WAVY

E.R. Wong

Abstract

A FORTRAN IV program written for expanding experimental angular distributions into Legendre polynomial series of any order (< 15) in all or even orders by the least square method. It also allows one to average simultaneously several (<20) excitation functions over any range of energy interval. It is the intention of this code to use both these functions for the analysis of yield curves taken at several angles. However, each of the aforementioned subroutines may be executed separately.

Program Description

Differential cross sections (or angular distributions) are frequently expanded into the Legendre polynomial series

$$W(\theta_i) = \sum a_k P_k (\cos \theta_i)$$

where

$W(\theta_i)$ = intensities at angle θ_i

$P_k (\theta_i)$ = Legendre polynomial of order k

a_k = coefficient of order k

The program uses the method of least square to fit an experimental angular distribution to these polynomials. As the procedure is well-known and has been described in detail elsewhere [1]) only a brief outline will be given here.

If the measured value is represented by $V(\theta_i)$ then the method of least square specifies that this be achieved by chosing a_k so that

$$\Delta = \sum w_i \left[W(\theta_i) - V(\theta_i)\right]^2$$

is a minimum. w_i is the weighting factor and generally expressed in terms of standard deviation, σ_i, by $w_i = \frac{1}{\sigma_i}$.

Since the errors of measurement (i.e. standard deviation, σ_i) are known, then Δ_{min} has a χ^2 distribution with $(n - m)$ degrees of freedom where n is the number of observations and m the number of fitted parameters.

Given a set of observations (angular distributions) the program will determine the a_k coefficients. The maximum order, k_{max}, of these coefficients is governed by the user. However, k_{max} must not exceed the number of observations or 15. An option is also provided in cases where only even order Legendre polynomial expansion is required, (e.g. reactions that exhibit symmetry about 90°). Aside from printing these a_k coefficients and their associated errors, the program will also give the χ^2 per degrees of freedom for the fit.

The other part of the program concerns the averaging process whereby an excitation function recorded with good energy resolution

may be averaged to simulate yield with poorer resolution. In particular by averaging two adjacent yield points one would simulate an excitation obtained with a target twice as thick. Consequently, increasing the averaging interval would correspond to thickening the target. Of course one may, on the other hand, regard it as deterioration of beam energy resolution. The program allows the user to impose lower and upper limits as well as the increment of the averaging process.

The averaging procedure may be combined with the least square fitting procedure to analyse yield curves obtained at several angles simultaneously. Thus the program will perform the least square fit after each averaging interval.

The program consists of a mainline which controls the input and output as well as the calling of subroutines. It also contains the option of writing the output into a disk file beside the normal printout. This latter option is handy when one wishes to plot the yield curves. The format with which the output is written onto the file is compatible with the input format of the plotting code, "AUTOPLOTTER" 4).

<u>Input</u>

A control, ICONTR, is used to distinguish between the different input quantities and dummy variables are then used to accept all input 2,3). The input cards are of the form

```
ICONTR, (DUM(I), I  I,7)     FORMAT (I2,F18.0,6F10.0)
```

Once a quantity has been entered it will be used until changed with the exception of ICONTR = 2 card which must be included for each set of averaging calculation, otherwise the default value will be used. The codes for control and dummy variables are tabulated in Table I and the default values for some variables in Table II.

As mentioned earlier the two parts of the program may be executed independently; the key control cards for calling the respective subroutines are ICONTR = 2 and ICONTR = 5. If ICONTR = 2 card is omitted, then the program will not call the averaging routine. On the other hand if on the ICONTR = 5 card, the quantity, NANG = 1, then no least square fitting will be performed.

In the averaging process, the number of yield points are determined from the maximum, minimum and increment and hence the ICONTR = 2 card must precede ICONTR = 4,6 and 7 cards. Yields for each energy are then expected to be entered on separate cards in order of increasing energy following ICONTR = 6 card. The normalization factors (ICONTR = 4) and yield errors (ICONTR = 7) are input in the similar manner. All quantities in general may be input in any sequence.

The program will start executing after the ICONTR = 7 series of cards have been read and will continue calculating for any number of sets of data until it encounters ICONTR = -1 or other terminating commands.

References

1) A.J. Ferguson, *Angular Correlation Method of Gamma-Ray Spectroscopy*, North Holland Publishing Company, p. 105.

2) W.P. Green, University of Alberta, Nuclear Research Centre Internal Report UAE-NPL-27.

3) E. Wong and B.O. Aaquist, University of Alberta, Nuclear Research Centre Internal Report UAE-NPL-47.

4) M. Easton, "AUTOPLOTTER", University of Alberta Computer Service Publication (1971).

TABLE I

ICONTR	DUM(I) I =	VARIABLE	COMMENT
-1			Stop
0		TITLE(I)	Title read on the following card (FORMAT 20A4)
1	1	KB	Maximum order of Legendre polynomial to be fitted (KB < 15)
	2	NOPT	0 only even orders fitted 1 all orders fitted
	3	NPLOT	0 no output for plot 1 output for plot without errors >1 output for plot with errors
2*	1	ENMIN	Minimum energy
	2	ENMAX	Maximum energy
	3	ENDEL	Energy increment
	4	XINTMI	Minimum energy interval to be averaged
	5	XINTMA	Maximum energy interval to be averaged
	6	XINTDE	Energy interval increment
3**		Q(I)	Attenuation coefficients follow on the next card or cards (FORMAT 8F10.0)
4		TEMP(I)	Normalization factors follow on the next card or cards (FORMAT 8F10.0)
5	1	NANG (< 20)	Number of experimental angles
6		YY(I)	Experimental angular distributions read in the order of angles on the next card or cards
7		YEY(I)	Experimental distribution errors corresponding to YY(I) on the following card or cards

Program starts execution after ICONTR = 7 series of cards are read.

* This card must precede ICONTR = 4, 6 and 7 cards if it is used.

** This card must follow ICONTR = 1 card if it is used.

TABLE II

DEFAULT	VARIABLE	DESCRIPTION
3	KB	Maximum number of order of the Legendre polynomial
0	NOPT	Option to fit only even orders of Legendre polynomial
0	NPLOT	Option of NO output for plot
1	NANG	Number of experimental angles = 1
1.0	Q(I)	Attenuation coefficients = 1.0
1.0	TEMP(I)	Normalization factors = 1.0

APPENDIX D

Volume 29B, number 9 PHYSICS LETTERS 4 August 1969

POSITIVE PARITY STATES IN ^{40}K *

P. J. TWIN **, W. C. OLSEN and E. WONG
Nuclear Research Centre,
The University of Alberta, Edmonton, Canada

Received 27 June 1969

Neutron and γ-ray angular distributions, and γ-ray polarisation correlations have been measured with the reaction ^{40}Ar(p, nγ)^{40}K. Positive parity states have been established at 1.644 MeV (0^+), 1.959 MeV (2^+), 2.261 MeV (3^+) and 2.290 MeV (1^+).

Recent interest in deformed states in nuclei around ^{40}Ca [1, 2] led us to search for such states in ^{40}K, where they would be characterised by their positive parity. The ^{39}K(d, p)^{40}K reaction [3] was known to preferentially excite the single p-h (negative parity) states, the four lowest states at 0, 30, 800 and 891 keV are $f_{\frac{7}{2}} d_{\frac{3}{2}}^{-1}$ states whilst those at 2047, 2070, 2103 and 2625 keV arise from the $p_{\frac{3}{2}} d_{\frac{3}{2}}^{-1}$ configuration. We have studied the ^{40}Ar(p, n)^{40}K reaction which strongly excites nearly all the low-lying levels in ^{40}K including the four lowest levels not described by single p-h configurations. These are at 1644, 1959, 2261 and 2290 keV.

The lifetime of the 1644 keV state of 0.49 μs [4] together with its mode of decay to both the 800 keV (2^-) and 30 keV (3^-) states indicate a probable assignment of 0^+. On the other hand, a negative parity with $J \leq 2$ is favoured by a recent DWBA analysis of data from the ^{40}Ar(τ, t)^{40}K reaction [5]. We have measured the neutron angular distributions from the five lowest levels in ^{40}K at a bombarding energy of 5.5 MeV using the pulsed proton beam and neutron time-of-flight facility at the University of Alberta. The only distribution to exhibit any marked anisotropy was that for neutrons exciting the 1644 keV state. The symmetry about 90° of this distribution, shown in fig. 1, indicates the dominance of the compound nuclear mechanism. The theoretical distributions shown were calculated with a Hauser-Feshbach computer program [6] which uses the average potentials of Rosen [7]. Small changes in the potentials did not affect the shape of the distributions which clearly indicate the 1644 keV state has spin 0. The negative parity assignment is ruled out as it requires an M3 enhancement factor of 10^4 for the 1614 keV γ-ray.

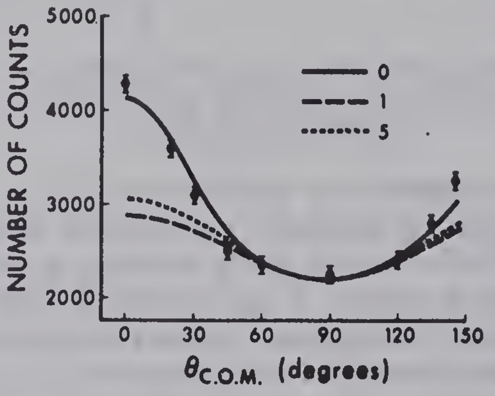

Fig. 1. Neutron angular distribution for 1644 keV state in the reaction ^{40}Ar(p, n)^{40}K at a proton bombarding energy of 5.5 MeV. The fitted curves are derived from a compound nuclear model calculation for spin assignments of 0, 1 and 5. The other possible spin values of 2, 3 and 4 give essentially isotropic distributions.

The 1959 keV state was studied at a proton energy of 4.44 MeV, 90 keV above its threshold excitation energy. We measured the angular distributions of both the 1159 keV (→ 800 keV 2^- state) and 1929 keV (→ 30 keV 3^- state) γ-rays with a 45 cm^3 Ge(Li) detector; the γ-γ correlation between the 1159 keV and 770 keV γ-rays with NaI crystals; and the polarisation direction correlation of the 1159 keV γ-ray with a Compton polarimeter with the 45 cm^3 Ge(Li) counter as the scatterer and two NaI crystals as the analysers. The data were fitted in terms of the 1959 keV level's magnetic substate populations, which were limited to lie within values calculated at threshold and 200 keV above threshold by the MANDY program of Sheldon and Van Patter [8], which is based on the compound nuclear

---

* Work supported in part by the Atomic Energy Control Board of Canada.

** On leave of absence from University of Liverpool, England.

model. The large a_2 Legendre coefficients of 0.40 ± 0.01 and -0.22 ± 0.02 for the angular distributions of the 1159 keV and 1929 keV γ-rays, respectively, could only be fitted by a spin 2 assignment to the level, which was confirmed by the γ-γ correlation. The polarisation of the 1159 keV γ-ray was measured at angles of $\theta = 90^{\circ}$, 45° and 0° relative to the beam direction, the results at 0° being used to correct for slight differences in the efficiency of the analysing crystals. The definition of polarisation used was

$$p = \frac{1}{R} \times \frac{N(\theta, \phi = 0) - N(\theta, \phi = 90)}{N(\theta, \phi = 0) + N(\theta, \phi = 90)}$$

where $N(\theta, \phi)$ is the number of counts in the photo-peak of the sum coincidence spectra at angles θ, ϕ. The efficiency, R, of the polarimeter was calculated with the solid-angle correction technique suggested by Ferguson [9] and checked by the results for the $2^+ \rightarrow 0^+$ 1460 keV transition in ^{40}Ar. The measured polarisation of -0.76 ± 0.21 (the efficiency calculation contributing most of the error) enabled the definite assignment of positive parity to the 1.959 MeV state. The χ^2 plot versus δ, shown in fig. 2, for various spin and parity assignments indicates pure E1 character for the 1159 keV γ-ray. The 1929 keV γ-ray was determined to have an M2/E1 mixing ratio of 0.10 ± 0.07.

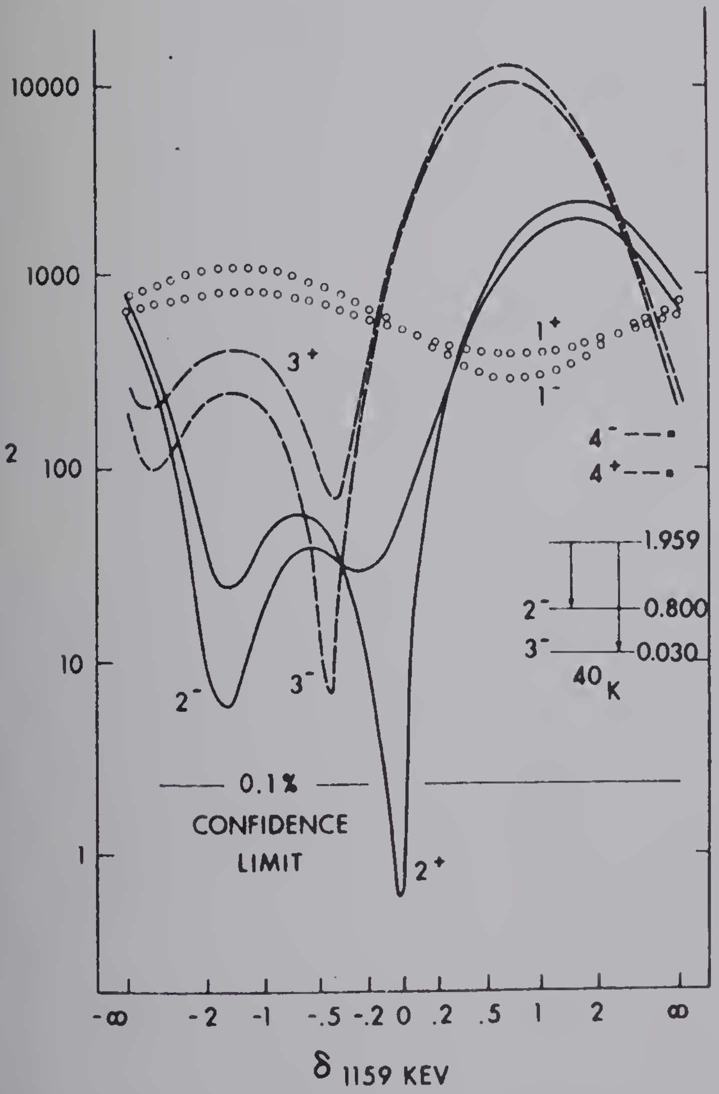

Fig. 2. A plot of χ^2 versus δ for various spin and parity assignments to the 1959 keV state. The angular distributions of the 1159 keV and 1929 keV γ-ray and the polarisation-direction correlation of the 1159 keV γ-ray are fitted simultaneously.

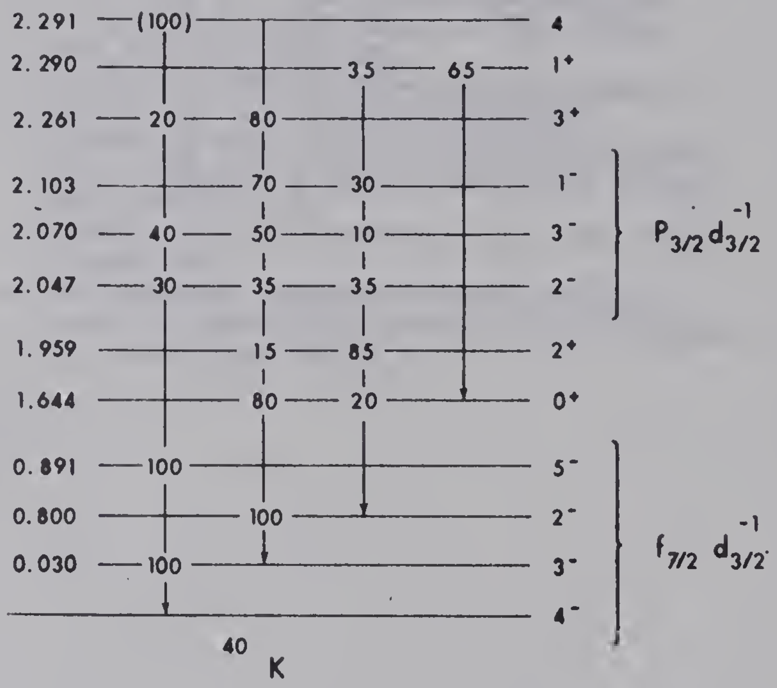

Fig. 3. A summary of the spin and parity assignments together with the γ-ray branching ratios for the low-lying states in ^{40}K.

From similar techniques the angular distributions of the 2231 keV and 2261 keV γ-rays indicate that the 2261 keV state has a spin of 3 whilst the polarisation correlation at $\theta = 90^{\circ}$, yielding p = -0.57 ± 0.28, shows that the state has positive parity. The 2290 keV state observed in the ^{39}K(d,p)^{40}K reaction [3] has been shown to be a doublet of energies 2290 and 2291 keV. The 2290 keV state decays to the 1644 keV 0^+ state (646 keV γ-ray) and the 800 keV 2^- state (1490 keV γ-ray) whilst the 2291 keV state decays to the 4^- ground state. The angular distribution of the 646 keV γ-ray can only be fitted with a spin assignment of 1 and the compound nuclear calculation also gives a fit three times better for 1^+ than for 1^-. The presence of the strong decay mode to the 0^+ state also indicates the state has positive parity. The angular distribution of the 2291 keV γ-ray with an a_2 of 0.55 ± 0.03 can only be fitted for a spin of 4 to the 2291 keV state.

These results, summarised in fig. 3, show that at least four positive parity states, with possible configuration $f_{7/2}^{2}d_{3/2}^{-2}$ and with spins 0^+, 1^+, 2^+ and 3^+, lie at the same energy in ^{40}K as the single p-h $p_{3/2}d_{3/2}^{-1}$ states.

[illegible]

[illegible]

[illegible]

The authors wish to thank Drs. W. J. McDonald, J. L. Honsaker and D. M. Sheppard, and Mr. T. P. G. Carola for their assistance with various parts of the experiment.

References

1. W. J. Geraee and A. M. Green, Nucl. Phys. 93 (1967) 110 and A123 (1969) 241.
2. B. H Flowers and L. D. Skouras, Nuel. Phys. A116 (1968) 529.
3. H. A. Enge, E. J. Irwin and D. H. Weaner, Phys. Rev. 115 (1959) 949.
4. J. G. Main et al., Phys. Letters 26B (1968) 295.
5. J. J. Wesolowski, L. F. Hansen and M. L. Stelts, Phys. Rev. 172 (1968) 1072.
6. N. E. Davison, Nuclear Research Centre Report, University of Alberta, 1968 (unpublished).
7. L. Rosen, in Proc. Second Intern. Symp. on polarisation phenomena of nucleons (Birkhauser Verlag, Basel, 1966) V, 253.
8. E. Sheldon and D. M. Van Patter, Revs. Mod. Phys. 38 (1966) 143.
9. A. J. Ferguson, Angular correlation methods in gamma-ray spectroscopy (North-Holland Publishing Co., Amsterdam, 1965) p. 40.

* * * * *

APPENDIX E

A Study of γ Rays of ^{37}Ar

Nuclear Physics **A192** (1972) 279—290; © *North-Holland Publishing Co., Amsterdam*

Not to be reproduced by photoprint or microfilm without written permission from the publisher

A STUDY OF γ-RAYS OF ^{37}Ar

E. WONG, B. C. ROBERTSON, K. V. K. IYENGAR [†], D. M. SHEPPARD
and W. C. OLSEN

Nuclear Research Centre, University of Alberta, Edmonton, Alberta, Canada [††]

Received 28 January 1972
(Revised 4 April 1972)

Abstract: The mean lifetime of levels in ^{37}Ar below 3.30 MeV excitation were measured via the ^{37}Cl(p, nγ)^{37}Ar reaction with the Doppler-shift attenuation method. Gamma-ray angular distributions were obtained at various incident energies and compared with the predictions of the statistical compound nuclear model. The angular distribution and lifetime results yield an assignment of $J^\pi = \frac{5}{2}^{(+)}$ for the 3.171 MeV level and $J^\pi = \frac{9}{2}^-$ for the 3.185 MeV level. The experimental results are discussed and compared with shell-model calculations.

E | NUCLEAR REACTION ^{37}Cl(p, nγ), $E = 3.25$–5.90 MeV; measured $\sigma(E; E_\gamma, E_n, \theta_\gamma)$, Doppler-shift attenuation. ^{37}Ar deduced levels, τ, γ-branching ratios, J^π, γ-mixing. Enriched targets; Neutron time-of-flight technique; Ge(Li) detector.

1. Introduction

Nuclei near doubly closed shells are of considerable interest due to the relatively simple shell-model configurations expected, and experimental data can be readily compared in detail with theoretical predictions. However, the fact that the simple shell model cannot account for even the number of levels in ^{37}Ar up to an excitation of 4 MeV [ref. [1])], suggests the presence of more complex configurations. The measurements of other properties such as the electromagnetic decay and lifetimes should provide useful information about these configurations.

The present experiment was undertaken to provide information on level spins, multipole mixing ratios, branching ratios and lifetimes for ^{37}Ar levels up to an excitation of 3274 keV. The results are compared with previous information, where available. The existence of the 3185 keV level [1,2]) is directly confirmed by a neutron time-of-flight measurement. The lifetime and mixing ratio results are discussed in terms of the available theoretical predictions.

2. The experiment

2.1. EXPERIMENTAL ARRANGEMENT

2.1.1. *Lifetime determination.* Levels in ^{37}Ar up to an excitation of 3.28 MeV were populated via the ^{37}Cl(p, nγ)^{37}Ar reaction ($Q = -1.596$ MeV) using a 5.70

[†] Present address: Nuclear Reactions Section, Tata Institute of Fundamental Research, Homi Bhabha Road, Colaba, Bombay, 5 India.

[††] This work has been supported in part by the Atomic Energy Control Board of Canada.

MeV proton beam from the University of Alberta 6 MV Van de Graaff generator. The target consisted of 500 $\mu g/cm^2$ of $PbCl_2$ (enriched to 87 % in ^{37}Cl) evaporated onto a 0.5 mm thick Au backing. Gamma rays were detected both in coincidence with neutrons and in singles by a 45 cm^3 Ge(Li) detector placed 10 cm from the target. Neutrons were detected in a 5.1 cm thick × (17.8 cm OD, 2.5 cm ID) NE218 annular neutron detector subtending angles between 157° and 177° to the beam axis and placed 15.8 cm from the target. The γ-flux in the neutron detector was suppressed by a 1.95 cm thick lead shield. Detected γ-rays were rejected by time-of-flight gating and pulse-shape discrimination. Details of the γ-rejection and n-γ coincidence circuits are given in ref. [3]).

Gamma-ray peaks from ^{88}Y and ^{60}Co sources were accumulated during all runs. In singles runs these were added directly to the spectra, but in the n-γ coincidence runs additional circuits were used to select γ-γ coincidences between the Ge(Li) detector and a 7.5 cm × 7.5 cm NaI(Tl) crystal placed nearby. This γ-γ coincidence source spectrum was accumulated in parallel with the n-γ spectrum and provided a continuous monitor of the system stability.

2.1.2. *Angular distribution measurements.* Gamma-ray distributions for levels up to an excitation of 3274 keV were measured in singles at several proton energies between 3.25 and 5.15 MeV. The Ge(Li) detector was mounted on a rotating trolley at a distance of 20 cm from the target. Measurements were carried out using thick targets [see ref. [3])] of enriched ^{37}Cl ($\approx$ 85 %) in the form of KCl deposited onto a 0.05 cm thick Ta backing as well as the evaporated $PbCl_2$ target. An additional small (6 cm^3) Ge(Li) detector fixed at 90° was used in the initial stage of the experiment to monitor the reaction yield.

2.2. DATA ANALYSIS

2.2.1. *Lifetime analysis.* Observed energy shifts for the various levels were obtained from the centroid position of the appropriate γ-rays by a least-squares fitting procedure. The mean initial recoil velocity was determined from kinematics, taking into account the energy loss of the incident beam through the target. For n-γ coincidence runs, the finite angle of the neutron detector was also taken into account. For the singles experiments, the influence of the neutron angular distribution on the mean initial recoil velocity was accounted for using the method of ref. [4]). Neutron angular distributions were also independently measured using a time-of-flight technique [see ref. [5])] to explicitly calculate the mean initial recoil velocity; results obtained using the two methods agreed in all cases to better than 1 %.

The $F(\tau)$ curves were calculated using a computer code [6]) which uses the formulae of Lindhard [7]) to calculate electronic and nuclear stopping. There is evidence [8]) for systematic deviation from the Lindhard predictions for electronic stopping of up to 30 %, and in fact the stopping power calculations of Firsov [9]) have been shown in many cases [10]) to give closer agreement with experiment than those of Lindhard. However, for Ar ions stopping in Cl, where the largest deviation from the Lindhard

prediction might be expected in the present experiment, the two predictions agree to within 1 %. Consequently the Lindhard values have been used throughout and a 20 % error assigned to the total stopping power.

2.2.2. *Angular distribution analysis and branching ratio determination.* Gamma-ray yields were obtained by summing counts over the full-energy peak of the appropriate γ-rays and normalizing to the yield of the isotropic decay of the 1410 keV ^{37}Ar level ($J^\pi = \frac{1}{2}^+$). Angular distributions were fitted to an even-order Legendre polynomial series and also compared with the predictions of the statistical model of Sheldon [11]). In addition, comparisons were made allowing the spin substate populations to vary in order to evaluate the dependence of extracted mixing ratios on the validity of the statistical model assumption (subsect. 3.3.1). The phase convention of Rose and Brink [12]) for mixing ratios was used throughout. Mixing ratios errors were estimated using the method proposed by Cline and Lesser [13]).

Angular distributions predicted by the statistical model were calculated and compared with experiment using the computer code AK [ref. [14])]. All kinematically allowed neutron exit channels as well as the proton elastic channel and the four strongest α-particle exit channels were included in the calculation. The necessary transmission coefficients were obtained [15]) using the optical-model parameters of Rosen [16]) for protons, Perey and Buck [17]) for neutrons and Davis [18]) for α-particles. Transmission coefficients were also obtained from the code ABACUS [ref. [19])] and yielded essentially the same results.

Branching ratios were determined using the zero-order Legendre polynomial coefficients and the previously measured detector efficiencies [20]).

3. Experimental results

3.1. EXCITATION ENERGIES AND DECAY SCHEMES

Excitation energies were inferred from the various γ-ray energies determined by the fitting procedure described in subsect. 2.2.1. Gamma-ray energies were determined independently from the singles and the coincidence data, and found to be in good agreement. The excitation energies are summarized in fig. 1, together with the branching ratio information. The present results are in generally good agreement with those of refs. [1, 2, 21–23]).

It has been proposed from γ-ray studies [1, 2]) that the 3.17 MeV level is a doublet, consisting of levels of 3171 and 3185 keV excitation. To obtain direct confirmation of the presence of the 3185 keV level, a neutron time-of-flight spectrum was accumulated using a pulsed proton beam [5]) at an incident proton energy of 5.90 MeV and a 100 μg/cm^2 thick PbCl$_2$ target (enriched to 87 % ^{37}Cl). A neutron group corresponding to the proposed level can be clearly seen (fig. 2) in the time-of-flight spectrum, giving direct confirmation of the existence of a level in ^{37}Ar at an excitation of 3185 keV.

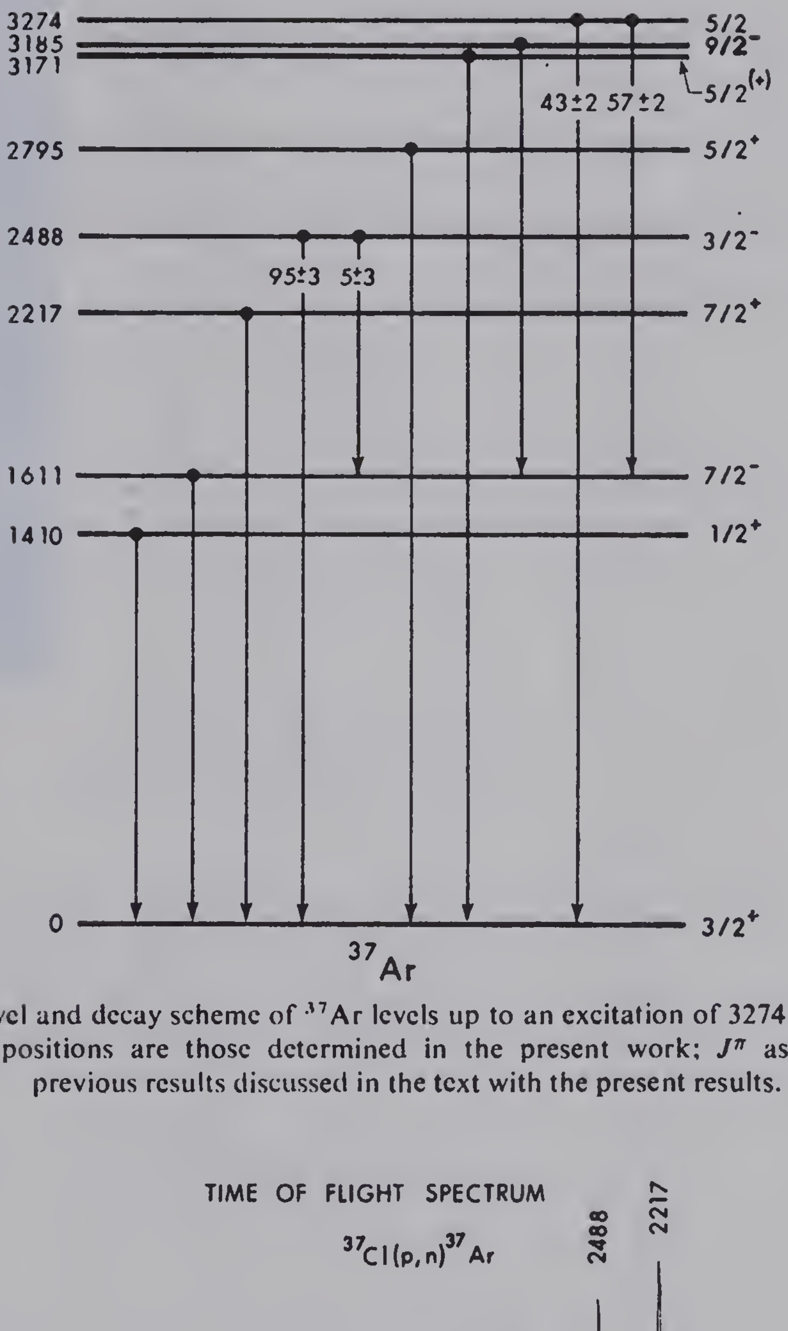

Fig. 1. Energy level and decay scheme of ^{37}Ar levels up to an excitation of 3274 keV. The branching ratios and level positions are those determined in the present work; J^π assignments combine previous results discussed in the text with the present results.

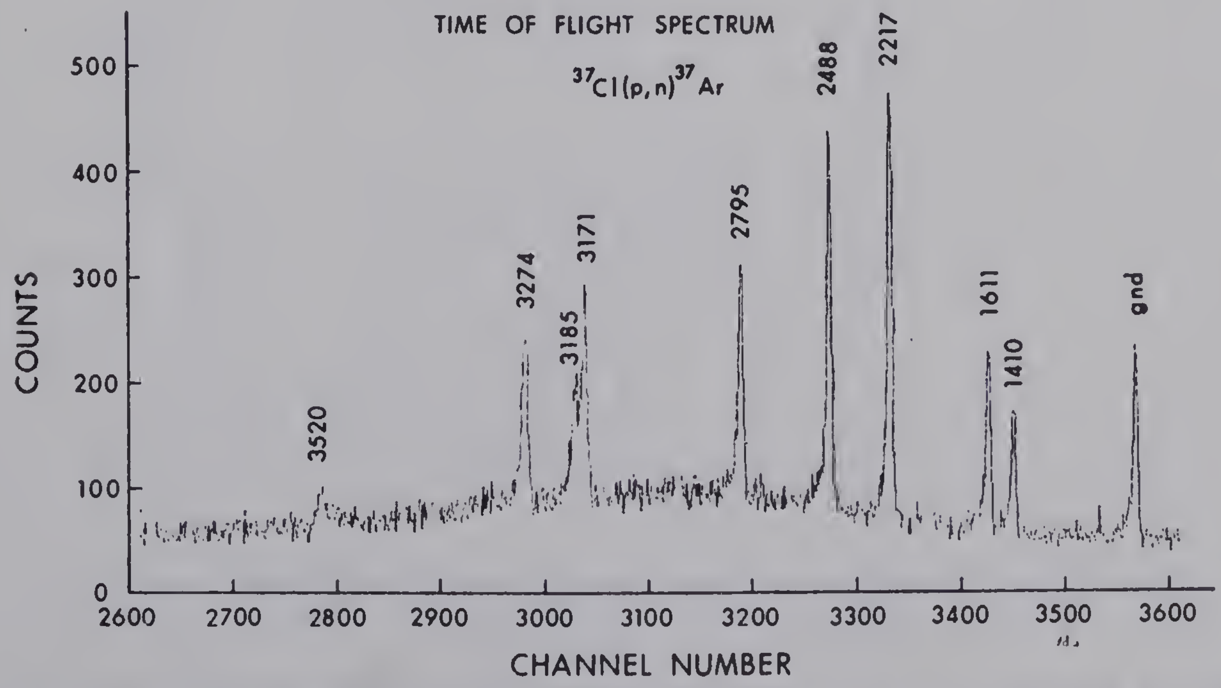

Fig. 2. Time-of-flight spectrum of neutrons from the ^{37}Cl(p, n)^{37}Ar reaction observed for a flight path of 6.37 m. Neutrons were detected at 0° to the beam axis in a NE213 liquid scintillator. The incident proton energy is 5.90 MeV.

[illegible]

[illegible]

TABLE 1

Summary of lifetime determinations

Transition		Attenuation factor $F(\tau)$		τ_m (fs)					
E_i (keV)	E_f (keV)	coinc.	singles	this experiment			Ivascu *et al.* ref. [2])	Ragan *et al.* ref. [21])	Caraca *et al.* ref. [23])
				coinc.	singles	average	coinc.	singles	singles
1410	g.s.	0.17 ± 0.02	0.11 ± 0.02	945^{+200}_{-120}	940^{+300}_{-160}	940^{+170}_{-100}	650 ± 350	1080^{+170}_{-130}	370^{+190}_{-110}
1611	g.s.	< 0.05		> 3000		> 3000	$> 10{,}000$		
2217	g.s.	0.26 ± 0.03	0.20 ± 0.04	520 ± 90	500 ± 90	510 ± 70	600 ± 180	380 ± 50	
2488	g.s.	0.19 ± 0.05	0.16 ± 0.04	700^{+460}_{-260}	640^{+300}_{-200}	660^{+250}_{-160}	400 ± 130	775^{+105}_{-89}	88 ± 24
2795	g.s.	0.91 ± 0.07	0.88 ± 0.12	22 ± 18	21 ± 20	22 ± 14	< 25	14 ± 11	< 8
3185	1611		0.31 ± 0.05		285 ± 60	285 ± 60	950 ± 450		
3274	g.s.		0.75 ± 0.12		47 ± 27	50 ± 20			
3274	1611		0.72 ± 0.10		52 ± 25		45 ± 30		

3.2. LIFETIMES

The lifetime of levels up to an excitation of 2795 keV were investigated using the coincidence technique and up to an excitation of 3274 keV in singles. Gamma-ray energy shifts between 0° and 120° for several levels are indicated in fig. 3. The present lifetime information is summarized in table 1 and also compared with previous results. The attenuation factors and lifetimes listed for the singles measurements have been corrected for cascade feeding and all the results include a small correction ($\lesssim$ 10 %) due to recoiling ^{37}Ar nuclei which decayed in the Au backing.

The lifetime of the 3185 keV level determined in the present experiment, $\tau = 285 \pm 60$ fs, is to be compared with $\tau = 950 \pm 450$ fs obtained by Ivascu *et al.* [2]).

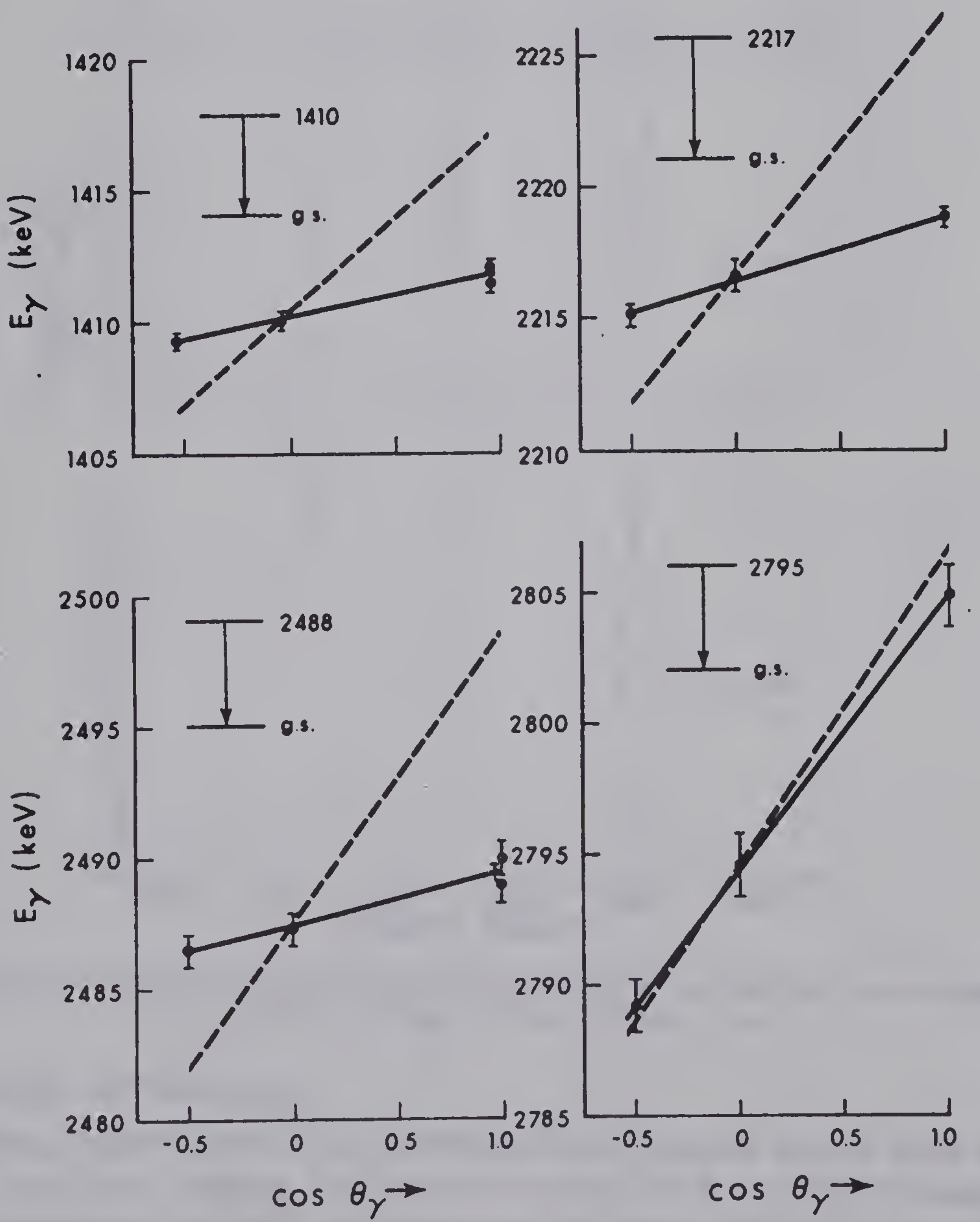

Fig. 3. Plots of γ-ray energy *versus* cos θ_γ for transitions in ^{37}Ar. The solid lines correspond to a least-squares fit to the experimentally observed energies and the dashed lines correspond to the full kinematic shifts. The plots shown are for coincidence experiments.

A spectrum of the 3185 → 1611 keV transition is shown in fig. 4 [cf. fig. 2 of ref.[2])].

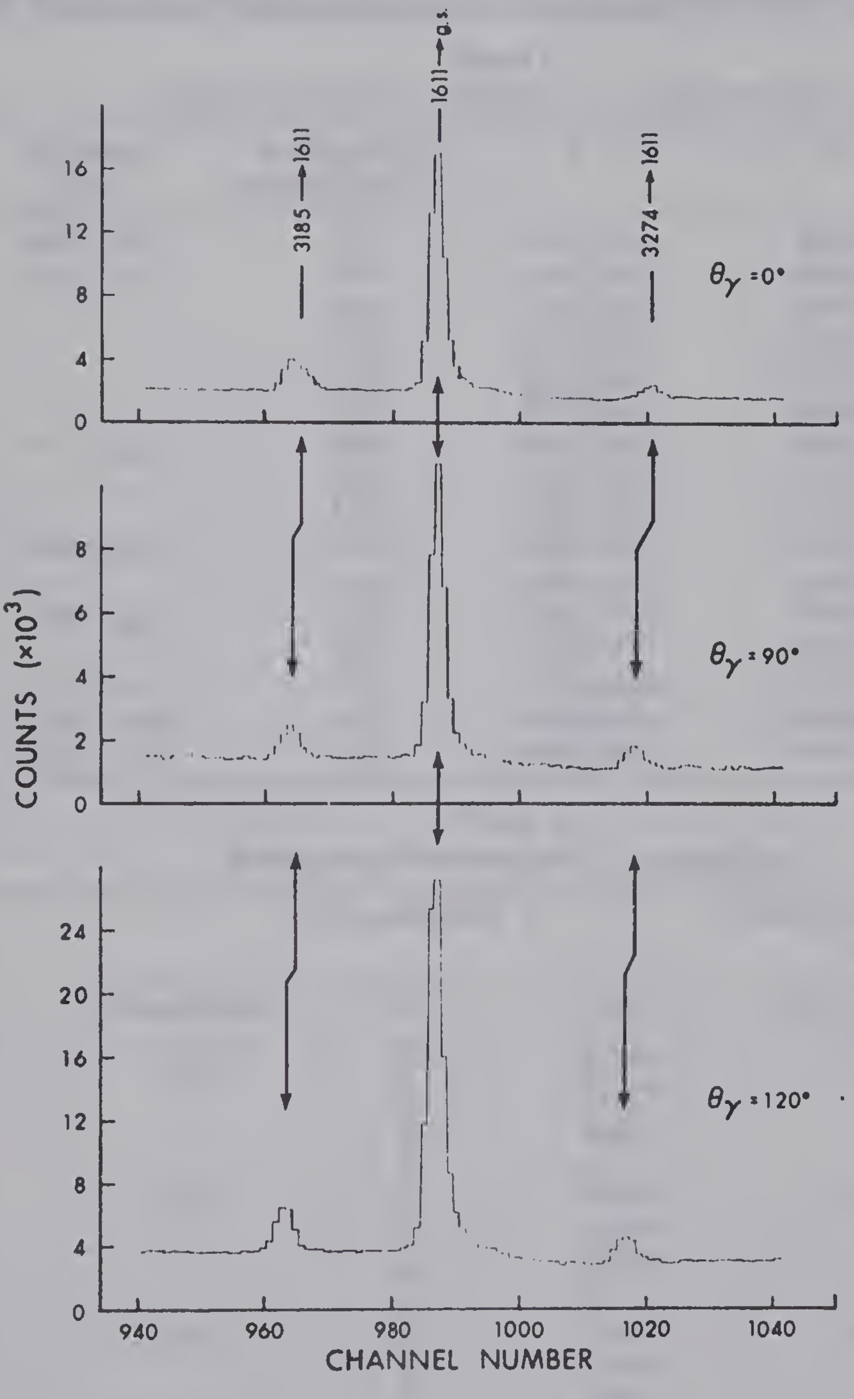

Fig. 4. Variation of energy with detection angle for the 1574, 1611 and 1662 keV γ-rays, originating from the 3185, 1611 and 3274 keV levels in ^{37}Ar.

3.3. ANGULAR DISTRIBUTIONS

Gamma-ray angular distribution measurements were carried out for levels up to 3274 keV excitation. Angular distributions measured at $E_p = 3.35$, 4.55 and 5.15 MeV were done with the $PbCl_2$ target; the rest were done with the KCl target. The angular distribution of γ-rays from the 1410 keV level ($J^\pi = \frac{1}{2}^+$), used to normalize all other γ-ray yields, was independently measured at a beam energy of 3.25 MeV to

be isotropic within 3 % using the small fixed Ge(Li) monitor. Legendre polynomial expansion coefficients for all measured angular distributions are listed in table 2; spin- and mixing-ratio determinations are summarized in tables 3 and 4.

TABLE 2
Legendre polynomial coefficients for angular distributions

Transition (keV)	Bombarding energy (MeV)	a_2	a_4
1410 → g.s.	3.25	-0.01 ± 0.03	0.00 ± 0.03
1611 → g.s.	3.35	0.24 ± 0.02	-0.10 ± 0.02
	3.40	0.18 ± 0.03	-0.07 ± 0.03
	4.05	0.18 ± 0.01	-0.03 ± 0.01
	4.30	0.16 ± 0.01	-0.03 ± 0.01
	4.55	0.17 ± 0.01	-0.08 ± 0.02
2217 → g.s.	4.05	0.44 ± 0.02	0.03 ± 0.02
	4.30	0.23 ± 0.01	-0.01 ± 0.01
	4.55	0.22 ± 0.01	-0.04 ± 0.01
2488 → g.s.	4.55	0.05 ± 0.01	0.00 ± 0.01
	5.15	0.05 ± 0.01	0.02 ± 0.01
2795 → g.s.	4.55	-0.01 ± 0.03	0.07 ± 0.03
	5.15	0.01 ± 0.01	0.02 ± 0.01
3171 → g.s.	5.15	-0.36 ± 0.08	-0.04 ± 0.08
3185 → 1611	5.15	0.47 ± 0.01	0.02 ± 0.02
3274 → g.s.	5.15	-0.08 ± 0.01	-0.01 ± 0.01

TABLE 3
Mixing ratio of the 1611 keV → g.s. transition

E_p (MeV)	SCN prediction			Best-fit population distribution determination	
	arctan δ(deg)	M	$P(M)$ [a]	arctan δ (deg)	$P(M)$
3.35	8 ± 4	$\frac{1}{2}$	0.239	8 ± 3	0.247
		$\frac{3}{2}$	0.179		0.173
		$\frac{5}{2}$	0.082		0.080
		$\frac{7}{2}$	0		0
3.40	12 ± 4	$\frac{1}{2}$	0.238	13 ± 4	0.233
		$\frac{3}{2}$	0.179		0.182
		$\frac{5}{2}$	0.083		0.085
		$\frac{7}{2}$	0		0
4.05	7 ± 4	$\frac{1}{2}$	0.205	10 ± 3	0.210
		$\frac{3}{2}$	0.165		0.162
		$\frac{5}{2}$	0.098		0.097
		$\frac{7}{2}$	0.032		0.031
4.30	8 ± 3	$\frac{1}{2}$	0.202	8 ± 3	0.203
		$\frac{3}{2}$	0.163		0.140
		$\frac{5}{2}$	0.099		0.115
		$\frac{7}{2}$	0.036		0.042
4.55	8 ± 4	$\frac{1}{2}$	0.199	10 ± 3	0.214
		$\frac{3}{2}$	0.162		0.168
		$\frac{5}{2}$	0.100		0.085
		$\frac{7}{2}$	0.039		0.033

[a] Populations are listed only for positive substates.

TABLE 4

Summary of spin and mixing-ratio assignments in ^{37}Ar

Transition E_i E_f	Present results J	δ	Champlin ref. 1) δ
2217 → g.s.	$\frac{7}{2}$	-0.03 ± 0.04	-0.03 ± 0.04
2488 → g.s.	$\frac{3}{2}$	unrestricted	
2795 → g.s.	$\frac{5}{2}$	-0.21 ± 0.13	0.00 ± 0.15
3171 → g.s.	$\frac{5}{2}$	$0.7^{+1.5}_{-0.6}$	$0.3\ \pm0.3$
3185 → 1611	$\frac{9}{2}$	-0.58 ± 0.09	
3274 → g.s.	$\frac{5}{2}$	-0.03 ± 0.13, $4.0^{+5.5}_{-1.5}$	0.20 ± 0.25 or 2.7 ± 0.5

3.3.1. *The* 1611 keV *level.* Angular distributions of the 1611 keV ground state transition were measured at $E_p = 3.35$, 3.40, 4.05, 4.30 and 4.55 MeV. A γ-ray yield function measurement [see ref. 22)], however, indicates that there is some non-statistical contribution on the reaction yield, bringing into question the accuracy of statistical compound nuclear (SCN) model predictions in the present experiment.

The presence of partial wave strength in addition to the expected statistical strengths could change the magnetic substate populations of a decaying level so that interpretation of an angular distribution using an unmodified SCN model calculation would result in an incorrect mixing-ratio assignment and, in extreme cases, an incorrect spin assignment. Consequently all the 1611 keV angular distributions have been analysed both with SCN predictions and by allowing magnetic substate populations to vary arbitrarily.

The 1611 keV γ-ray angular distribution analysis resulted in a unique $J = \frac{7}{2}$ assignment; this is in good agreement with the previous assignment 21, 22) of $J^\pi = \frac{7}{2}^-$. Also, the mixing ratios at all beam energies are in good agreement (table 3). The accepted value for the mixing ratio ($\delta = 0.16\pm0.04$) is in good agreement with the value of Champlin *et al.* 1), 0.15 ± 0.04, Ragan *et al.* 21), 0.09 ± 0.03 and Taras *et al.* 22), 0.22 ± 0.11. It was therefore concluded that the observed yield fluctuations are insufficient to cause any appreciable error due to using SCN model predictions, and accordingly they have been used throughout the following analysis.

3.3.2. *The* 2217, 2488, 2795 *and* 3274 keV *levels.* Analysis of the measured angular distributions of the ground state decays of the 2217, 2488, 2795 and 3274 keV levels yield results in agreement with the previous assignments of $\frac{7}{2}^+$ [ref. 21)], $\frac{3}{2}^-$ [ref. 1)], $\frac{5}{2}^+$ [ref. 21)] and $\frac{5}{2}$ [ref. 2)], respectively. The mixing ratios obtained in the present work are also in good agreement with the previous results (see table 4).

3.3.3. *The* 3171 *and* 3185 keV *levels.* The yield of the 3171 keV γ-ray was obtained by subtracting the contribution due to the ^{35}Cl 3162 keV γ-ray using a Gaussian lineshape. It was possible to make a unique $J = \frac{5}{2}$ assignment to the 3171 keV level. Although it is not possible to completely rule out negative parity, due to the large mixing-ratio error, positive parity is more likely.

The angular distribution of the 1574 keV transition from the 3185 keV level (fig. 5) is consistent only with $J = \frac{9}{2}$ or $\frac{11}{2}$. Furthermore, using the measured lifetime and mixing ratios, it is possible to assign $J^{\pi} = \frac{9}{2}^{-}$ to the 3185 keV level.

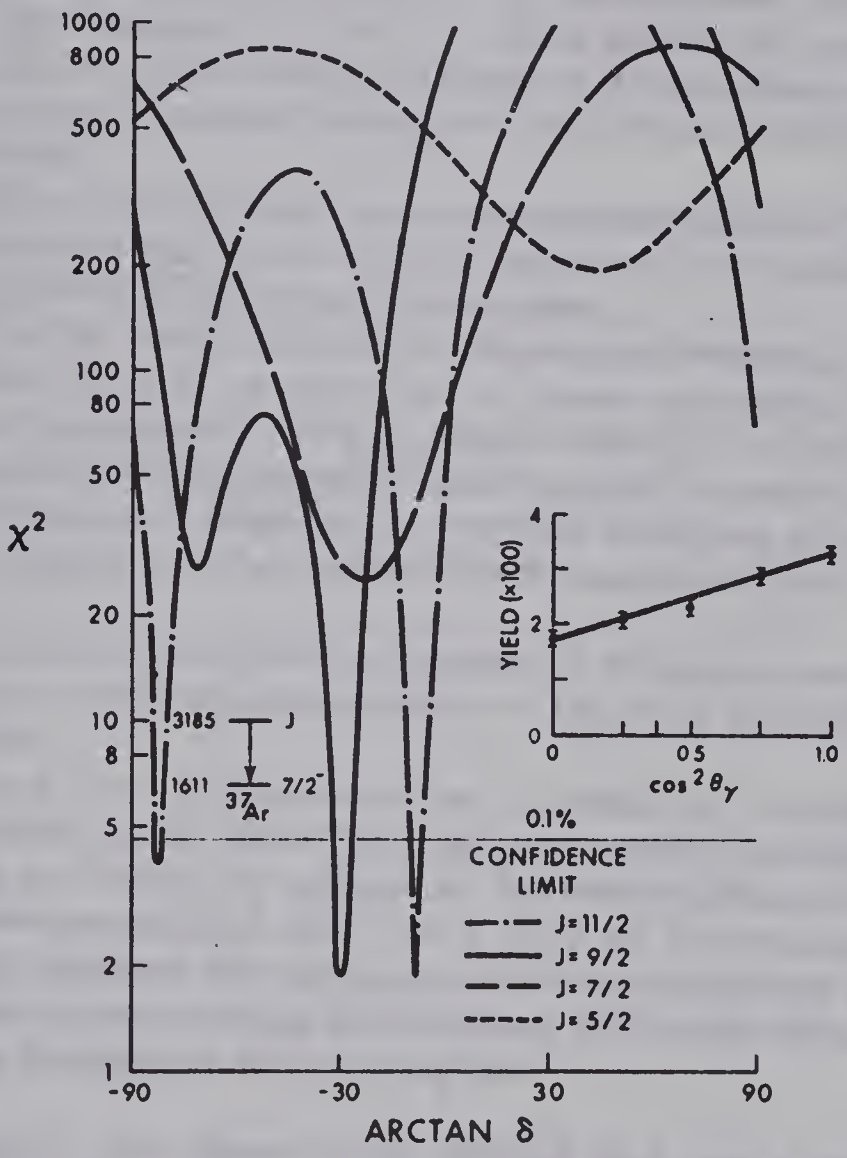

Fig. 5. Gamma-ray angular distribution (insert) and χ^2 plots for the 1574 keV transition from the 3185 keV level to the 1611 keV level measured at a proton energy of 5.15 MeV. The solid and dotted lines indicate the best fit for various spin and mixing-ratio combinations.

4. Discussion

Several DSA lifetime determinations exhibit a large variation between different experiments. In particular, in ^{37}Ar the recent results of Caraca *et al.* [23]) show a difference from other work of up to a factor of 10 (see table 1), which cannot be accounted for by the normally expected uncertainties. They concluded that the only possible reason for the observed discrepancy is that the nuclear stopping-power prediction is strongly underestimated by the Lindhard theory for light ions in high-Z solids below certain critical velocities. However, it is not clear that this is the *only* possible explana-

tion. It is instructive to look at the difference in the quoted lifetimes for the 1410 and 2488 keV levels between the results of Caraca *et al.* and both those of Ragan *et al.* and the present results. In each case a time difference of approximately 650 fs is indicated. This time difference would correspond to the recoiling nuclei travelling approximately 0.5 μm (assuming $\beta = 2.8 \times 10^{-3}$) before starting the slowing-down process described by the $F(\tau)$ calculation. As Caraca *et al.* used a thin target, thick backing configuration, a mean target-backing gap of about 0.5 μm would also explain the quoted differences.

Two shell-model transition-rate calculations for positive-parity states in ^{37}Ar up to 2796 keV excitation have been reported [21]). The calculations, of Dieperink and of Wildenthal, use the whole 2s-1d shell configuration space.

The 1410 keV level M1 lifetime predicted by Dieperink and Wildenthal are 730 fs and 470 fs, respectively. Both are faster than the present experimental value of 940^{+170}_{-100} fs. Similarly a lifetime of $\approx$ 3.5 fs is predicted for the 2795 keV level by both calculations, compared with the experimental value 22 ± 14 fs. The absolute values of the mixing ratio prediction of Dieperink, $|\delta| = 0.07$ and Wildenthal, $|\delta| = 0.12$ for the ground state transition are to be compared with the experimental value -0.21 ± 0.13.

The E2 lifetime of the 2217 keV level was calculated by Wildenthal to be 420 fs, in reasonable agreement with the experimental value $\tau = 510 \pm 70$ fs. This level was not treated by Dieperink.

The 1611 keV level ($J^{\pi} = \frac{7}{2}^{-}$) has most of the $1f_{\frac{7}{2}}$ strength in ^{37}Ar and is most likely of a single-particle nature. Harris [24]) has calculated the theoretical M2 lifetime and E3/M2 mixing ratio using a $1f_{\frac{7}{2}}$ configuration. The predicted lifetime of 12 ns is to be compared with the measured value [25]) of 6.5 ± 0.3 ns. The predicted mixing ratio is 0.087, in fair agreement with the experimental value of 0.16 ± 0.04. However it should be pointed out that correcting the discrepancy with the M2 lifetime would result in worsening the agreement for the mixing ratio.

Note added in proof: The lifetime of the 3185 keV level, among others, has recently been measured by Luketina *et al.* [26]). They obtained an average lifetime of $\tau = 300 \pm 60$ fs, in good agreement with the present value.

References

1) J. W. Champlin, A. J. Howard and J. W. Olness, Nucl. Phys. **A164** (1971) 307
2) M. Ivascu, D. Popescu and G. van Middelkoop, Nucl. Phys. **A163** (1971) 418
3) B. C. Robertson, T. P. G. Carola, D. M. Sheppard and W. C. Olsen, Nucl. Phys. **A160** (1971) 137
4) E. K. Warburton, J. W. Olness and A. R. Poletti, Phys. Rev. **160** (1967) 938
5) K. V. K. Iyengar, E. Wong and G. C. Neilson, Nucl. Phys. **A155** (1970) 582
6) B. C. Robertson, R. A. I. Bell, J. L'Ecuyer, R. D. Gill and H. J. Rose, Nucl. Phys. **A126** (1969) 431
7) J. Lindhard, Mat. Fys. Medd. Dan. Vid. Selsk. **28**, no. 8 (1954);
J. Lindhard, M. Scharff and H. E. Schiøtt, *ibid.* **33**, no. 14 (1963)

8) J. H. Ormrod, J. R. MacDonald and H. E. Duckworth, Can. J. Phys. **43** (1965) 275
9) O. B. Firsov, ZhETF (USSR) **26** (1959) 1517
10) B. Fastrup, P. Hvelplund and C. A. Sautter, Mat. Fys. Medd. Dan. Vid. Selsk. **35**, no. 10 (1966)
11) E. Sheldon, Rev. Mod. Phys. **35** (1963) 795
12) H. J. Rose and D. M. Brink, Rev. Mod. Phys. **39** (1967) 306
13) D. Cline and P. M. S. Lesser, Nucl. Instr. **82** (1970) 291
14) P. W. Green, University of Alberta internal report UAE-NPL-27 (1971)
15) N. E. Davison, University of Alberta internal report UAE-NPL-8 (1969)
16) L. Rosen, Proc. 2nd Int. Symp. on polarization phenomena of nucleons, ed. P. Huber and H. Schopper (Birkhauser Verlag, Basel, 1966)
17) F. G. Perey and B. Buck, Nucl. Phys. **32** (1962) 353
18) R. H. Davis, Symp. on nuclear reaction mechanisms and polarization phenomena, ed. B. Cujec, Q. Ho Kim and R. J. Slobodrian (Les Presses de L'Université Laval, Quebec, 1970)
19) E. H. Auerbach, Brookhaven report BNL 6562 (1964)
20) W. H. Chung, University of Alberta internal report UAE-NPL-23 (1970)
21) C. E. Ragan, C. R. Gould, N. R. Roberson, G. E. Mitchell and D. R. Tilley, Phys. Rev. **C3** (1971) 1152
22) P. Taras, A. Turcotte, R. Vaillancourt and J. Matas, Can. J. Phys. **49** (1971) 1215
23) J. M. G. Caraca, R. D. Gill, P. B. Johnson and H. J. Rose, Nucl. Phys. **A176** (1971) 273
24) G. I. Harris, Proc. Int. Conf. on properties of nuclear states, Montréal, ed. M. Harvey *et al.* (Presses de L'Université de Montréal, Montréal, 1969) p. 192
25) W. L. Randolph, Jr., R. R. Borchers, R. Michaelsen, D. W. Haag and W. Ribbe, Phys. Rev. Lett. **27** (1971) 603
26) I. J. Luketina, J. E. Brock and A. R. Poletti, Phys. Rev., to be published

Appendix F

Listing of 'OXDS' - a program to calculate $F(\tau)$

```
                                                   OS ALGOL F

                                                SOURCE PROGRAM
  SC       SOURCE STATEMENT

 00000     'BEGIN'
 00000     'REAL' A1A,A2A,ERR1,M,RH,VMIN,DELTA,ERR2,BC,DUM,AC,INT2,AV,BTAU,A1,
 00000     A2,A3,A4,VMAX,TMIN,A0,AA1,ACCC,PPF,AAA,BBB,FUDGNU,FUDGEL,NNEN,PATH,
 00000     RANGE;
 00001     'INTEGER' NSS,NEN,I,NUCLEAR,NF,N,TK,COUNTT,J,K,F1,F2,F10,F,ZI,II,
 00001     R,NL,PP,STEPS,SUP,NVMAX,IJKL;
 00002     'REAL' 'ARRAY' Q,RHO,A,Z(/1:6/),EXN,RES,COL,COL1(/0:10/),
 00002     E,DE,TAU(/0:40/),VMAXX(/1:50/),EXPC,SHAPE,LIM,TIME,VINT,
 00002     DEC,VELEFF(/-1:201/),C01(/0:10,0:10/);
 00003     'PROCEDURE'WRITE(DV,F,N);'VALUE'DV,F,N;'INTEGER'DV,F;'REAL'N;'CODE';
 00008     'PROCEDURE'WRITETEXT(DV,S);'VALUE'DV;'STRING'S;'INTEGER'DV;'CODE';
 00013     'INTEGER''PROCEDURE'FORMAT(S);'STRING'S;'CODE';
 00016
 00016     'PROCEDURE'COPY;
 00017     'BEGIN'
 00017     'INTEGER'BEG,I,J;'INTEGER''ARRAY'COPY(/1:30/);
 00019     SEARCH:INSYMBOL(0,'('*')',BEG);'IF'BEG¬=1'THEN''GOTO'SEARCH;
 00021     I:=0;
 00022     INPUT:I:=I+1;
 00023     INSYMBOL(0,'('*ABCDEFGHIJKLMNOPQRSTUVWXYZ0123456789()/.,'')',COPY(/I/));
 00024
 00024     'IF'COPY(/I/)¬=1'THEN''GOTO'INPUT;
 00025     'FOR'J:=1'STEP'1'UNTIL'I-1'DO'
 00025     OUTSYMBOL(1,'('*ABCDEFGHIJKLMNOPQRSTUVWXYZ0123456789()/.,'')',
 00025     COPY(/J/));
 00026     WRITETEXT(1,'(''('C')'')');
 00027     'END';
 00028
 00028     'REAL' 'PROCEDURE' LINDEL(Z1,Z2,A2,E);
 00029     'VALUE' Z1,Z2,A2,E; 'REAL'Z1,Z2,A2,E;
 00031     'BEGIN' 'COMMENT' E IN MEV/NUCLEON,LINDEL=DE/DX IN MEV-CM2/MG;
 00031     LINDEL:=73.0*(Z1**(7/6))*Z2*SQRT(E)/A2/((Z1**(2/3)+Z2**(2/3))**(3/2));
 00032     'END';
 00033
 00033     'REAL' 'PROCEDURE' MK(Z1,Z2,A1,A2,V);'VALUE'Z1,Z2,A1,A2,V;
 00035     'REAL' Z1,Z2,A1,A2,V;
 00036     'BEGIN' 'REAL' EP,K,R,AL,RL,IU,IL,EF,NL,AFS,EE;
 00037     EE:=(465.5*V**2)/(9.0'4);
 00038     EP:=(3.24*1.0'4*A1*A2*EE)/(SQRT(Z1**0.6667+Z2**0.6667)*Z1*Z2*(A1+A2));
 00039     NL:=(RH/(A2*1.66))*1.0'3;
 00040     AFS:=1.096/(Z1**0.6667+Z2**0.6667);
 00041     R:=A1/A2;
 00042     AL:=(1+R)/2;BE:=(AL**2)/R;
 00044     K:=0.0;
 00045     'IF' EP<=0.380001 'THEN' 'BEGIN' IL:=3.14159;'GOTO' E2E; 'END';
 00048     'IF' EP<=3.00001 'THEN' 'BEGIN' IU:=3.14159; 'GOTO'SA;'END';
```

```
                                        SOURCE PROGRAM
  SC       SOURCE STATEMENT

 00051     RL:=2*ARCTAN((3/SQRT(EP**2-9)));IU:=RL;
 00053     SA:IL:=2*ARCTAN((0.38/SQRT((EP**2-0.1444))));
 00054     'IF' EP<=1.0001 'THEN' 'GOTO' B;
 00055     K:=K+II1(R,RL,3.14159)/(EP**2);
 00056     B:K:=K+0.814*(II3(R,IU)-II3(R,IL))/EP-0.2*II2(R,IL,IU);
 00057     B2B:'IF'EP**2*1.0'4-1>1.0'-20 'THEN'
 00057     K:=K+0.87*(II3(R,IL)-II3(R,2*ARCTAN(1/SQRT(EP**2*1.0'4-1))))/EP;
 00058     MK:=(K*3.14159*NL*AFS)/2;
 00059     'END';
 00060
 00060     'REAL' 'PROCEDURE' RARCSIN(X); 'VALUE'X; 'REAL'X;
 00063     'BEGIN' 'IF'(1-X**2)<1.0'-10 'THEN' 'BEGIN' RARCSIN:=3.14159/2;
 00064     'GOTO'NJB; 'END'; RARCSIN:=ARCTAN((X/SQRT(1-X**2)));
 00067     NJB:'END';
 00068
 00068     'REAL' 'PROCEDURE' II1(R,AL,AU);'VALUE'R,AL,AU;   'REAL'R,AL,AU;
 00071     'BEGIN' 'REAL' ALF,BE,PHL,PHU;
 00072     ALF:=(1+R)/2; BE:=ALF**2/R;
 00074     PHL:=RARCSIN((SIN(AL/2)/SQRT(BE)));
 00075     PHU:=RARCSIN((SIN(AU/2)/SQRT(BE)));
 00076     II1:=(-1/(2*(SIN(AU/2))**2)+1/(2*(SIN(AL/2))**2))
 00076     -(ALF/(2*BE*SQRT(R*BE)))*((-COS(PHU)/((SIN(PHU))**2))
 00076     +LN(1/SIN(PHU)-COS(PHU)/SIN(PHU)))
 00076     -LN((COS(PHU/2)/SIN(PHU/2))))/SQRT(R*BE)
 00076     +(ALF/(2*BE*SQRT(R*BE)))*((-COS(PHL)/((SIN(PHL))**2))
 00076     +LN(1/SIN(PHL)-COS(PHL)/SIN(PHL)))
 00076     +LN((COS(PHL/2)/SIN(PHL/2))))/SQRT(R*BE);
 00077     'END';
 00078
 00078     'REAL' 'PROCEDURE' II2(R,AL,AU); 'VALUE' R,AL,AU; 'REAL' R,AL,AU;
 00081     'BEGIN' 'REAL' ALF,BE,PHL,PHU;
 00082     ALF:=(1+R)/2; BE:=ALF**2/R;
 00084     PHU:=RARCSIN(SIN(AU/2)/SQRT(BE));
 00085     PHL:=RARCSIN((SIN(AL/2)/SQRT(BE)));
 00086     II2:=LN(SIN(AU/2)/SIN(AL/2))-(1/SQRT(R))*(SQRT(ABS(BE-(SIN(AU/2.0))**2))
 00086
 00086     -SQRT(ABS(BE-(SIN(AL/2.0))**2)))
 00086     -(ALF/SQRT(BE*R))*LN((1/SIN(PHU)-COS(PHU)/SIN(PHU))/(1/SIN(PHL)
 00086     -COS(PHL)/SIN(PHL)));
 00087     'END';
 00088
 00088     'REAL' 'PROCEDURE' II3(R,AL);'VALUE'R,AU; 'REAL'R,AU;
 00091     'BEGIN' 'REAL' ALF,BE,PHU;
 00092     ALF:=(1+R)/2.0;      BE:=ALF**2/R;
 00094     PHU:=RARCSIN((SIN(AU/2.0)/SQRT(BE)));
 00095     II3:=-1.0/SIN(AU/2.0)+(ALF/(BE*SQRT(R)))*(SQRT(ABS(BE-(SIN(AU/2.0))**2))
 00095
 00095       /SIN(AU/2.0))+PHU/SQRT(R);
```

CENTRAL STORES HF-565

```
                                          SOURCE PROGRAM
  SC        SOURCE STATEMENT

 00096      'END';
 00097
 00097      'REAL' 'PROCEDURE' NDEDX(Z1,Z2,A1,A2,EE);'VALUE' EE,Z1,Z2,A1,A2;
 00099      'INTEGER' Z1,Z2; 'REAL' A1,A2,EE;
 00101      'BEGIN' 'REAL' EP,AE,ID;
 00102      EP:=(3.24'4*A1*A2*EE)/(SQRT((Z1**0.6667+Z2**0.6667))*Z1*Z2*(A1+A2));
 00103      ID:=(Z1*Z2*A1*8.475)/(1.66*A2*(A1+A2)*SQRT(Z1**0.6667+Z2**0.6667));
 00104      'IF' EP<14 'THEN' 'GOTO'RRF;
 00105      'IF'EP<13 'THEN' 'GOTO'RA;
 00106      NDEDX:=((ID*LN(2.259*EP))/2.0*EP);
 00107      'GOTO' FINI;
 00108      RA:AE:=SQRT(EP);
 00109      NDEDX:=ID*0.25*((LN(2.259*EP)*(EP-14))/(2.0*EP)+(13-EP)
 00109      *(1.97*AE*EXP(-1.82*AE)+0.0225*AE));
 00110      'GOTO' FINI;
 00111      PRR:EP:=SQRT(EP);
 00112      AE:=('IF'EP>(2.2-SQRT(6.5/4.1)) 'AND'EP<(2.2+SQRT(6.5/4.1))
 00112      'THEN'(0.065-0.041*((EP-2.2)**2)) 'ELSE' 0.0);
 00113      NDEDX:=ID*((1.97*EXP(-1.32*EP)*EP+0.0225*EP)+AE);
 00114      FINI:'END';
 00115
 00115      'PROCEDURE' PRINT(ACO,ARES,ADEG); 'VALUE' ACO,ARES,ADEG;'INTEGER'ADEG;
 00118      'ARRAY'ACO,ARES;
 00119      'BEGIN' 'INTEGER' AI,AJ,RO;
 00120      WRITETEXT(1,'(''('CC')'DEGREE****COEFFICIENT*PLUS*RESIDUE'('CC')'')');
 00121      RO:=FORMAT('('-D.DDD'-ND')');
 00122      WRITE TEXT(1,'(''('3S')'')');
 00123      'FOR'AI:=0'STEP'1'UNTIL'ADEG 'DO''BEGIN'WRITE(1,F2,AI);
 00124      'FOR'AJ:=0'STEP'1'UNTIL'AI 'DO''BEGIN'WRITE TEXT(1,'(''('3S')'')');
 00125      WRITE(1,RO,ACO(/AI,AJ/));
 00126      'END';
 00127      WRITE TEXT(1,'(''('3S')'')'); WRITE(1,RO,ARES(/AI/));
 00129      WRITE TEXT(1,'(''('C')'')');
 00130      'END';'END'OF PRINT;
 00132
 00132      'REAL''PROCEDURE' EXPINT(LO,UP,TAU);'VALUE'LO,UP,TAU;'REAL'LO,UP,TAU;
 00135      'BEGIN'    EXPINT:=-TAU*(EXP(-UP/TAU)-EXP(-LO/TAU));
 00136      'END';
 00137
 00137      'REAL''PROCEDURE'POLY(X,A,M,N);
 00138      'VALUE'X,N,M;'REAL'X;'ARRAY'A;'INTEGER'N,M;
 00142      'BEGIN''INTEGER'I;'REAL'P;P:=A(/N/);
 00145      'FOR'I:=N-1'STEP'-1'UNTIL'M'DO'P:=P*X+A(/I/);
 00146      POLY:=P
 00146      'END';
 00147
 00147      'PROCEDURE'CURVEFIT(N)POINTS:(X,Y)MAXDEGREE:(DEG)COEFFICIENTS:(C)
 00147      RESIDUALS:(RES); 'VALUE'N,X,Y,DEG;'INTEGER'N,DEG;'ARRAY'X,Y,C,RES;
```

CENTRAL STORES HF.385

```
                                      SCURCE PROGRAM
 SC       SOURCE STATEMENT

00151     'BEGIN''INTEGER'I,J,P;'REAL'SUMX,SUMY;
00153     'ARRAY'R(/1:N/),CC,D,M(/0:DEC/),T(/0:DEG,1:N/),B(/0:DEG,0:DEG/),
00153     PI,RO(/1:DEG/);SUMX:=SUMY:=0.0;
00155     'FOR'I:=1'STEP'1'UNTIL'N'DC''BEGIN'SUMX:=SUMX+X(/I/);
00156     SUMY:=SUMY+Y(/I/);
00157     'END';
00158     'FOR'P:=0'STEP'1'UNTIL'DEG'DC''FOR'J:=P+1'STEP'1'UNTIL'DEG'DO'
00158     C(/P,J/):=0.0; RES(/0/):=0.0;
00160     M(/0/):=N;D(/0/):=SUMY;C(/0,0/):=CC(/0/):=D(/0/)/M(/0/);
00163     B(/0,0/):=B(/1,1/):=1;B(/1,0/):=-SUMX/N;
00165     'FOR'I:=1'STEP'1'UNTIL'N'DO''BEGIN'T(/0,I/):=1;
00166     T(/1,I/):=X(/I/)+B(/1,0/);
00167     RES(/0/):=RES(/0/)+(Y(/I/)-C(/0,0/))**2'END';
00168     'FOR'P:=1'STEP'1'UNTIL'DEG'DO'
00168     'BEGIN'RES(/P/):=D(/P/):=M(/P/):=PI(/P/):=RO(/P/):=0.0;
00169     'FOR'I:=1'STEP'1'UNTIL'N'DO'
00169     'BEGIN'M(/P/):=M(/P/)+T(/P,I/)*T(/P,I/);
00170     D(/P/):=D(/P/)+Y(/I/)*T(/P,I/);
00171     'IF'P¬=DEG'THEN''BEGIN'RO(/P/):=RO(/P/)+X(/I/)*T(/P,I/)
00171     *T(/P-1,I/);PI(/P/):=PI(/P/)+X(/I/)*T(/P,I/)*T(/P,I/)
00172     'END';'END';
00174     C(/P,P/):=CC(/P/):=D(/P/)/M(/P/);
00175     'IF'P¬=DEG'THEN''BEGIN'RO(/P/):=RO(/P/)/M(/P-1/);
00176     PI(/P/):=PI(/P/)/M(/P/);
00177     'FOR'I:=1'STEP'1'UNTIL'N'DC'
00177     T(/P+1,I/):=(X(/I/)-PI(/P/))*T(/P,I/)-RC(/P/)*T(/P-1,I/);
00178     B(/P+1,0/):=-PI(/P/)*B(/P,0/)-RO(/P/)*B(/P-1,0/);
00179     'FOR'J:=0'STEP'1'UNTIL'P-2'DC'
00179     B(/P+1,J+1/):=B(/P,J/)-PI(/P/)*B(/P,J+1/)-RO(/P/)*B(/P-1,J+1/);
00180     B(/P+1,P/):=B(/P,P-1/)-PI(/P/);B(/P+1,P+1/):=1'END';
00182     'FOR'J:=0'STEP'1'UNTIL'P-1'DO'C(/P,J/):=C(/P-1,J/)+CC(/P/)*B(/P,J/);
00183     'FOR'I:=1'STEP'1'UNTIL'N'DO'
00183     'BEGIN'R(/I/):=Y(/I/);
00184     'FOR'J:=0'STEP'1'UNTIL'P'DC'R(/I/):=R(/I/)-C(/P,J/)*
00184     ('IF'J=0'THEN'1'ELSE'X(/I/)**J);
00185     RES(/P/):=RES(/P/)+R(/I/)*R(/I/)'END';
00186     'END';'END'CURVEFIT;
00188
00188     'PROCEDURE' SIMRULE(A,B,F,INTEGRAL,C,ACC,FAIL);
00189     'VALUE'A,B,ACC;'REAL'A,B,INTEGRAL,C,ACC;
00191     'LABEL'FAIL;'REAL''PROCEDURE'F;
00193     'BEGIN''INTEGER'M,N,NN;'REAL'D,H,G0,G1,G2,G3,G4,A0,A1,A2,RES,X;
00195     'ARRAY'S1,S2,S3(/1:15/);RES:=C:=0.0:M:=N:=0;NN:=15;
00199     G0:=F(A);G2:=F((A+B)/2.0);G4:=F(B);
00202     A0:=(B-A)*(G0+4.0*G2+G4)/2.0;
00203     AA:D:=2.0**N;H:=(B-A)/(4.0*D);X:=A+(4.0*M+1.0)*H;
00206     G1:=F(X);G3:=F(X+2.0*H);
00208     A1:=H*(G0+4.0*G1+G2);A2:=H*(G2+4.0*G3+G4);
```

SOURCE PROGRAM

```
SC       SOURCE STATEMENT

         'IF'ABS(A1+A2-A0)>ACC/C 'THEN'
         'BEGIN'M:=M+M;N:=N+1;
         'IF'N>NN 'THEN''GOTO'FAIL;
         A0:=A1;S1(/N/):=A2;S2(/N/):=G3;S3(/N/):=G4;G4:=G2;G2:=G1;
         'GOTO'AA;'END''ELSE''BEGIN'
         RES:=RES+(A1+A2)/3.0;M:=M+1;C:=A+M*(E-A)/D;
         BB:'IF'M=2*(M'/'2) 'THEN'
         'BEGIN'M:=M'/'2;N:=N-1;'GOTO'BB;'END';
         'IF'M¬=1'OR'N¬=0'THEN'
         'BEGIN'A0:=S1(/N/);
         G0:=G4;G2:=S2(/N/);G4:=S3(/N/);
         'GOTO'AA;'END';'END';
         MJ:INTEGRAL:=RES;'END';


         'REAL''PROCEDURE'DX(V);'VALUE'V;'REAL'V;
         'BEGIN''REAL'PO,A1B.A2B;'INTEGER'K;
         'IF'V<=(E(/1/))'THEN''GOTO'MA;
         POL:PO:=POLY(V,COL1,0,6);
         'GOTO'EG;
         MA:PO:=(POLY(E(/1/),COL1,0,6)*V)/E(/1/);
         EG:'IF'NUCLEAR<0.5'THEN''GOTO'JR5;A1B:=0;A2B:=0;
         'FOR'K:=1'STEP'1'UNTIL'NSS'DO'
         'BEGIN'
         A1B:=A1B+Q(/K/)*A(/K/)*
         NDEDX(ZI,Z(/K/),(M/0.0664),A(/K/),(5.172'-3*(V**2)));
         A2B:=A2B+Q(/K/)*A(/K/);
         'END';
         PO:=PO+(0.3204*FUDGNU*RH*A1B)/A2B;
         JR5:DX:=M/PO;
         'END'OF DX;


         'REAL''PROCEDURE'READ;
         'BEGIN''REAL'V;INREAL(0,V);READ:=V;
         'END';


         'REAL''PROCEDURE'MKDX(V);'VALUE'V;'REAL'V;
         'BEGIN''INTEGER'E;'REAL'A1C,A2C;A1C:=A2C:=0.0;
         'FOR'E:=1'STEP'1'UNTIL'NSS'DO'
         'BEGIN'A1C:=A1C+A(/E/)*C(/E/)*MK(ZI.Z(/E/),(M/0.0664).A(/E/),V);
         A2C:=A2C+Q(/E/)*A(/E/);
         'END';
         MKDX:=FUDGNU*(V*DX(V)*A1C)/A2C;
         'END';


         SYSACT(15,12,1); SYSACT(1.6,132);SYSACT(1.12.1);
         STARTA:WRITETEXT(1,'(''('CC')'')');
         COPY;
         ININTEGER(0,NSS);'IF'NSS<0.5'THEN''GOTO'FIN:
```

CENTRAL STORES HY-585

```
                                        SOURCE PROGRAM
  SC       SOURCE STATEMENT

 00277     INREAL(0,RH);INREAL(0,M);ININTEGER(0,ZI);
 00280     'FOR'I:=1'STEP'1'UNTIL'NSS'DO'C(/I/):=READ;
 00281     'FOR'I:=I'STEP'1'UNTIL'NSS'DO'A(/I/):=READ;
 00282     'FOR'I:=1'STEP'1'UNTIL'NSS'DC'Z(/I/):=READ;
 00283     ININTEGER(0,NEN);
 00284     'IF'NEN<0.1'THEN''BEGIN'NNEN:=-10;NEN:=1;INREAL(0,FUDGEL);
 00287     'END''ELSE'NNEN:=10;
 00288     'IF'NNEN<0'THEN'E(/I/):=0.I'ELSE''FCR'I:=1'STEP'1'UNTIL'NEN'DO'
 00288     E(/I/):=READ;
 00289     'FOR'I:=1'STEF'1'UNTIL'NEN'DC''EEGIN'
 00289     A1A:=0;A2A:=0;
 00291     'FOR'II:=1'STEP'1'UNTIL'NSS'CO''BEGIN'
 00291     AIA:=A1A+(Q(/II/)*A(/II/)*('IF'NNEN<0'THEN'LINDEL(ZI,Z(/II/),
 00291     A(/II/),0.I)*FUDGEL'ELSE'READ));
 00292     A2A:=A2A+Q(/II/)*A(/II/);
 00293     'END';
 00294     DE(/I/):=A1A/A2A;
 00295     'END';
 00296     'IF'NEN=1'THEN''BEGIN'NEN:=7;
 00297     'FOR'I:=2'STEP'1'UNTIL'7'DC''BEGIN'
 00297     E(/I/):=E(/1/)*I;DE(/I/):=DE(/1/)*SGRT(I);
 00299     'END';'END';
 00301     FI:=FORMAT('('SNCC.DDDSS')');
 00302     'IF'NNEN<0'THEN''BEGIN'WRITETEXT(1,'(''('CC')'LINDHARD*STCPPING*WITH*ELE
 00302
 00302     CTRONIC*FACTOR*=*****')');
 00303     WRITE(1,F1,FUDGEL);WRITETEXT(1,'(''('CC')'')');
 00305     'END';
 00306     WRITETEXT(1,'(''('C')'E(MEV/AMU)**DE/DX(MEV.CM/MG'('2C')'')');
 00307     F10:=FORMAT('('-SSC.DDC'-NC')');
 00308     'FOR'I:=I'STEP'I'UNTIL'NEN'DC''BEGIN'
 00308     WRITE(I,F10,E(/I/));WRITE(1,F10,DE(/I/));WRITETEXT(1,'(''('C')'')');
 00311     E(/I/):=300.0*SORT(E(/I/)/465.5);
 00312     'END';
 00313     NP:=NEN;ININTEGER(0,NVMAX);
 00315     'FOR'I:=1'STEP'1'UNTIL'NVMAX'DC'VMAXX(/I/):=READ;
 00316     INREAL(0,VMIN);ININTEGER(0,N);ININTEGER(0,TK);
 00319     'IF'TK<0.5'THEN''BEGIN'TAU(/1/):=0.002;TAU(/2/):=0.004;TAU(/3/):=0.01;
 00322     'FOR'I:=4'STEP'1'UNTIL'16'DO'TAU(/I/):=10*TAU(/I-3/);TK:=16;
 00324     'END' 'ELSE''FOR'I:=1'STEP'1'UNTIL'TK'DO'TAU(/I/):=2'12 *(READ);
 00325     INREAL(0,ACCC);ININTEGER(0,SUP);
 00327     INREAL(0,FUDGNU);'IF'FUDGNU<-0.1'THEN'NUCLEAR:=0'ELSE'NUCLEAR:=1;
 00329     WRITETEXT(1,'(''('CC')'MASS*CF*ICN'('SSS')'CHARGE*****DENSITY**Z*AND*A**
 00329
 00329     OF**EACKING'('CC')'')');
 00330     F1:=FORMAT('('SNDD.DDDSS')');F2:=FORMAT('('SSSSNDDSSS')');WRITE(1,F1,M);
 00333
 00333     WRITE(1,F2,ZI);WRITE(1,F1,FF);
```

CENTRAL STORES HF-303

```
                              SCURCE PROGRAM
 SC     SOURCE STATEMENT

00335   'FOR'I:=1'STEP'1'UNTIL'NSS'DC''BEGIN''IF'I>1.5'THEN'
00335   'BEGIN'WRITETEXT(1,'(''('C')'')');WRITETEXT(1,'(''('28S')'')');
00337   'END';WRITE(1,F2,Z(/I/));WRITE(1,F1,A(/I/));
00340   'END';
00341   WRITETEXT(1,'(''('CC')'MIN*VELCCITY*=***')');WRITE(1,F10,(VMIN*10**8));
00343   'IF'NUCLFAR>0.)'THEN''BEGIN'
00343   WRITETEXT(1,'(''('CC')'WITH*NUCLEAR*FACTOR*=****')');
00344   WRITE(1,F1,FUDGNU);
00345   'END';
00346   WRITETEXT(1,'(''('CC')'')');
00347   M:=M*0.0664;
00348   'FOR'I:=1'STEP'1'UNTIL'NP'DO'DE(/I/):=C.3204*RH*DE(/I/);
00349   CURVEFIT(NP,E,DE,5,C01,RES);
00350   PRINT(C01,RES,5);
00351   'FOR'I:=0'STEP'1'UNTIL'5'DO'CCL1(/I/)              :=C01(/5,I/);
00352   'FOR'IJKL:=1'STEP'1'UNTIL'NVMAX'DC''BEGIN'VMAX:=VMAXX(/IJKL/);
00353   DELTA:=LN(VMAX/VMIN)/N;
00354   EXPO(/0/):=0;INT2:=0.0;TIME(/C/):=0.0;VINT(/0/):=VMAX;
00358   DE(/1/):=POLY(E(/1/),CCL1,0,6);
00359   'BEGIN'
00359   PATH:=RANGE:=0.0;VELEFF(/0/):=VMAX;
00361   'FOR'II:=1'STEP'1'UNTIL'N'DC''BEGIN'
00361   VINT(/II/):=VINT(/II-1/)*EXP(-DELTA);
00362   AC:=DX(VINT(/II/));
00363   'IF'SUP<1.9'THEN''GOTC'QS1;
00364   WRITE TEXT(1,'(''('C')'')');
00365   WRITE(1,F10,AC);
00366   QS1:'END';
00367   WRITETEXT(1,'(''('CSSS')'VELOCITY****TIME********COSBAR******VELEFF*****
00367
00367   **PATHLENGTH**MEANRANGE***(THE LATTER IN MG/CM2)'('C')'')');
00368   'FOR'II:=1'STEP'1'UNTIL'N'DO''BEGIN'
00368   VINT(/II/):=VINT(/II-1/)*EXP(-DELTA);
00369   AC:=ABS((VINT(/II-1/)-VINT(/II/))*DX((VINT(/II-1/)+VINT(/II/))/2.0)/
00369   (400.0*ACCC));
00370   'IF'SUP<1.9'THEN''GOTO'QS2;
00371   WRITETEXT(1,'(''('C')'')');
00372   WRITE(1,F10,AC);
00373   QS2:SIMPULE(VINT(/II/),VINT(/II-1/),DX,INT2,DUM,AC,FAIL1);
00374   TIME(/II/):=TIME(/II-1/)+INT2;
00375   AC:=ABS((VINT(/II-1/)-VINT(/II/))*MKDX((VINT(/II/)+VINT(/II-1/))/2)/
00375   (400*ACCC));
00376   SIMRULE(VINT(/II/),VINT(/II-1/),MKDX,INT2,DUM,AC,FAIL5);
00377   EXPO(/II/):=EXPO(/II-1/)+INT2;
00378   VELEFF(/II/):=VINT(/II/)*EXP(-EXPO(/II/));
00379   PATH:=PATH+0.5*(VINT(/II-1/)+VINT(/II/))*(TIME(/II/)-TIME(/II-1/));
00380   RANGE:=RANGE+0.5*(VELEFF(/II-1/)+VELEFF(/II/))
00380   *(TIME(/II/)-TIME(/II-1/));
```

```
                                   SOURCE PROGRAM
 SC      SOURCE STATEMENT

00381    WRITETEXT(1,'(''('C')'')');
00382    WRITE(1,F10,(VINT(/II-1/)*10**8));
00383    WRITE(1,F10,(TIME(/II-1/)*5.0/(1'13)));
00384    WRITE(1,F10,EXP(-EXPO(/II-1/)));
00385    WRITE(1,F10,VELEFF(/II-1/)*10**8);WRITE(1,F10,PATH*PH/20);
00387    WRITE(1,F10,RANGE*RH/20);
00388    'END';
00389    WRITETEXT(1,'(''('CC')'LIFETIME******FTAU********CUTERR*****INTERR'('C
00389    ')'')');
00390    'FOR'II:=1'STEP'1'UNTIL'IX'DO''BEGIN'AC:=BC:=0.0;
00391    'FOR'I:=0'STEP'1'UNTIL'N'DO'DEC(/I/):=EXP(-TIME(/I/)/TAU(/II/));
00392    'FOR'I:=1'STEP'1'UNTIL'N'DO'
00392    'BEGIN''IF'VELEFF(/I-1/)*DEC(/I-1/)<1'-6*VMAX'AND'I>3'THEN''GOTO'TERM;
00393    AAA:=(VELEFF(/I-1/)*TIME(/I/)-VELEFF(/I/)*TIME(/I-1/))/(TIME(/I/)
00393    -TIME(/I-1/));
00394    BBB:=(VELEFF(/I/)-VELEFF(/I-1/))/(TIME(/I/)-TIME(/I-1/));
00395    AC:=AC+(AAA+BBB*(TIME(/I-1/)+TAU(/II/)))*DEC(/I-1/)
00395    -(AAA+BBB*(TIME(/I/)+TAU(/II/)))*DEC(/I/);
00396    'END';
00397    TERM:ERR1:=VELEFF(/I/)*DEC(/I/)/VMAX;
00398    ERR2:=(VELEFF(/1/)-VELEFF(/2/))*2/(VELEFF(/1/)+VELEFF(/2/));
00399    AC:=AC/VMAX;
00400    WRITETEXT(1,'(''('C')'')');
00401    WRITE(1,F10,TAU(/II/)*5'-13);
00402    WRITE(1,F10,AC);
00403    WRITE(1,F10,ERR1);WRITE(1,F10,ERR2);
00405    'END';'END';
00407    WRITETEXT(1,'(''('5C')'')');
00408    'END';
00409    'GOTO'RSD2;
00410    FAIL1:WRITETEXT(1,'(''('C')'FAIL1'('C')'')');'GOTO'RSD2;
00412    FAIL5:WRITETEXT(1,'('FAIL5'('C')'')');
00413    RSD2:'GOTO'STARTA;
00414    FIN:'END';
```

B30122